MONSOON SURGES, TROPICAL CYCLONES AND EXTREME RAINFALL EVENTS IN NW MADAGASCAR

Abdallah Nassor

Oceanography Department, University of Cape Town

A thesis submitted in fulfillment of the requirements

for the degree of Master of Science

March 1995

ABSTRACT

Rainfall variability in NW Madagascar and the kinematics and thermodynamics of flood-producing weather systems affecting the region are examined. Daily rainfall in the austral summer are used to select 16 cases for the composite analysis of flood events in the period 1987-1992. In addition two cases of flood events are studied individually. The first flood event occurred in 1991 and brought 420 mm of rainfall in 24 hours at Maintirano during the passage of tropical cyclone (TC) Cynthia, an eastward moving TC from the Mozambique Channel. The second flood event occurred in 1992 and brought 347 mm of rainfall in 24 hours at Mahajanga due to the passage of TC Bryna, a westward moving TC from the Indian Ocean.

Inter-annual rainfall variability is correlated with the indices: TC day frequency, QBO and SOI, and a useful value is found with the first index but not with the two latter global indices. An intraseasonal analysis indicates that wet spells have a duration of 15 to 20 days. Daily spectra-analysis of rainfall reveals the complexity of interplay between the convective forcing features. Cycles of 10-20 days are contributed by easterly waves, while 40 day cycles are produced by monsoon surges. The composite analysis identifies the following features: an eastward shift of active convection from Mozambique across Madagascar in conjunction with a surge of the NW monsoon and weakening of the easterlies in the lower troposphere. These factors promote TC genesis. Other supporting influences include the development of an anticyclonic circulation in the upper level over the island with northwestward outflow. This often coincides with an east phase QBO, an upper level eastward moving mid-latitude trough and a persistent moisture flux convergence over the island throughout TC passage.

The topography of Madagascar plays an important role in the intensification of the flood-producing weather system by enhancing the cloud vortex in the NW region of the island.

CONTENTS

PREFACE

The Mozambique Channel west of Madagascar is one of the few regions of the world where rapid tropical cyclone (TC) genesis takes place; it is also an area of convergence of monsoon flow and trade winds, creating deep convection which often moves eastward toward the northwest region of Madagascar. Many tropical storms initiated in the Mozambique Channel or SW Indian Ocean (SWIO) hit the island of Madagascar, resulting in considerable destruction due to strong winds and floods. Daily rainfall in the region is highly variable. The topography of the island plays an important role in initiating the cloud vortex of the flood-producing system over the area. The real threat for the population in the region is a storm moving eastward from the Channel, its lifespan is short and its rapid development makes the task of weather forecasting more difficult. It is then, of major concern to know the dynamics of these storms for disaster prevention in the region.

The aim of this dissertation is to contribute to a better understanding of the origin of flood-producing systems affecting the region as well as the dynamics and evolution of such systems. Spatial map and vertical section composites form the data analyses in this thesis which is presented on a sequential event scale.

The major themes of the thesis are:

1] to identify the global indices and regional patterns modulating inter-annual as well as intra-seasonal variability of the monsoon rainfall;

2] to establish differences in the mean and anomalous synoptic fields of meteorological parameters associated with composite wet events;

3] to determine the origin of the moisture flux and to examine the synoptic features of flood-producing systems, particularly monsoon surges and TCs developing in the SWIO.

The thesis is divided into 7 chapters and diagrams are appended at the end of each. In Chapter 1, the climatology of the region, and the rain-producing systems affecting the area are reviewed. The motivation and hypotheses to be tested are outlined at the end of the chapter. In Chapter 2, background to the various studies undertaken in the field of monsoon and TC development in the Indian, Australian and SWIO region as well as climate variability in the latter region is provided. In Chapter 3, the data, methodology and the various meteorological parameters used in this study are discussed. In Chapter 4, the inter-annual and intra-seasonal variability of summer rainfall and the structure of meteorological patterns associated with the dry spell are examined. In Chapter 5, the results of the historical mean and composite case in terms of dynamic/kinematic, moisture and thermodynamic processes are examined. In Chapter 6, analyses of the meteorological parameters associated with two cases of floods in 1991 and 1992 due to TC Cynthia and TC Bryna respectively, are discussed. Chapter 7 interprets the results in the form of a discussion. All conclusions derived are also summarized in this chapter.

LIST OF FIGURES

Figure

LIST OF TABLES

Table

APPENDICES

Appendix

CHAPTER 1

INTRODUCTION

1.1 Climate of Madagascar :

Monsoon circulations and tropical cyclones (TCs) are factors controlling summer rainfall in many countries bordering the Indian Ocean. Meteorological studies on the area have indicated that the Southwest Indian Ocean (SWIO) and the Mozambique Channel are important sources for severe weather systems (Duvergé, 1949; Donque, 1975; and Jury and Pathack, 1991). The semi-permanent low-level depression in the eastern Channel is an area of convergence of monsoons and easterly flows. It is also an area of TC-genesis where sea surface temperatures often exceed 28°C between December and March.

The island of Madagascar in the SWIO (Fig 1.1) separated from the African continent by the Mozambique Channel, is one of these countries affected by monsoon rain and TC. It extends 1580 km north-south and is 500 km wide. Its relief consists of a juxtaposition of coastal plains and plateau with mountains > 2000 m elevation in some locations (Fig 1.2 and 1.3). The aim of this study is to analyse the evolution of weather patterns associated with the occurrence of heavy rainfall events affecting the northwest region of Madagascar, caused by monsoon vortices and locally generated TCs.

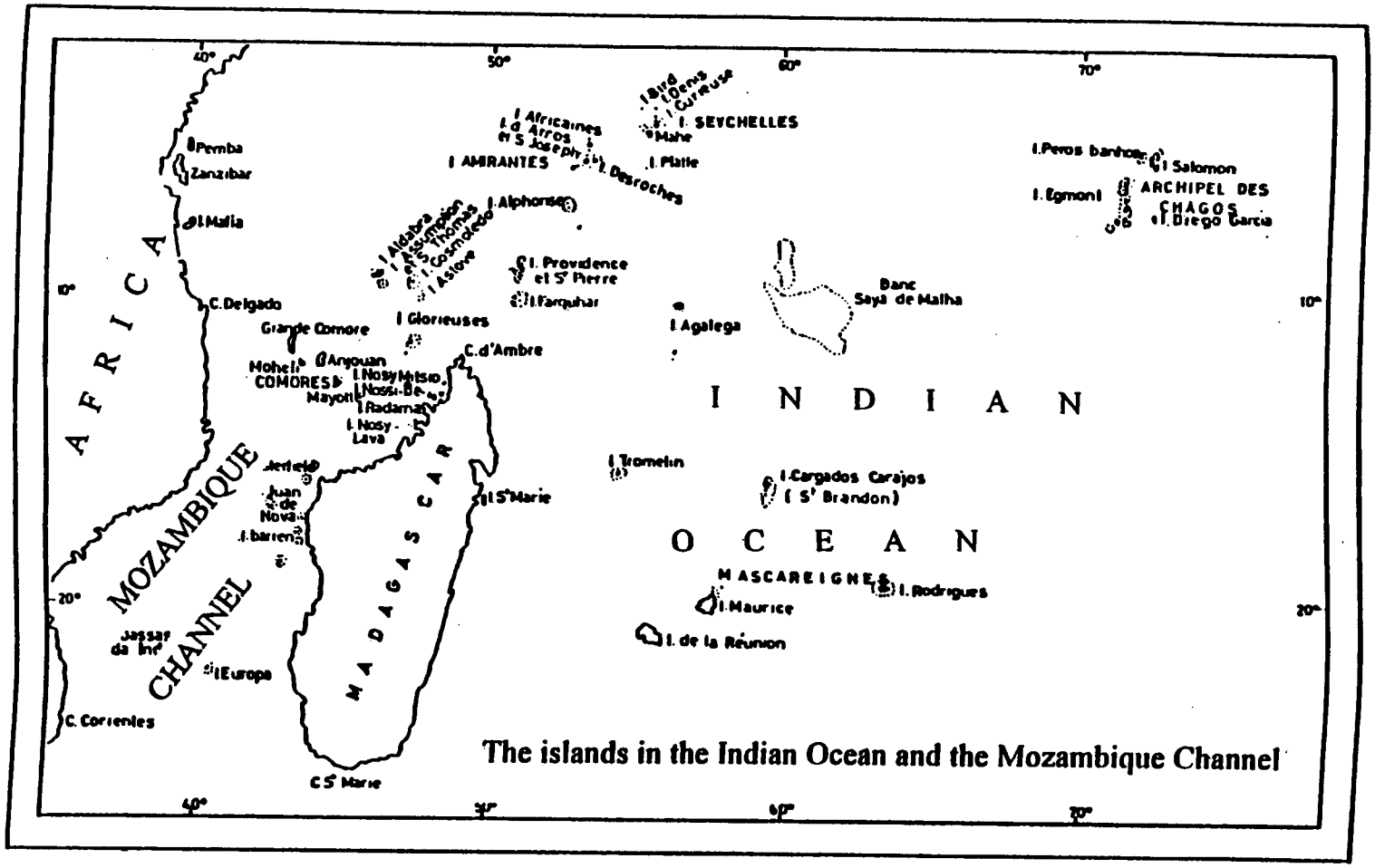

The islands in the Indian Ocean and the Mozambique Channel

(from Donque, 1975)

Figure 1.1 : The Southwest Indian Ocean

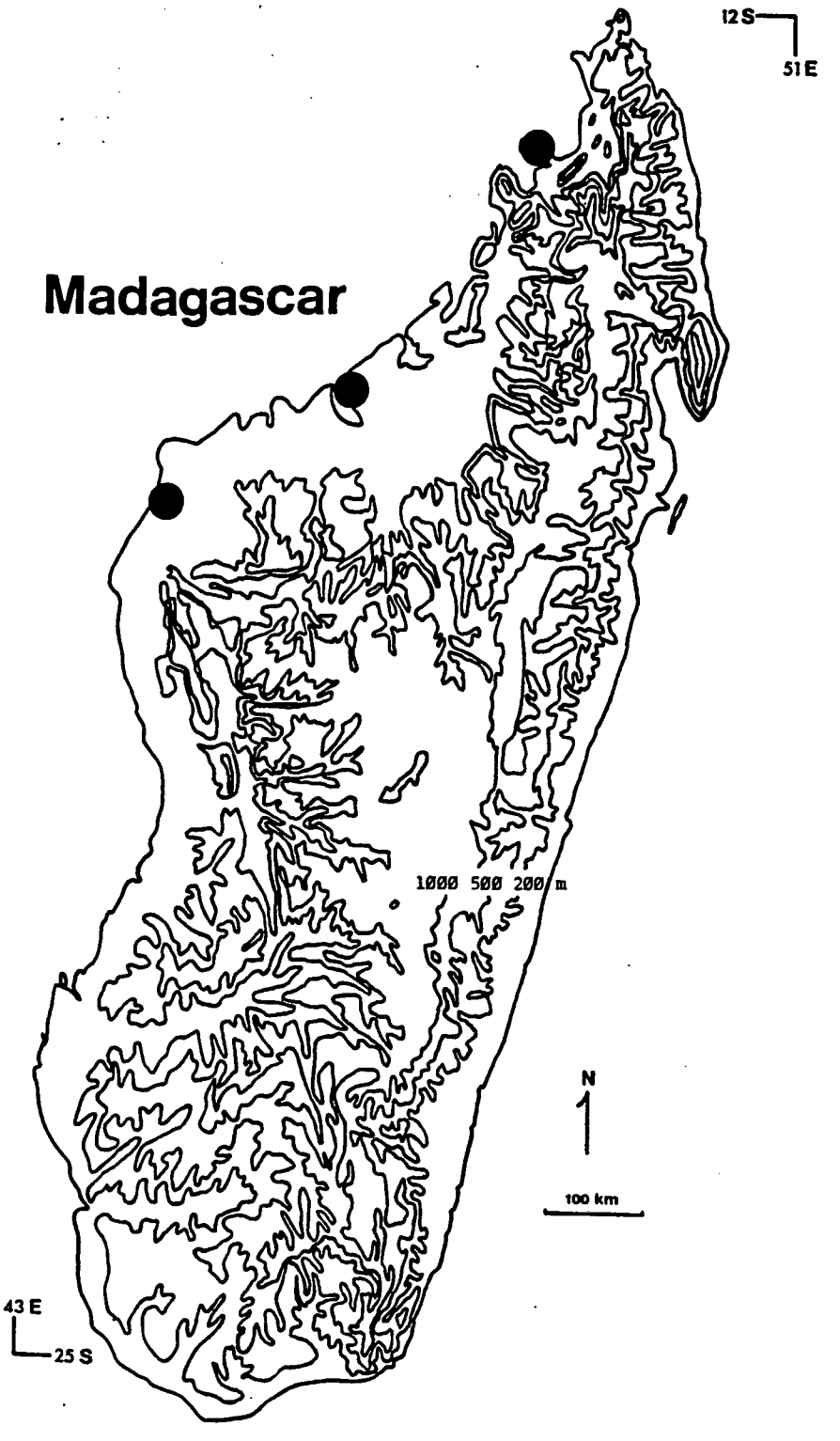

Figure 1.2: Topography of Madagascar and location of rainfall stations used in this study.

● = station location.

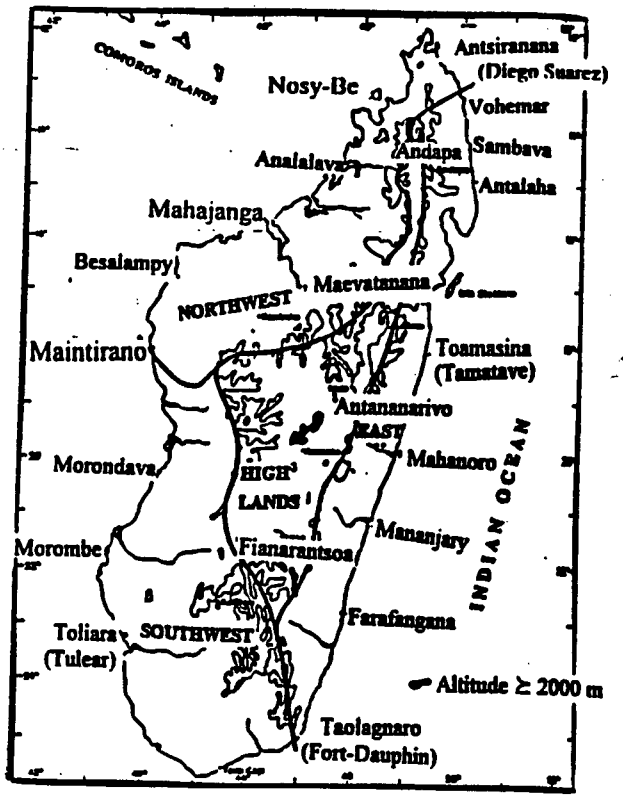

Figure 1.3.a: The climatic region of Madagascar.

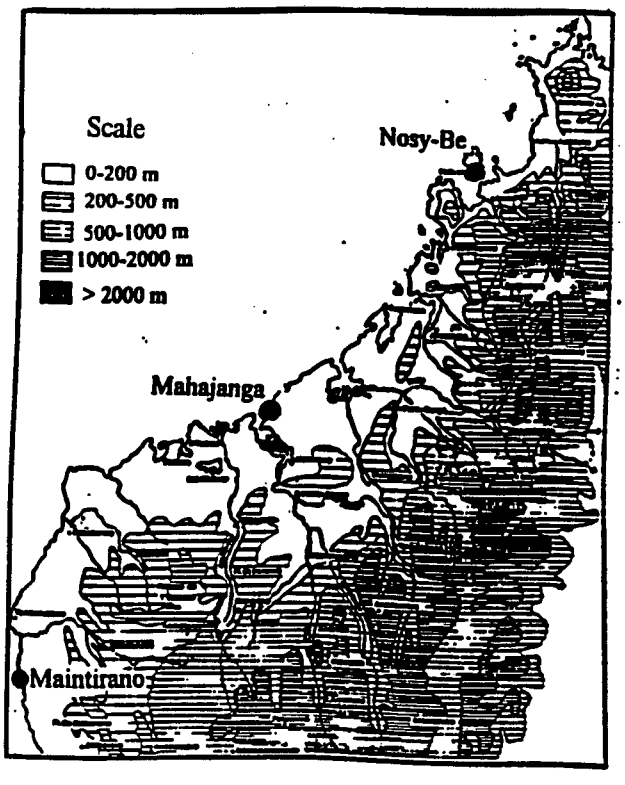

Figure 1.3.b: The Northwest region with elevations.

1.1.1 The climatic regions :

The location and topography of Madagascar play an important role in its climate. During the southern hemisphere winter, the weather is mainly influenced by trade winds and subtropical high pressure cells to the south of the island, moving continuously from the west to east. During summer (November to April), it is influenced firstly by monsoon winds and eventually tropical cyclones forming in the area. Many attempts have been made to define and classify the climate of its various regions, most notably by Donque (1975) and Williams (1990) who determined four climatic regions, namely:

a) The East (Fig 1.3.a): wet throughout the year, where the weather is determined by the strength of the trade wind.

b) The Highlands: cool with one rainy season and one dry season, where the weather is determined by the dynamic interaction of trade winds, monsoon flow and the subtropical anticyclones.

c) The Southwest: leeward dry zone with little rainfall even during the summer season, where the weather is determined by the characteristics and the frequency of southerly fronts, and the strength of the trade wind.

d) The Northwest: warm with summer rainy season and dry winter season, where the weather is determined by the strength of the monsoon.

1.1.2 Main rain-producing systems in summer :

The major rain-bearing systems over Madagascar are the Inter Tropical Convergence Zone (ITCZ), monsoons and tropical cyclones (Donque, 1975; Jury and Pathack, 1991). It is noteworthy to indicate that in the SWIO, a TC is defined where the 10 min mean wind speed is more than 32 $m s^{-1}$ and the minimum pressure is less than 997 hPa.

1.1.2.1 The ITCZ and monsoon vortex :

The summer rainfall over Madagascar is mainly of convective origin, during which the ITCZ moves southwards from the equator to be located between 10 and 15°S (Donque, 1975; Le Borne, 1987; and Jury and Pathack, 1991). The ITCZ reaches its southern-most position about 20°S in the Mozambique Channel (40 - 45°E) and is located at 10°S to the east of Madagascar in January and February. This southward penetration is associated with northwesterly monsoon winds flowing off the east coast of Africa toward Madagascar. Heavy rainfall is often experienced in the afternoon following the seasonal onset of the monsoon, and varies considerably from day to day. Often a " V " shaped cloud vortex is present at 15°S, 45°E.

1.1.2.2 The tropical cyclone :

The second rain-producing weather systems in Madagascar are tropical cyclones which initiate either in the Mozambique Channel or to the northeast of Madagascar. TCs are rotary storms, which form over ocean waters with temperatures greater than 27°C in tropical regions. Their outer circulation can extend more than 1000 km from the storm center. It is one of the most life

threatening and destructive natural phenomenon due to its strong winds, torrential rainfall and storm surge (Montgomery and Farrell, 1993).

In the Mozambique Channel, the area of cyclogenesis is confined mainly between 13 and 20°S. East of 50°E, it is generally equatorward of 15°S (Le Borne, 1987; Ecormier, 1992; and Jury, 1993). The occurrence of TC in the Mozambique Channel is not regular each year. The least active seasons for TC-genesis in the Mozambique Channel were 1982, 1987 and 1988 with no formation, while the most active were 1971, 1975 and 1986 with three formations each. Observation of TC in the area have improved since the use of satellite imagery in 1968. During the seasons 1968 to 1992, 36 TC have formed within the Channel (Ecormier, 1992), 21 had eastward trajectories and 27 formed in January or February. The characteristics of TC genesis in the Channel are its rapid development, small size, short life span (Le Borne, 1987).

1.2 Motivation and hypothesis :

1.2.1 Motivation :

This thesis will concentrate on the northwest region of Madagascar. This is the area most affected by monsoon flow and tropical cyclogenesis. Motivation for this work can be found in locally destructive impacts. In 1987/1988, four TC moving westward from the Indian Ocean influenced the weather of the area; a gust of 61 m s^{-1} was recorded at Besalampy on 27 January, due to TC Doaza. In 1988/1989, two TC passed through the area, 329 mm of rain was recorded at Juan de Nova on 12 January and a gust of 51 m s^{-1} was recorded at Maintirano on 14 January. In 1989/1990, one TC crossed the area with gusty winds on Nosy-Lava,

the precipitation associated with TC Hanta was less important. In 1990/1991, two TC passed the area, 604 mm of rain with peak gust of 51 m s^{-1} was recorded at Maintirano on 16 and 17 February. In 1991/1992, two TC passed over the area, the wind associated with these storms were weak but they brought heavy rain; 347 mm was recorded at Mahajanga on 3 January due to TC Bryna and 92 mm on 24 February due to TC Elisabetha.

From the events mentioned, it can be seen that heavy rain and strong wind from TC are significant. The amount of daily rainfall for each season is highly variable. In general, the diagram of daily rainfall for each season (Fig 1.4) shows 2 to 3 peaks of maxima above 70 mm. From 1960 to 1992, 30 events of heavy (>70 mm) daily rainfall data were observed in the NW area, 15 caused by the passage of TC near the observing stations. The highest daily rainfall on record is 462 mm recorded at Besalampy on 7 February 1977 due to TC Emilie.

The region is inhabited by two million people and there are many rivers in the area. Like other developing countries, most of the population (80%) live in rural areas and depend on subsistence agriculture. The passage of a TC or occurrence of floods often destroy in a few hours the timeless effort of the peasants' crop production of rice, cotton and sugarcane. The peasants are left hopeless, due to the destruction of houses, roads, plantations and loss of human life. Such situations happen almost every year. It is a serious problem for the government because when floods or destructive TC-winds occur, the area must rely on relief from outside the country. Instead of exporting goods to other regions, the NW area must be supplied and economic progress is slowed.

The main threat to the region comes from the Mozambique Channel where storms develop so rapidly that only 24 hours after formation, a TC may hit the NW coast of Madagascar with such intensity that the damage over the region is considerable. In the northwestern region of Madagascar for example, when TC

Cynthia crossed the area from the Mozambique Channel, thousands of houses were destroyed, 87,654 were left homeless, and 65 dead or missing people were reported to the national meteorological service. It is noteworthy to mention that TC Cynthia had a lifespan only three days (16 to 19 February 1991).

Many rivers exist in the Mahajanga watershed, but there is no dam to control the eventual rise of their level. The risk of flooding is omnipresent. Although the problem is important, only a few attempts have been made to study the meteorology of the Mozambique Channel. Most of these studies deal with the SWIO, focusing on the area east of Madagascar. Therefore, it is essential to understand the mechanisms responsible for the rapid formation, intensity and trajectory of TC in the Mozambique Channel, as well as the monsoon vortex causing torrential rain in the area. This will enable the national weather office to better forecast the event for disaster prevention and to improve chances of economic development of the region.

1.2.2 Hypotheses to be tested :

1.2.3.1 Cyclogenesis is triggered by:

a) the pre-existence of an initial convective disturbance;
b) well organized monsoon and trade wind flow with cyclonic vorticity in the low to middle troposphere and upper air divergence;
c) weak vertical easterly wind shear;
d) an upper trough and post frontal high pressure cell over the southern Mozambique Channel;
e) warm sea surface temperatures (> 28°C) and high EPT values (> 350°K) below 850 hPa.

1.2.3.2 TC intensification occurs when:

a) the monsoon westerlies strengthen;

b) the low-level cyclonic circulation builds up;

c) the upper-level outflow increases during the early stages of development;

d) the storm moves southeastward.

1.2.3.3. TC structural characteristics include:

a) a warm moist mid-troposphere;

b) maximum wind speed and convection area in the NE sector;

c) monsoon vortex and deep convection near Mahajanga due to the convergence of westerlies and easterlies over the steep topography of the area.

The hypothesis will be investigated using composite ECMWF weather data for the period four days before to two days after a severe event, selected from six consecutive summers from 1987 to 1992 inclusive.

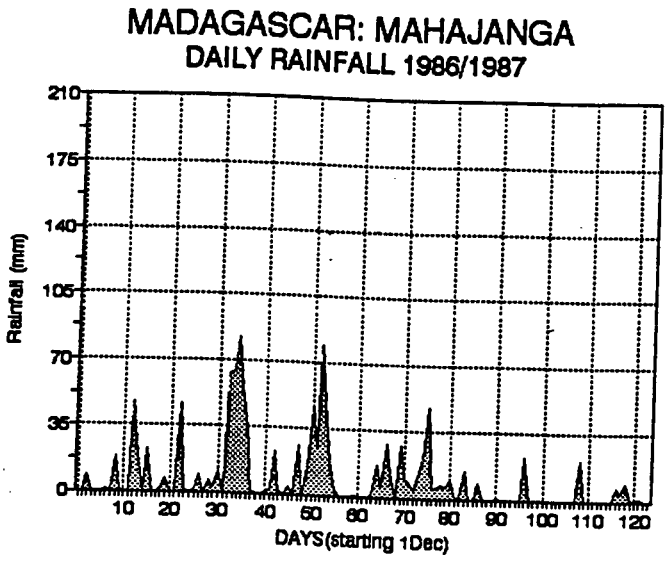

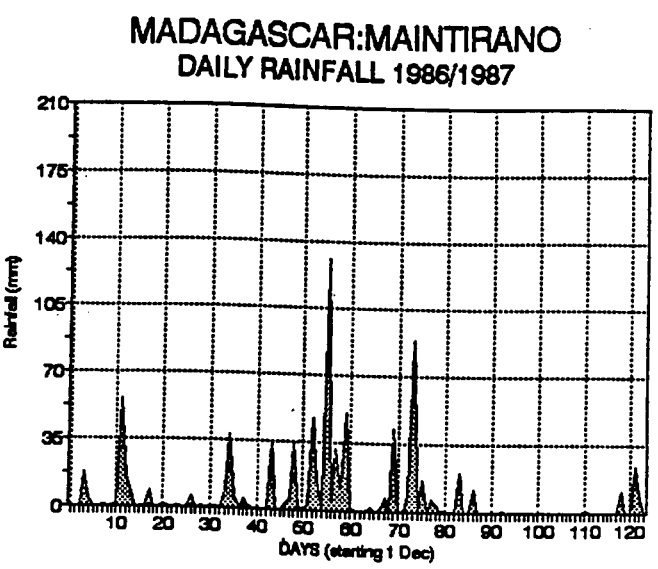

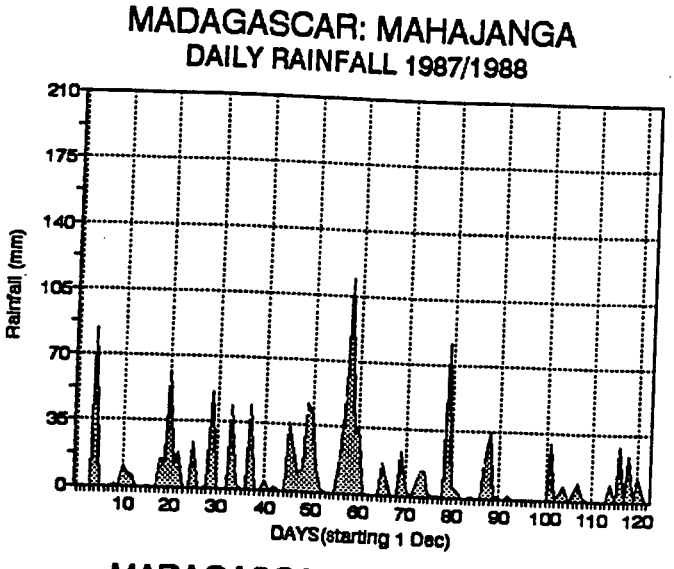

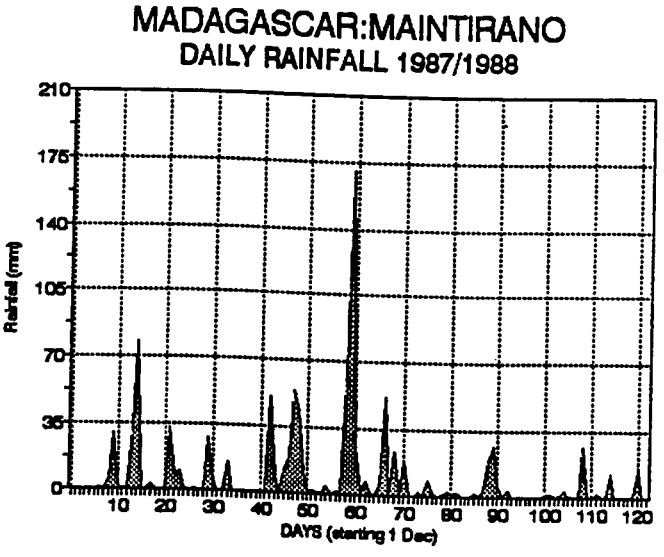

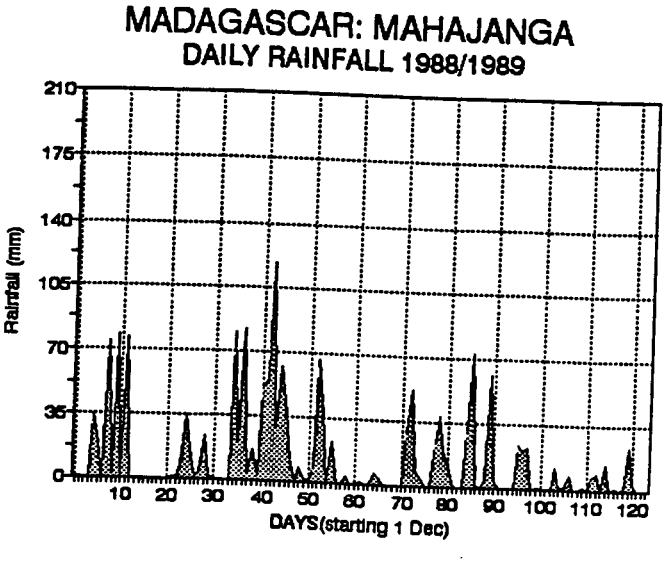

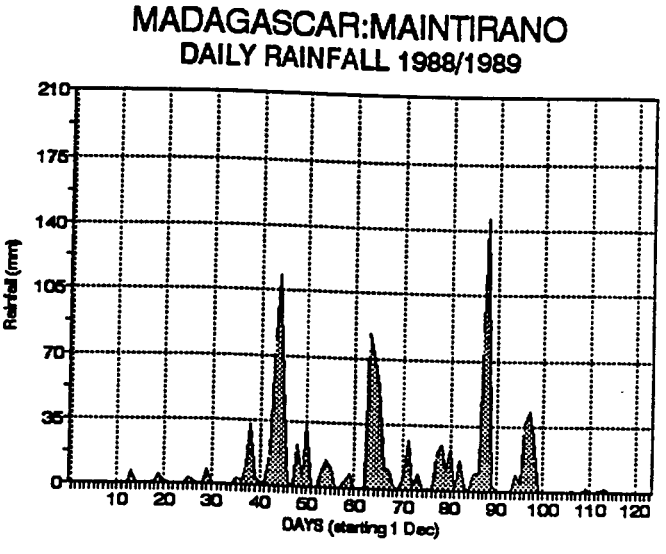

Figure 1.4.a: Daily rainfall (December-March) at Mahanjanga.

Figure 1.4.b: Daily rainfall (December-March) at Maintirano.

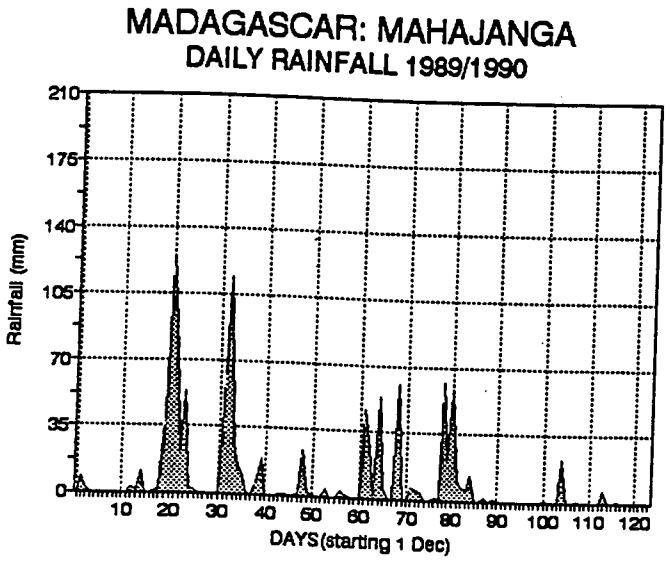

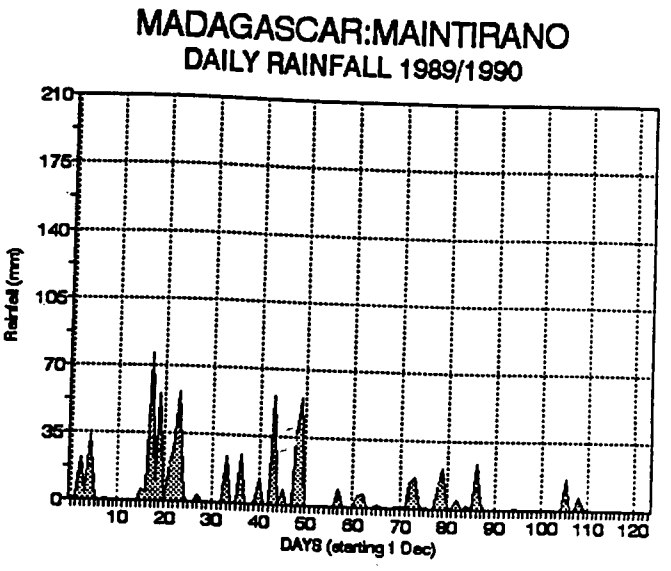

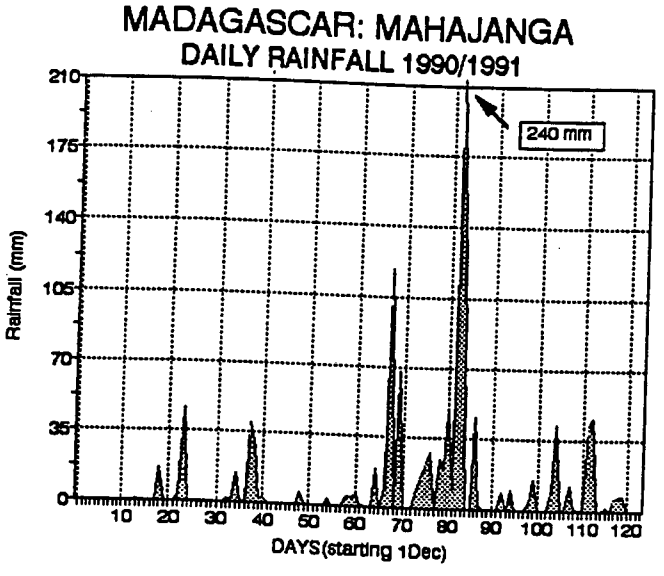

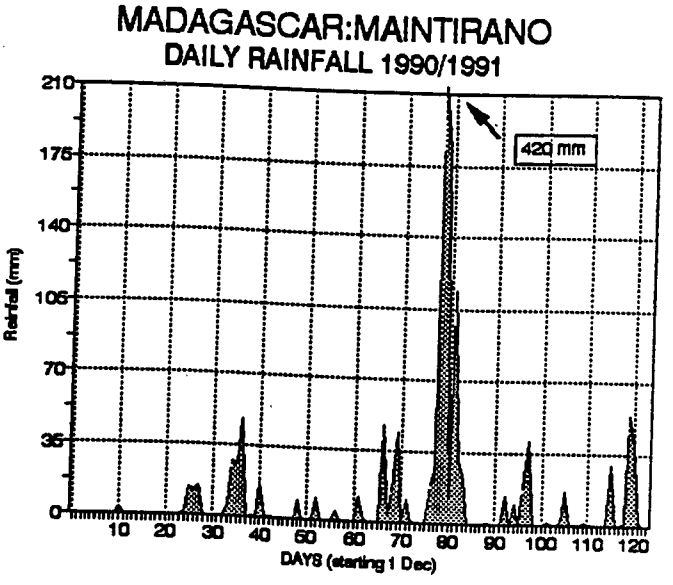

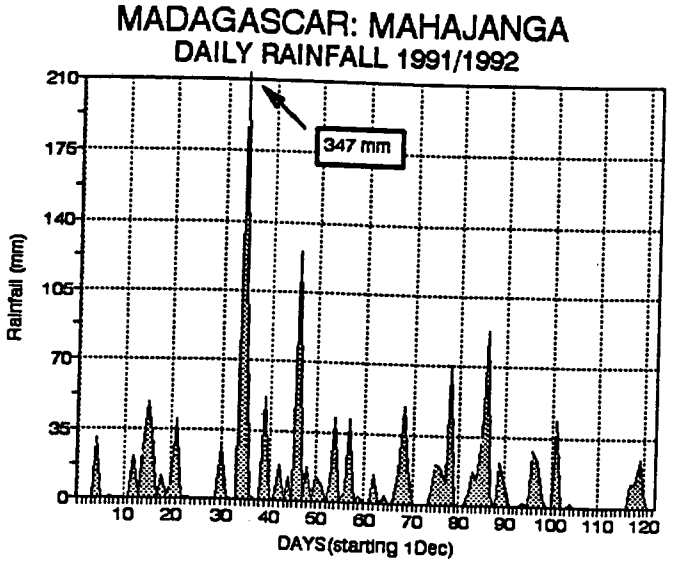

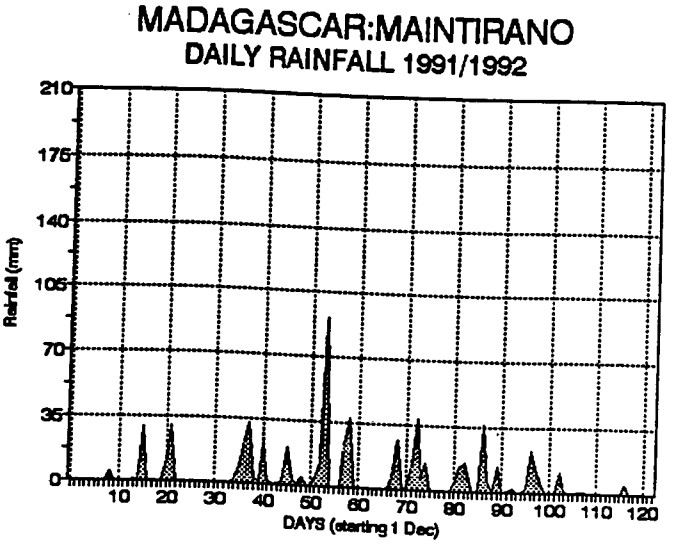

Figure 1.4.a (continued)

Figure 1.4.b (continued)

CHAPTER 2

LITERATURE REVIEW

2.1 Climatology of the Intertropical Convergence Zone (ITCZ) and its seasonal changes :

The ITCZ is a prominent feature of the earth's tropical atmosphere. In satellite imagery, the ITCZ appears as discontinuous zonal cloud bands of 2-5 degrees of latitude in width. The ITCZ forms the ascending branch of the large-scale meridional Hadley circulation through which the mid-latitudes are linked to the tropics. Sea surface temperature (SST) gradients often determine the position of the ITCZ by enhancing boundary-layer convergence over the warmest axis via hydrostatically induced pressure gradients (Schneider and Lindzen, 1977; Lindzen and Nigam, 1987; Tiedtke et al., 1988). Interhemispheric asymmetries may also affect the position of the ITCZ. There are tropical regions, where SST gradients are weak, such as in the Indian and western Pacific Oceans. There SST gradients may not affect the location of the ITCZ but rather the convective and boundary-layer processes surrounding it (Hess et al., 1993). During the November-March season, the ITCZ moves from the Northern to Southern Hemisphere and reaches its southern-most position in February (Donque, 1975; Le Borne, 1987; and Jury and Pathack, 1991). This southward movement is associated with shifting of the rainfall area (> 200 mm per month) south of the equator.

In the SWIO, the shape and intensity of the ITCZ is modulated by the strength of the NW monsoon off the coast of east Africa and by standing and transient vortices. The intensity of the ITCZ is discontinuous, the convection is indicated to beat a maximum over Africa between 20 to 35°E with OLR values < 220 W m^{-2}, while over the Mozambique Channel the OLR is higher, but rainfall is at its maximum intensity. The interaction of easterly trade winds and the topography of Madagascar, the cross equatorial penetration of monsoon winds off east Africa, and the SW-NE trend of SST > 28°C contribute to the differing latitudinal position and character of the ITCZ. Following the seasonal transition in the monsoon circulation, the ITCZ develops near the equator to the east of 60°E in October, gradually shifts southwest-ward toward Madagascar, wherein an interaction occurs between the NW monsoon and topographically deflected easterly flow. The ITCZ reaches its most intense development in February, and shifts rapidly northward in the March-April monsoon transition. It is found that the interannual variability of the ITCZ is linked to changes in the regional low level circulation and SST field, and a break in the ITCZ along 50-55°E is often associated with the penetration of subsident easterly winds off the northern end of Madagascar (Jury et al., 1994).

2.2 Monsoon flow :

2.2.1 Monsoon onset and its characteristics :

Many studies have been made around the monsoon, mainly in the Indian and Australian region. The Southern Hemisphere (SH) summer monsoon is recognized to have an impact on the global circulation. Troup (1961) and more recently Hendon and Liebmann (1990) found the existence of many similarities between Asian and Australian monsoon features.

In the Australian region, circulation changes that accompany the onset have been studied by Hendon and Liebmann (1990) using composites. They found that the onset is accompanied by the expansion of the upper tropospheric easterlies about the equator, and shifting of the subtropical jet poleward at onset coinciding with the first occurrence of a convectively active 40-50 day Madden-Julian oscillation. The mean onset date for the Australian summer monsoon is 25 December and the duration of the "wet-westerly" event is about 15-20 days.

In the Indian region, the onset of Indian boreal summer monsoon is associated with persistent heavy cloudiness over the southeast Arabian Sea, the establishment of a low-level westerly jet off the coast of Africa and over the Arabian sea, called the Somali Jet, and an upper tropospheric easterly jet over the Indian peninsula and adjoining seas, known as the Tropical Easterly Jet. These jets are associated with a strong low-level cross-equatorial flow from the Southern Hemisphere and an upper tropospheric divergent flow (Slingo et al., 1988; Soman and Kumar, 1993). Over Kerala, it has been shown that there is a clear demarcation between pre-monsoon rainfall and rainfall that heralds the onset of the monsoon. The wet spell has a mean duration of 15 days (Ananthakrishnan and Soman, 1988).

The monsoon onset is governed by the seasonal cycle in the summer hemisphere. Interaction between tropical convection, El Niño Southern Oscillation phenomenon (ENSO), 30-60 day oscillation, and mid-latitude synoptic disturbances contribute to the onset (Hendon et al., 1989 and Chen et al., 1992). Soman and Kumar (1993) studied the structure of the monsoon onset, and found a change in the direction of the temperature gradient in the middle and upper troposphere. The gradient turns strongly positive 15 days after the onset, by which time the lower-level westerlies and upper-level easterlies have developed owing to a thermal wind response. A stationary east-west trough line appears

about 10 days before the onset at the tip of the Indian peninsula from 700 to 400 hPa, and then moves rapidly northward after the onset.

Magana and Yanai (1991) showed a periodicity of 30 to 60 days on the intensification of convective activity during the Indian boreal summer monsoon. Fluctuation in the intensity of the subtropical circulations are reflected in the alternating time evolution of easterlies and westerlies at 200 hPa. Significant relationships have been demonstrated between the onset dates, the outgoing longwave radiation (OLR) and the southern oscillation index (SOI) (Murakami et al., 1986; Holland, 1986).

Laing and Fritsch (1993) found that the seasonal progression of mesoscale convective complexes (MCC) from ocean to land are similar to the progression of the monsoon moisture flux. The monsoon also appears to influence the monthly distribution of MCC which often develop into tropical depressions after moving from land to locations over the ocean. Chen et al. (1992) stated that the quasi-periodic behavior of the summer monsoon life cycle is a most unique phenomenon. The time evolution of the Indian monsoon is related to the location of northward migrating monsoon troughs and ridges.

Little attention has been paid to the SWIO region until recently. Jury and Pathack (1991) studied the structure and variability of the summer climate and tropical synoptic scale weather systems transiting the SWIO. They found that during January and February, easterly flow and shear in the layer above the trade winds 700-300 hPa are persistent and most conducive to barotropic instabilities. In the warm oceans north of 15°S where SST > 28°C, the winds are westerly. Southeasterly trades are found to the south. Near Madagascar the northwest monsoon and a topographically induced lee trough shift the convective maximum to the 15-20°S latitude band. The lower tropospheric moist layer

deepens and becomes more unstable to the west of 50°E during the summer season. The weather systems drift with the 500-700 hPa layer winds according to their findings.

Jury et al. (1991) found westward moving waves in the 10-20°S latitude band during some years and in the 20-30°S latitude band during other years. They found that wet summers over southern Africa correspond to more westward moving convective systems in the SWIO. The lifespan of the convective disturbances range between 10 to 20 days.

Garanganga (1989) studied the onset of 1982/83 austral summer monsoon over southern Africa and found some similarities and differences in its behaviour compared to Australia. Australia typically lags by 6-8 weeks the onset over southern Africa, where the convection is dominated by an easterly wind regime. Over Australia westerly flow dominates the low-level circulation during convectively active phases.

Over southern Africa, the high phase of the Southern Oscillation (SO) is associated with increased rainfall and the low phase with decreased rainfall. The major rain-producing system over South Africa are the cloud bands connecting tropical systems over central Africa with mid-latitude depressions to the south of the subcontinent. The displacement of cloud bands between southern Africa and Madagascar occurs between high and low phases of the SO in association with the reversals in the direction of the anomalous zonal Walker circulation over the Indian Ocean (Lindesay et al., 1986; Lindesay, 1988). This statement agrees with Jury (1992) who found the existence of a dipole between Botswana and Mauritius, where the low phase of the SO associated with the east phase of the Quasi-biennial Oscillation (QBO) implies lower tropospheric convergence over Madagascar.

2.2.2 Monsoon and its relationship to the El Niño/Southern Oscillation (ENSO) phenomenon :

Bjerknes (1969) was among the first to describe the ENSO as a coupled phenomenon. This phenomenon has held much attention because of its impact on the regional and global climate (Rasmusson and Carpenter 1982). Kiladis and van Loon (1988) showed that in the year before a warm event a strong South Pacific High is associated with below normal surface pressure over northern Australia and the central Indian Ocean; and during the cold event, the opposite happens. The Southern Oscillation Index (SOI) is observed to vary coherently on interannual time scales. A negative anomaly in the SOI corresponds to a weak pressure gradient across the Pacific, resulting in a weak trade winds. A positive anomaly on the other hand leads to stronger easterly winds, and equatorial and west coast upwelling. The ENSO is described as an oscillation between a warm and cold phase referred to as El Niño and La Niña respectively. The existence of a cycle enables ENSO predictions to be made up to lead times of about one year implying the possibility of long range climate predictions in the tropics (Latif et al., 1993).

Chao and Philander (1993) stated that the SO signal transfers warm surface water zonally across the tropical Pacific. The anomalies of the meridional component of the surface wind are southerly during La Niña and northerly during El Niño, and correspond to a northward (during La Niña) or southward (during El Niño) displacement of the ITCZ. Cadet (1985) and Jury et al (1994) have identified that central Indian Ocean SST are closely related to the ENSO cycle.

Tyson (1986) related that as the Walker circulation increases, the upper-level poleward flow in the Hadley cell increases and the subtropical jet over Marion Island strengthens during the high phase of the SO (La Niña). During the low phase of the SO,

the ascending branch of the Walker circulation lies over the longitude of Madagascar. Ropelewski et al. (1992) showed that tropospheric biennial variability is an integral part of the SO, and the Indian Ocean may play an important role in the evolution of the SO. Shukla and Paolino (1983) associated the Darwin pressure anomaly and the monsoon rainfall over India, and demonstrated that the phase of the SO could be used as a predictor of monsoon rainfall.

Streten (1980) analysed some prominent features of the Indian Ocean and found that the SWIO subtropical High exhibits a clear bi-annual cycle of movement migrating some 17° westward in winter from its spring and summer position. It is most stable in location in summer. Over the tropical SWIO the atmosphere is barotropic and the sea level pressure is indicative of much of the lower troposphere (Padya, 1989).

2.3 Tropical cyclones :

2.3.1 TC formation :

Some factors are believed to be important for TC formation, these are SST, a pre-existing cyclonic disturbance, a favourable thermodynamic profile to support deep convection, weak vertical easterly wind shear and an environmental pattern favorable for anticyclonic outflow in the upper troposphere (Donque, 1975; Riehl, 1979; Anthes, 1982; Le Borne, 1987; Zehnder, 1991; Montgomery and Farrell, 1993; and Jury, 1993).

Davidson and Hendon (1989) showed a progressive vorticity increase on the eastward side of monsoon troughs. The process resulted in many TC formations over northern Australia and the South Pacific. McBride and Keenan (1982) noted the existence of upper troughs during cyclogenesis events which they suggested would provide favourable genesis conditions.

Jury and Pathack (1991) identified a ENE-WSW trend of TC genesis points across the SWIO region, paralleling a similar trend in SSTs and the ITCZ (OLR or outgoing longwave radiation minimum). A subtropical trough over the Mozambique Channel often triggers rainfall over Madagascar. They found also that increased SSTs to the northeast of Madagascar in the preceding spring and a QBO east phase creates conditions for more frequent cyclogenesis and increased rainfall over the island. They stated that transient convective waves in the SWIO are often implicated as precursors to TC and in rainfall events over SE Africa and Madagascar.

Davidson and Kumar (1990) suggested that the convective enhancement over the genesis area is triggered by increased outflows induced by the encroaching tropical upper tropospheric troughs (TUTT). Lyons (1991) demonstrated the interaction of eastward propagating midlatitude troughs, and monsoon troughs moving southward across east Africa. The merged troughs are associated with a prominent band of low OLR (deep convection).

2.3.2 TC structures, development, and forecasting indices :

Davidson et al. (1990) supported the finding of Gray (1979) and McBride and Zher (1981), and indicate that large-scale low level cyclonic vorticity, weak vertical wind shear over the system center, and large horizontal gradients of wind across the system are

precursor conditions for genesis. An increase in the low-level convergence and sustained inner core deep convection marked the intensification phase. The maintenance of the core convection depended critically on surface evaporation. Shi et al. (1990) showed that the superposition of an upper tropospheric ridge over a TC is a favorable condition for the intensification of a mature TC. Molinary and Valaro (1990) speculated that the approach of a mid-tropospheric trough often precedes deepening of the TC.

Padya (1989) and Jury and Pathack (1991) found that the SWIO experiences regular organized convective activity leading to an average of 11 disturbances reaching tropical depression intensity each summer. Jury et al. (1993a) found that in the Indian Ocean, the factors contributing to intense TC are the existence lower level cyclonic and convergent circulation anomalies, high water vapour fluxes in the equatorial westerlies, a deep layer of moisture along a NW-SE axis over Madagascar, and upper-level easterly anomalies (associated with QBO).

Jury (1993) showed that during a summer with high TC frequency, the following climatological features are noticeable: a Walker Cell anomaly involving upper level easterlies and lower level westerlies over the equatorial monsoon area, increased subtropical trade winds and a strengthened southern Hadley circulation, and poleward shift and reduction of westerlies in the mid-latitudes.

Douglas (1992a and b) showed the existence of maximum divergence is at 200 hPa level and the largest value of the vertical wind at 500 hPa level. He also stated that the vorticity increase associated with the onset of the monsoon vortex over India was more pronounced in the mid-troposphere than at lower levels. He observed that the location of the rain areas of northern hemisphere depressions is in the southwest of the circulation center.

In their work Montgomery and Farrell (1993) found that near the tropopause there is a region of very low (negative) potential vorticity, and strong anticyclonic flow in the ascent region. The formative time scale for tropical cyclones in association with upper-level forcing is sensitive to the vertical distribution of the moist static stability parameter. Migratory upper-level troughs can initiate and strongly influence tropical cyclone formation, even in cases with weak upper-level shear and no surface temperature gradients. Observations also suggest that a warm core forms at upper levels well before the mature stage, and the juxtaposition between a transient upper level trough and easterly moving low-level tropospheric disturbance is associated with spin up. (Yanai 1968; Riehl 1979, Bosart and Bartlo 1991).

The strengthening of monsoon westerlies over a large longitudinal span and a sub-tropical and easterly flow south of the development area is associated with TC development in the Australian region (Davidson and Holland, 1987; and Davidson et al., 1990). Consequently, in the lower troposphere, there is increasing large-scale cyclonic vorticity in the monsoon trough and suppression of poleward outflow from the tropics. In the upper level, an anticyclone strengthens over western-central Australia two days before the genesis of TC, and a TUTT shear zone develops and moves equatorward along the eastern Australian coast.

The above literature review has demonstrated a gap in our detailed understand of TC evolution and monsoon interaction in the SWIO. In the following sections of this thesis the above concepts are tested using observational data and conceptual models are developed which indicate that TC in the Mozambique Channel are somewhat unique.

CHAPTER 3

DATA AND METHODOLOGY

3.1. Data and methodology :

3.1.1 Rainfall Data :

Daily rainfall data in the northwest coastal region of Madagascar were obtained at various stations for the months December to March in the period 1960-1992 . After quality checking the data for missing records, three stations were left: Nosy Be, Mahajanga, and Maintirano (Fig 1.3). As illustrated previously in Figure 1.4, the rainfall varies considerably from day to day. Extreme events were selected on the basis of a rainfall criteria: >70 mm/day. In this study the criteria was exceeded on 16 occasions in the period 1987 to 1992 as outlined in Table 3.1 below:

Table 3.1: Period of events where the rainfall exceeded 70 mm.

Case 1 : 03 January 1987	**Case 9 :** 12 January 1989
Case 2 : 24 January 1987	**Case 10 :** 01 February 1989
Case 3 : 11 February 1987	**Case 11 :** 25 February 1989
Case 4 : 14 December 1987	**Case 12 :** 20 December 1989
Case 5 : 28 January 1988	**Case 13 :** 05 February 1990
Case 6 : 17 February 1988	**Case 14 :** 15 January 1992
Case 7 : 09 December 1988	**Case 15 :** 16 February 1992
Case 8 : 05 January 1989	**Case 16 :** 24 February 1992

3.1.2 Composite Procedure :

Composites were formed by averaging data for wet cases shown in Table 3.1. The procedure consists first of adding each parameter (for instance geopotential height) value at the same level, at every 2.5° grid-point in the domain used for the 16 cases, then dividing the sum by 16 to get the mean value at each grid-point. The advantage of this method is to reduce the total number of maps and figures associated with each case study.

The composite analysis technique has been used extensively in the field of climatology (Tyson 1981; Lindesay 1988 and Walker 1989) and meteorology (Ferranti et al., 1990 and Lyons 1991). This technique is useful in showing inter-annual structure, and in transient intra-seasonal weather systems. The primary benefit of compositing is that common features inherent in particular events may be easily recognized. Here, a time frame is adopted for compositing: the day of heaviest rainfall (>70mm) is Day 0; Day-4 is four days prior to the event; day-2, two days prior; and day+2, two days after the event.

In addition to the 16-case composite, two individual cases have been analysed because of their intensity. The first case was on 17 February 1991 which brought 420 mm rainfall at Maintirano, and the second one on 3 January 1992 with 347 mm rainfall at Mahajanga. In these extreme cases, the analysis was carried out in the same way as the composite; except that the structure six days prior to the extreme event is examined, in addition to the -4, -2, 0 and +2 day details. These TC tracks are shown in appendix B.

In the 16-case composite, the data are analysed in terms of the anomaly. This is done by computing the mean fields for all the parameters used in the analysis from 1 January to 28 February from 1987 to 1992, and subtracting from the mean composite value at each grid-point. In the case of extreme TC events, the actual value is maintained for operational purposes.

3.1.3. Seasonal and inter-annual rainfall analysis :

In addition to the analysis of daily rainfall and extreme events, the seasonal distribution of NW Madagascar rainfall and its inter-annual variability were analyzed. To filter the daily variability pentads (5 day means) were used. The season is comprised of 24 pentads starting from pentad 1: 2-6 December, to pentad 24: 27-31 March. This period December to March is chosen since it encloses the period of monsoon rains and TC formation in the region. For the study of drought, daily rainfall data from 1960 to 1992 were converted to pentad averages and normalized using the statistical formula:

$$z = (xi - x) / \sigma \qquad \text{Eq 3.1}$$

where:

z = normalized departure

xi = individual data point

x = historical mean

σ = historical standard deviation

The following criteria were used for defining dry pentads :

departure < -1

and composites were similarly formed using pentad field data. This approach is not used for wet pentad analysis as the composite is similar to Day 0, so only the dry composite is presented. Also the short lifespan of Mozambique Channel TCs does not lend itself to pentad sequential analysis.

Inter-annual variability of summer rainfall departures was analysed for the 1960-1992 period using spectral analysis of area-averaged rainfall. Cross correlation coefficients were evaluated between the various station data (Table 3.2) and the area mean.

Table 3.2: Croos corelation between stations and the area mean.

	Area mean	Mah mean	Mai mean	Nos mean
Area mean	1.00	0.88	0.87	0.92
Mah mean	0.88	1.00	0.60	0.70
Mai mean	0.87	0.60	1.00	0.76
Nos mean	0.92	0.70	0.76	1.00

Where:

Area mean = seasonal rainfall for the period 1960-1992 in NW Madagascar

Mah = Mahajanga, Mai = Maintirano, Nos = Nosy-Be.

Degrees of freedom is 30, so all values are statistically significant at the 99 % confidence limit. So the formulation of the three stations index is justified.

3.1.4 Global indices and statistical tests :

The Southern Oscillation Index (SOI = Tahiti - Darwin pressure anomaly) and the Quasi-biennial Oscillation (QBO = Singapore 30 hPa zonal wind departure) were obtained from the Climate Analysis Centre (CAC) bulletins. These are used to test for global inter-annual influences at the regional scale through correlation analyses.

3.1.5 European Centre for Medium Range Weather Forecasts (ECMWF) field data:

The observational stations in the region are very sparse and mainly land stations, since the main composante of the area is the Ocean, the data set from these stations are not sufficient for a correct analysis. Due to this fact the ECMWF data set are used to assist in forecasting. In practice the numerical prediction from the european product are

reliable up to 48 hours, hence the product is considered reliable for operational forecasting.

The ECMWF data were obtained from the European Centre for Medium range Weather Forecasts and World Climate Research Program (WCRP) Level III-A Global Atmospheric Data Archive in Reading, United Kingdom. Data from 1987 to 1992 were used for the weather data processing in the area enclosed by 15-75°E, 0-40°S except for the velocity potential and the streamfunction of the water vapour flux where the area of study is reduced by 5° at each side. The data are at a resolution of 2.5° x 2.5° (Fig 3.1), and are available for the 1000, 850, 700, 500, 300, 200, 100 hPa levels.

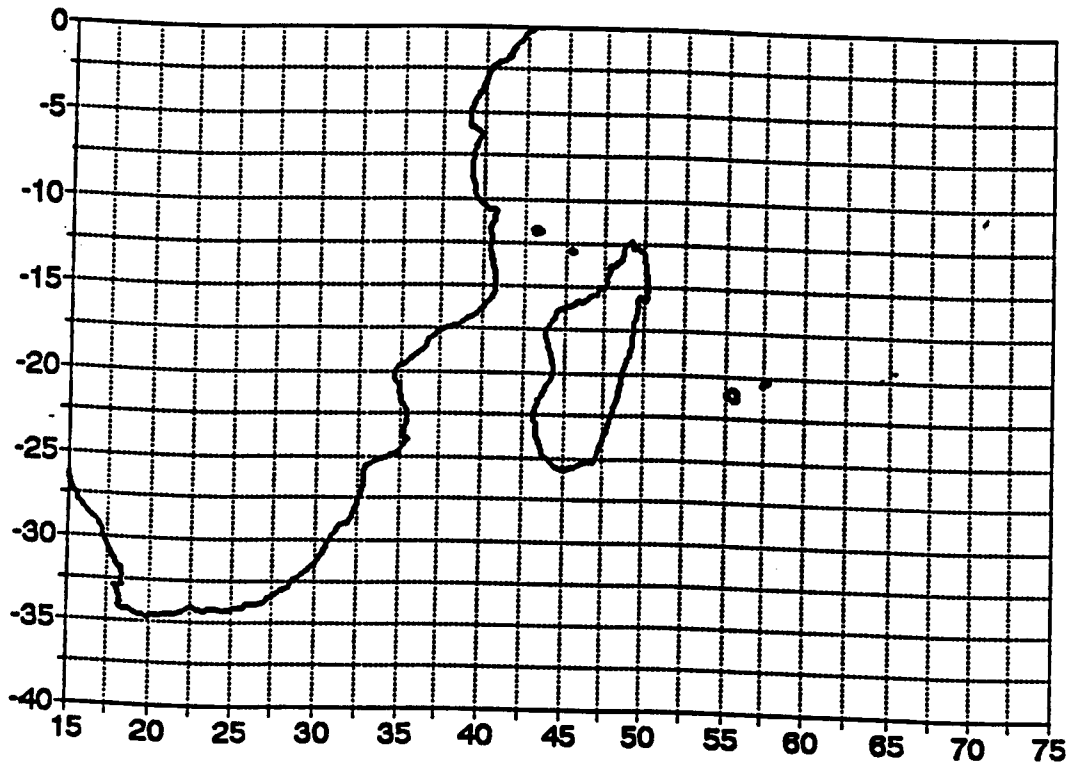

Figure 3.1 : Regional domain used in this study has northern boundary at the equator, western boundary at 15°E, southern boundary at 40°S and eastern boundary at 75°E; with data at every 2.5° grid-point resolution.

The following are the basic ECMWF assimilated grid point variables:

- Geopotential height (gpm)
- Temperature (°C)
- Zonal wind (m s^{-1})
- Meridional wind (m s^{-1})
- Vertical motion (Pa s^{-1})
- Humidity (%)

In addition, the following derived parameters were computed:

- Horizontal wind velocity
- Divergence
- Vorticity
- Precipitable water
- Water vapour flux
- Divergent and non-divergent water vapour flux
- Specific humidity
- Equivalent potential temperature

Three atmospheric levels were analyzed: 1000, 500 and 200 hPa. These level were chosen because, in the operational field, the 1000 hPa level is close to the station level and is the level of destructive winds; vertical motion is maximum at 500 hPa and the divergence field is strongest at 200 hPa level. Additionally N-S and E-W vertical cross sections were analysed.

3.2 Dynamic computations :

The total two-dimensional horizontal wind vector can be written in terms of rotational and irrotational components by the Helmholtz' s Theorem (Asnani, 1993). That is :

$$V = V\psi + V\chi \qquad \text{Eq 3.2}$$

where $V\psi$ is the non-divergent or streamfunction (rotational) component and $V\chi$ is the divergent or velocity potential (irrotational) component of the total horizontal wind. In the tropics, the horizontal gradient of pressure is very weak; then in a large synoptic scale, the velocity potential (χ) and streamfunction (ψ) are very useful in analysing climatic forces. The vorticity and the divergence also can be expressed in these terms but highlight smaller scale features associated with convective weather systems.

3.2.1 Vorticity :

The vorticity is defined as the measure of fluid rotation, that is the relative spin about the local vertical. In the SH a negative (relative) vorticity is one in which there is a tendency for the air to rotate in a clockwise (cyclonic) sense. The components of the vorticity in the total two-dimensional field are as follows :

$$\begin{aligned} \text{Vorticity} = \zeta &= (\nabla x\, V) \\ &= \partial v / \partial x - \partial u / \partial y \\ &= \nabla^2 \psi \end{aligned} \qquad \text{Eq 3.3}$$

where ψ is the streamfunction

3.2.2 Divergence :

The divergence is defined as the acceleration experienced by the air in the local horizontal plane. A region of divergence on an isobaric surface is one from which there is a net out flow of air. The components of the divergence in the total two-dimensional field is as follows :

$$\text{Divergence} = \delta = (\nabla \bullet V)$$
$$= (\partial u / \partial x) + (\partial v / \partial y)$$
$$= \nabla^2 \chi \qquad \text{Eq 3.4}$$

where χ is the velocity potential

3.3 Thermodynamic and moisture computations :

The water vapour content of moist air can be expressed through a number of different variables, several of which are in common use in meteorology.

3.3.1 Precipitable Water :

Precipitable water (PW) is the amount of water vapour in the atmosphere and defined as the mass of water vapour in a vertical column of the atmosphere having unit cross-sectional area. It is usually expressed in millimeters. Theoretically, it is the depth of

water that would be obtained if all the water in a column of air were condensed onto a horizontal plane of unit area.

Mathematically, it is defined between two specified levels as:

$$PW = \frac{1}{g}\int_{p_1}^{p_2} x \delta p \qquad \text{Eq 3.5}$$

where :

x = mixing ratio between pressure set levels p_1 and p_2,

p_1 = 1000-850 hPa surface level

p_2 = 300 hPa surface level

g = 9.80665 m s^{-2} (gravitation constant)

PW is usually integrated between 850 to 300 hPa (Chen and Tzeng, 1989); in this study, it is integrated from the 1000 hPa level if the data grid point was below 1000 meters above sea level, and from the 850 hPa level if the data grid point is above 1000 meters. This was done to better represent moisture parameters over the SWIO.

3.3.2 Water Vapour Flux :

Water vapour flux (WVF transport) is defined as the advection of PW by the total horizontal wind. The total horizontal mean flux of water vapour Q is obtained through vertical integration :

$$Q = \frac{1}{g}\int_{p_1}^{p_2} qV \delta p \qquad \text{Eq 3.6}$$

where :

q = specific humidity (g kg^{-1})

g = gravitation constant (m s^{-2})

V = horizontal wind vector in the layer (m s^{-1})

p_1 = 1000-850 hPa surface level

p_2 = 500 hPa surface level

It is expressed in grams per kilogram meter per second (g kg^{-1} m s^{-1}).

The individual qu and qv components of the total two-dimensional horizontal wind are combined to give a water vapour flux vector (QV), which has both direction and magnitude.

Magnitude of the vector is calculated from :

$$\sqrt{(qu)^2 + (qv)^2} \qquad \text{Eq 3.7}$$

and direction from :

$$\arctan\left(\frac{qu}{qv}\right) \qquad \text{Eq 3.8}$$

The moisture in the atmosphere is concentrated mainly in the lower and mid-troposphere, the weighted vector average of WVF often reflects flow below 500 hPa. Therefore, the integration is from the surface, as with PW, to the 500 hPa level.

3.3.3 Divergent water vapour flux :

The water vapour flux divergence is the velocity potential of water vapour flux. The velocity potential function is solved once the water vapour flux components have been calculated using equation 3.6. Water vapour flux divergence is therefore a vertically integrated resultant meteorological variable and gives valuable insight into the spatial regional patterns of the divergent (non-rotational) nature of moisture in the integrated atmosphere. It is a more useful forecasting tool than velocity potential alone, since water vapour is included.

3.3.4 Non-divergent water vapour flux :

The non-divergent water vapour flux is the rotational component (streamfunction) of the total two-dimensional horizontal water vapour flux circulation. It is also a vertically integrated resultant meteorological variable and may be useful in analysing the spatial features of the rotational component of the water vapour flux vector. This variable is calculated once the water vapour flux components have been calculated using equation 3.6.

3.3.5 Specific Humidity :

Specific humidity is the weight of water vapour per unit weight of air expressed as grams of water vapour per kilogram of air (g kg^{-1}). Specific humidity is calculated as follows:

$$q = (0.622 \times e) / (p-[0.378 \times e]) \qquad \text{Eq 3.9}$$

where :

e = vapour pressure (see appendix)

p = set-level pressure (hPa)

3.2.6 Equivalent Potential Temperature :

The equivalent potential temperature (θ_e or EPT) is the potential temperature a parcel of air has when its mixing ratio has been reduced to zero and all the latent heat is converted into sensible heat (Betts 1974, Bolton 1980). The temperature and moisture content in the atmosphere can be combined into θ_e, usually represented as a vertical profile showing regions of suppressed or enhanced convection. It is expressed in degree Kelvin (°K) and calculated as follows :

$$\theta_e = Tk\left(\frac{1000}{p}\right)^{a} \exp\left[\left(\frac{3.376}{Tl} - b\right)c\right] \qquad \text{Eq 3.10}$$

where :

$a = 0.2854(1 - 0.28 \times 10^{-3} r)$

$b = 0.00254$

$c = r(1 + 0.81 \times 10^{-3} r)$

T_k = absolute temperature

r = mixing ratio (see appendix)

T_l = absolute temperature at the lifting condensation level (see appendix)

CHAPTER 4

CLIMATOLOGY OF RAINFALL, THE HISTORICAL MEAN AND DRY SPELLS OF NW MADAGASCAR

Using three coastal stations in the NW of Madagascar, seasonal and pentad rainfall departures were analyzed for the period 1960-1992, and daily rainfall departures for the ECMWF period 1987-1992. The summer (December-March) mean rainfall distribution varies from year to year (Fig 4.1), that is 1977 versus 1978 and from period to period, 1968-1973 (wet) versus 1985-1992 (dry). In the following sections the rainfall series at various time scales are analysed for spectral cycles and relationships; and the dynamics of dry spells are analysed from ECMWF composite fields.

4.1 Analysis of summer rainfall:

4.1.1 Interannual variability :

The summer, area-averaged rainfall time series reveal six wet years, 1962, 1969, 1971, 1973, 1977, 1984 and three dry years 1961, 1978, 1990 (Fig 4.1). The rainfall periodogram shows a dominant cycle of 2.45 years and two relatively weak peaks of 2.2 and 3.6 years cycle (Fig 4.2). The 2.45 and 2.2 year cycles in the NW-region rainfall may be attributed to the QBO, the 3.6 year cycle to the SOI. This is in contrast with the findings of Jury and Pathack (1991) which identified a six-year cycle in smoothed Madagascar central highlands rainfall.

In Madagascar, an abundance of summer convective rainfall is related to the passage of TC in the region (Donque, 1975). According to Ecormier (1992), during the wet years, in 1962 for example, 13 TC were recorded in the region, among which four crossed Madagascar and the Mozambique Channel. In 1969, eight TC were experienced

in the region, two formed in the Mozambique Channel and another two crossed Madagascar from the Indian Ocean (I-O). In 1971, 15 TC were observed in the region. One TC from the I-O crossed the island, and four TC formed in the Channel. In 1973, 13 TC were observed in the region among which five hit the island and two TC formations were observed in the Channel. In 1977, nine TC were observed in the region, among which four crossed the island from the I-O into the Channel, where no genesis was observed. In 1984, 10 TC were recorded in the region among which five hit the island mainly in its northwestern region. In the Channel, two TC formations took place. Jury et al (1993a) have outlined details of this destructive TC season. More recent work has identified a prominent 10 year cycle in TC days in the SWIO.

During the dry years, in 1961, five TC-genesis were observed in the SWIO region, but none affected Madagascar. It is noteworthy to mention that to the west of 75°E, only two TC formations took place: Eva had a three day lifespan generated at 13°S, 71°E and Doris formed on 24 January at 10°S, 59°E and moved southeastward. In 1978, 15 TC formations occurred, but only four TC were experienced in the area west of 55°E; TC Georgia from 17°S, 43°E in the Channel crossed the southwest coast of the island. In 1990, nine TC were recorded in the region but Alibera is the only TC which hit the island on its southeastern region. Most of the TC affected the area to the east of 60°E between Mauritius and Australia.

From the above seasonal summaries it is apparent that during wet years, the NW of the island is affected by the passage of TC in agreement with Donque (1975). According to Jury et al. (1993b), the TC frequency cycle is 2.6 years in the period 1960-1990. Therefore the 2.45 year cycle of the NW Madagascar rainfall may be attributed to TC passage and relationships to global indices such as the SOI and QBO.

4.1.2 Summer Rainfall and SOI and QBO relationships :

Relationships between NW-region rainfall and global indices of the Southern Oscillation Index (SOI) and Quasi-biennial Oscillation (QBO) are studied using linear correlation. The SOI is the difference of the surface pressure anomaly between Tahiti and Darwin. The QBO phenomena is the regular alternation of zonally symmetric westerly and easterly winds in the mean zonal winds of the tropical stratosphere (30 hPa) with a periodicity of 24-30 months (Xu, 1992 and Ogallo et al, 1993).

Both the SOI and QBO are weakly correlated with NW Madagascar summer rainfall at 0.15 and -0.11, respectively. The correlations improve only slightly at lag -1 month (December) for the SOI (-0.2) and at lag -2 (November) for the QBO (-0.31). These results suggest that the transfer of global signals to the local climate is not efficient. Jury et al (1993b) have found that TC frequency in the I-O east of Madagascar is poorly correlated with the SOI at 0 lag (near 0), but is relatively better with the QBO (-0.37). TC frequency and SOI are highly correlated with oceanic sea surface temperature (SST) in the central equatorial Indian Ocean, however upper westerly wind shear suppresses a direct response between SOI, SST and NW Madagascar rainfall (Jury et al 1993a). The QBO is best correlated with OLR and rainfall over SE Madagascar.

The El Niño-Southern Oscillation (ENSO) has a time scale of 2-8 years (Barnett, 1991). The El Niño is characterized by the occurrence of anomalously warm surface waters in the entire Pacific for about a year (Rasmusson and Carpenter, 1982). The Southern Oscillation (SO) consists of a seesaw in the surface pressure that involves opposite changes in the eastern and western hemisphere (Berlage, 1957). The role played by the SO in the interannual variability of the climate system of the tropical atmosphere is unquestionable (Kiladis and van Loon, 1988). However, for NW Madagascar the SOI is not a useful predictor, owing to the above mentioned conflicting signals. Opposing limbs of the Walker circulation anomaly associated with the ENSO fall on either side of the island and not directly over it.

Although the QBO may be a useful predictor in some areas (i.e. Zimbabwe and SE Madagascar), it is not the case in NW Madagascar. For instance during the wet year 1962, the QBO index has a positive value of 0.68, during the dry year 1990 it was near zero.

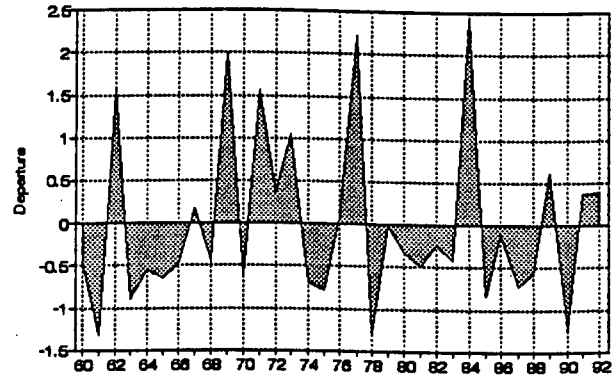

Figure 4.1: Mean Dec-Mar rainfall anomaly for the NW region.

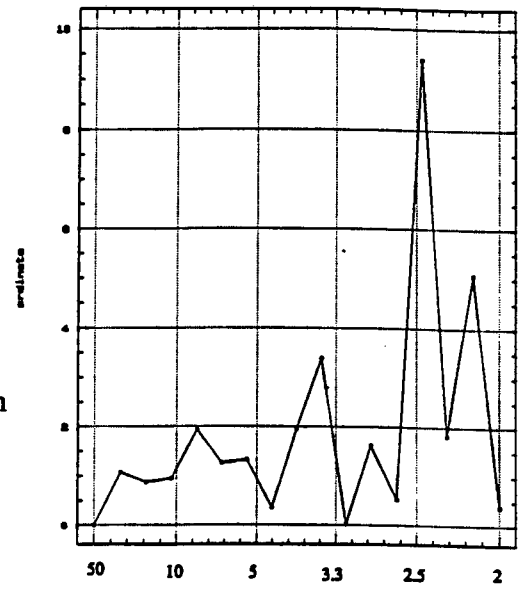

Figure 4.2: Periodogram for the mean annual summer rainfall in the NW region from 1960 to 1992

4.2 Pentad rainfall distribution:

4.2.1 Rainfall frequency and onset :

The mean pentad rainfall distribution from 1960 to 1992 (Fig 4.3) shows that from pentad 1 that is 2 to 6 December up to pentad 7 which is 1 to 5 January, the rainfall amount increases from 35 to 65 mm per pentad. From pentad 17 that is 20 to 24 February the trend goes down to 25 mm per pentad at pentad 24 which is 27 to 31 March. The

Madagascar national weather service defines the onset of the rainfall season where the amount in ten successive days exceeds 10 mm per day. Thus the mean onset pentad where the amount of rainfall is at least 50 mm is pentad 5.

The mean pentad rainfall anomaly for the ECMWF period 1987-1992 reveals a number of wet spells between pentad 5 to 18 (Fig 4.4). Considerable intraseasonal variation is evident and requires accurate forecasting through analysis of meteorological factors related to the wet and dry pentad.

The mean pentad rainfall anomalies for each summer: 1987, 1988, 1989, 1990, 1991, 1992 in the NW-region reveals large intraseasonal variation. Wet and dry spells (+1 and -1 deviation respectively) within the season are as follows:

Table 4.1 : wet and dry pentads.

	86-87	87-88	88-89	89-90	90-91	91-92
Wet pentad	7, 11, 14	10, 12	9	4, 7	16	7
Dry pentad	20, 22	xxx	12	2, 19, 23	xxx	xxx

Where: pentad 1 = 2 to 6 December; xxx = no dry spell.

4.2.2 Historical mean analysis :

In this section the historical mean structure for various fields is analysed and interpreted as a background for understanding the evolution of composite anomalies. The historical means are constructed from ECMWF data for the period January-February 1987-1992 in the domain 0-40°S, 15-75°E. The mean is therefore based on 360 days of input data and is considered representative, although in this period area-rainfall and TC days were slightly below the longer term means (Figure 4.1).

4.2.2.1 Dynamic and kinematic results :

4.2.2.1.1 Geopotential height :

At the lower 1000 hPa level (Fig 4.5), a low pressure area of 80 gpm is over Africa around 20°S, over the north of the Mozambique Channel and to the east of Madagascar with an axis along 15°S. This low pressure area corresponds to the mean location of the ITCZ in summer. Over southern Africa a trough separates the South Atlantic anticyclone from the Indian Ocean anticyclone located to the SE of Madagascar. At 500 hPa level, there exists a trough to the SE of Madagascar, and two anticyclones one to the NE of the island and another one over Southern Africa. At the 200 hPa level, a zonal ridge extends along 15°S from Africa to Madagascar.

4.2.2.1.2 Temperature gradient between 500-100 hPa :

The temperature gradient in the upper troposphere (Fig 4.6.a) indicates instability through radiative cooling at 100 hPa and latent heat release at 500 hPa in the area to the north of 20°S. This confirms the presence of deep convection within the ITCZ.

4.2.2.1.3 Vertical wind :

The 500 hPa field (Fig 4.6.b) reveals sustained upward motion over Madagascar (0.16 Pa s^{-1}) indicative of strong convective activity over the area. Over Africa, there is upward motion of 0.08 Pa s^{-1} at 5°S, 20°E and 15°S, 30°E. This suggests that in the ITCZ the convection is more intense in those areas. Over the eastern escarpment of South Africa an area of upward motion is also found due to orographic uplift of the lower level easterlies over 2000 m mountains.

The E-W vertical section of the mean vertical wind along 16°S (Fig 4.6.c) reveals the existence of strong upward motion over the longitude of Madagascar. Its N-S section

along 46°E (Fig 4.6.d) shows that the upward motion is confined over the island extending from the surface to 150 hPa level with a mean maximum value at 500 hPa. Along the latitude band 12-17°S the upward motion starts from 950 hPa due to the topographic effect over NW Madagascar. The 500 hPa level is found to be the level of maximum vertical velocity, this level corresponds with the finding of Douglas (1992a) for the monsoon depression.

4.2.2.1.4 Horizontal winds :

The lower tropospheric pattern of 1000 hPa wind (Fig 4.7) shows zonal belts of the monsoon flow and easterlies, which converge over the west coast of Madagascar. In the south part of the Mozambique Channel, flow is towards Mozambique. The monsoon flows are slightly stronger than the subtropical easterly flow. In the 500 hPa level, the monsoon flow and the southerly flow from the southern part of the Channel is converging toward Africa along the latitude band 10°S. Easterlies are weaker in the Indian Ocean, while over Southern Africa there is an anticyclonic circulation with strong westerlies on its polar side. In the upper troposphere at 200 hPa level, there is an anticyclonic outflow off northeast Madagascar joining the southeasterly flow to the north of 10°S. There exists a weak trough axis to the southwest of Madagascar on 45°E.

The N-S vertical section of the mean zonal wind along 46°E (Fig 4.7.d) indicates the existence of easterlies at the equator (0-7°S) throughout the troposphere. In the latitude band 8-17°S the lower-level westerly monsoon wind is weak; between 17-36°S the lower-level easterlies are stronger with a mean maximum of 6 m s^{-1} at 27°S in the surface level. In the upper level, strong westerlies are found to the south of 15°S with a mean maximum value at 200 hPa over 40°S representing the circumpolar jet stream.

4.2.2.1.5 Divergence :

In the 1000 hPa field (Fig 4.8), there is strong convergence (negative) over South Africa, due to the topography of the area. At higher levels, it is replaced by a positive divergence (1.5 x 10^{-6} s^{-1} at 500 hPa). Over Madagascar, there exists a convergence area of -10 x 10^{-6} s^{-1}at 1000 hPa. In the 500 hPa level there is an area of convergence over Africa along 10-20°S, over Madagascar off its NE coast and along the latitude band 5-15° S in the Indian Ocean. In the upper level, the pattern shows maximum divergence (6 x 10^{-6} s^{-1} at 200 hPa) over Madagascar, and two cells of 4 x10^{-6} s^{-1}, one over Africa (10°S, 25 °E) and the other over the Indian Ocean (5°S, 60°E). This upper-level divergence is superposed with lower-level convergence along the area of the ITCZ.

The E-W vertical section of the divergence field along 16°S (Fig 4.8.d) reveals the existence of a convergence area in the lower troposphere extending up to 450 hPa from Africa to Madagascar, and upper-level divergence with a maximum value of 6 x 10^{-6} s^{-1} at 200 hPa over the island. The N-S vertical section along 46°E (Fig 4.8.e) indicates the existence of a dipole, lower convergence-upper divergence over the island suggesting the role played by the topography and lower level monsoon flow and easterlies.

4.2.2.1.6 Vorticity :

The lower level at 1000 hPa level (Fig 4.9.a) shows cyclonic vorticity -12 x 10^{-6} s^{-1} over southern Madagascar and 8 x 10^{-6} s^{-1} to the east of the island along the latitude band 10-20°S. There is an anticyclonic vorticity area to the north and south of the Mozambique Channel. In the upper level, the area south of 5°S shows anticyclonic vorticity owing to encroachment of sub-tropical westerlies, with maximum value of 20 x 10^{-6} s^{-1} over Southern Africa oriented NW-SE which continues to the south of the Mozambique Channel.

The zonal vertical section of the mean vorticity along the latitude 16°S (Fig 4.9.d) shows that there is cyclonic vorticity up to 500 hPa from 25-65°E with a maximum value

near 800 hPa, and anticyclonic vorticity at 200 hPa with a maximum value over 15°S. The meridional vertical section along 46°E (Fig 4.9.e) shows that the cyclonic vorticity is centered at 25°S.

4.2.2.2 Moisture and thermodynamic results :

4.2.2.2.1 Precipitable water :

The precipitable water integrated from surface to 300 hPa (Fig 4.10.a) reveals that there exists a maximum amount of 55 mm over the north part of Madagascar as well as over central Africa at 5°S, 15°E. This agrees with the position of a trough over the Congo basin where there is intense convective activity. Over South Africa an area of minimum PW (25 mm) is found.

4.2.2.2.2 Vertical gradient of specific humidity :

The vertical gradient of specific humidity at low level, between 1000-850 hPa level (Fig 4.10.b) shows three maxima of which one is over the south part of the Channel (6.5 g kg^{-1}), one over Africa about 2°S, 25°E (7 g kg^{-1}) and the last near the Comoros Islands 5°S, 50°E (7 g kg^{-1}) where monsoon surges originate.

4.2.2.2.3 Water vapour flux :

The surface-500 hPa integrated WVF pattern exhibits considerable similarity with the horizontal wind at the lower level (Fig 4.10.c); there is convergence of moisture from the monsoon flow and the easterlies. It indicates that the moisture content brought by the monsoon flow is greater than the one from the easterly winds. Thus, the strength of the monsoon flow is an important contributor to rainfall dynamics in the area. Over Africa the flux of moisture is small.

4.2.2.2.4 Velocity potential of water vapour flux :

The potential function of water vapour flux (χ_Q) and the divergent water vapour flux (Q_{div}) integrated from surface to 500 hPa shows convergence of flux over Madagascar (20 x 10^9 kg s^{-1}). This area of convergence extends along a line into Mozambique and along the east coast of South Africa (Fig 4.11.a and b).

4.2.2.2.5 Streamfunction of water vapour flux :

The non-divergent water vapour flux (ψ_Q) integrated from surface to 500 hPa shows a cyclonic circulation (6 x 10^9 kg s^{-1}) oriented NW-SE off the northeast coast of Mozambique to the southeast of Madagascar. An anticyclonic area is located to its NE (-4 x 10^9 kg s^{-1}). This is to be expected since the main axis of moisture flux is from the NW along the $\psi = 0$ line (Fig 4.11.c).

4.2.2.2.6 Equivalent potential temperature :

The equivalent potential temperature (EPT) pattern shows at the lower level a warm area extending from Africa to the Indian Ocean along the latitudinal band 5°- 20°S. In the 1000 hPa level (Fig 4.12.a), the 350°K-isoline covers Africa from the equator up to 25°S, then it narrows over the Channel (between 5° and 20°S) to be located north of Mauritius in the Indian Ocean. The 500 hPa level (Fig 4.12.b) shows a similar pattern, the 336°K-isoline covers the area between the equator up to 17°S, and it narrows over the Indian Ocean to be located between 5° and 15°S.

The vertical structure of the EPT along the latitude 16°S (Fig 4.12.c) shows that there is warm moist unstable air at 25°E and at 50°E in the lower troposphere which suggests the existence of convective areas in these locations. The meridional vertical section along 46°E (Fig 4.12.d) indicates that the unstable area is situated at 20°S. This suggest that the area of convective activity is over central Madagascar, owing partly to the steep orography.

The mean summer meteorological patterns mentioned above reveal the existence of deep convective activity over Africa at 15°S, 25°E and over Madagascar. There is a convergence of monsoon flux and trade winds at the surface over the NW of the island creating background conditions for tropical convective vortices.

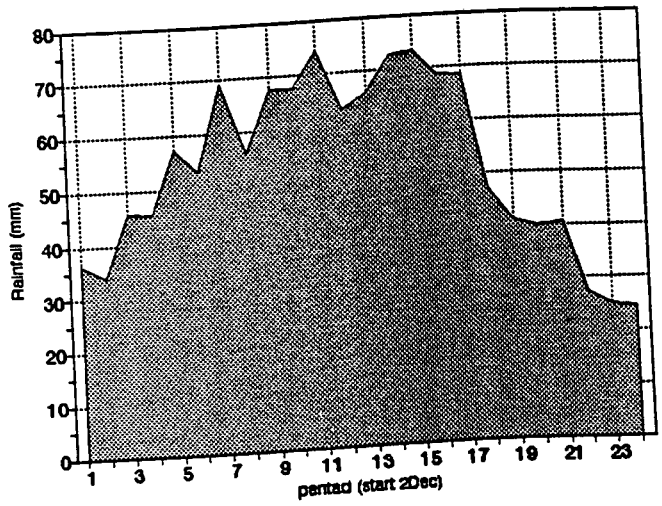

Figure 4.3: Mean pentad summer rainfall in the NW region for the period 1987 to 1992

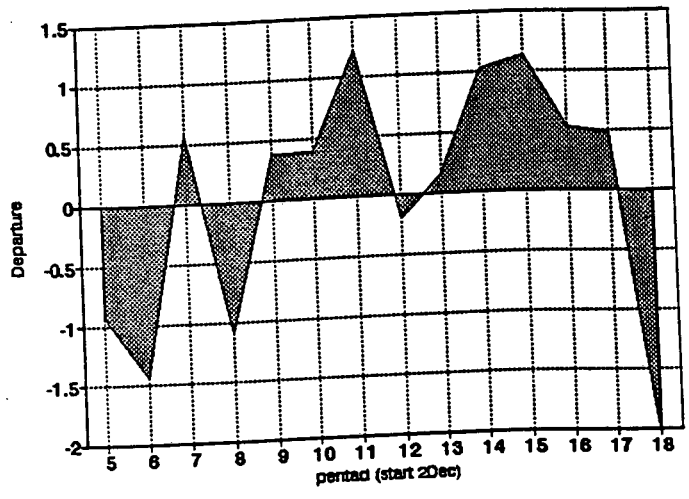

Figure 4.4: Mean pentad anomaly showing wet spells in summer rainfall

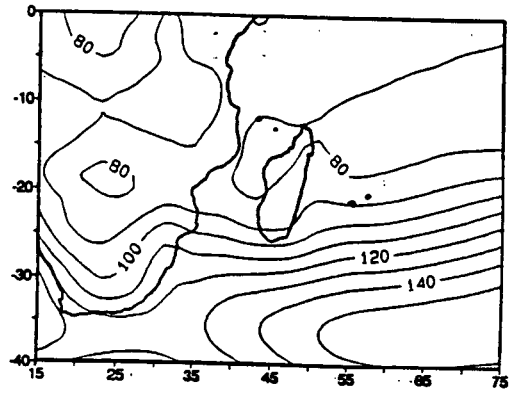

Figure 4.5.a: Mean geopotential height at 1000 hPa.
Contour interval 10 gpm

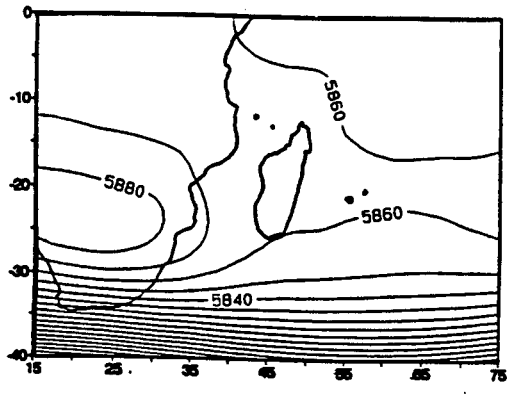

Figure 4.5.b: Mean geopotential height at 500 hPa.
Contour interval 10 gpm

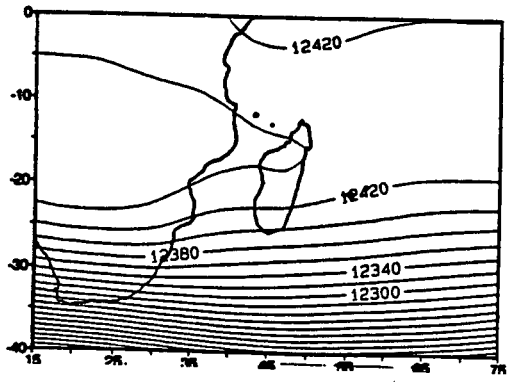

Figure 4.5.c: Mean geopotential height at 200 hPa.
Contour interval 20 gpm.

a

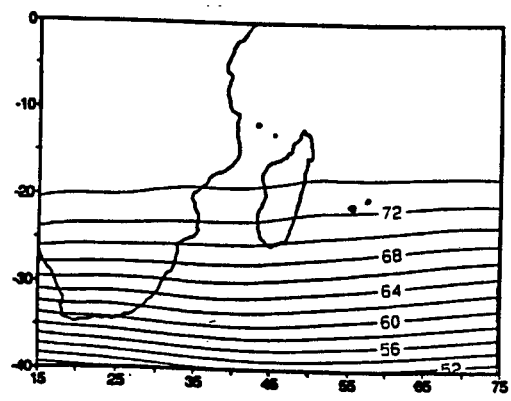

Figure 4.6.a: Mean temperature gradient beween 500-100 hPa.
Contour interval 2°C

b

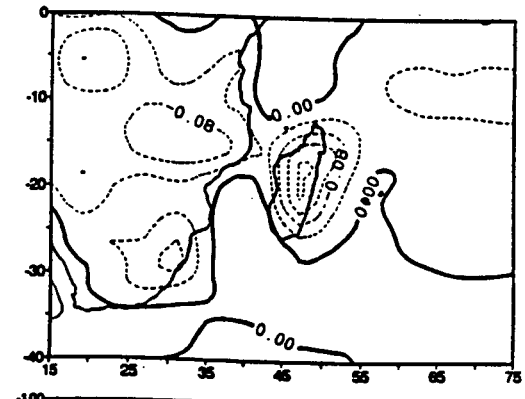

c

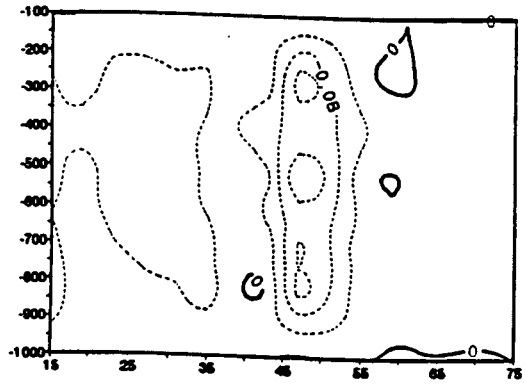

d

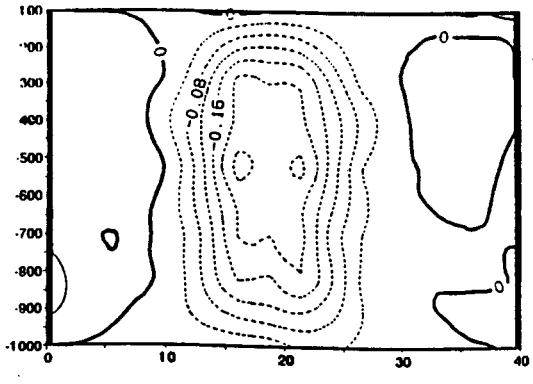

Figure 4.6.b: Mean vertical wind at 500 hPa.
c and d: Its vertical section along 16°S and 46°E.
Contour interval 0.04 Pa s^{-1}.

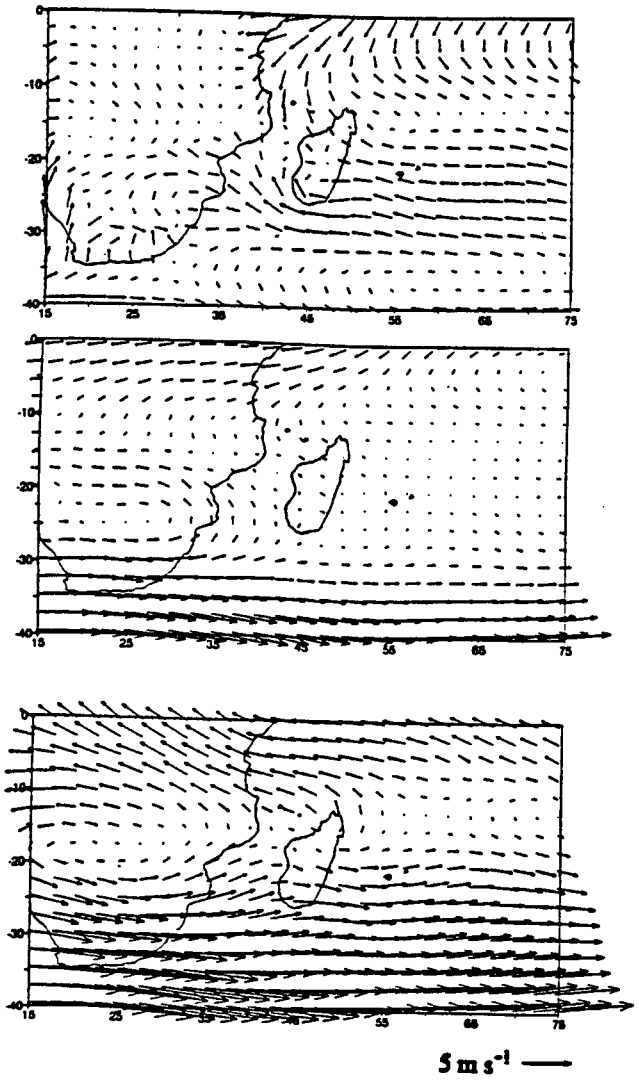

Figure 4.7.a-b-c: Mean horizontal wind at 1000, 500 and 200 respectivelly.

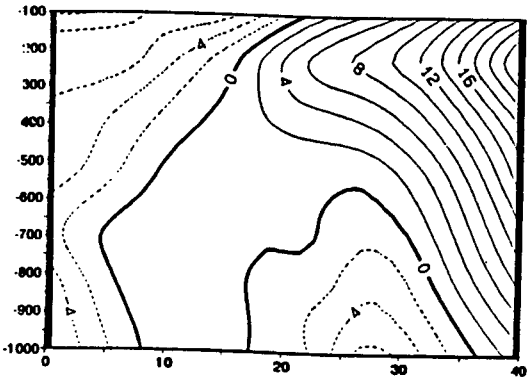

Figure 4.7.d: Vertical section of the mean zonal wind u along 46°E. Contour interval 2 m s^{-1}.

Figure 4.8.a-b-c: Mean divergence at 1000, 500, 200 hPa. Contour interval 2 x 10^{-6} s^{-1}
d-e: Its vertical section along 16°S and 46°E. Contour interval 1 x 10^{-6} s^{-1}.

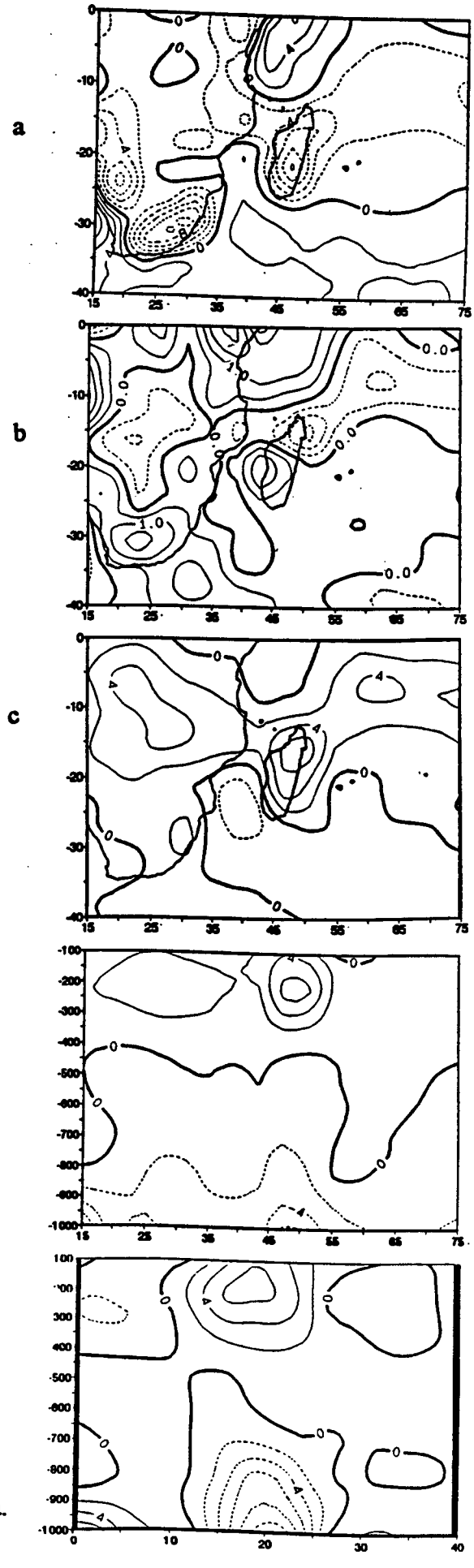

Figure 4.8

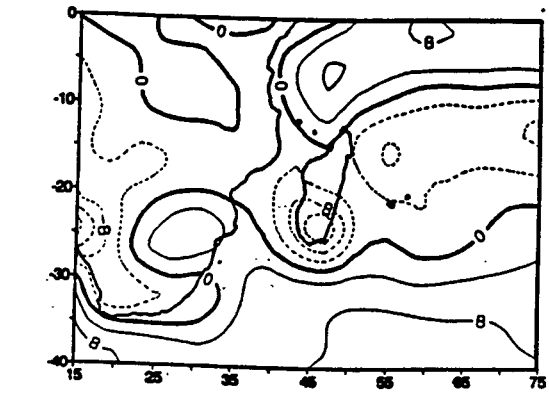

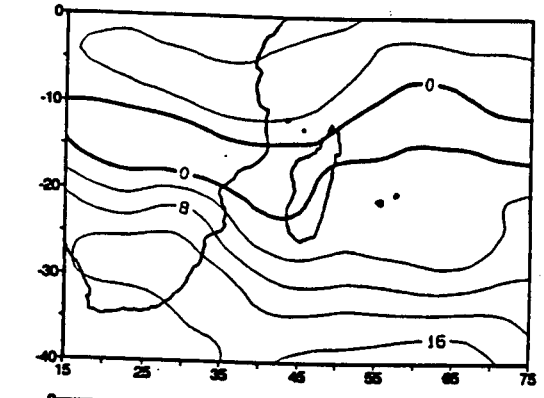

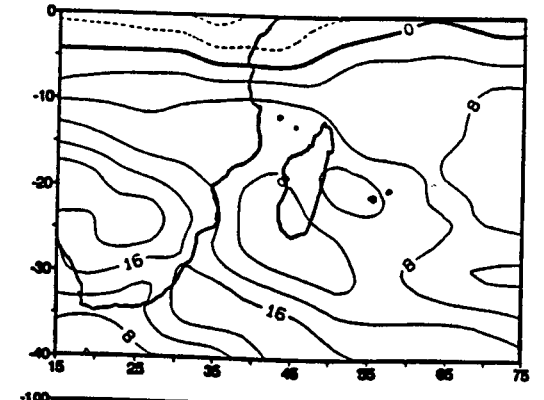

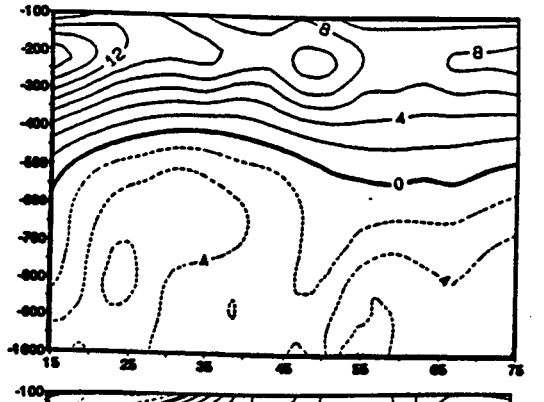

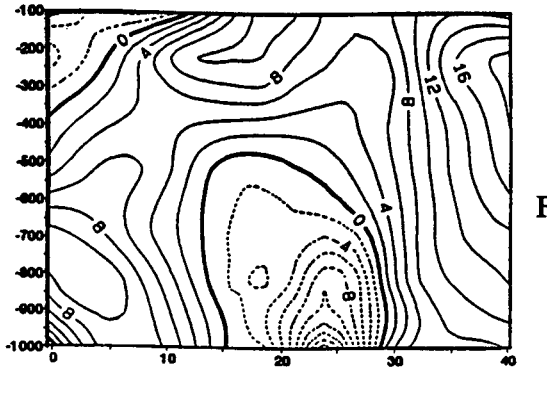

Figure 4.9

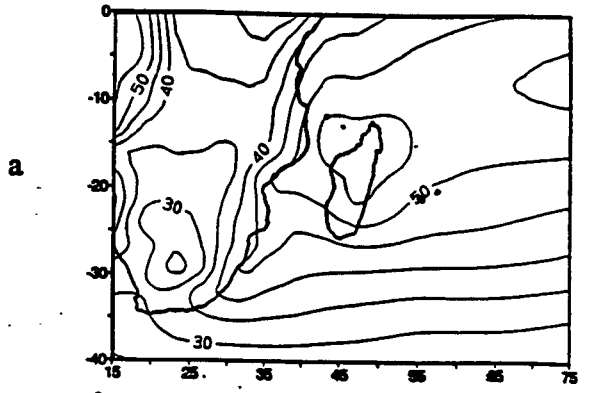

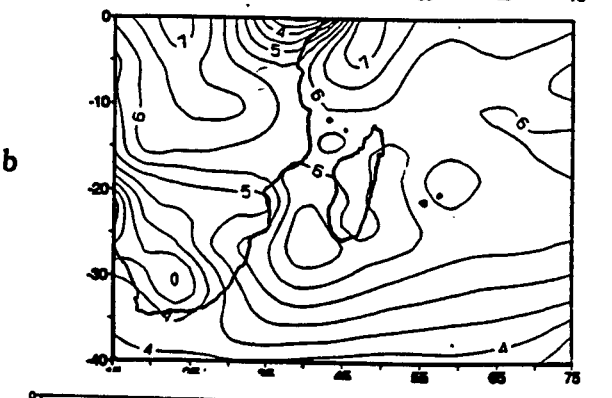

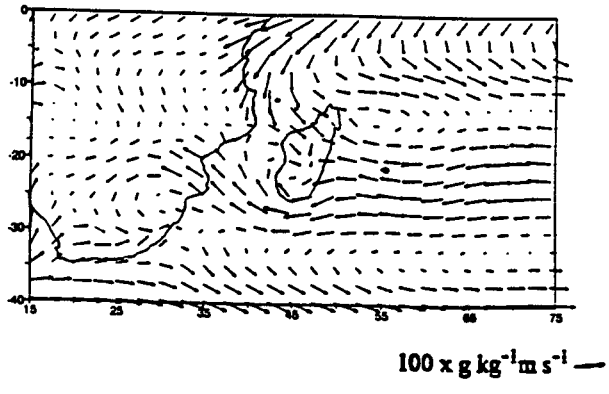

100 x g kg^{-1}m s^{-1}

Figure 4.10.a: Mean precipitable water integrated from surface up to 300 hPa. Contour interval 10 mm.
b: Mean specific humidity gradient between 1000-850 hPa. Contour interval 0.5 g kg^{-1}
c: Mean water vapour flux integrated from surface to 500 hPa.

Figure 4.9.a-b-c: Mean vorticity at 1000, 500, 200 hPa. Contour interval 4 x 10^{-6} s^{-1}
d-e: Its vertical section along 16°S and 46°E. Contour interval 2 x 10^{-6} s^{-1}.

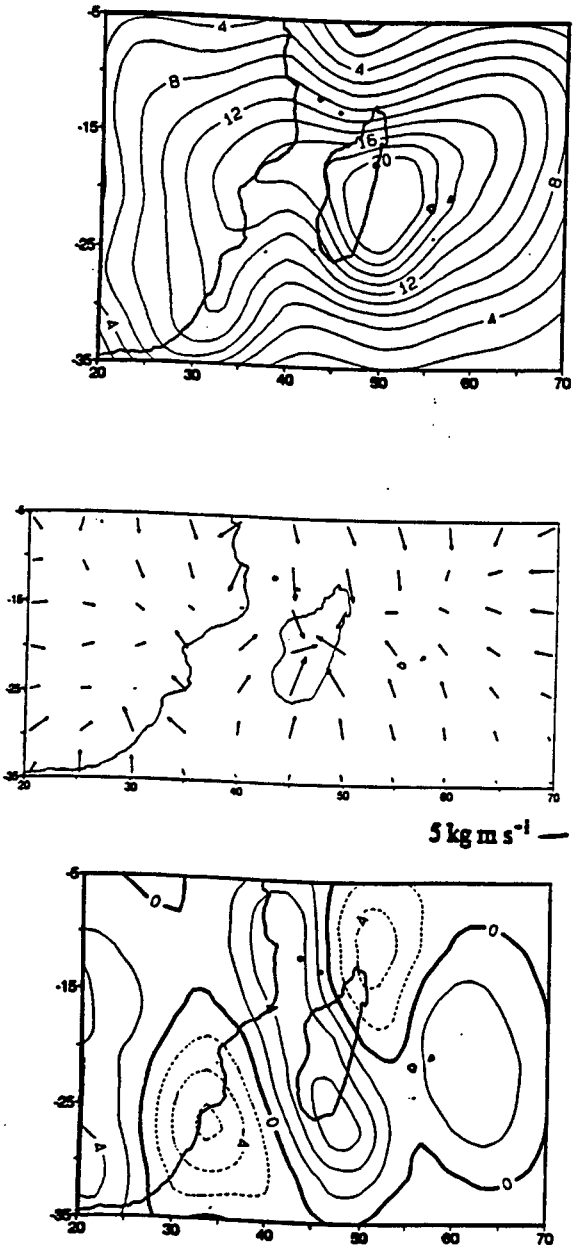

Figure 4.11.a: Mean velocity potential of water vapour flux (χ_Q) integrated from the surface to 500 hPa. Contour interval 2 x 10^9 kg s^{-1}

b: Mean divergent water vapour flux (Q_{div}) integrated from the surface to 500 hPa.

c: Mean streamfunction of water vapour flux integrated from the surface to 500 hPa. Contour interval 2 x 10^9 kg s^{-1}

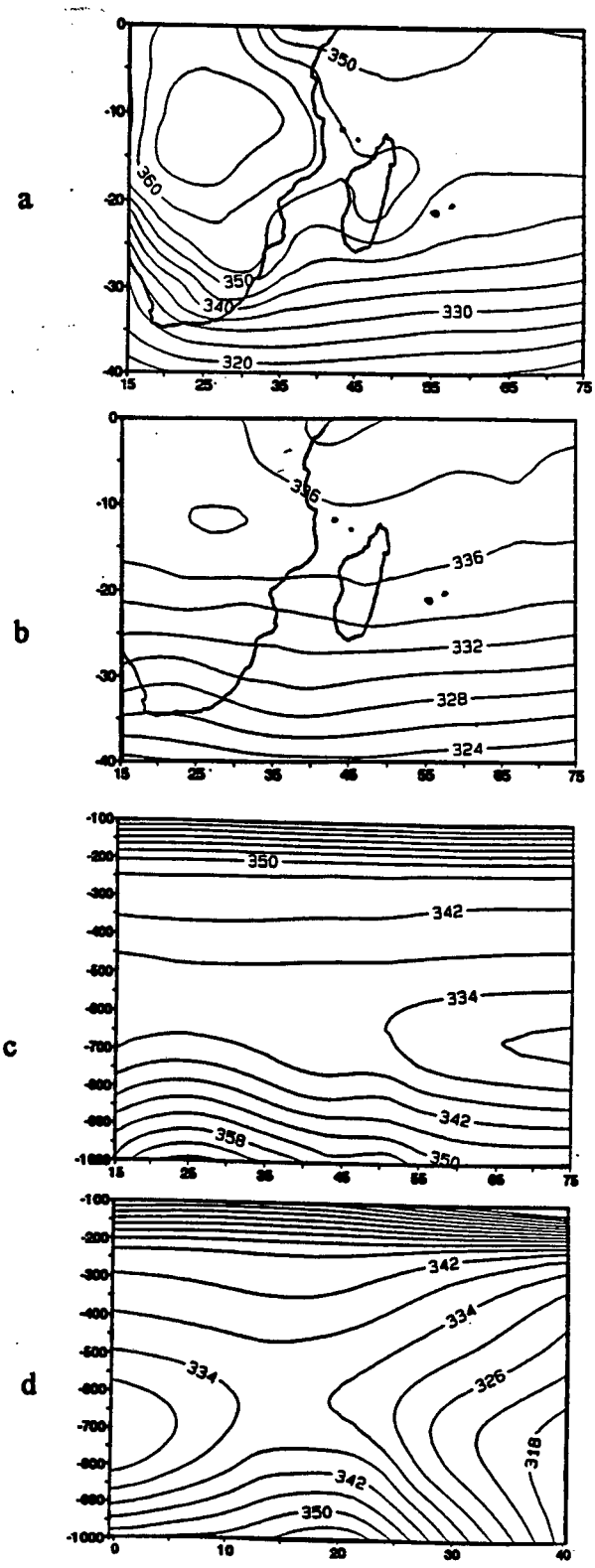

Figure 4.12.a-b: Mean EPT at 1000, 500 hPa. Contour interval 2°K

c-d: Its vertical section along 16°S and 46°E. Contour interval 2°K

4.2.3 Dry pentad structure :

The study of meteorological structure and dynamics of wet spells shows similar patterns to the composite of heavy rainfall events discussed in Chapter 5, therefore they are not considered here. For the dry pentad composite, meteorological parameters have been analysed for P 0 the dry event and for P-1 the period five days prior, according to table 4.1. The various fields are analysed as six dry pentads minus the January-February mean, hereafter defined as the anomaly.

4.2.3.1 geopotential height :

The structure (Fig 4.13) shows that at P-1 in the lower level (1000 hPa), there is a negative anomaly area (>8 gpm) to the south of Madagascar, a positive anomaly area to the west of the island over the Mozambique Channel and a ridge oriented NW-SE over South Africa. In the mid-troposphere (500 hPa), the negative anomaly area to the south of the island is more pronounced with a maximum value of 38 gpm to the south of the Channel; a positive anomaly area (8 gpm) is centered over Africa at 15°S, 25°E; the northwest of Madagascar is covered by a positive anomaly area while the rest of the island lies under the negative area. In the upper level (200 hPa), the negative anomaly area covers southern Africa and Madagascar with maximum value of 80 gpm at 30°S, 35°E to the southwest of the Channel; to the north of 10°S the positive anomaly area has its maximum value off the coast of East Africa (16 gpm). The overall structure of the anomalies is zonal, with low in the subtropics and high in the tropics at P-1.

At P 0 (Fig 4.14), the 1000 hPa level indicates that the negative anomaly area is moved east into the Indian Ocean while intensifying to maximum -13 gpm at 35°S, 54°E and the ridge from South Africa is now located to the south of the Channel. In the 500 hPa level, the negative anomaly is further eastward at 33°S, 45°E, south of Madagascar

with maximum value of -44 gpm. The whole island is covered by the negative area. In the upper level (200 hPa), the negative anomaly area (-104 gpm) is located at 33°S, 43°E and the area of maximum positive anomaly is located over Tanzania.

4.2.3.2 The horizontal wind :

At P-1 (Fig 4.15), in the 1000 hPa level there is a cyclonic circulation area to the SE of the Channel, and to the north of 15°S off the NW coast of Madagascar in a broad band, a strong northwestward wind anomaly exists and illustrates a weakening of the monsoon. In the Indian Ocean to the east of Mauritius, there is a cyclonic circulation centered at 20°S, 75°E. The 500 hPa level pattern shows a broad band of westerlies between 20-30°S , and a ridge oriented NW-SE to the SE of Mauritius. In the 200 hPa level the westerly wind anomaly lies between the latitude band 15-30°S throughout.

At P 0 (Fig 4.16), the 1000 hPa level shows a cross equatorial southeasterly flow anomaly to the north of 10°S. From the subtropics to the south of Madagascar, the southeasterly flow diverges towards the south coast of South Africa and to the east coast of Madagascar. In the 500 hPa level, an anticyclonic circulation over Africa at 15°S, 30°E is found in the dry spell, a subtropical cyclonic circulation at 35°S, 45°E and a westerly flow anomaly between these two systems up to the Indian Ocean. In the upper level the subtropical westerly anomaly strengthens and penetrates up to the equator in the longitudes of Madagascar 40-55°E. This and the weaker monsoon are obvious circulation features associated with dry spells over NW Madagascar.

4.2.3.3 The water vapour flux, its streamfunction and velocity potential :

The water vapour flux anomaly pattern shows at P-1 (Fig 4.17.a) easterly winds to the east of 65°E which diverge into the subtropics and northward toward the east African coast. In the south part of the Mozambique Channel, the upper branch of the cyclonic

circulation gives diffluent westerly wind anomalies toward Madagascar. At P 0 (Fig 4.17.b), to the north of 15°S the southeasterly anomalies are intensified as well as the subtropical southeasterlies to the south of Madagascar.

The velocity potential of the water vapour flux anomaly integrated from the surface to 500 hPa level shows at P-1 (Fig 4.18.a), a negative area over the whole region with a maximum value of -10 x 10^9 kg s^{-1} at 15°S, 60°E in the Indian Ocean suggesting an area of divergence. At P 0 (Fig 4.18.b), the pattern shows that the negative area lies from Mozambique toward the Indian Ocean with its maximum value 10 x 10^9 kg s^{-1} over Madagascar and a positive area oriented N-S over southern Africa to the west of the negative area.

The streamfunction of the water vapour flux anomaly integrated from the surface to 500 hPa level shows at P-1 (Fig 4.18.c), a negative area extending from southern Africa to Madagascar with maximum value -6 x 10^9 kg s^{-1} and another one in the Indian Ocean with maximum value -8 x 10^9 kg s^{-1} at 25°S, 63°E. These negative areas correspond to an anticyclonic circulation. At P 0 (Fig 4.18.d), there exists a positive area in the Indian Ocean up to the east part of Madagascar and negative area from the west part of the island westward. The line of zero streamfunction overlies Madagascar with a meridional orientation during dry spells, suggesting northward (equatorward) rotational flow in a divergent irrotational environment.

4.2.3.4 The precipitable water :

The precipitable water anomaly integrated from the surface to 300 hPa level shows at P-1 (Fig 4.19.a), the existence of negative area with maximum -8 mm over western Madagascar and a positive area over the east African coast (2 mm). At P 0 (Fig 4.19.b), the dry axis strengthens to a maximum negative value over the island of -10 mm and the positive area is 4 mm.

4.2.3.5 The temperature gradient and equivalent potential temperature :

The gradient of temperature between 500 hPa and 100 hPa level (Fig 4.19.c and d) shows at P-1 a positive anomaly area 1°C to the NE of Madagascar in the Indian Ocean and negative anomaly of -4°C to its SW off the eastern coast of South Africa at 27°S, 33°E. At P 0, the positive anomaly area extends westward over eastern Africa and the negative area anomaly intensifies to a maximum value of -5.6°C at its centre over 30°S, 40°E in a pattern similar to the upper geopotential.

The vertical cross-sections of the EPT along the latitude 16°S (Fig 4.20.a and b) shows at P-1, a positive anomaly area in the lower and middle troposphere at 75°E which suggests that an area of enhanced convection is located in the SE Indian Ocean. Over Africa and Madagascar the area of negative anomaly runs from the surface to 200 hPa level. At P 0 there is an area of positive anomaly over Africa up to the 800 hPa level at 20°S while over Madagascar the area of suppressed EPT, hence convection persists. Surface EPTs are less than -7°K below the mean prior to the dry spells.

The vertical cross-sections of the EPT along the longitude 46°E (Fig 4.20.c and d) reveal at P-1 the existence of a positive anomaly area with maximum of 3°K at 700 hPa level near the equator while to the south of 10°S there is a negative anomaly area in the lower and mid-troposphere with a maximum value near the surface between the latitude band 15-25°S. At P 0 the pattern does not vary much from the P-1 field.

The meteorological patterns of the dry spell indicate in the lower level, the existence of a cyclonic circulation anomaly in the subtropics five days prior to P 0. This moves eastward and brings a band of westerly winds into the tropics. To the north of 15°S equatorward flow is prevalent. In the upper level (200 hPa), the cyclonic circulation to the south of the Mozambique Channel moves eastward and to the north of 30°S, westerly flow dominates the entire area. The velocity potential of the water vapour flux reveals the

existence of divergent flow to the north of Mauritius moving toward Madagascar five days prior to the dry spell. The subtropical cyclonic circulation suggests the weakening of the migratory Indian Ocean anticyclone, and a positive anomaly in the Channel suggests that the ITCZ lies further north. This is confirmed by the existence of positive precipitable water over East Africa and deficiency over Madagascar. The vertical cross section of the EPT along the longitude of Mahajanga shows that the area of active convection lies near the equator. The withdrawal of monsoon support to the ITCZ is a major factor of dry spells over NW Madagascar.

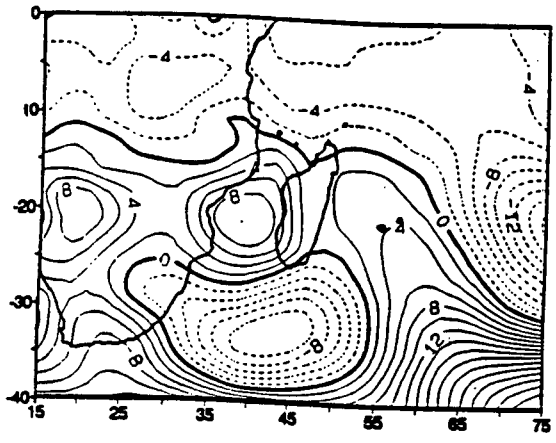

Figure 4.13.a: Geopotential height anomalies at 1000 hPa for pentad-1. Contour interval 2 gpm.

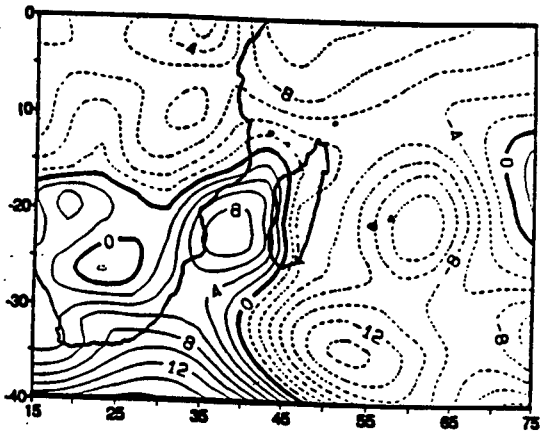

Figure 4.14.a: Geopotential height anomalies at 1000 hPa for pentad 0. Contour interval 2 gpm.

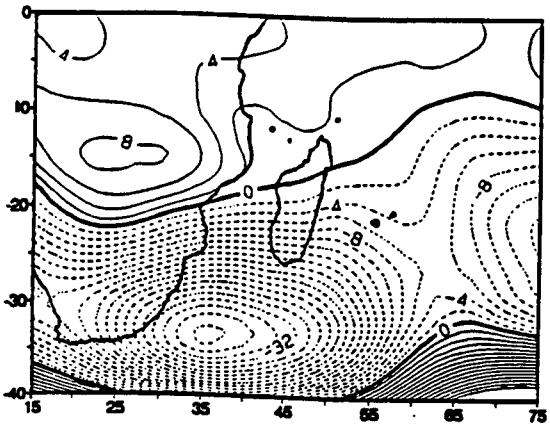

Figure 4.13.b: Geopotential height anomalies at 500 hPa for pentad-1. Contour interval 2 gpm.

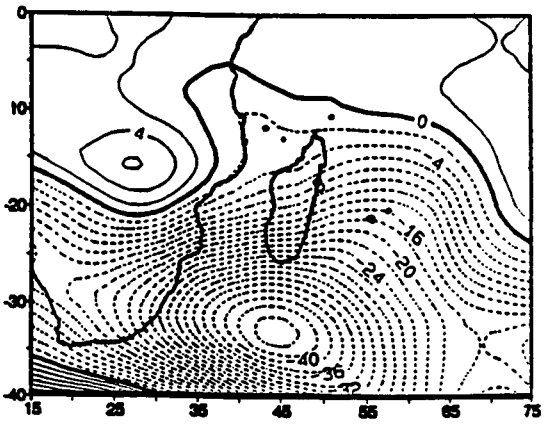

Figure 4.14.b: Geopotential height anomalies at 500 hPa for pentad 0. Contour interval 2 gpm.

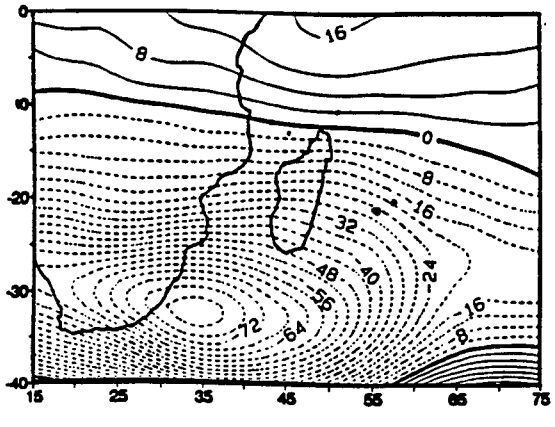

Figure 4.13.c: Geopotential height anomalies at 200 hPa for pentad-1. Contour interval 4 gpm

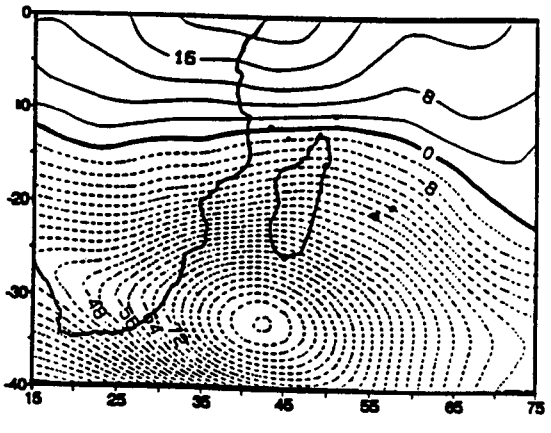

Figure 4.14.c: Geopotential height anomalies at 200 hPa for pentad 0. Contour interval 4 gpm

" DRY SPELL "

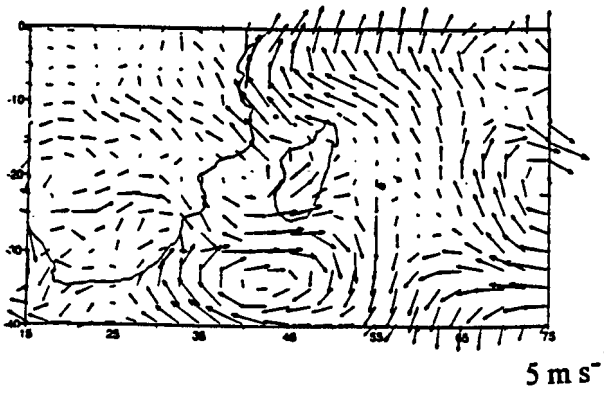

5 m s^{-1}

Figure 4.15.a: Horizontal wind anomalies at 1000 hPa for pentad-1.

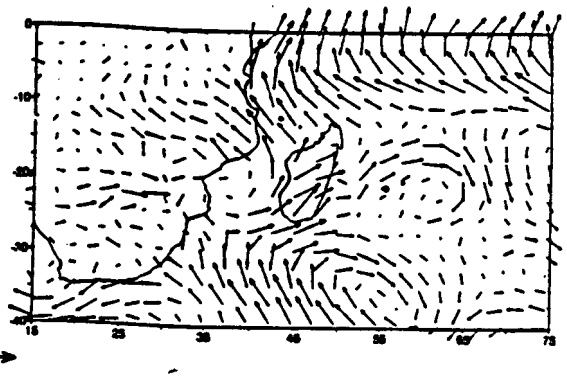

Figure 4.16.a: Horizontal wind anomalies at 1000 hPa for pentad 0.

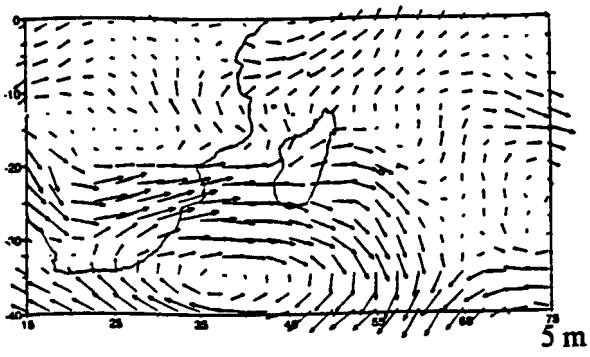

5 m s^{-1}

Figure 4.15.b: Horizontal wind anomalies at 500 hPa for pentad-1.

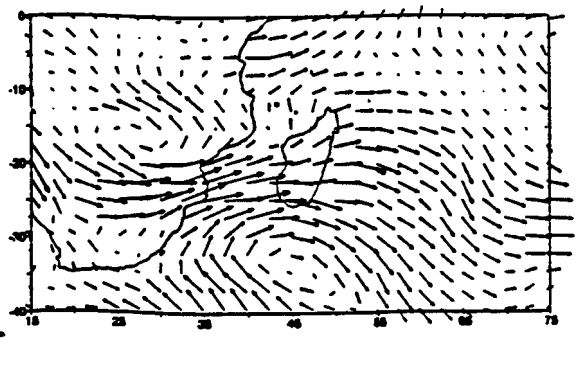

Figure 4.16.b: Horizontal wind anomalies at 500 hPa for pentad 0.

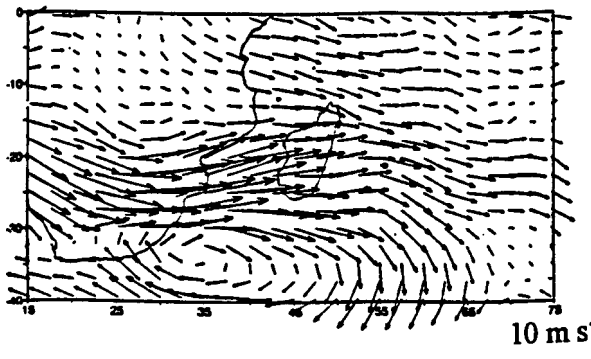

10 m s^{-1}

Figure 4.15.c: Horizontal wind anomalies at 200 hPa for pentad-1.

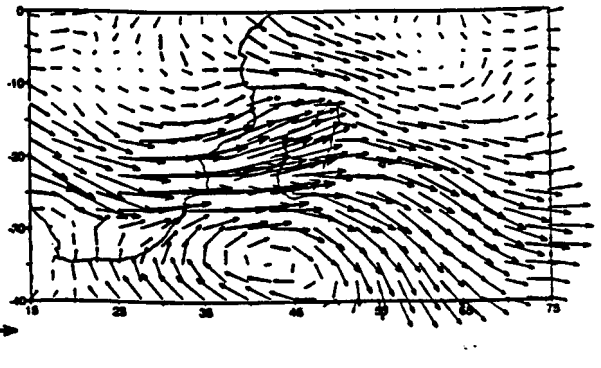

Figure 4.16.c: Horizontal wind anomalies at 200 hPa for pentad 0.

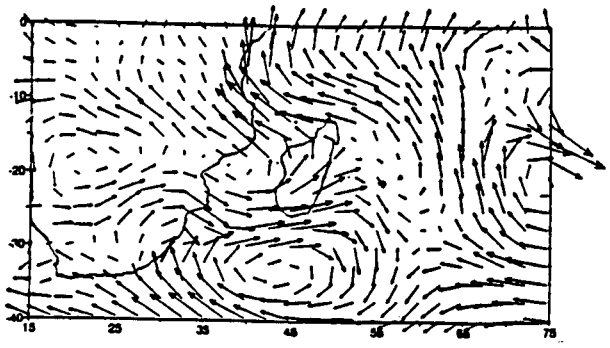

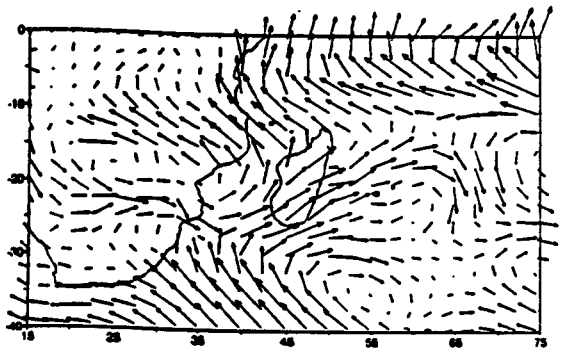

100 g kg^{-1} m s^{-1}

Figure 4.17.a: Water vapour flux anomalies integrated from the surface to 500 hPa for pentad-1.

Figure 4.17.b: Water vapour flux anomalies integrated from the surface to 500 hPa for pentad 0.

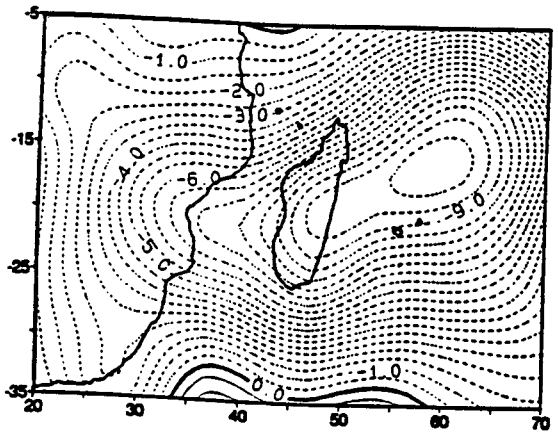

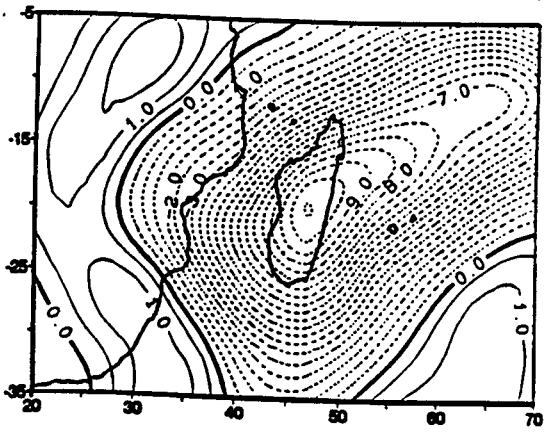

Figure 4.18.a: Velocity potential of water vapour flux (χ_Q) anomalies integrated from the surface to 500 hPa for pentad-1.
Contour interval 0.5 x 10^8 kg s^{-1}

Figure 4.18.b: Velocity potential of water vapour flux (χ_Q) anomalies integrated from the surface to 500 hPa for pentad 0.
Contour interval 0.5 x 10^8 kg s^{-1}

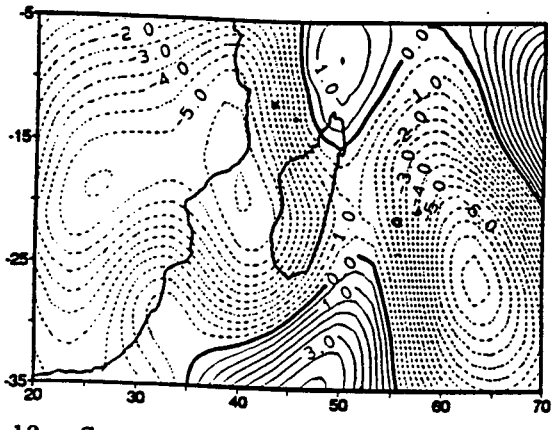

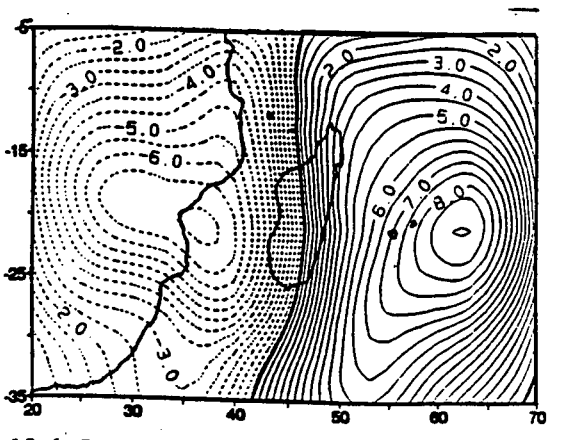

Figure 4.18.c: Streamfunction of water vapour flux anomalies integrated from the surface to 500 hPa for pentad-1.
Contour interval 0.5 x 10^8 kg s^{-1}

Figure 4.18.d: Streamfunction of water vapour flux anomalies integrated from the surface to 500 hPa for pentad 0.
Contour interval 0.5 x 10^8 kg s^{-1}

" DRY SPELL "

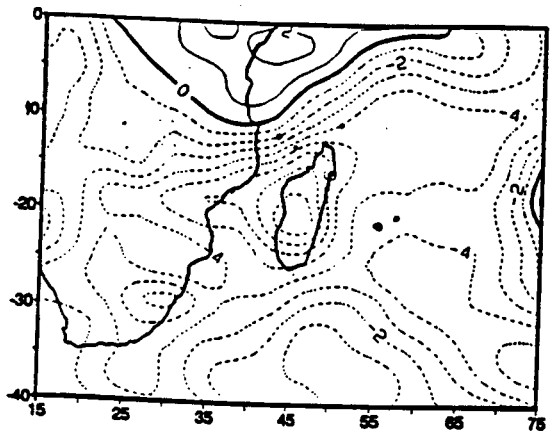

Figure 4.19.a: Precipitable water anomalies integrated from the surface up to 300 hPa for pentad-1. Contour interval 1 mm.

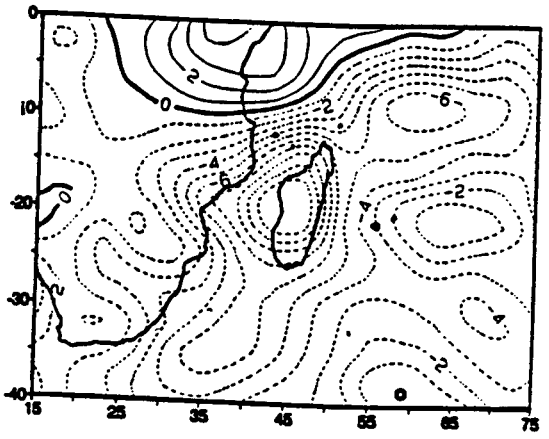

Figure 4.19.b: Precipitable water anomalies integrated from the surface up to 300 hPa for pentad 0 Contour interval 1 mm.

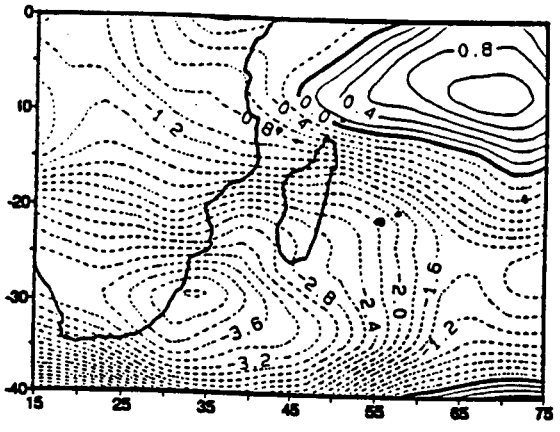

Figure 4.19.c: Temperature gradient anomalies between 500-100 hPa for pentad-1. Contour interval 0.2°C

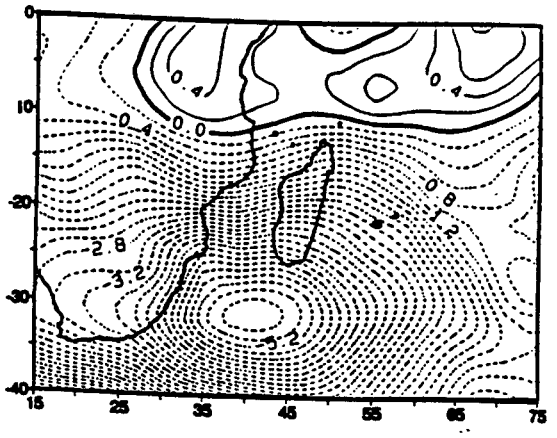

Figure 4.19.d: Temperature gradient anomalies between 500-100 hPa for pentad 0. Contour interval 0.2°C

" DRY SPELL "

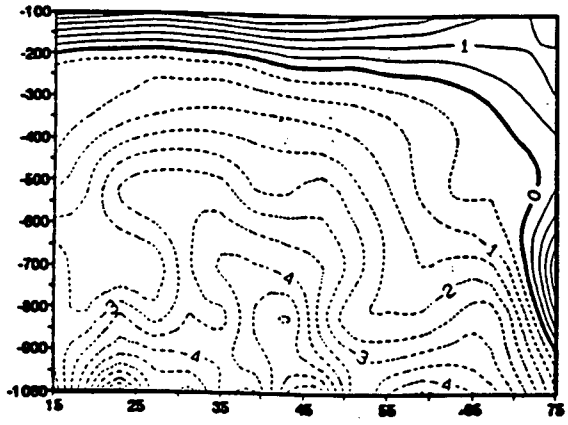

Figure 4.20.a: Vertical section of EPT anomalies along 16°S for pentad-1. Contour interval 0.5°K

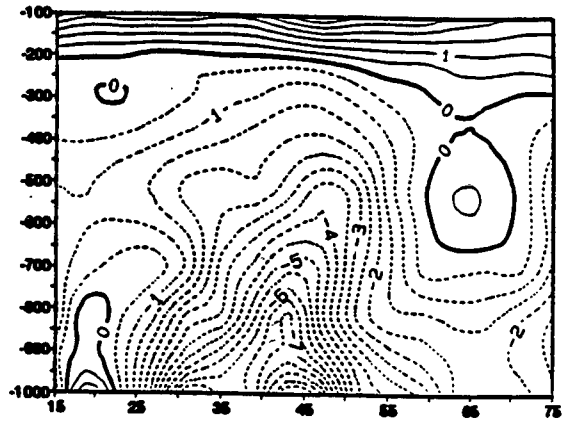

Figure 4.20.b: Vertical section of EPT anomalies along 16°S for pentad 0. Contour interval 0.5°K

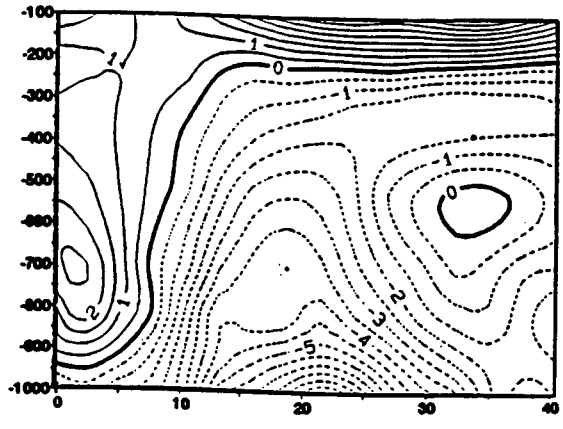

Figure 4.20.c: Vertical section of EPT anomalies along 46°S for pentad-1. Contour interval 0.5°K

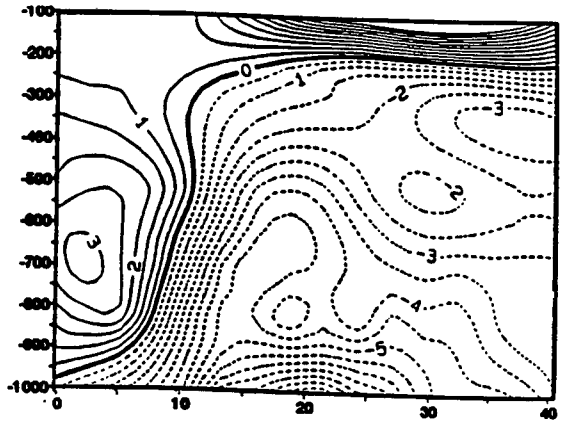

Figure 4.20.d: Vertical section of EPT anomalies along 46°S for pentad 0. Contour interval 0.5°K

4.3 Daily rainfall spectra-analysis :

The daily NW Madagascar summer rainfall spectra-analysis evidences considerable change between 1987-1992. As mentioned in the introduction to this chapter, this period exhibits rainfall 10 % below normal relative to the 1960-1992 period.

The spectra-analysis of the mean daily rainfall in the period 1987-1992 (Fig 4.21.a) has three weak cycles of 4.8, 7.6 and 11.1 days. The 1987 season shows two peaks of 10.1 and 20.3 days cycle (Fig 4.21.b). The 1988 has one peak of 9.3 days cycle (Fig 4.21.c). In 1989, the periodogram exhibits two peaks of 40.7 and 8.7 days cycle (Fig 4.21.d) and a relatively weak cycle peak of 11.1 days. The season 1990 has only one cycle of 15.3 days and the 1991 has two cycles of 4.1 and 40.7 days (Fig 4.21.e and f). Finally the 1992 season reveals three peaks of 3.7, 4.7 and 17.4 days cycle (Fig 4.21.g). Maximum spectral energy is found in 1989 and 1991 at 40.7 days.

From this analysis, the 40 days cycle can be attributed to the Madden-Julian oscillation and associated surges in the monsoon. The 10-20 days cycles which are apparent in most cases can be attributed to the transient "easterly" waves with a similar period according to Jury and Pathack, (1991). The variation from longer or singular peaks: 1987, 1990 to shorter chaotic cycles: 1988, 1992 reveals the complexity of interplay between the convective forcing features: monsoon surges, easterly waves, African tropical troughs and mid latitude westerly waves.

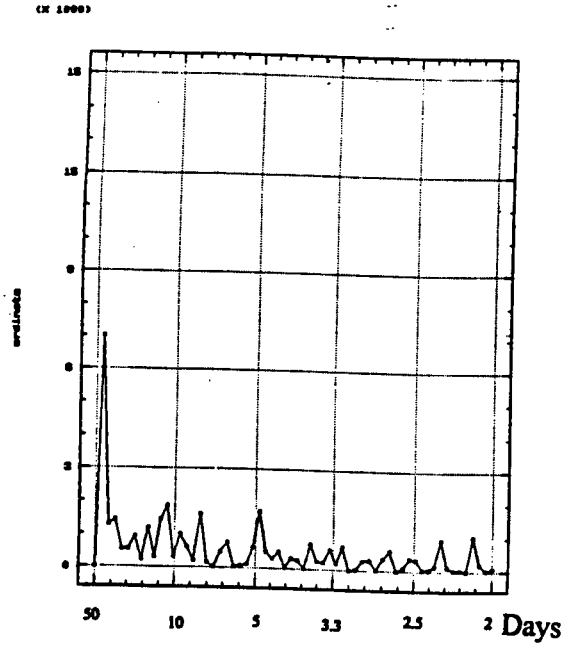

Figure 4.21.a: Periodogram for the mean daily summer rainfall in the NW region from 1987 to 1992

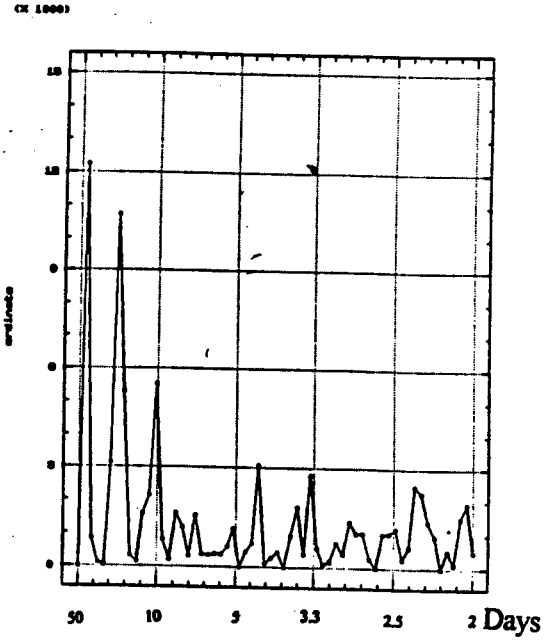

Figure 4.21.b: Periodogram of the mean daily rainfall in the NW region for the summer 1987

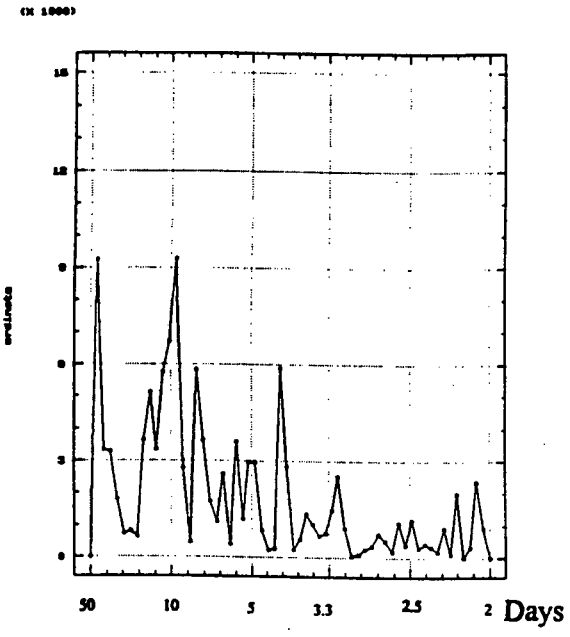

Figure 4.21.c: Periodogram of the mean daily rainfall in the NW region for the summer 1988

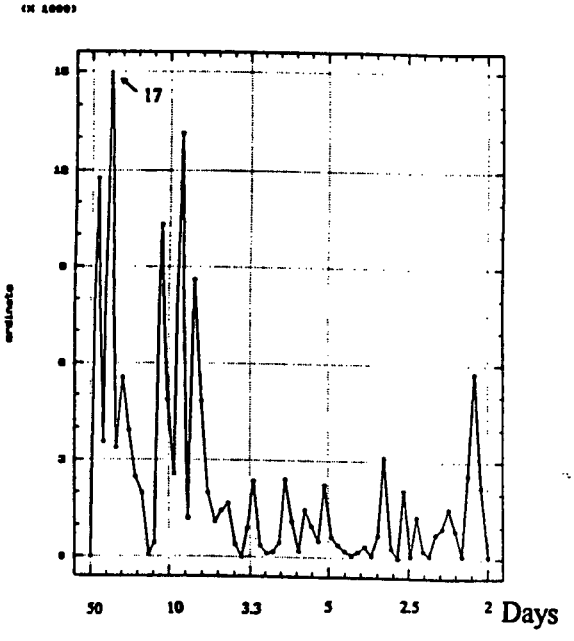

Figure 4.21.d: Periodogram of the mean daily rainfall in the NW region for the summer 1989

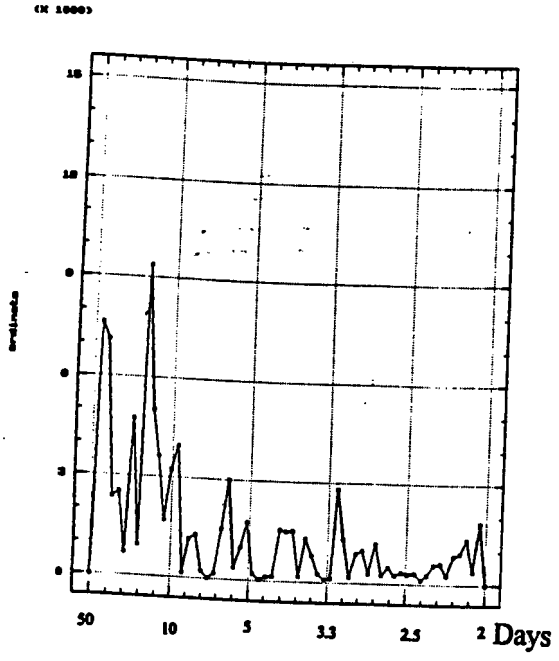

Figure 4.21.e: Periodogram of the mean daily rainfall in the NW region for the summer 1990

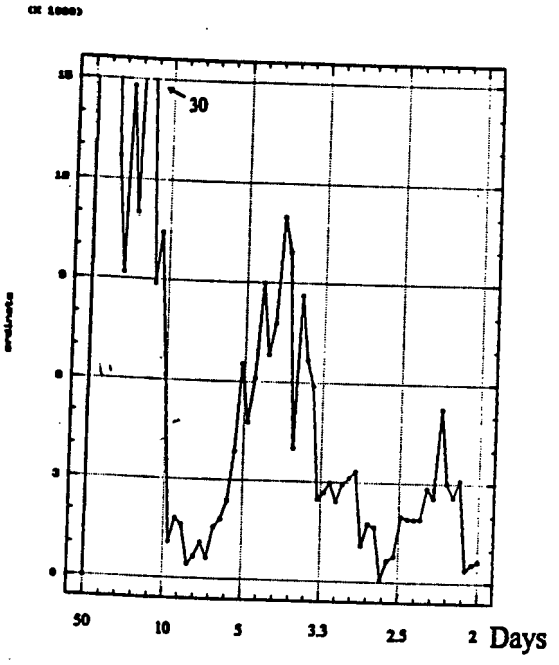

Figure 4.21.f: Periodogram of the mean daily rainfall in the NW region for the summer 1991

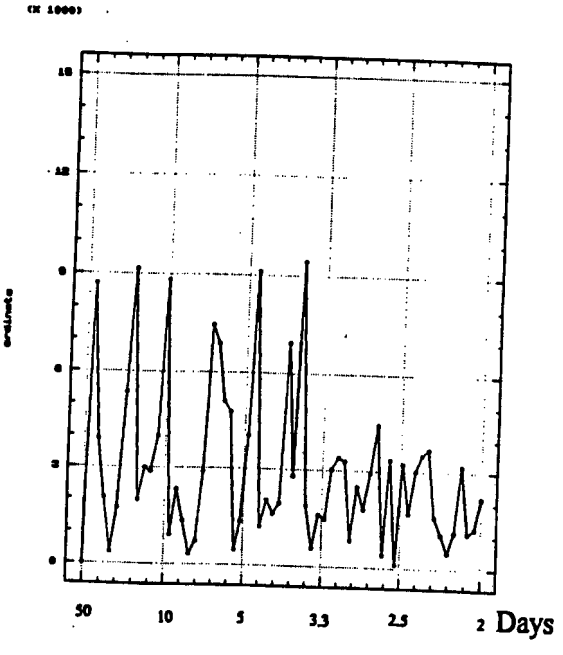

Figure 4.21.g: Periodogram of the mean daily rainfall in the NW region for the summer 1992

CHAPTER 5

COMPOSITE CLIMATOLOGY FOR EXTREME RAINFALL EVENTS

In this Chapter, ECMWF data are composited to study the evolution of extreme rainfall events over NW Madagascar. As outlined in Chapter 3, 16 events are selected and the field data averaged over a time frame from -4 to +2 days. The meteorological patterns, processes and dynamics are most evident through analysis of departures from historical mean conditions.

5.1 Anomaly composite analysis :

The anomaly results presented below form the major focus of this thesis. Changes taking place from day-4 to day+2 of the composite wet event are clearly shown in the anomaly sequences. These are based on 16 selected days minus the two-month mean discussed in Chapter 4.

5.1.1 Dynamic and kinematic structure :

5.1.1.1 The Geopotential height :

At the lower level the sequence generally illustrates a negative anomaly area over the east coast of Africa and the Channel, while at the upper-level an area of positive anomaly to the east of Madagascar moves westward (Fig 5.1). A prominent feature is strong negative anomalies in the upper level over the mid-latitudes.

At day-4, in the 1000 hPa level an area of negative anomalies exists with a maximum of -8 gpm to the east and west of Madagascar along the 15°S latitude. A

positive anomaly is located to the southwest of the Mozambique Channel and negative anomalies to the east. In the upper level a positive anomaly of 2 gpm in the Indian Ocean lies to the north of the Mascarenes and a strong negative anomaly area (< -60 gpm) is to the south of Madagascar. Two days after at day-2, in the 1000 hPa level, the systems weaken and an area of positive anomaly (5°S, 20°E) moves southward. In the 200 hPa level, the area of positive anomaly moves toward Madagascar while intensifying (10 gpm) and the area of negative anomaly to the south of the island weakens (-34 gpm). At day 0 the area of negative anomaly at the surface deepens to value of -10 gpm with a maximum over the west coast of Madagascar. The positive anomaly area over the west part of southern Africa increases to a value of 8 gpm. In the upper level the area of positive anomaly intensifies up to 14 gpm with maximum off the east coast of Madagascar (17°S, 52°E) extending westward over Africa. At day+2, there is a belt of negative anomalies extending from Mozambique eastward along the latitude band 15-30°S at the surface. In the upper level, the positive anomaly area weakens to the value of 8 gpm while moving southwestward over the south part of the Mozambique Channel. A quasi-stationary negative anomaly in the mid-latitudes prevails trough the sequence, and adjusts to the poleward intrusion of the positive anomaly. This highlights a degree of convective forcing by long wavelength westerly waves in the SWIO.

5.1.1.2 Vertical temperature gradient:

In the upper level, the temperature gradient between 500-100 hPa shows an area of unstable positive anomaly moving westward from the northwest of Mauritius while increasing from day-4 to day 0. The area of negative anomaly to the south of the Channel at day-4 weakens while moving eastward (Fig 5.2.a). In general the pattern is similar to the 200 hPa geopotential anomalies.

Four days prior to the event, there is a positive anomaly area 0.8°C located at 15°S-62°E in the Indian Ocean. At day-2, that area moves over the northern part of the Channel (14°S, 46°E) while intensifying to the value of 1°C and extending a ridge toward the Mascarenes. At day 0, the positive anomaly area covers the region north of 25°S with its maximum value (1.4°C) over the north of Madagascar. Two days after the event, the positive area of maximum upper instability moves to the southern part of the Mozambique Channel.

5.1.1.3 Vertical wind :

The 500 hPa level (Fig 5.2.b) shows an area of positive anomaly 4 x 10^{-1} Pa s^{-1} (sinking) over SE Africa at day-4. A weak positive anomaly 2 x 10^{-1} Pa s^{-1} over Madagascar strengthens at day-2. Over the Mozambique Channel an area of negative anomaly weakens; also off the east of Madagascar up to Reunion island another negative anomaly area intensifies up to -4 x 10^{-1} Pa s^{-1}. It appears that negative (rising motion) anomalies over east Africa and the SWIO converge onto Madagascar from day-2 to 0. At day 0 an area of negative anomaly expands from the Mascarenes into the Channel, then moves east at day+2 while over Madagascar there is an area of positive anomaly of 4 x 10^{-1} Pa s^{-1}.

5.1.1.4 Horizontal winds :

Four days prior to the extreme rainfall event (day-4), at the surface a cyclonic vortex is found in the SWIO to the northeast of Reunion at 15°S, 60°E (Fig 5.3); over the Mozambique Channel the anomalous wind flow converges toward the Mozambique coast from Madagascar, and from the subtropical area south of the Channel. In the Indian Ocean, the flow from the subtropical easterlies in the latitude band 20-30°S converges toward the southeast. In the 200 hPa level, the surface cyclonic flow anomaly is superposed with an anticyclonic anomaly

area. There exists a trough oriented NW-SE over southern Africa with strong northwesterly flow to the east of it. Two days later (day-2), at the surface the cyclonic vortex moves to the northeast coast of Madagascar in the I-O and the easterly anomaly over the tropics weakens. In the Mozambique Channel northerly monsoon flow (10 m s^{-1}) surges toward NW Madagascar. In the southern part of the Mozambique Channel a northerly flow anomaly is found off the Mozambique coast into the subtropics. The upper-level anticyclonic circulation has moved over the NW Madagascar with northwestward outflow while in the latitude band 20-30°S a subtropical jet of westerlies converges over the southern tip of the island. A trough axis moves over the Channel. At day 0, the 1000 hPa wind pattern shows that the cyclonic vortex moves into the Channel off the west coast of Madagascar and the monsoon surge still prevails over the NW. In the I-O east of 55°E, the easterly flow anomaly is replaced by a westerly flow anomaly. In the upper level, there is a zonal ridge along 20°S from Zimbabwe to Madagascar, and a trough axis is located over the south of the island. Two days after the event (day+2), in the 1000 hPa level the cyclonic circulation is over the west coast of Madagascar but the monsoon flow anomaly has weakened. In the I-O a cyclonic circulation forms over Mauritius. In the upper level the trough axis moves to the SE of Mauritius and the anticyclonic circulation is well organized over Zimbabwe with continued northwesterly outflow over Madagascar.

5.1.1.5 Divergence :

Four days prior to the extreme rainfall event, the surface level shows an area of negative -2 x 10^{-6} s^{-1} anomaly over the east coast of Africa and positive anomaly 2 x 10^{-6} s^{-1} over Madagascar as well as over the southern tip of Africa which extends into the subtropics southeastward. In the upper level, the pattern is reversed, negative over Madagascar and the Mascarenes as well as over the

southern tip of Africa, and positive over the east coast of Africa and the Channel. Two days prior to the event (day-2), at the surface the positive anomaly area over Madagascar is confined over its west part separating a negative anomaly area over the north of the Channel and a second one to the west of Reunion. Noteworthy is also the negative anomaly area -3 x 10^{-6} s^{-1} over the southeast coast of South Africa. In the 200 hPa level exists a band of positive divergence oriented NW-SE from 5°S, 20°E up to 35°S, 65°E with its maximum value 3 x 10^{-6} s^{-1} to the east of Madagascar and a negative anomaly of -3 x 10^{-6} s^{-1} over the SW of the island. At day 0 the low-level negative area expands over the Channel up to the east of Madagascar while a positive area of 2 x 10^{-6} s^{-1} persists to the north of the Mozambique Channel. In the upper level the band of positive anomaly is shifted eastward to be located off the east coast of Tanzania extending to 40°S, 75°E with its maximum value 3 x 10^{-6} s^{-1} off the east coast of the Island. Two days after the event (day+2), the surface-level pattern shows that the positive anomaly to the north of Madagascar extends in a ridge into the NW of the island and there are negative anomaly areas over the northeast coast of Mozambique, over the southeast coast of South Africa and over the Mascarenes in the I-O. In the 200 hPa level, the band of positive anomaly splits into three cells with maximum value 4 x 10^{-6} s^{-1} over the Mascarenes (Fig 5.4).

5.1.1.6 Vorticity :

Four days prior to the event, there is in the 1000 hPa level a cyclonic vorticity anomaly (-4 x 10^{-6} s^{-1}) centered at 10°S, 60°E in the I-O and a second one (-8 x 10^{-6} s^{-1}) to the SE of Madagascar. In the south part of the Mozambique Channel, there is an anticyclonic vorticity anomaly (4 x 10^{-6} s^{-1}) centered off the SW coast of the island. It is worth mentioning the existence of a weak cyclonic vorticity anomaly over the NE coast of Mozambique. In the 200 hPa level, in the I-

O there is exists an anticyclonic vorticity anomaly (8 x 10^{-6} s^{-1}) at 15°S, 57°E; and over southern Africa there is a cyclonic vorticity anomaly (-12 x 10^{-6} s^{-1}). Two days prior to the event, the 1000 hPa surface level shows that the cyclonic circulation anomaly in the I-O weakens and is located over the NE coast of Madagascar. The cyclonic vorticity anomaly from the Mozambique coast moves over the Channel while the positive vorticity anomaly area persists over the SW tip of Madagascar. The upper-level pattern shows that the anticyclonic vorticity anomaly strengthens to the value of 10 x 10^{-6} s^{-1}, and moves over the NW of the island, while the cyclonic vorticity anomaly over southern Africa is intensified to -16 x 10^{-6} s^{-1} and moves eastward to be located to the south of the island at 35°S, 47°E. The vorticity anomaly field shows at day 0 that the negative anomaly area over the Channel moves southeastward reaching the value of -4 x 10^{-6} s^{-1} off the west coast of Madagascar. In the I-O the second cyclonic anomaly moves to the NW of Reunion. In the upper level, the area of positive anomaly shifts southeastward, while in the subtropics an area of negative anomaly from South Africa continues its eastward movement. Two days after the event, the surface-level pattern shows the two negative cell anomalies are now one over Madagascar and is joined by another cell over Mauritius with the same intensity (-4 x 10^{-6} s^{-1}). In the upper level, the positive anticyclonic vorticity anomaly from the I-O moves to the south of the Channel and is linked with the second one over the southern Africa (Fig 5.5.a and b).

The divergence and vorticity patterns indicate that the low-level convective area shifts from the Mozambique coast to Madagascar throughout the process. The lower-level convergence is superposed with an upper-level divergence up to day 0 then the systems tilt afterward.

The kinematic analysis indicates the existence of diffluent upper-level westerlies inthe sub-tropics before and during the event which steered the TC

southeastward and enhanced anticyclonic outflow. Intensification of a TC under conditions of westerly shear is a characteristic of the Mozambique Channel.

5.1.2 Moisture and thermodynamic results :

5.1.2.1 Precipitable water :

Vertically integrated water vapour from the surface to 300 hPa shows that the state of the atmosphere over the Island changes from relatively dry to wet within four days (Fig 5.6.a).

At day-4, an area of negative anomaly of -2 mm exists over Madagascar, while to its west over Mozambique exists an area of positive anomaly of 2 mm. To the south of the Channel, there is also a negative anomaly of -4 mm extending toward South Africa. Two days later (day-2), the pattern shows that the negative anomaly over the island has moved southward and merges with one to the south of the Mozambique Channel. The positive anomaly over Mozambique extends eastward over the Channel. At day 0, the area of positive anomaly moves over the island and its value increases up to 3 mm. Two days later, the positive cell anomaly continues its eastward movement and is now centered at 17°S, 60°E over the Mascarenes. In general the movement of the positive PW anomalies is eastward from Africa to Madagascar.

5.1.2.2 Vertical gradient of specific humidity :

The vertical gradient of the specific humidity field (Fig 5.6.b) shows that four days prior (day-4) to the event, there is an area of positive anomaly to the north of the Channel as well as over northern Mozambique and another one off the SW coast of South Africa; in the I-O there is a negative anomaly cell of -8×10^{-1} g kg^{-1} located at 10°S, 55°E which indicates convective mixing in the surface layer.

Two days later, the positive anomaly shifts NW and increases to a value of 4 x 10^{-1} g kg^{-1} centered at 5°S, 25°E extending up to 25°S. A second positive cell to the north of the Mozambique Channel expands over the sector; while the negative anomaly in the I-O elongates southward up to Madagascar. At day 0, the positive cell anomaly to the north of the Channel intensifies up to 4 x 10^{-1} g kg^{-1} and extends over the north region of the island. The positive cell retreats northward at day+2. The area to the north of Madagascar is an area of sharp vertical moisture gradients indicative of an evaporative source region.

5.1.2.3 Water vapour flux :

The pattern of integrated water vapour flux (WVF) from the surface to 500 hPa shows some similarity with the lower level wind circulation, that is the existence of an area of cyclonic circulation anomaly over the Indian Ocean (15°S, 60°E) moving toward the Mozambique Channel and strengthening of the monsoon flux (Fig 5.7.a).

At day-4, an anomalous flux associated with the cross equatorial monsoon is found off the east coast of Africa and northern Madagascar which flows into the cyclonic circulation in the I-O. To the south of the Mozambique Channel a westerly trough appears which promotes the confluence of subtropical flows and the trade wind anomalies. Two days prior to the heavy rainfall event, the northwesterly monsoon flow anomaly strengthens and converges onto the NW of the island while the I-O cyclonic circulation moves over its east coast. Simultaneously the trade wind anomaly becomes northeasterlies. The monsoon inflow continues to strengthen and converges on the northwest of Madagascar at day 0, and the cyclonic circulation is now off the west coast of the island. In the I-O the trade wind anomaly is replaced by a westerly flow anomaly. Two days after the event, the monsoon flow anomaly and the southerly flow anomaly from the

south of the Mozambique Channel converge on the NW region of the island to merge with the westerly flow anomaly in the I-O.

5.1.2.3 Velocity potential of water vapour flux :

At day-4 an area of positive anomaly (convergence) of 4.5 x 10^9 kg s^{-1} over the Channel and a negative anomaly (divergence) cell of -1 x 10^9 kg s^{-1} over the NE coast of Madagascar is noted in the velocity potential of WVF integrated from the surface to 500 hPa. In the I-O to the east of Mauritius, there is also a positive anomaly cell indicating a convergence of WVF over the area. Two days prior to the event, the pattern shows that the negative anomaly area extends meridionally from the north to the south of the Mozambique Channel with two cells of maxima, one to the north of Madagascar at 7°S, 45°E (-2 x 10^9 kg s^{-1}) and the other over the south tip of the island (-1.5 x 10^9 kg s^{-1}). The positive anomaly area in the I-O moves over the Mascarenes. At day 0, the positive anomaly area is intensified to the value of 4.5 x 10^9 kg s^{-1} and moves over Madagascar while to the north of the island there is a negative cell anomaly. Two days after the heavy rainfall event, there is a negative cell anomaly over Mozambique and a second one to the NE of Madagascar extending up to the northern part of the island, which indicates divergence of WVF. The area of positive cell anomaly moves southward to be located south of the island extending from the SE coast of South Africa to the Mascarenes with a SW-NE axis (Fig 5.7.b and 5.8.a). Prominent in the vector representations is the southward monsoon flux at day-2 and 0.

5.1.2.4 Streamfunction of water vapour flux :

At day-4, the streamfunction of WVF integrated from the surface to 500 hPa shows that there is a positive anomaly area over the region, with a strong value of 10 x 10^9 kg s^{-1} located at 15°S, 62°E in the I-O which indicates the

existence of cyclonic circulation in that sector. At day-2, it moves over the Mozambique Channel while weakening to a value of 4 x 10^9 kg s^{-1}, and negative anomaly areas develop to the east and SE of Madagascar with -5 x 10^9 kg s^{-1} and -2 x 10^9 kg s^{-1} respectively. At day 0 the positive anomaly area expands from east Africa to Madagascar with two maxima of 5.5 x 10^9 kg s^{-1} each, one over Mozambique and the other over Madagascar while the negative cell anomaly in the I-O weakens (-3 x 10^9 kg s^{-1}). The tight gradient over the north of the island indicates that the monsoon inflow is stronger in that sector. Two days later, the pattern shows that the positive anomaly area moves eastward (Fig 5.8.b).

5.1.2.6 Equivalent potential temperature :

The pattern (Fig 5.9.a and b) shows at the lower level an eastward moving positive anomaly of higher equivalent potential temperature (EPT) from the east coast of Africa which suggests that the convective area starts from northern Mozambique and moves southward toward the island.

At day-4, the 1000 hPa level shows an area of positive anomaly of 3°K centered at 10°S, 25°E. In the 500 mb level, the pattern shows an area of positive anomaly oriented NW-SE crossing the north tip of Madagascar, with maximum value 1°K on the east coast of Africa to the north of the Channel and 0.5°K to the southeast of Mauritius. Two days later, the surface-level pattern shows that the positive cell anomaly weakens by 1°K while to the south of the island, there is a negative cell anomaly of -4°K centered at 30°S, 40°E. In the 500 hPa level the area of positive anomaly shifts south to cover Mozambique, the Channel, Madagascar and displays two maxima one over the Channel and the other off the east coast of the Island. At day 0, the surface pattern shows that the positive cell anomaly covers the region of the Channel up to the equator; and the 500 hPa level shows a positive cell centered off the east coast of the island with a value of 1.5°K. Two

days later the systems weaken; the 1000 hPa level shows that the positive area has shifted over Africa.

The section 5.1 and 5.2 showed that there is a cyclonic circulation anomaly moving southwestward from the central Indian Ocean. Strong NW monsoon is associated with strong pressure gradient between this cyclonic circulation anomaly and the anticyclone to the North of Madagascar at day-4. By day-2 an upper level anticyclonic circulation anomaly has moved and enhanced over NW Madagascar with prominent northwestward outflow. At day 0, the westerly ridge merges with the subtropical ridge and forms a strong easterly current emerges equatorward of the Zimbabwe-Madagascar high. The moisture source lies in the upstream region where meridional monsoon sureges originate.

5.1.3 Vertical section analysis of the 1000-100 hPa layer :

The vertical section analysis is carried out E-W zonally and N-S meridionally along fixed coordinates (16°S and 46°E) over NW Madagascar.

5.1.3.1 Vertical section of the divergence field :

The E-W vertical section of the divergence field along 16°S (Fig 5.10.a) indicates at day-4 the existence at the surface of a weak negative area over the interior of Africa, the Mozambique Channel, Mascarenes, and a positive anomaly area over Madagascar. In the upper level negative anomaly areas of -1×10^{-6} s^{-1} lay over Africa and Madagascar above 300 hPa. At day-2, a positive anomaly area develops over Africa in the mid-troposphere under a negative anomaly area of -2×10^{-6} s^{-1} aloft. Over the Channel and Madagascar, there is convergence in the lower level superposed with a divergence area at 200 hPa. At day 0, the lower-level convergence area extends from Mozambique to the Mascarenes and upward

to 300 hPa over Madagascar. Aloft the divergence area intensifies and extends westward. At day+2, in the lower level exists a positive anomaly area over Africa and Madagascar. The convergence area shifts eastward. In the upper level a negative anomaly area lays over Africa and a positive anomaly area from the Channel to the Mascarenes.

The N-S vertical section of the divergence field along 46°E (Fig 5.10.b) shows at day-4, the existence of a positive anomaly area in the lower troposphere in the tropics with a maximum value of 3×10^{-6} s^{-1} at 17°S; above this maximum divergence anomaly lays a negative area of -1×10^{-6} s^{-1} at 200 hPa. At day-2, the upper-level negative anomaly area strengthens and extends within the latitude band 10-35°S. At day 0, a weak negative anomaly lays in the lower troposphere over NW Madagascar. A positive anomaly of a maximum value of 5×10^{-6} s^{-1} develops at 200 hPa. At day+2, over NW Madagascar, there is a positive anomaly area in the lower level and a negative anomaly area above it at 200 hPa.

5.1.3.2 Vertical section of the vorticity field :

The zonal cross-section of the vorticity anomaly along 16°S (Fig 5.10.c) shows that at day-4, areas of negative (cyclonic vorticity) anomaly exist over Mozambique, the Channel and between 55-65°E in the lower level while the upper troposphere exhibits an area of positive (anticyclonic vorticity) anomaly with maximum value at 200 hPa. At day-2, the lower-cyclonic vorticity anomaly extends from Mozambique to Madagascar, superposed with a positive anomaly aloft which strengthens to a maximum value of 10×10^{-6} s^{-1} at 200 hPa. At day 0, the lower negative anomaly area extends from 25°S to 55°S in the lower and mid-troposphere while the positive area aloft shifts eastward. Two days later, the negative anomaly area dominates in the region between 35-60°E up to 250 hPa.

The meridional vertical section along 46°E (Fig 5.10.d) shows that at day-4, in the lower level there is an alternation between positive and negative area. At day-2, a weak positive-negative dipole area develops in the lower level to the north of 20° and aloft the pattern exhibits a negative-positive dipole with a maximum value of 12 x 10^{-6} s^{-1} and -18 x 10^{-6} s^{-1} at 200 hPa over 15 and 35°S respectively. At day 0, the negative area over 20°S strengthens and extends up to 300 hPa, the negative area aloft weakens. Two days later, the negative area continues to strengthen along 15-25°S throughout the troposphere.

5.1.3.3 Vertical section of the vertical wind field :

The E-W vertical section of the vertical wind along 16°S (Fig 5.10.e) reveals at day-4, the existence of an upward motion anomaly over the Mozambique Channel up to 200 hPa. Over Madagascar, a downward motion anomaly prevails in the lower troposphere. Above it, there is an upward motion anomaly extending upward. At day-2, over Africa lays an area of positive anomaly with a maximum value of 6 x 10^{-2} Pa s^{-1} at the 500 hPa level. To the east of Madagascar over 55°E, a deep negative anomaly extends up to 200 hPa. In the mid-troposphere, a positive anomaly area develops over Madagascar. At day 0, the upward motion anomaly intensifies and extends from the Channel to 65°E with a maximum value of -8 x 10^{-2} Pa s^{-1} in the mid-troposphere. At day+2, the upward motion anomaly confined over 55-65°E weakens while over the Channel and Madagascar a positive anomaly area develops with maximum value in the mid-troposphere.

The N-S vertical section of the vertical wind field along 46°E (Fig 5.10.f) reveals at day-4 the existence of a dipole positive-negative area anomalies tilting toward the equator with height, the positive area has a maximum value of 6 x 10^{-2} Pa s^{-1} at 300 hPa over 15°S and a negative area -6 x 10^{-2} Pa s^{-1}. At day-2, the

dipole system weakens and moves down with the positive area centered at 600 hPa and the negative at the surface. At day 0, the negative area deepens and extends throughout the troposphere over NW Madagascar. Two days later a positive anomaly area develops over the island with a maximum value of 8×10^{-2} Pa s^{-1} at 550 hPa.

5.1.3.4 Vertical section of the EPT field :

The zonal vertical cross-section of the EPT along 16°S (Fig 5.10.g) shows that there is a positive anomaly area in the lower troposphere at day-4 between 25 to 45°E from the surface up to 600 hPa. From day-2, this positive area increases upward to cover the troposphere at day 0 from the surface to 200 hPa level between 30 and 60°E. The EPT maxima moves eastward at day+2 by which time a negative anomaly area exists in the lower troposphere over the Mozambique Channel. The meridional cross-section along the 46°E (Fig 5.10.h) shows at day-4, the existence of positive anomaly areas in the lower troposphere up to 750 hPa level and in the middle troposphere from the equator to 5°S. These positive areas move south to be located at day 0 between 10 to 20°S extending from the surface to 200 hPa level. At day+2, in the mid-troposphere exists a negative anomaly area to the north of 10°S and a positive area to its south, while at the surface there is a negative anomaly area extending southward from 10°S. A significant feature is the surface layer negative EPT anomaly at day -4 and -2 near 20°S, 46°E which may offer useful operational forecast guidance prior to an extreme rainfall event.

5.1.3.5 Vertical section of the zonal wind field :

The N-S vertical section of the zonal wind field along 46°E (Fig 5.10.i) indicates at day-4, the existence of westerly wind anomalies throughout the troposphere to the south of 20°S and above 900 hPa to the north of 10°S. Over

NW Madagascar above 800 hPa exists an area of easterly wind anomalies. Two days later at day-2, a dipole regime of negative-positive anomaly areas develops aloft with a maximum values of -4 m s^{-1} and 10 m s^{-1} centered over 5°S and 30°S respectively at 200 hPa. A lower-level westerly anomaly develops over NW Madagascar. At day 0, the pattern is similar to day-2 but lower-level easterly anomalies develop in the subtropics. Two days later, the dipole system aloft weakens and in the lower and mid-troposphere over the NW region of the island the westerlies intensify with a maximum of 4 m s^{-1} at 700 hPa.

The composite ECMWF weather anomalies demonstrate that four days prior to the heavy rainfall event, there exists an area of strong convection over the east coast of Africa extending toward the NW Madagascar area, associated with low-level cyclonic vorticity; and a post frontal high pressure cell to the south of the Mozambique Channel overlaid by an upper trough. The wind flow and WVF show that in the lower level the monsoon surges over the northern Mozambique Channel two days prior to the event, while the trade winds weaken over the Indian Ocean. In the upper level the superposition of an anticyclonic circulation with diverging northwestward outflow completes the necessary conditions for extreme rainfall.

The analysis indicates that there is:

1] Increased instability and uplift over Mozambique and an eastward shift to Madagascar, coincident with strengthening of upper level divergence over the island.

2] an intensification of low-level cyclonic vorticity over the Mozambique Channel and a strengthening of upper anticyclonic vorticity, assisted by the sub-tropical jet.

3] a surge of monsoon flow and weakening of trade wind easterlies in the low levels, and development of northwestward outflow aloft.

4] an eastward shift in the velocity of the WVF field indicating moisture convergence and wave-CISK over the island.

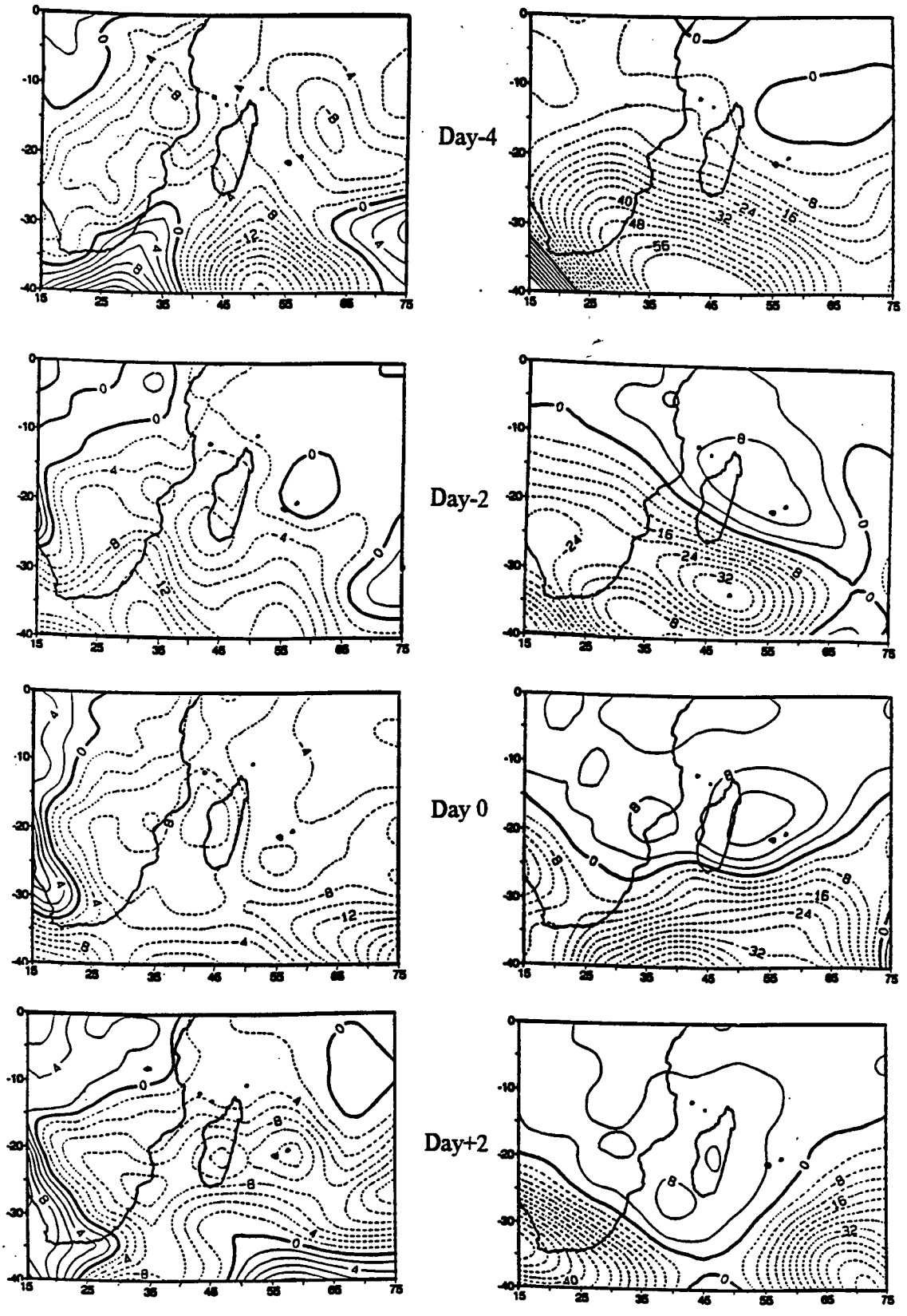

Figure 5.1.a: Geopotential height anomalies at 1000 hPa for day-4 to day+2. Contour interval 2 gpm.

Figure 5.1.b: Geopotential height anomalies at 200 hPa for day-4 to day+2. Contour interval 4 gpm

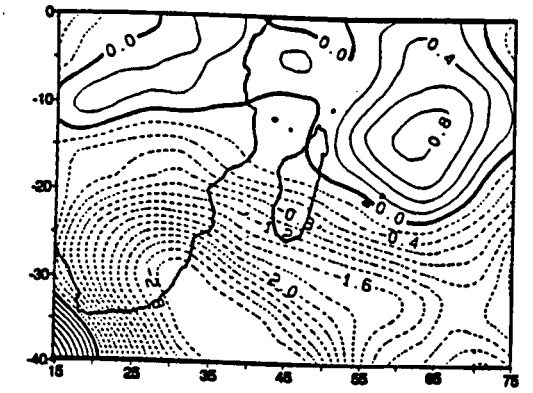

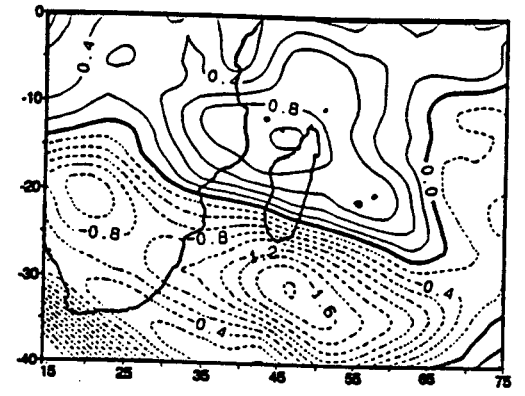

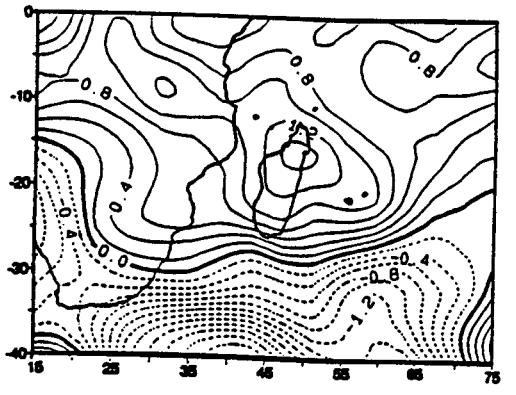

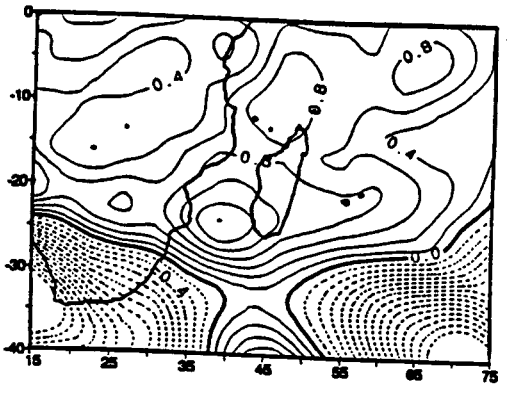

Figure 5.2.a: Temperature gradient anomalies between 500-100 hPa for day-4 to day+2. Contour interval 0.2°C

Day-4

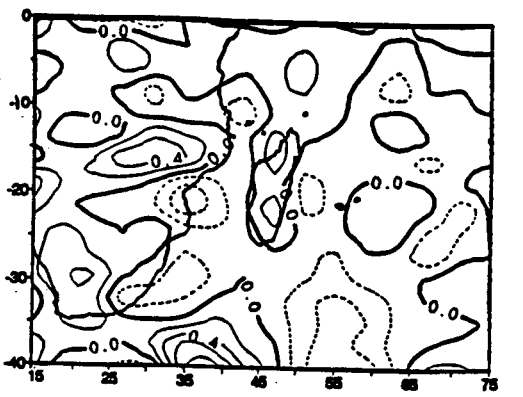

Day-2

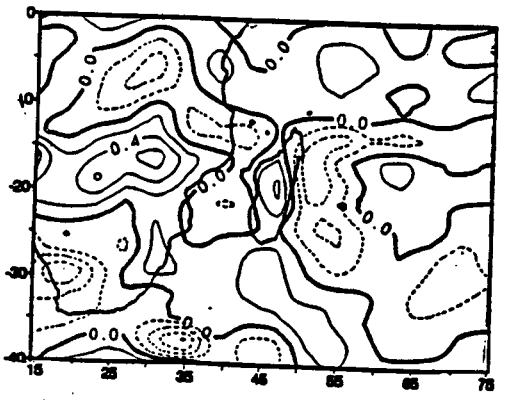

Day 0

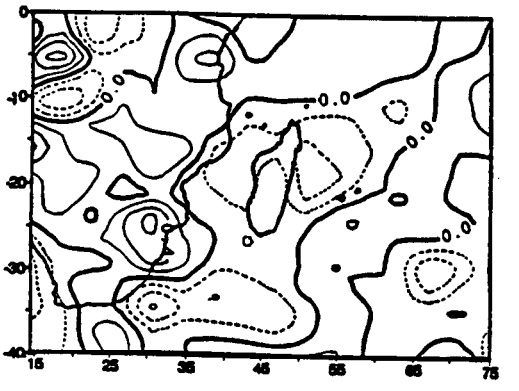

Day+2

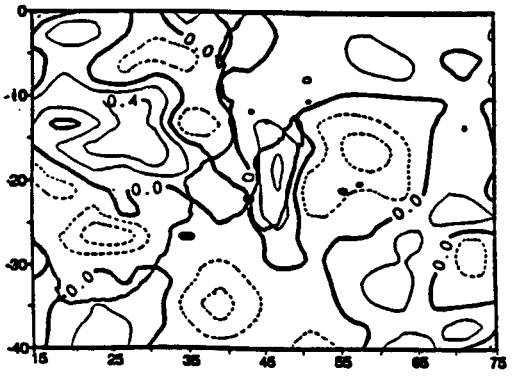

Figure 5.2.b: Vertical wind anomalies at 500 hPa for day-4 to day+2. Contour interval 0.2 Pa s^{-1}

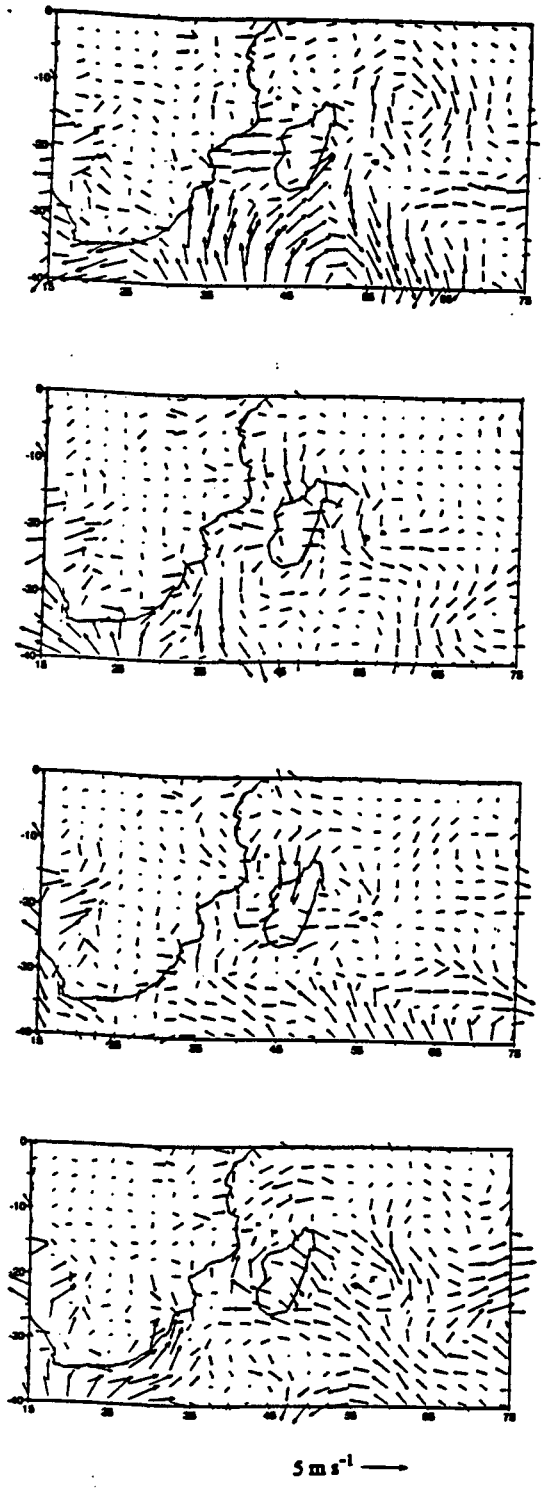

Figure 5.3.a: Horizontal wind anomalies at 1000 hPa for day-4 to day+2.

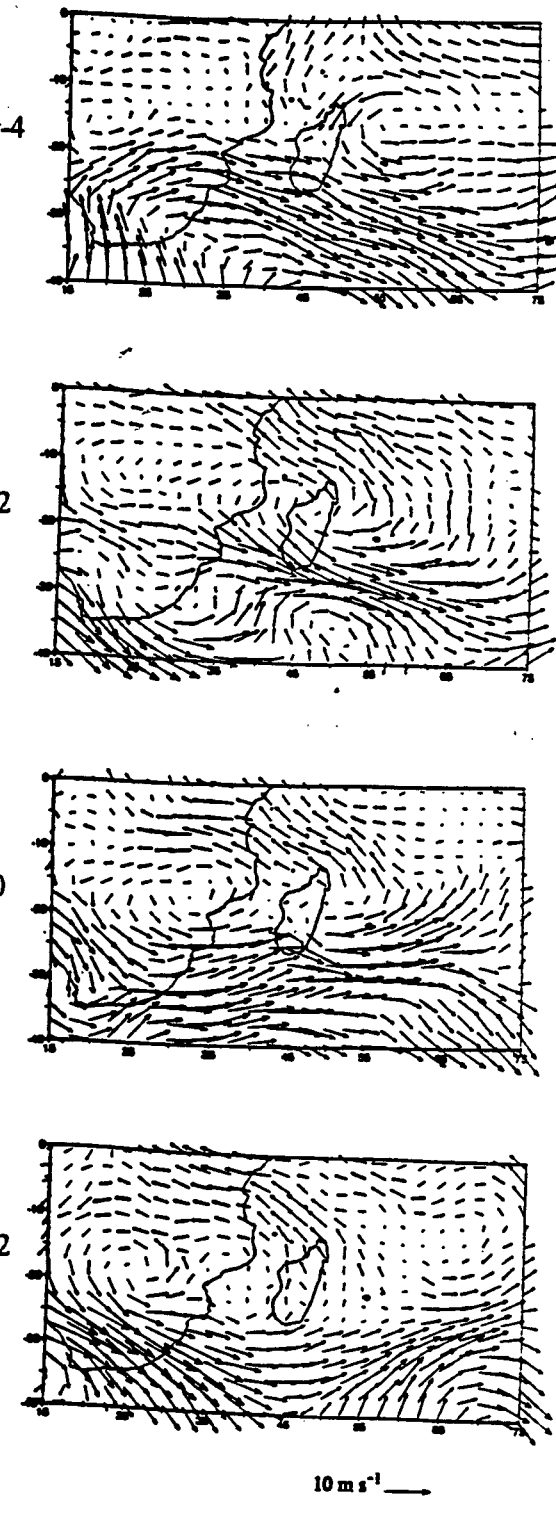

Figure 5.3.b: Horizontal wind anomalies at 200 hPa for day-4 to day+2.

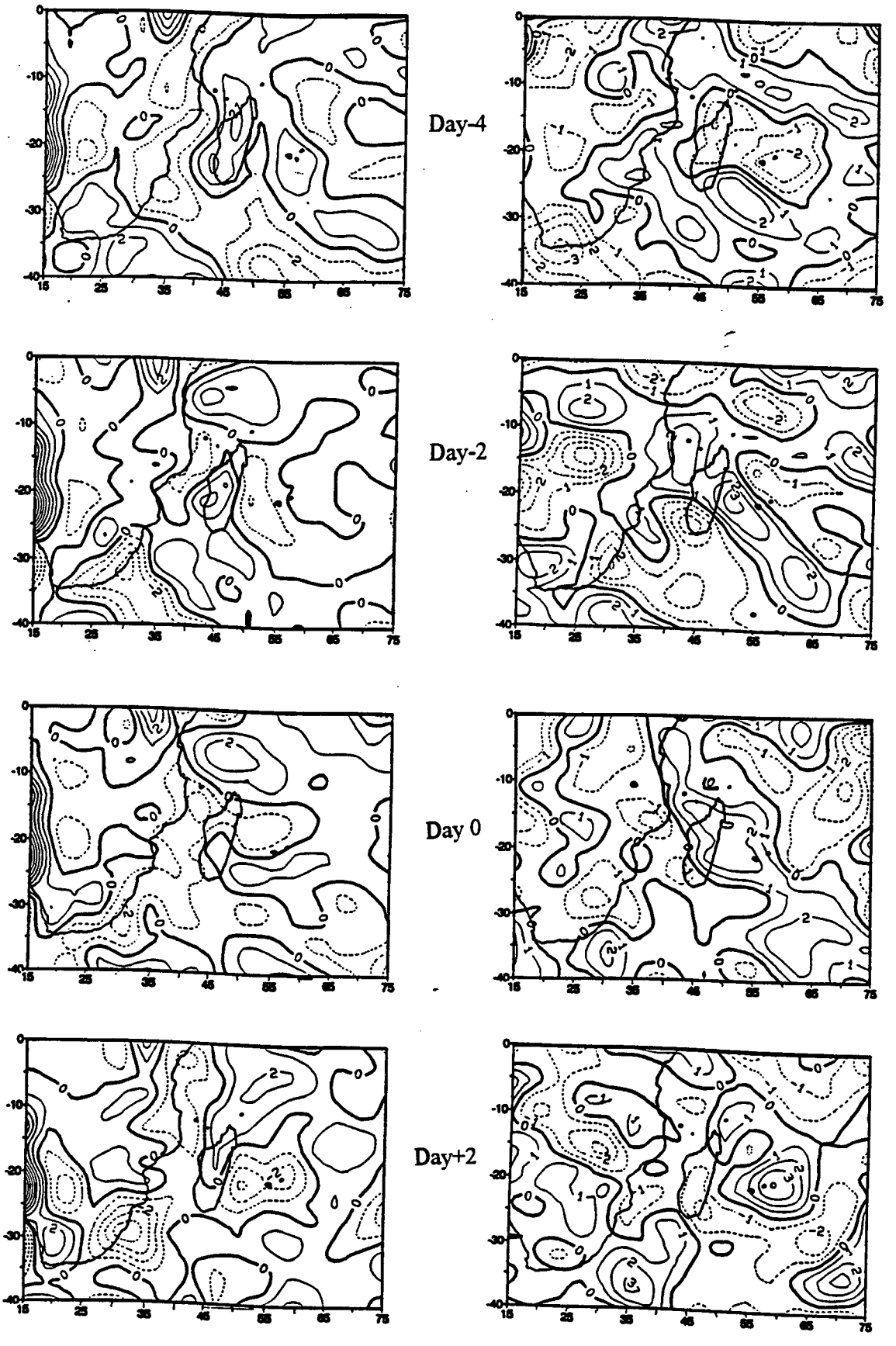

Figure 5.4.a: Divergence anomalies at 1000 hPa for day-4 to day+2. Contour interval 1 x 10^{-6} s^{-1}

Figire 5.4.b: Divergence anomalies at 200 hPa for day-4 to day+2. Contour interval 1 x 10^{-6} s^{-1}

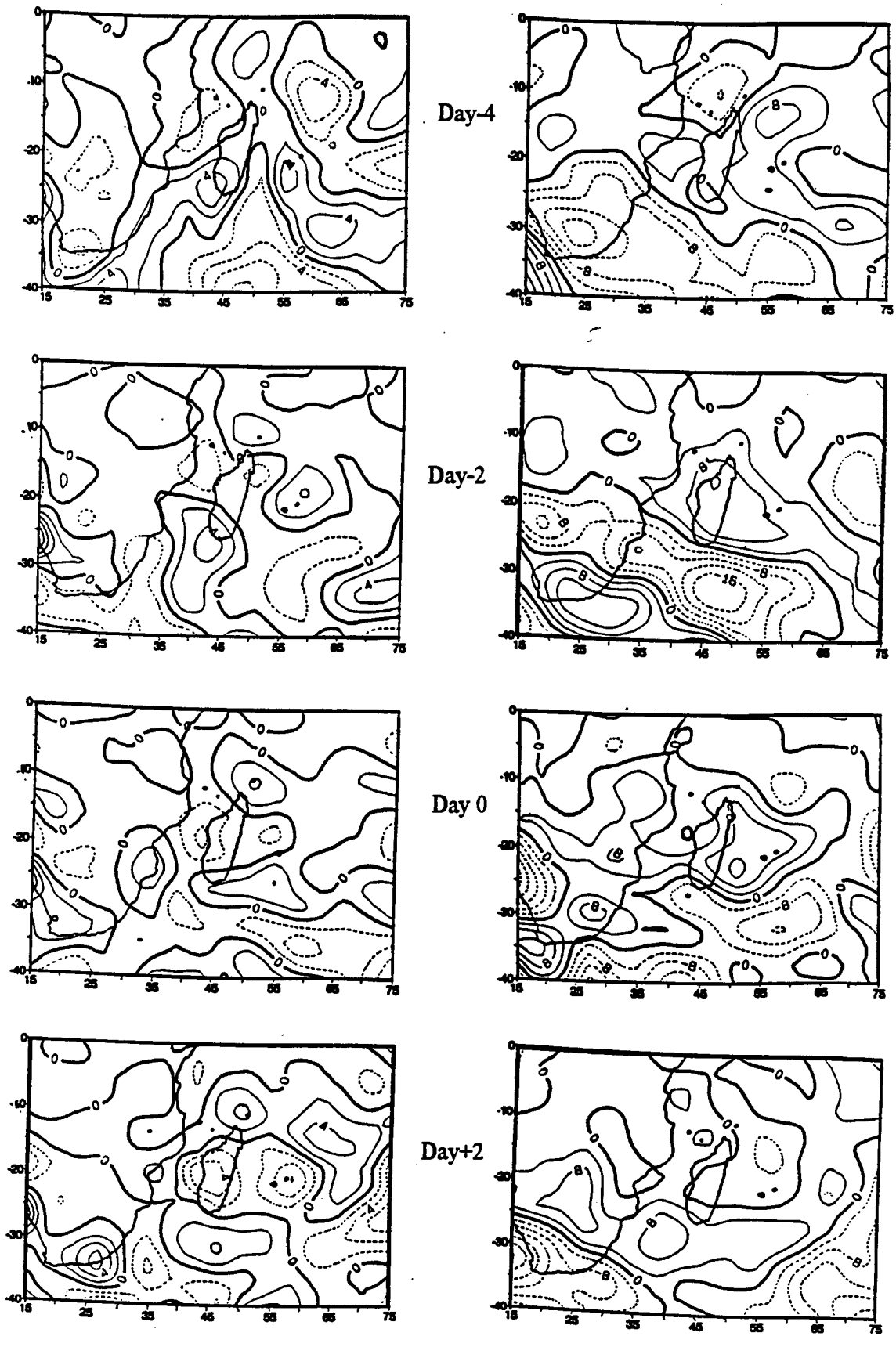

Figure 5.5a: Vorticity anomalies at 1000 hPa for day-4 to day+2. Contour interval 2 x 10^{-6} s^{-1}

Figure 5.5.b: Vorticity anomalies at 200 hPa for day-4 to day+2. Contour interval 4 x 10^{-6} s^{-1}

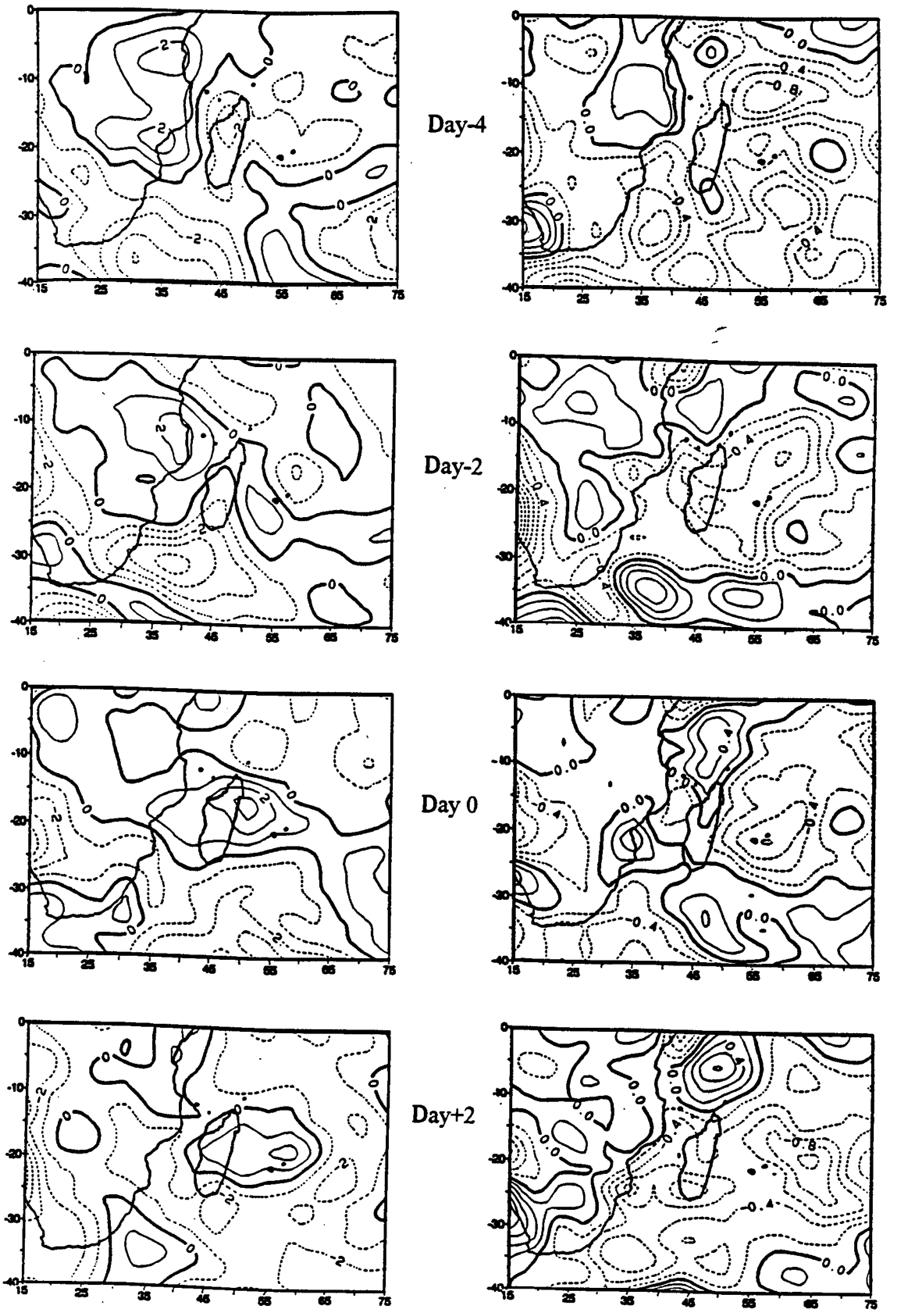

Figure 5.6.a: Precipitable water anomalies integrated from the surface up to 300 hPa for day-4 to day+2. Contour interval 1 mm.

Figure 5.6.b: Gradient specific humidity anomalies between 1000-850 hPa for day-4 to day+2. Contour interval 0.2 g kg^{-1}

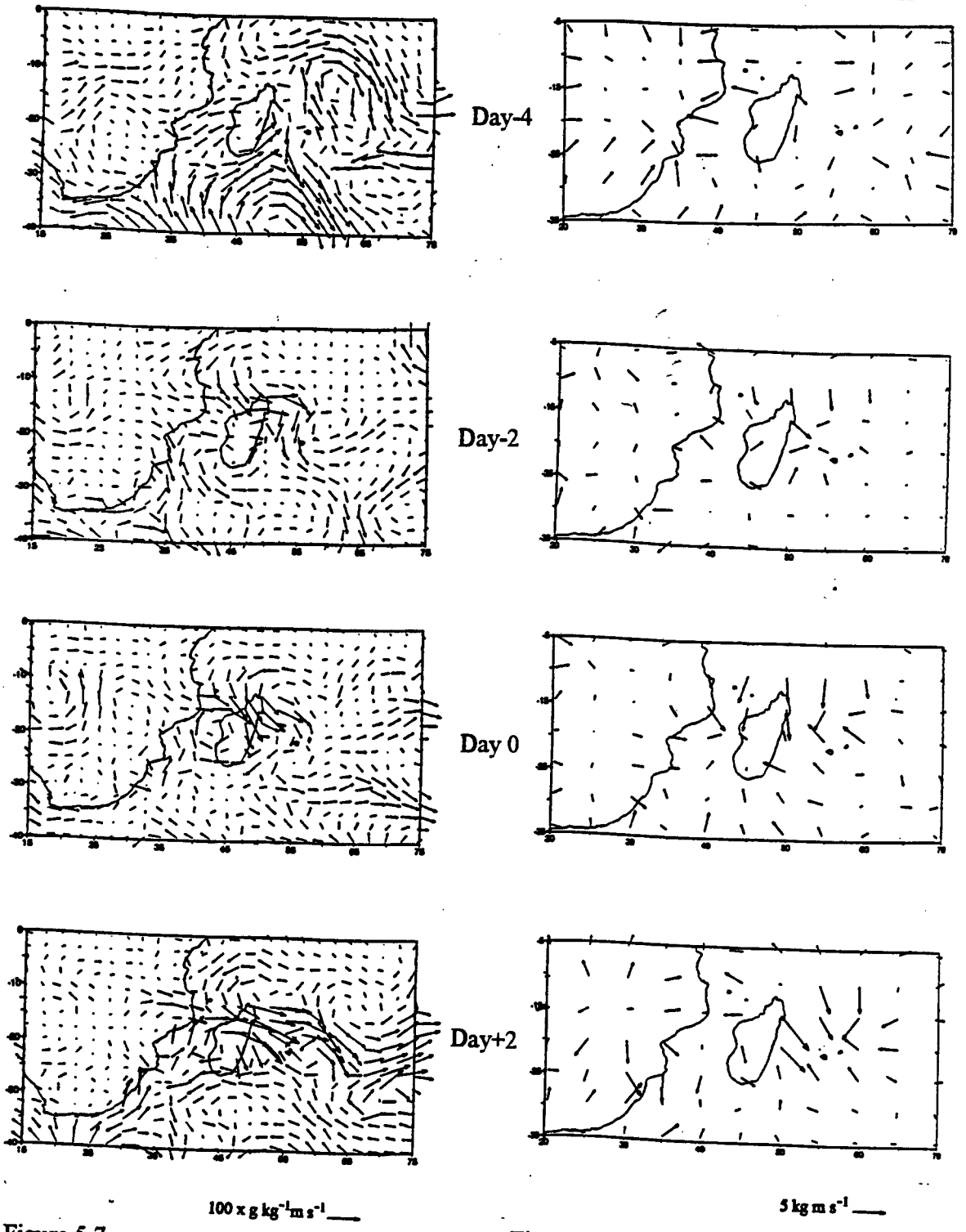

100 x g kg^{-1}m s^{-1}

Figure 5.7.a: Water vapour flux anomalies integrated from the surface to 500 hPa for day-4 to day+2.

5 kg m s^{-1}

Figure 5.7.b: Divergent water vapour flux (Q_{div}) integrated from the surface to 500 hPa for day-4 to day+2.

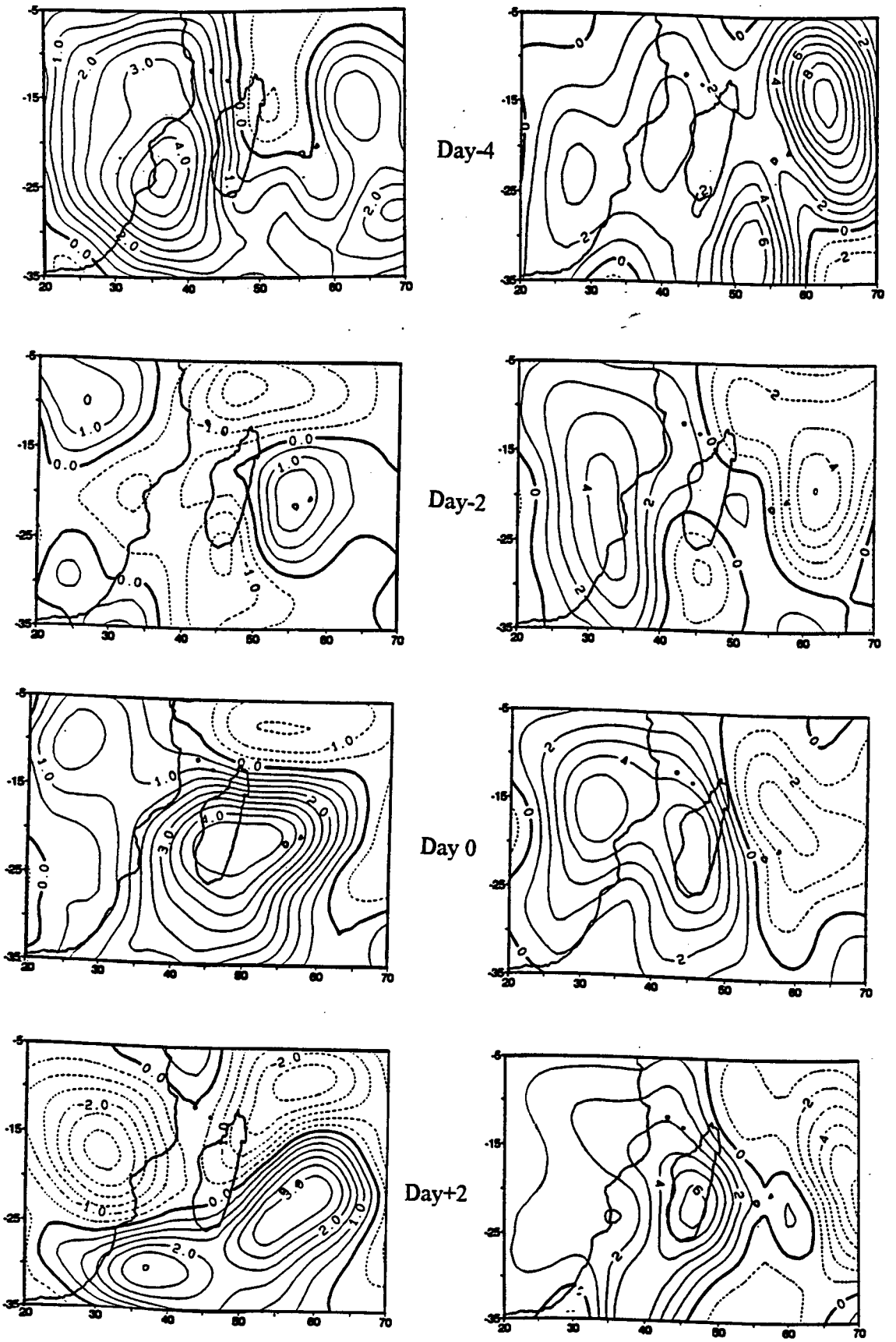

Figure 5.8.a: Velocity potential of water vapour flux (χ_Q) anomalies integrated from the surface to 500 hPa for day-4 to day+2. Contour interval 0.5 x 10^8 kg s^{-1}

Figure 5.8.b: Streamfunction of water vapour flux anomalies integrated from the surface to 500 hPa for day-4 to day+2. Contour interval 1 x 10^8 kg s^{-1}

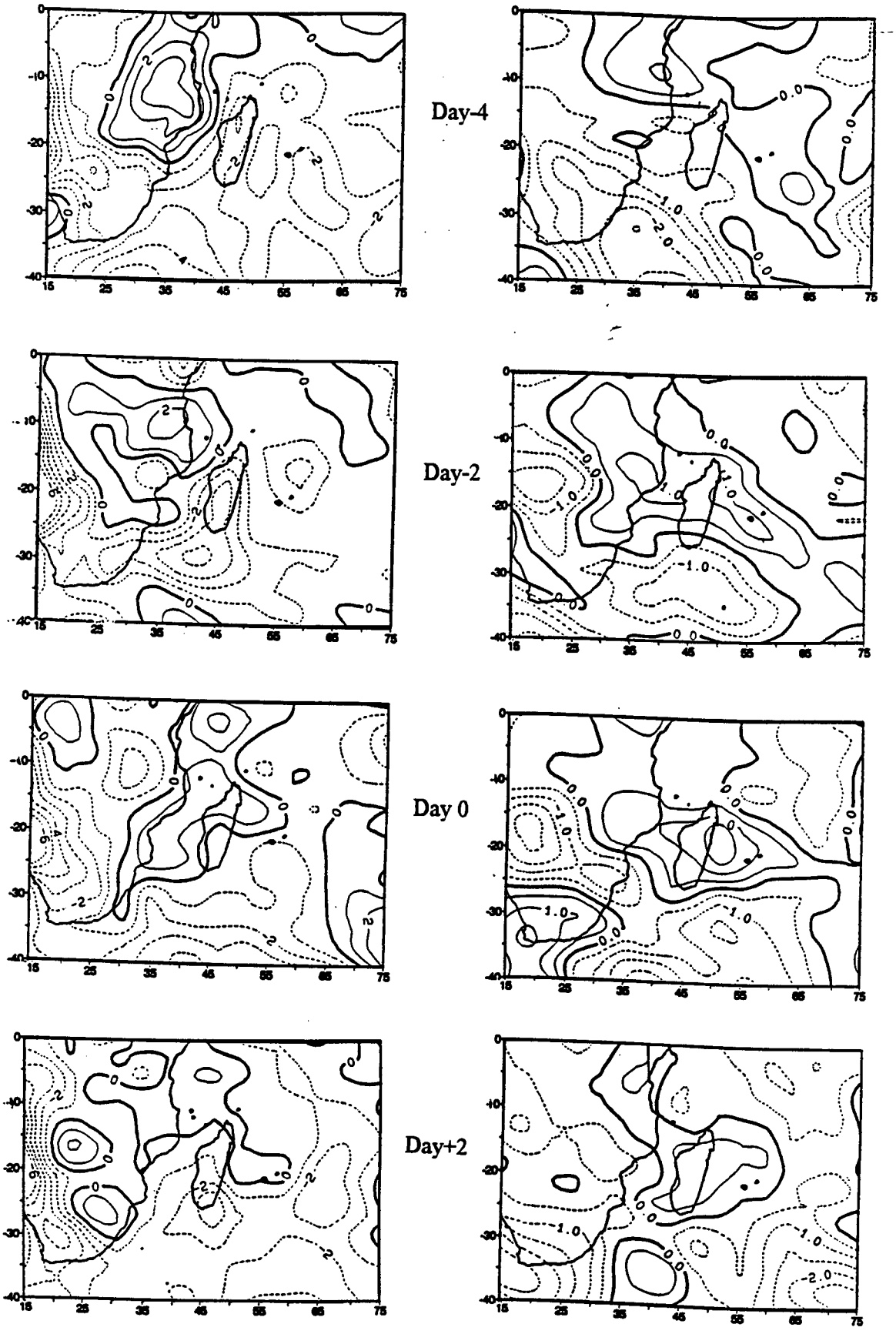

Figure 5.9.a: Equivalent potential temperature anomalies at 1000 hPa for day-4 to day+2. Contour interval 1°K

Figure 5.9.b: Equivalent potential temperature anomalies at 500 hPa for day-4 to day+2. Contour interval 0.5°K

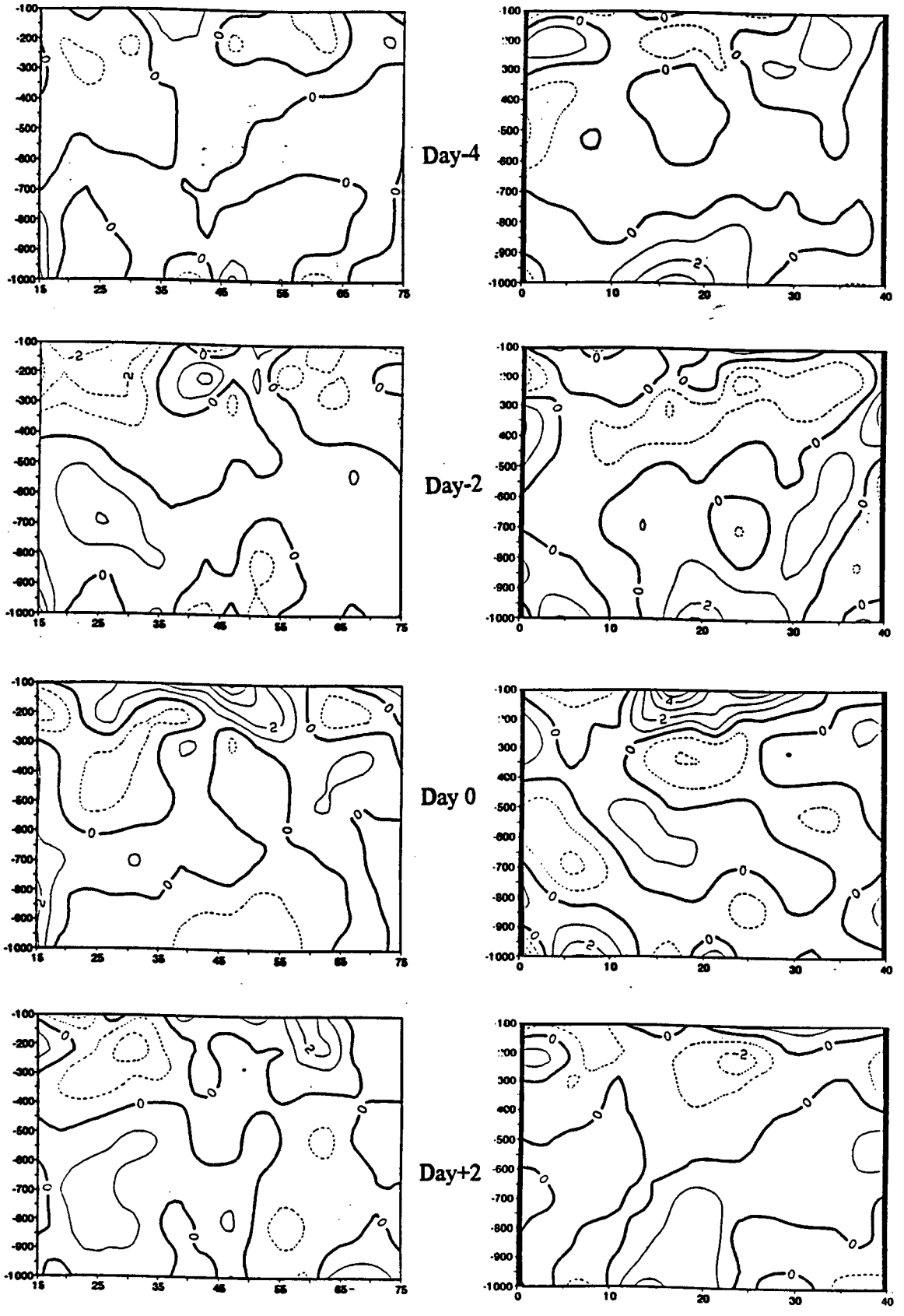

Figure 5.10.a: Vertical section of divergence anomalies along 16°S for day-4 to day+2. Contour interval 1 x 10^{-6} s^{-1}

Figure 5.10.b: Vertical section of divergence anomalies along 46°E for day-4 to day+2. Contour interval 1 x 10^{-6} s^{-1}

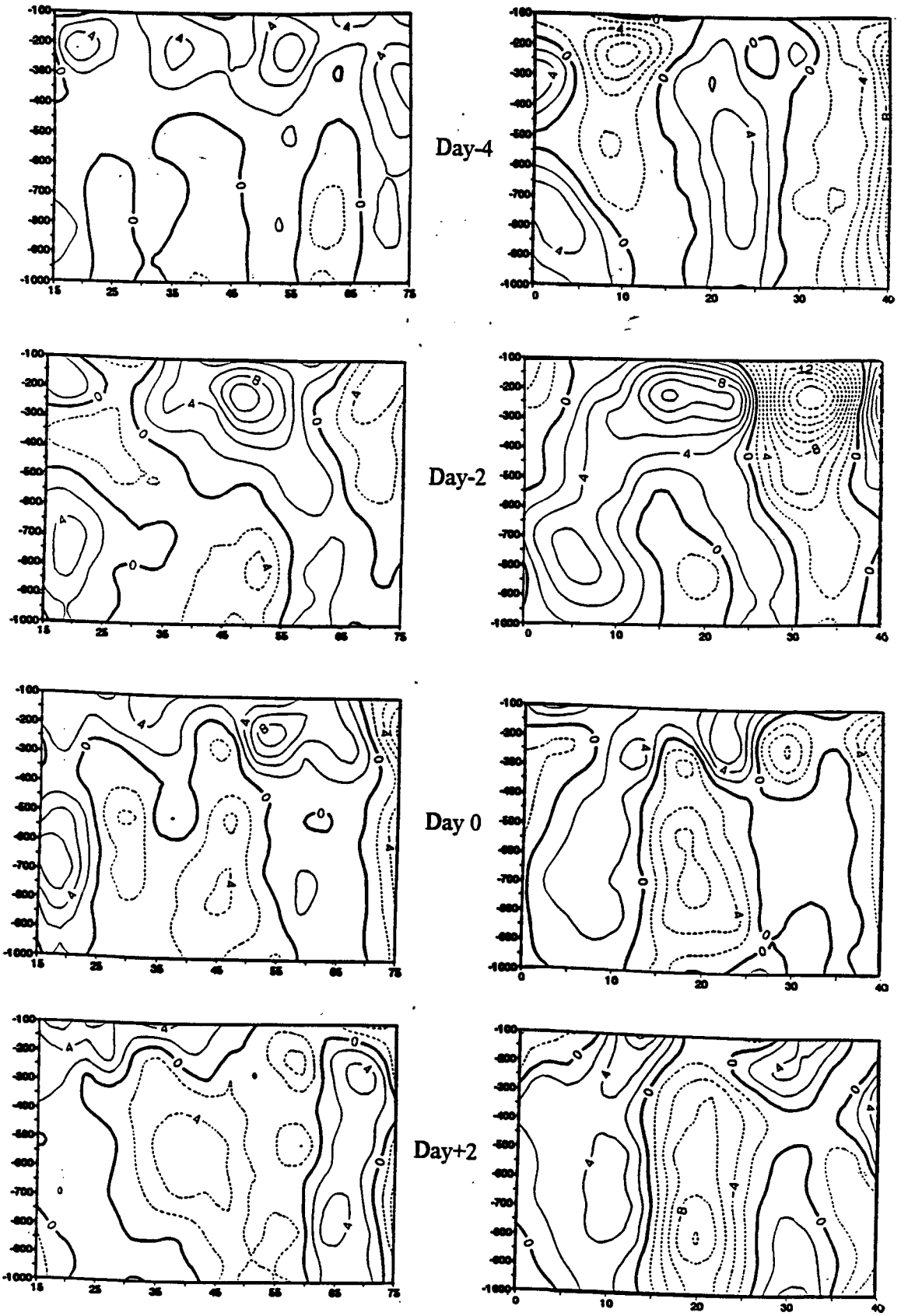

Figure 5.10.c: Vertical section of vorticity anomalies along 16°S for day-4 to day+2. Contour interval 2 x 10^{-6} s^{-1}

Figure 5.10.d: Vertical section of vorticity anomalies along 46°E for day-4 to day+2. Contour interval 2 x 10^{-6} s^{-1}

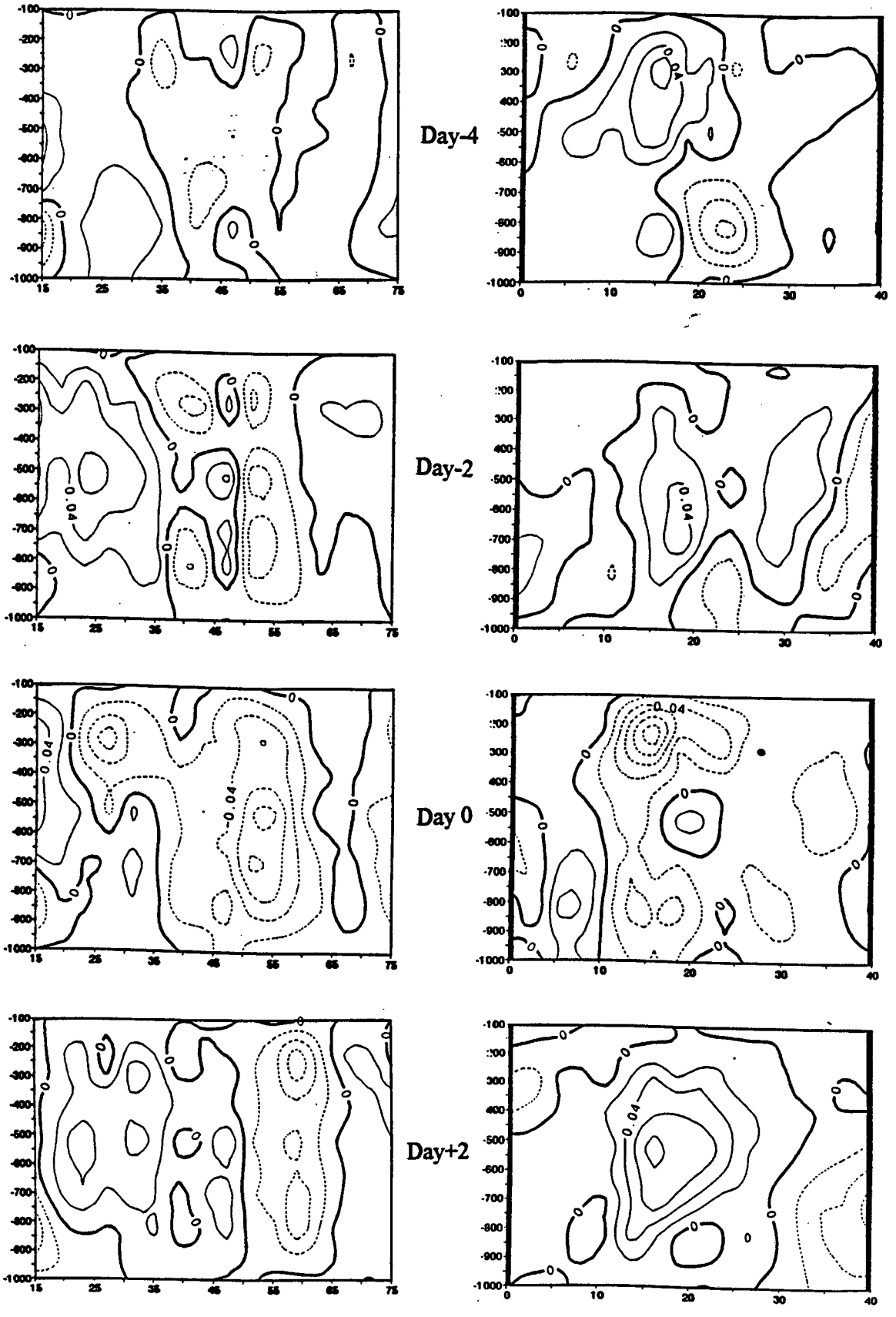

Figure 5.10.e: Vertical section of vetical wind anomalies along 16°S for day-4 to day+2. Contour interval 0.02 Pa s^{-1}

Figure 5.10.f: Vertical section of vertical wind anomalies along 46°E for day-4 to day+2. Contour interval 0.02 Pa s^{-1}

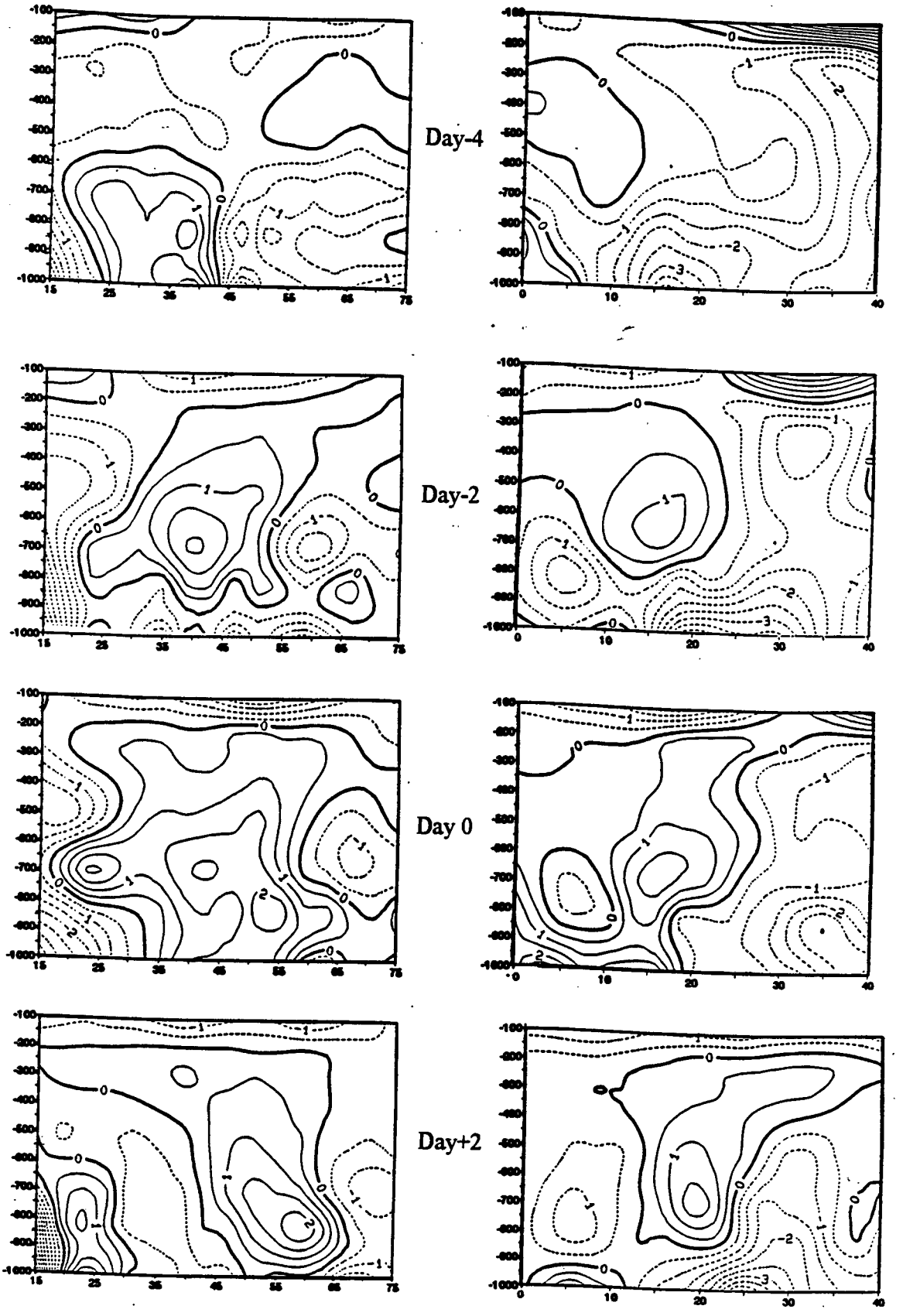

Figure 5.10.g: Vertical section of EPT anomalies along 16°S for day-4 to day+2. Contour interval 0.5°K

Figure 5.10.h: Vertical section of EPT anomalies along 46°E for day-4 to day+2. Contour interval 0.5°K

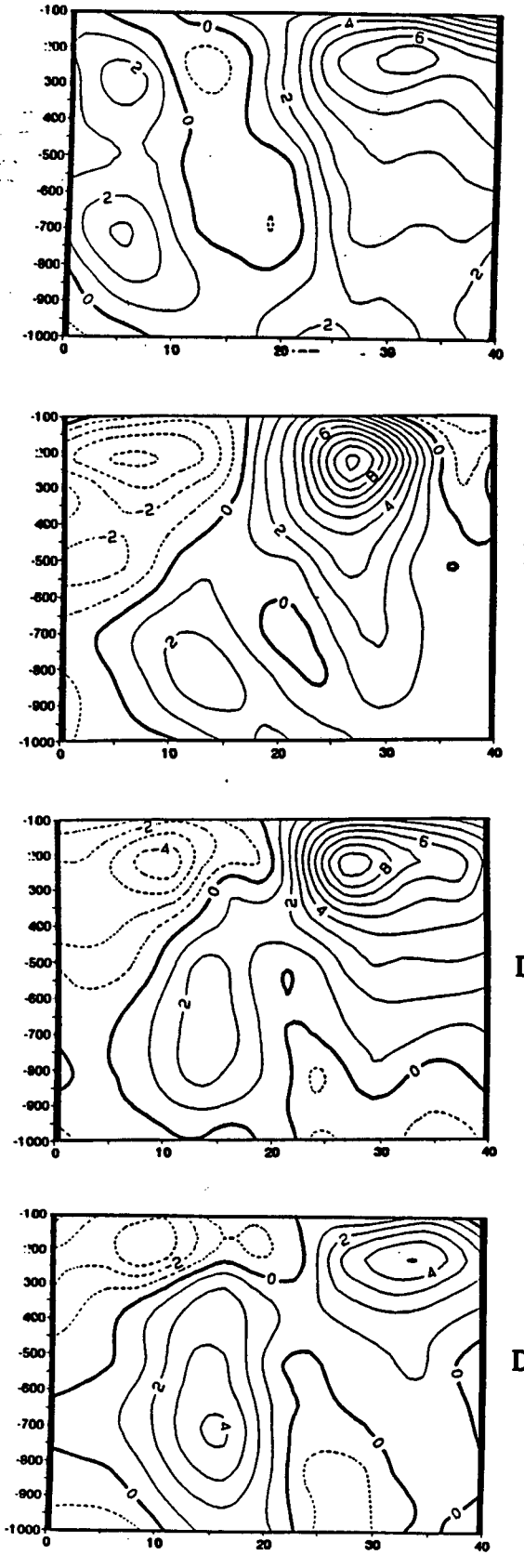

Figure 5.10.i: Vertical section of zonal wind anomalies along 46°E for day-4 to day+2. Contour interval 1 m s^{-1}

CHAPTER 6

CASE STUDY ANALYSIS OF EXTREME FLOOD EVENTS

During the period 1987-1992, the NW region of Madagascar experienced two major flood-producing weather systems. The first episode occurred in February 1991, due to TC Cynthia resulting in 420 mm of rainfall in 24 hours with gusts of 50 m s^{-1} being recorded at Maintirano. The second event occurred in January 1992, due to TC Bryna. In this case 347 mm rainfall with gusts of 23m s^{-1} were recorded in 24 hours at Mahajanga. This chapter aims to analyse the two cases studies to further understand the physics and dynamics during TC activity through analysis of all stages in the same way as in Chapter 5. Here though, the analysis starts from day-6. Instead of the anomaly, the actual values are used for operational purposes. The chapter also investigates the predictability of TC-related weather forecasting in the Madagascar region. These TC tracks are shown in appendix B.

6.1 The 1991 extreme rainfall event :

In mid-February 1991, Maintirano in NW Madagascar experienced a flood event during the passage of TC Cynthia causing considerable damage over the region. TC Cynthia formed as the ITCZ became active over Malawi and shifted eastward in early February 1991. A low system observed over Mozambique (20°S, 30°E), then developed into TC Cynthia when crossing the Mozambique Channel where the SST was 29°C. The evolution of the system is analysed using daily ECMWF data.

6.1.1 Dynamic and kinematic results :

6.1.1.1 Geopotential height :

At the 1000 hPa level on 11 February 1991 (Fig 6.1), a low pressure area of 80 gpm lay over the Mozambique Channel at 20°S, 37°E. An anticyclone of 180 gpm to the south of Madagascar in the subtropics extends from the east coast of South Africa. In the upper level at 200 hPa, a high pressure area lay over the tropics from Africa to Madagascar. To the SW of the Channel, an upper-level trough is oriented NW-SE. On 13 February, the low pressure area in the Channel deepens to 60 gpm while the subtropical anticyclone intensifies to a value of 220 gpm and moves eastward. A trough is located to the SE of Africa. In the upper level, the trough over the SW of the Channel is more apparent and to the SW of Mauritius a ridge is oriented meridionally along 65°E. On the 15th, the low system at the surface continues to deepen (40 gpm) and moves over the Mozambique coast. In the subtropics the anticyclone intensifies to 240 gpm and continues its eastward movement, as well as the trough axis which is now to the south of the Channel. In the upper level, the ridge is centered over Zimbabwe and a cut-off low exists to the SW of Mauritius at 28°S, 62°E. On the 17th, the low system at the surface is named TC Cynthia and moves eastward to be located over the SW of Madagascar. At the 200 hPa level higher heights lay over southern Madagascar, and the upper trough is to the SE of Reunion island. On the 19th, a low level ridge axis appears to the SW of the Channel, the TC moves east and deepens over SW Madagascar. The TC continues to be overlaid at the 200 hPa level by a high pressure area.

6.1.1.2 Horizontal wind :

The horizontal wind vectors on the 11th of February at the 1000 hPa level show monsoon flow and easterly flow converging toward Madagascar, creating a cyclonic flow over the Mozambique Channel and off the northeastern coast of Madagascar due to the topography of the island. To the south of the island, the easterlies are diverging toward the SE coast of southern Africa. In the 200 hPa level, an anticyclonic circulation lies over southern Africa with an northwestward outflow to the north of 20°S (Fig 6.2). On the 13th, the 1000 hPa pattern reveals that the cyclonic circulation to the NE of Madagascar moves slightly to the west while the NW monsoon flow strengthens. To the south of 20°S, the easterlies from the subtropical anticyclone intensify while blowing toward the SE of Madagascar. The cyclonic circulation over the Channel shifts to the Mozambique coast. In the upper level (200 hPa), an anticyclonic circulation is apparent to the east of Madagascar and the zonal ridge over the tropics moves north over 20°S extending from Africa toward the island. Subtropical upper westerly flow to the south of the ridge axis is in the latitude band 20-30°S from Africa to the Mascarenes, where a trough oriented along the longitude 70°E forces the flow to move equatorward joining the upper easterly flow. On the 15th, the subtropical surface-level anticyclonic circulation continues to move east. The NW monsoon flow intensifies further and blows toward the cyclonic circulation over Madagascar and toward the low system over the Mozambique coast, which is now more organized (weak stage of TC Cynthia). Coastal South Africa is under southerly winds associated with an anticyclone to its south in the subtropics. In the upper level, the anticyclonic circulation over Africa is more circular, with an axis of westerly outflow diverging toward Madagascar in the subtropics and a relatively strong southeasterly outflow equatorward of 15°S. To the SE of the Mascarenes exists a cyclonic circulation. On the 17th, the 1000 hPa pattern shows that the NW monsoon wind intensifies

and converges into the TC which is now over western Madagascar, while the easterly wind in the I-O weakens. Another cyclonic circulation develops near 17°S, 66°E. In the subtropics, the anticyclone from the south Atlantic Ocean moves to the south of the Channel. In the upper level, the system is superposed with an upper air diffluence with a predominantly northwestward outflow. Over South Africa, the westerly jet intensifies in the subtropics, blowing from the Atlantic Ocean into the I-O. On the 19th, the surface pattern reveals the existence of a trough to the SW of the Channel. The monsoon wind weakens, consequently the system weakens over southern Madagascar. In the upper level (200 hPa) a large anticyclonic outflow circulation is tilted SE, the upper-level tropical easterly wind weakens and off the east coast of South Africa lies a trough axis oriented N-S along 30°E.

6.1.1.3 Temperature gradient :

On 11 February 1991, the upper-tropospheric temperature gradient (Fig 6.3.a) shows high instability in the tropics from Africa to Madagascar with maximum (77°C) centered over Mozambique. This instability intensifies 0.5°C per day up to 15 February where it reaches 79°C. On the 17th, the warm area (78°C) covers the region from Mozambique to Madagascar along 20°S . It moves over southern Madagascar on the 19th. Latent heating in the mid-level and upper radiative cooling of stratosphere-penetrating clouds contributes to positive feedback in the convective process. The eastward shift of the maximum area from the SE Africa to Madagascar is evident.

6.1.1.4 Vertical wind :

On the 11th, the vertical wind pattern at 500 hPa level (Fig 6.3.b) shows the existence of upward motion over Africa along 20°S , over the NE of Madagascar

along 15°S and over the SE of South Africa due to the orographic effect there. On the 15th over Madagascar, the field of upward motion (-4 x 10^{-1} Pa s^{-1}) covers the entire island. On the 17th, it covers the southern 3/4 of the island while increasing to a value of -8 x 10^{-1} Pa s^{-1}, with its centre over central Madagascar (20°S, 47°E). Two days later the system weakens to a value of -6 x 10^{-1} Pa s^{-1} over the region of Antananarivo.

6.11.5 Divergence :

The 1000 hPa divergence pattern reveals on the 11th that there is a convergence area oriented SW-NE from the Mozambique Channel to near the equator in the I-O with a maximum value of -16 x 10^{-6} s^{-1} off the NE coast of Madagascar. A second area of convergence lies from Namibia to the SE coast of South Africa; a positive divergence area extends from Mozambique into the I-O to the south of 25°S. In the upper level (200 hPa) over the tropics, the lower-level convergence is superposed by an upper-level divergence. Over Madagascar the area of upper-level divergence has a maximum value of 16 x 10^{-6} s^{-1}. In the early stages the divergence patterns are oriented to the NE of the system (Fig 6.4). On the 13th, at 1000 hPa the area of maximum convergence over Madagascar moves slightly over land but weakens to a value of -12 x 10^{-6} s^{-1}, while in the upper level it is superposed with an area of maximum divergence of 24 x 10^{-6} s^{-1}. On the 15th, the surface level pattern is similar to the 13th except that the isolines of -4 x 10^{-6} s^{-1} extend into the tropical area from SW Africa to the east of Madagascar. However, in the upper level the area of maximum divergence over Madagascar continues to move southwestward and covers the whole island. It is surrounded to its SW and SE by two cells of convergence -8 x 10^{-6} s^{-1} and to its E and NW by two cells of -16 x 10^{-6} s^{-1}. On the 17th, the lower-level pattern shows the increase of the convergence area at the surface (-24 x 10^{-6} s^{-1}) centered over western

Madagascar, and in the 200 hPa level it is overlaid by a maximum divergence of 32 x 10^{-6} s^{-1} also over central Madagascar. On the 19th, the lower-level convergence over the island weakens (-16 x 10^{-6} s^{-1}) and the upper-level divergence weakens (24 x 10^{-6} s^{-1}) over the NW. Only in the later stage do the upper divergence-lower convergence maxima begin to tilt, and only by 1 grid point (i.e. 2.5°) to the north.

6.1.1.6 Vorticity :

The pattern (Fig 6.5) shows on the 11th in the surface level, one area of cyclonic vorticity (-24 x 10^{-6} s^{-1}) over southern Africa, another (-16 x 10^{-6} s^{-1}) over the Mozambique Channel, a third over the NE coast of the island and finally one over the I-O at 10°S, 70°E; all in a northeastward alignment. In the upper level, anticyclonic vorticity covers southern Africa and Madagascar, while to the south of the Channel there is a cyclonic vorticity area. On the 13th, the 1000 hPa level reveals the existence of weak cyclonic vorticity over the SE coast of Africa, over the north and south tip of Madagascar owing to the steep topography and in the I-O to the NE of Mauritius along 10°S. In the 200 hPa level over the tropics, the cell of maximum anticyclonic vorticity shifts eastward to cover the area from Zimbabwe to the Mascarenes. Along the latitude band 25-30°S runs an area of cyclonic vorticity up to Madagascar, then northeastward in the I-O. On the 15th in the lower level, the negative area (cyclonic) over the Mozambique coast strengthens (-24 x 10^{-6} s^{-1}) while the one over Madagascar weakens and covers the east part of the island. In the upper level, southern Africa is covered by a positive area except in its SW tip; the negative area moves east to cover the area from the NW of Madagascar toward the I-O. On the 17th in the 1000 hPa level, cyclonic vorticity intensifies over the west coast of Madagascar to a value of -32 x 10^{-6} s^{-1} and in the I-O a negative area of -16 x 10^{-6} s^{-1} moves toward Mauritius

and is centered at 20°S, 70°E. In the 200 hPa level, anticyclonic vorticity is strong over the south Mozambique Channel, while from the Mascarenes into the subtropics, there is an area of negative vorticity oriented NW-SE. On the 19th, the negative area in the 1000 hPa level moves over SE Madagascar, and represents feedback between the shearing effect of the topography and the cyclonic inflow of the TC. A negative area to the east of Mauritius intensifies to a value of -24×10^{-6} s^{-1}. In the 200 hPa level, a broad band of anticyclonic vorticity is oriented NW-SE from 10°S, 15°E to 40°S, 55°E. The southeastward shift of upper-level anticyclonic vorticity "leads" the TC. Over the southeast coast of South Africa and east of Madagascar in the subtropics exists areas of negative vorticity.

6.1.2 Moisture and thermodynamic results :

6.1.2.1 Precipitable water :

The precipitable water (PW) pattern integrated from the surface to 300 hPa level (Fig 6.6.a) in general shows an oversupply of moisture exceeding 60 mm throughout the sequence. On the 11th of February the 50 mm isoline covers a large area over Madagascar from the Mozambique coast up to the Mascarenes extending northeastward to the equator with two maxima (60 mm), one over southern Mozambique and another over northern Madagascar. On the 13th, the pattern is similar to the 11th except that the area of maximum PW content (60 mm) covers the northern 3/4 of the island and extends a narrow band over the southern Channel. On the 15th, the area of maximum PW content covers the Channel and most of the island. On the 17th, the 50 mm isoline covers a broad area from the SE coast of Africa to the I-O oriented SW-NE, while the area of maximum PW content (70 mm) is located over the island. On the 19th, the 50 mm isoline covers

the most part of the SWIO to the east of 30°E, while over the interior of southern Africa, the PW content decreases to under 20 mm.

6.1.2.2 Water vapour flux :

The water vapour flux (WVF) pattern is similar to the lower-level wind circulation. Throughout the development of the TC, a large cyclonic vortex moves southeastward from 10°S, 70°E in the I-O to 25°S, 65°E by the 19th.

On the 11th February (Fig 6.6.b), the easterly flow carries more moisture into the cyclonic circulation over the NE of Madagascar. The monsoon flux initiates off the east coast of Africa and over the Mozambique coast. On the 13th, the monsoon flux converges into the low system over the north of the island which is now better developed; the second low system over Mozambique remains stationary while to the south of South Africa exists a frontal low moving eastward. On the 15th, the monsoon flux intensifies. The low system (TC Cynthia) over Mozambique develops at the expense of the low over Madagascar. On the 17th, the cyclonic WVF vortex associated with TC Cynthia moves southeastward over Madagascar and the monsoon flux continues to strengthen while the easterly WVF weakens in the I-O. The frontal low in the subtropics remains quasi-stationary to the SW of the Channel. On the 19th, the monsoon flux starts to weaken and the cyclonic circulation associated with the TC widens to a radius more than 1000 km and covers the Channel and Madagascar.

6.1.2.3 Velocity potential of water vapour flux :

The velocity potential of WVF integrated from the surface to the 500 hPa level shows on the 11th of February an area of positive values (convergence) over the region with a maximum of 44 x 10^9 kg s^{-1} centered off the east coast of Madagascar. On the 13th, the moisture flux convergence weakens and an area of

negative value of -8 x 10^9 kg s^{-1} lies over the subtropics to the SE of Madagascar. On the 15th, the positive area intensifies and covers the whole region with a maximum value of 56 x 10^9 kg s^{-1} over the east coast of Madagascar. On the 17th, the system moves south and is centered off the SE coast of the island with value of 52 x 10^9 kg s^{-1}. On the 19th, the pattern is similar to the one on the 17th except there is a weak negative area oriented meridionally along 25°E over Africa (Fig 6.7.a). The persistence of this χ_Q signal may make it useful in forecasting flood events.

6.1.2.4 Streamfunction of water vapour flux :

The streamfunction of WVF integrated from the surface to the 500 hPa level (Fig 6.7.b) reveals on the 11th of February, a negative area (anticyclonic circulation) over southern Africa as well as over the I-O with values of -16 x 10^9 kg s^{-1}, and -32 x 10^9 kg s^{-1} respectively. Over the Mozambique Channel exists a positive area (cyclonic circulation) of 12 x 10^9 kg s^{-1} centered at 25°S, 40°E. On the 13th, the positive area covers the longitude band from the east coast of Africa to the west coast of Madagascar extending a ridge to the NE of the island, while the negative area weakens. On the 15th, the positive area intensifies (52 x 10^9 kg s^{-1}) and covers the area to the west of 46°E and the SE of Madagascar. The centre of the positive area moves over the SE of the island while the negative area in the I-O intensifies to -24 x 10^9 kg s^{-1} centered at 15°S, 57°E. An area of cyclonic circulation appears to the east of Mauritius at 70°E. Finally on the 19th, the positive area over Madagascar continues to move SE while the one from the I-O moves west, weakening the negative area over the Mascarenes. In general, the patterns are quite meridional; the strengthening of the positive area west of Madagascar is a key feature associated with monsoon inflow.

6.1.2.5 Equivalent potential temperature :

The EPT field (Fig 6.8 a and b) at the 1000 hPa level on the 11th of February reveals an area of warm sector extending from Africa to Madagascar bounded by the 350°K isoline and another area to the east of 60°E along the latitude band 5-15°S. In the 500 hPa level the warm sector is confined to the area between 7-25°S from Africa to Madagascar, then shifted over the latitude band 2-12°S in the I-O. On the 13th, the >350°K area in the 1000 hPa level, covers most of southern Africa into the I-O but shifts NE to the east of the island toward the equator, with a maximum value of 360°K over interior tropical SE Africa as well as over central Madagascar. In the middle troposphere, the warm sector pattern is similar to the one on the 11th. On the 15th, the area of warm sector intensifies with a maximum of 370°K over Africa at 12°S, 20°E in the 1000 hPa level. In the mid-troposphere the >340°K area runs from Zimbabwe to Madagascar. On the 17th, the centre of warm sector moves over Zimbabwe in the surface level. In the 500 hPa level, the 340°K area extends from Mozambique to Madagascar with a maximum value of 350°K over Madagascar. On the 19th, in the 1000 hPa level the area covered by the 360°K isoline narrows over Africa and over Madagascar it covers 3/4 of the island. In the 500 hPa level, the 340°K isoline covers the Mozambique coast, another warm cell covers the Madagascar region.

6.1.3 Vertical section analysis of the 1000-100 hPa layer :

The vertical sections of the meteorological parameters analysed in this section are either zonally E-W along the latitude 16°S or meridionally N-S along the longitude 46°E using ECMWF data from 1000 to 100 hPa levels.

6.1.3.1 The vertical section of the divergence field :

The E-W vertical section of the divergence field along 16°S (Fig 6.9.a) reveals on the 11th of February the existence of a convergence area over Mozambique between 25-35°E with maximum (-16 x 10^{-6} s^{-1}) at 800 hPa. Over Madagascar a weak area of convergence is noted. These two convergence areas lay under fields of divergence in the 200 hPa level with a maximum value of 12 x 10^{-6} s^{-1} over Mozambique. On the 13th, the divergence field at 200 hPa over the island intensifies to 28 x 10^{-6} s^{-1} and in the lower level, the convergence field extends from Africa to Madagascar up to the 500 hPa level; over Mozambique it weakens in favour of the one over the island. On the 15th, the two systems are more organized from Mozambique to the island; a lower-level convergence area with a maximum of -20 x 10^{-6} s^{-1} at 800 hPa over Madagascar lays under an upper-level divergence area of 24 x 10^{-6} s^{-1} at the 200 hPa level. On the 17th, the lower-level convergence area over the Channel extends up to 500 hPa while over the island it extends up to 700 hPa only. In the upper level, the positive area over the island weakens to 20 x 10^{-6} s^{-1}. On the 19th, the two systems are concentrated over the island. In the lower level at 800 hPa exists a negative area with a maximum of -16 x 10^{-6} s^{-1} and at 200 hPa a positive area with a maximum of 24 x 10^{-6} s^{-1} (Fig 6.9.a).

The N-S vertical section of the divergence along 46°E shows on the 11th that a dipole system lay over the NW Madagascar (16°S) with convergence extending up to 600 hPa. On the 13th, the dipole system intensifies, the negative area extends up to 450 hPa and the positive one strengthens to 32 x 10^{-6} s^{-1}. On the 15th, the systems weaken while shifting southward from the latitude band 10-20°S to 15-25°S. On the 17th, the systems become more organized and more intense with a value of 40 x 10^{-6} s^{-1} at 200 hPa and -24 x 10^{-6} s^{-1} at 800 hPa over 20°S on the west coast of Madagascar. On the 19th, the lower convergence area

strengthens and continues to move south. In the upper level the positive area weakens and shifts northward (Fig 6.9.b).

The vertical section of the divergence shows that the convergence area is located to the south of 10°S with maximum value at 800 hPa level. The fields suggest that the area of convergent flow and convective activity which was over Mozambique on the 11th moves toward Madagascar and becomes more active over the warm water in the Channel. On encountering the topography of the island the upper level divergence intensifies.

6.1.3.2 The vertical section of the vorticity field :

The E-W vertical section of the vorticity along 16°S (Fig 6.10.a) exhibits on the 11th of February cyclonic vorticity in the lower level with a maximum of -24 x 10^{-6} s^{-1} over Mozambique (along 35°E) at 700 hPa. To the east of 40°E lays an area of anticyclonic vorticity. The upper level is dominated by an anticyclonic vorticity field with a maximum of 40 x 10^{-6} s^{-1} over 55°E at the 300 hPa level. On the 13th, the negative area at the lower level extends east over Madagascar and in the upper level the area of maximum positive value shifts upward to the 200 hPa level. On the 15th, the lower-level cyclonic vorticity field becomes more organized over the area between Mozambique and Madagascar. In the upper level, the area of maximum positive value (at 200 hPa) moves east over 60°E and weakens to 32 x 10^{-6} s^{-1}. On the 17th the negative area over the Channel extends from 900 to 300 hPa and in the upper level the area of maximum anticyclonic vorticity is located at 50°E. On the 19th, the area of cyclonic vorticity is confined over the Channel between 900 and 500 hPa.

The meridional vertical section of vorticity along 46°E (Fig 6.10.b) reveals, on the 11th, the existence of a weak cyclonic area at the surface over Madagascar (19-27°S) tilted northward with height. The upper level is dominated by an

anticyclonic vorticity area with a maximum of 32 x 10^{-6} s^{-1} laying equatorward of 22°S. On the 13th, the negative area in the lower level intensifies over 15°S in the 900-600 hPa layer with a maximum of -32 x 10^{-6} s^{-1}. On the 15th, the area of cyclonic vorticity in the lower level shifts southward with its maximum at 800 hPa over 20°S. To the north of 15°S there is an area of anticyclonic vorticity from the surface up to 200 hPa. On the 17th, the negative area at the lower level continues to shift south but is confined to the layer between the surface and 500 hPa level. Above it a positive area extends between 10-30°S in the upper level with a maximum value of 48 x 10^{-6} s^{-1} at 200 hPa. On the 19th, the lower-level cyclonic area extends upward, and the upper-level positive area moves southward and intensifies to 54 x 10^{-6} s^{-1}.

The vertical section of the vorticity shows that the circulation vortex situated in the layer 700-800 hPa moves from Mozambique south-eastwards to Madagascar while strengthening over the Channel.

6.1.3.3 The vertical section of the EPT field :

The E-W vertical cross section of EPT along the 16°S (Fig 6.11.a) reveals low-level instability imposed by elevated heat fluxes over the plateau of SE Africa and Madagascar. On the 11th, in the mid-troposphere an area of 338°K exists at 15°E over Africa and another one of 326°K centered at 75°E in the I-O. On the 13th, the surface layer becomes thermodynamically cooler and in the mid-troposphere the dry stable layer in the I-O moves westward and becomes warmer by 4°K. On the 15th, in the mid-troposphere the low EPT area in the I-O (334°K) continues to move west, while increases in lower level instability characterize the area over the Mozambique Channel. This warming suggests an improved environment for deep convection over the area. On the 17th, the lower-level warming continues over the Mozambique Channel spreading eastward toward

Madagascar while the mid-troposphere cools down. On the 19th, at the surface, there is a cooling over the interior of southern Africa suggesting an area of suppressed convective potential. The warming over the Channel extends up to 700 hPa. In the I-O the mid-troposphere continues to warm up to the east of Mauritius. The low EPT layer potentially eroding the TC is 700-500 hPa, although minor asymmetries are apparent. The zonal widening of the band of high EPT is a characteristic feature of the sequence.

The meridional cross section of EPT along the longitude 46°E (Fig 6.11.b) shows that, on the 11th, the convective environment is unstable up to 800 hPa over the latitude band 10-25°S. This convectively active high EPT area shifts southward on the 13th to be located south of 15°S. On the 15th, there is a cooling over Madagascar in the lower layer. On the 17th, the area of high EPT at the lower level over Madagascar becomes more intense and by the 19th it spreads southward over the island indicating a deep convective area following the southward movement of the TC.

6.1.3.4 Vertical section of the zonal wind field :

The N-S vertical section of the zonal wind (u-component of the horizontal wind) along the longitude 46°E exhibits double dipole structure between the lower and upper level of the troposphere.

On the 11th of February (Fig 6.12), in the lower level to the north of 15°S there is a positive (westerly wind) area with a maximum wind of 4 m s^{-1} and to its south lay a negative (easterly wind) area with a maximum of -8 m s^{-1}. Above 500 hPa in the tropics, easterlies up to -18 m s^{-1} at 250 hPa level are found. In the subtropics upper-level westerlies of a similar magnitude are noted. Such strong shear in the precursor TC stage is relatively unique. This dipole pattern is more organized on the 13th with low-level tropical westerlies extending up to 450 hPa.

On the 15th, the dipole structure is tilted. Monsoon westerlies in the lower layer shift southward and upper-level easterlies move northward and weaken. The areas of positive and negative zonal winds in the lower level continue to strengthen (+10 and -10 m s^{-1} respectively) and the lower-level tropical westerlies link with the upper-level subtropical jet. On the 17th, the pattern shows some similarity to the 11th of February. The lower-level easterly trades weaken while the westerlies intensify with maximum winds of 14 m s^{-1} at 650 hPa. In the upper level the tropical easterlies and subtropical westerlies enhance anticyclonic outflow. On the 19th, the upper-level easterlies shift southward and connect to the lower-level easterlies which strengthen and extend upward.

The meridional section of the zonal wind shows that, at the beginning of development of the TC, the vertical wind shear is not weak. It is significant that the genesis point is not located in the longitude of the cross section. The surface easterlies weaken as the monsoon westerlies intensify, up to the mature stage of TC development. The reverse process takes place at the decay stage. Noteworthy is the equatorward tilt with height of the 0-isoline two days prior to this event.

6.1.4 Summary :

The extreme flood event in February 1991 was caused by TC Cynthia which developed in the Mozambique Channel. Although the TC had a short lifespan (three days), the damage caused over NW Madagascar was considerable. The kinematic, dynamic and thermodynamic analyses of the TC indicates that the system originates over Mozambique and shifts eastward toward the island. The patterns reveal that prior to the event, there is: an increase of the subtropical surface anticyclone intensity, in the upper level a trough moves from the SW Mozambique Channel to the I-O, monsoon flow strengthens, the 500-100 hPa temperature gradient shifts from Mozambique to Madagascar, and upper-level

divergence is superposed with lower-level convergence. Throughout the process, the velocity potential of WVF exhibits the persistence of an increasing convergence area over Madagascar and its streamfunction, the strengthening of the cyclonic circulation over the western region of the island associated with the monsoon flow. The vertical section of tropospheric structure suggests that the convective activity over Mozambique moves eastward and intensifies over the warm Channel. The topography of Madagascar enhances the cloud vortex, and the uplift is assisted by the upper-level divergence field. Heat fluxes over the SE Africa plateau and the Madagascar highlands contribute to low-level instability seen in the vertical section of EPT. It confirms also that the deep convection shifts toward the island during the period. The vertical section of the zonal wind indicates that lower easterlies weaken as the monsoon westerlies strengthen, and the subtropical upper-level westerly winds intrude two days prior to the event.

The meteosat imagery (Fig B-1 and 2) during the period of development of TC Cynthia shows a cloud band from the Congo basin spreading south to a low depression area over Beira, Mozambique. To the south of the Mozambique Channel a cold front is moving eastward, as confirmed by geopotential heights in figure 6.1.a. The northwesterly monsoon flow from the north of the Channel increases progressively from 13 February to reinforce the cloud vortex over the area (Fig 6.2.a). The system moves southeastward toward Madagascar while intensifying. The NOAA satellite imagery on 15 February shows two cloud clusters, one on the northwest coast of Madagascar and the other near Beira Mozambique. On the 16th at 1100Z, the two clusters fused to form one cloud system with outflow of cirrus to the north and east, and deep convection to the southwest (16.5°S, 41.0°E). The TC reached the west coast of Madagascar near Morondava and the topographic effects of the region changed the system's

trajectory to SE. The presence of a transient trough on the 19th to the southwest of the Channel assisted in steering the system southward. The system dissipated following the intrusion of subtropical westerlies.

Although the TC had only 3 day's lifespan, the Madagascar National Weather Service reported that the damage in the region of NW Madagascar was considerable: 76 deaths and missing people, destruction of bridges, roads and houses with 88,000 refugees.

The data from surface observing meteorological stations indicate that maximum wind and heavy rainfall were recorded on the left side of the system or northern quadrant at maturity (Fig 6.2.a, 17 February 1991). On the 16th, at Juan de Nova island, when the system was just to its south, minimum surface pressure was 997.5 hPa, a peak gust of 33 m s^{-1} and rainfall of 392 mm/day were recorded. Maintirano felt the destructive effects of the TC's northern quadrant with surface pressure of 996.8 hPa, wind speed 43 m s^{-1} gusting to 50 m s^{-1}, and rainfall of 420 mm. While at Morondava in the TC's southern quadrant, on 17th the surface pressure was 979.1 hPa, the wind speed 26 m s^{-1} gusting to 31 m s^{-1} and rainfall of 196.2 mm were recorded.

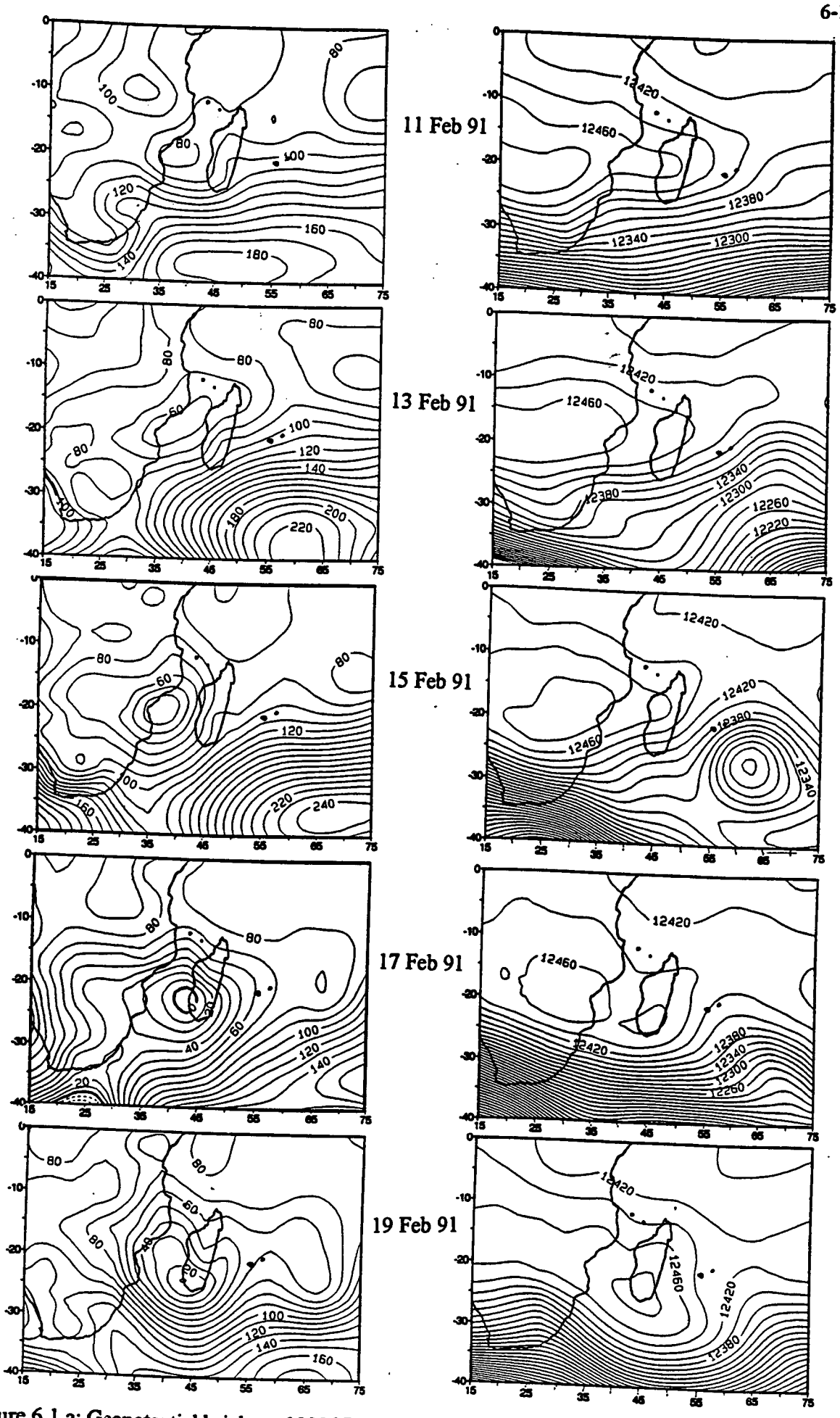

Figure 6.1.a: Geopotential height at 1000 hPa. Contour interval 10 gpm.

Figure 6.1.b: Geopotential height at 200 hPa. Contour interval 20 gpm

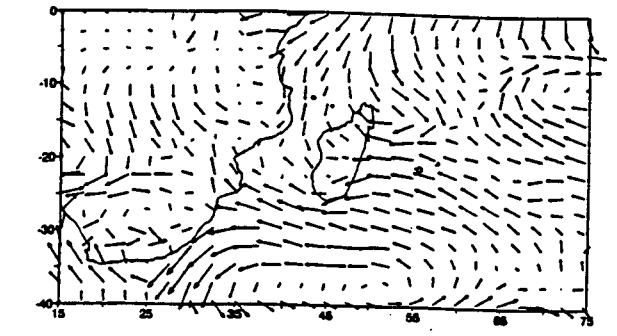

11 Feb 91

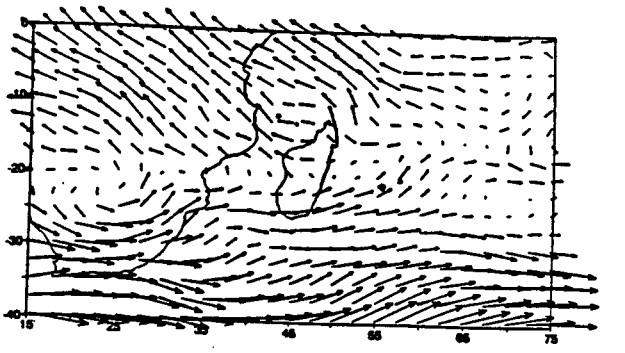

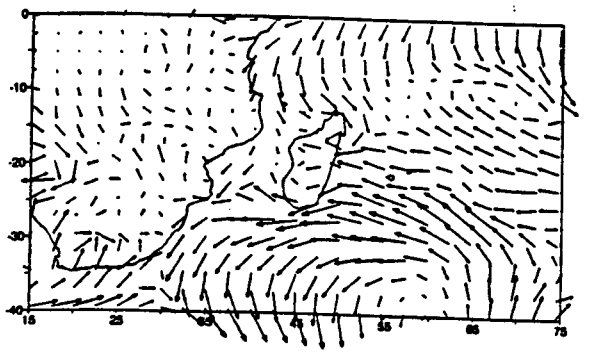

13 Feb 91

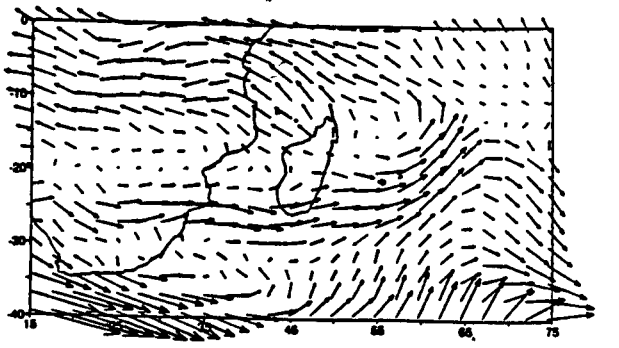

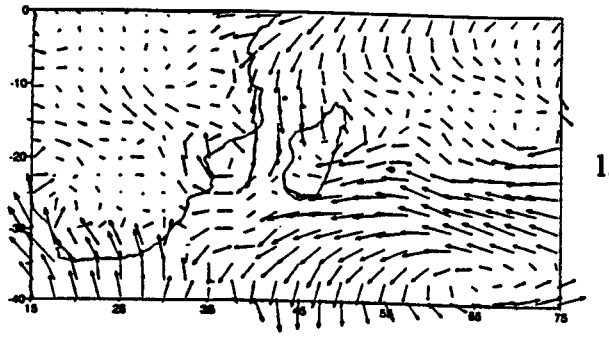

15 Feb 91

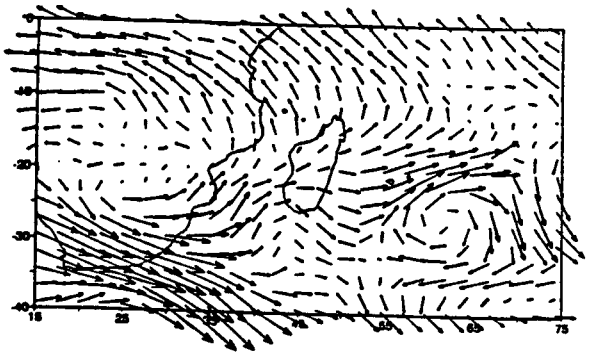

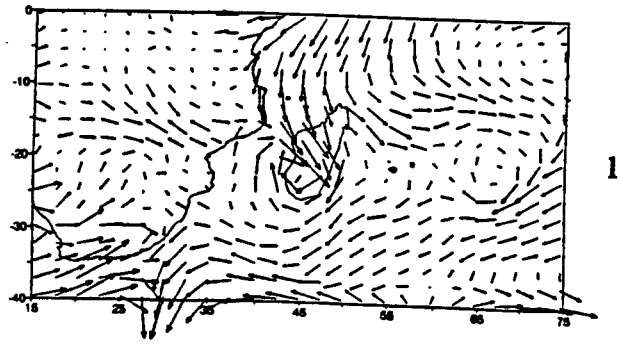

17 Feb 91

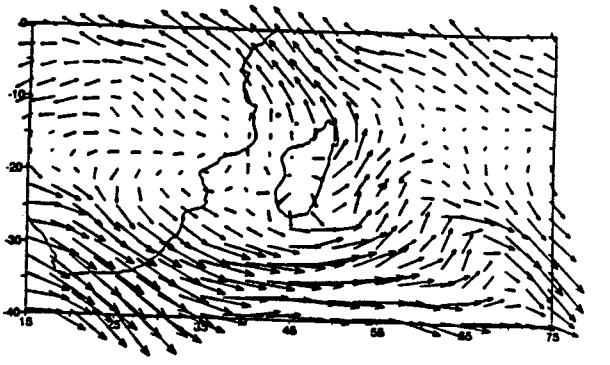

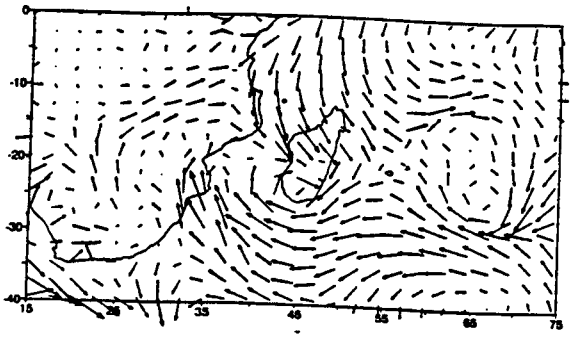

19 Feb 91

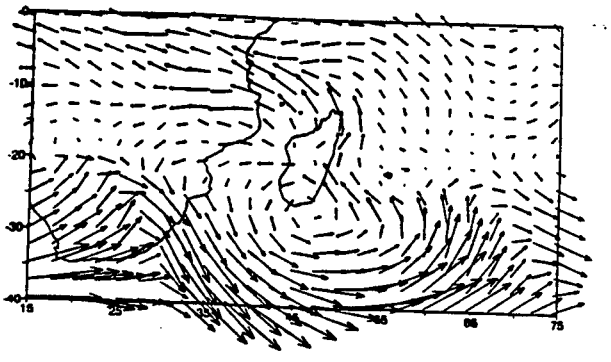

10 m s^{-1} —

Figure 6.2.a: Horizontal wind at 1000 hPa.

50 m s^{-1} ⟶

Figure 6.2.b: Horizontal wind at 200 hPa.

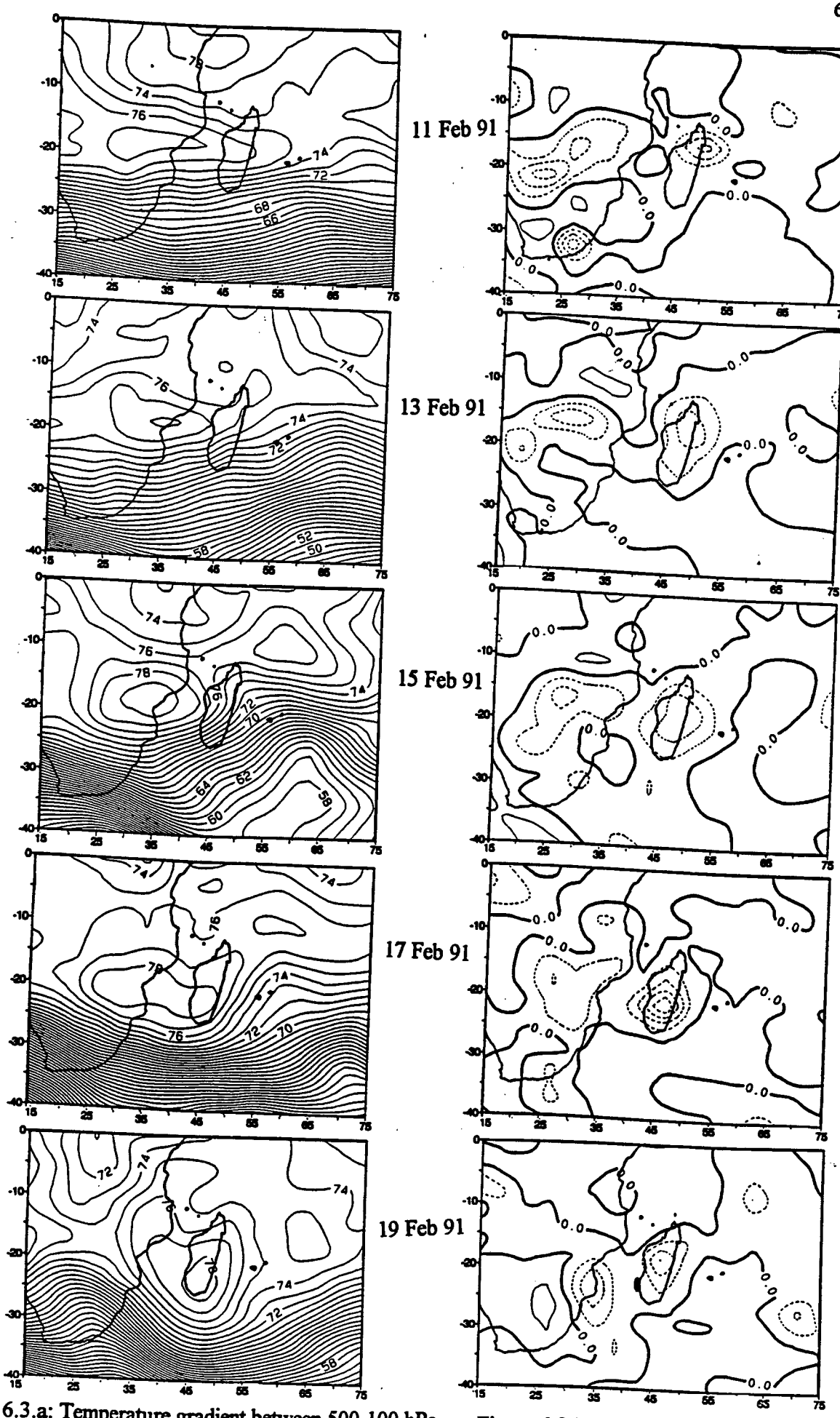

Figure 6.3.a: Temperature gradient between 500-100 hPa. Contour interval 1°C

Figure 6.3.b: Vertical wind at 500 hPa. Contour interval 0.2 Pa s^{-1}

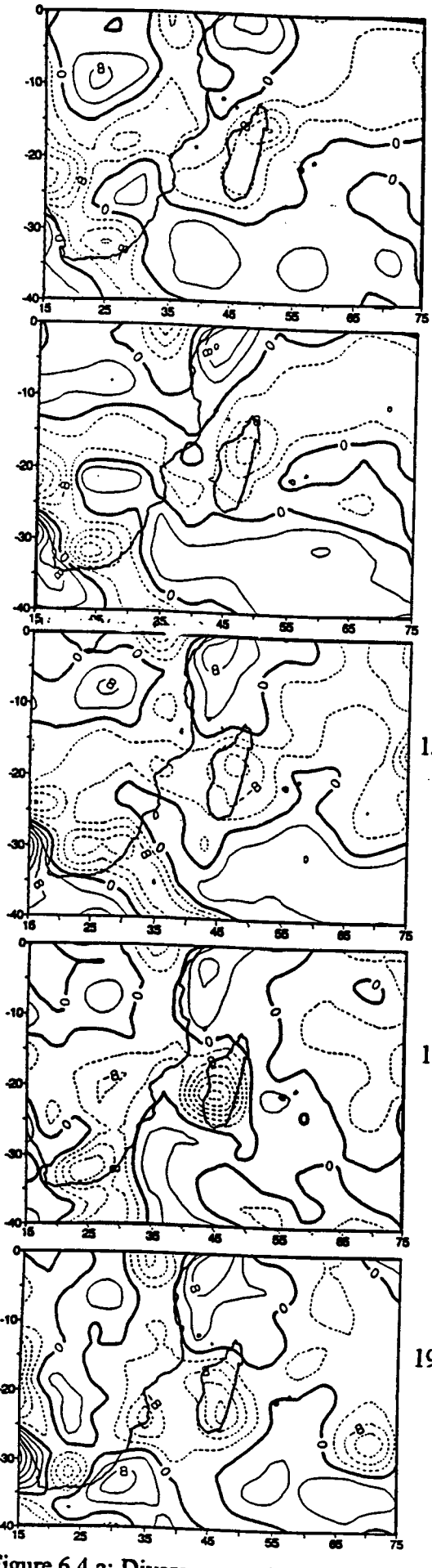

Figure 6.4.a: Divergence at 1000 hPa.
Contour interval 4 x 10^{-6} s^{-1}

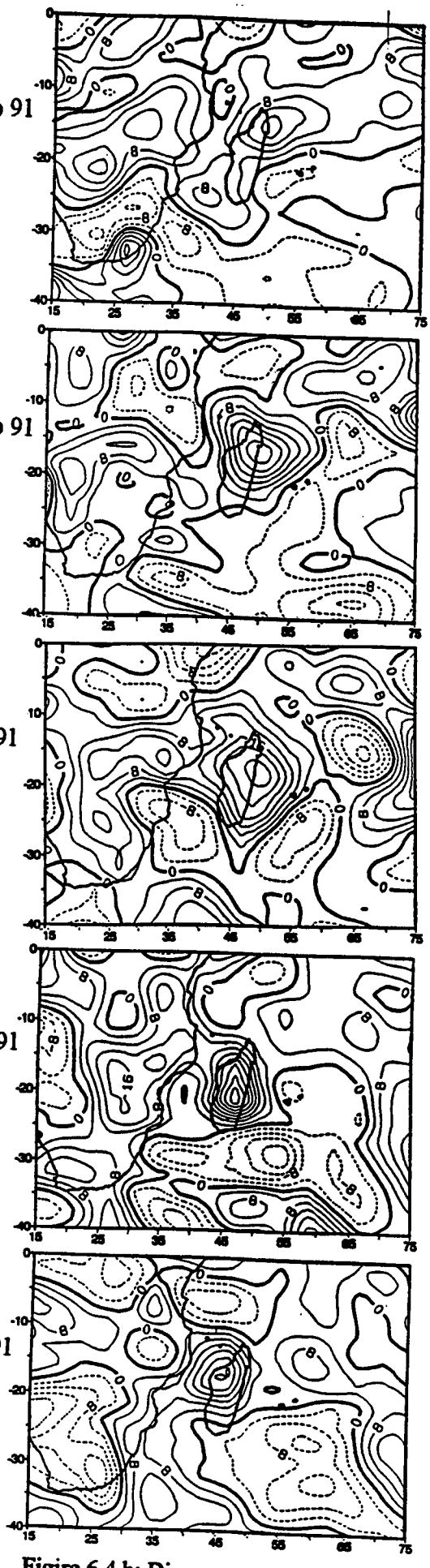

Figire 6.4.b: Divergence at 200 hPa.
Contour interval 4 x 10^{-6} s^{-1}

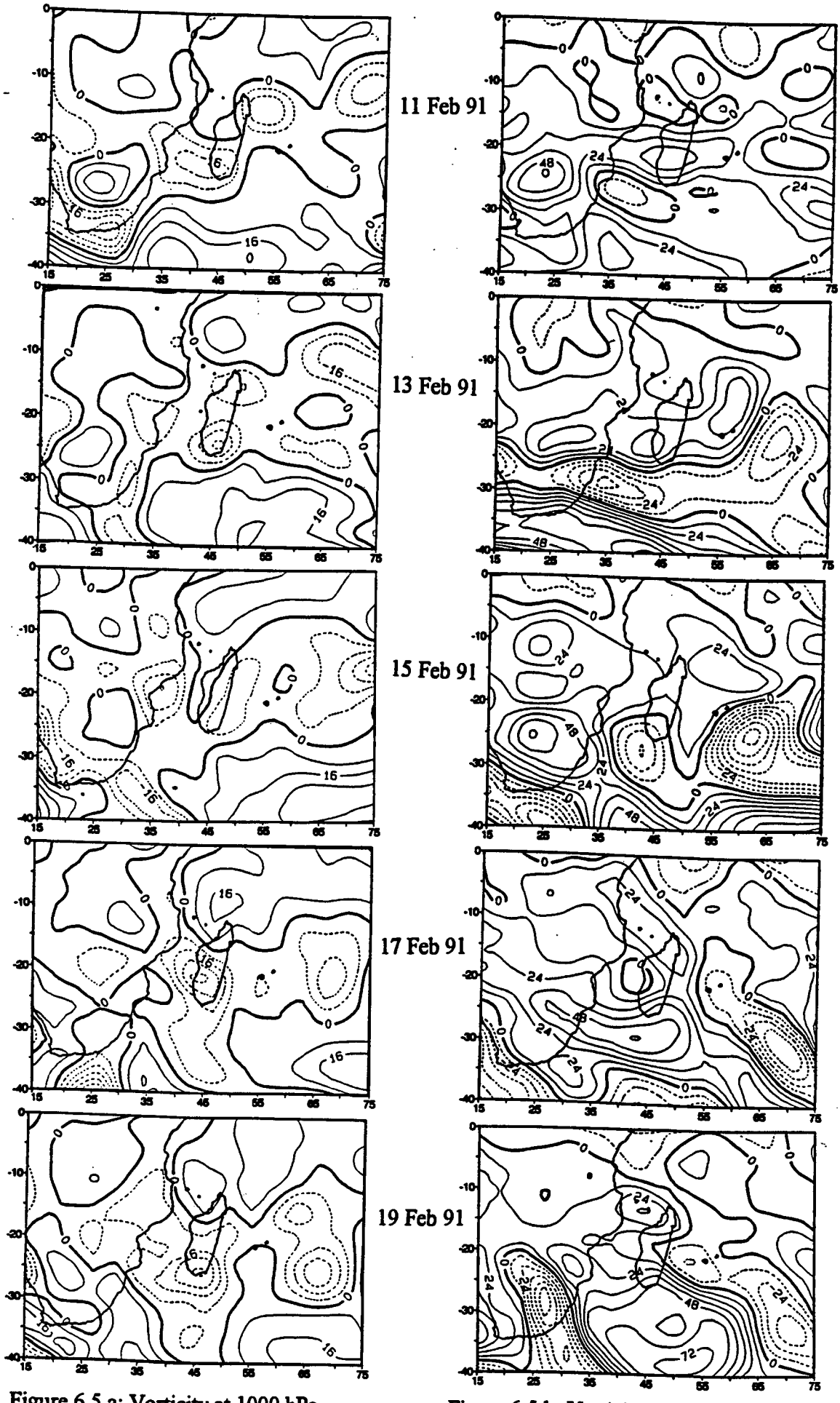

Figure 6.5.a: Vorticity at 1000 hPa.
Contour interval 8 x 10^{-6} s^{-1}

Figure 6.5.b: Vorticity at 200 hPa.
Contour interval 12 x 10^{-6} s^{-1}

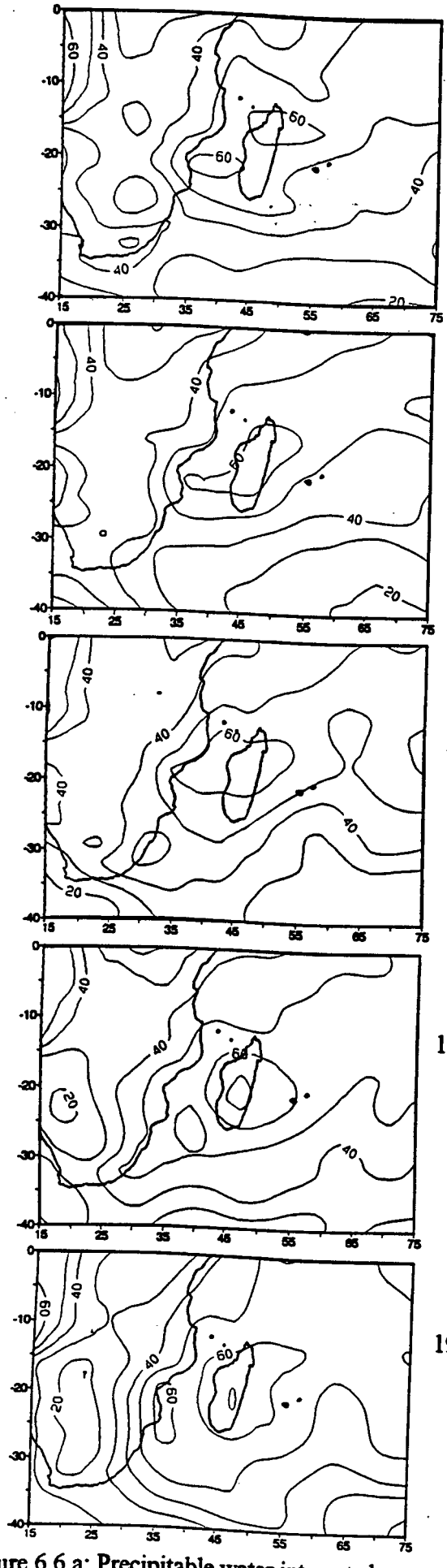

Figure 6.6.a: Precipitable water integrated from the surface up to 300 hPa. Contour interval 10 mm.

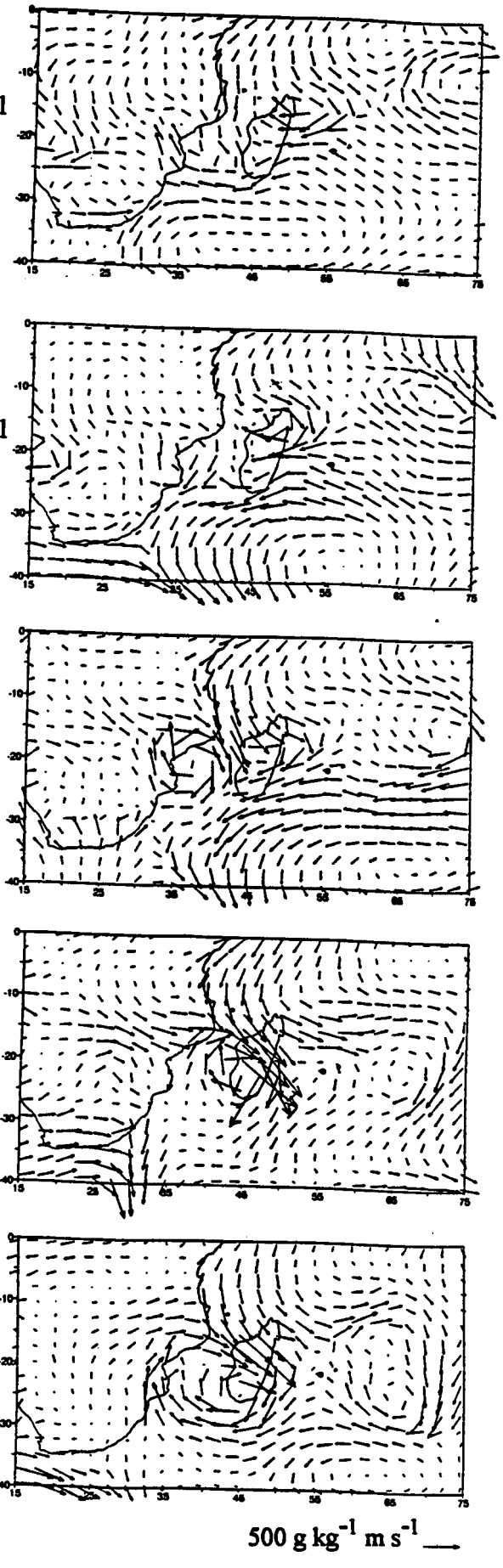

Figure 6.6.b: Water vapour flux integrated from the surface up to 500 hPa.

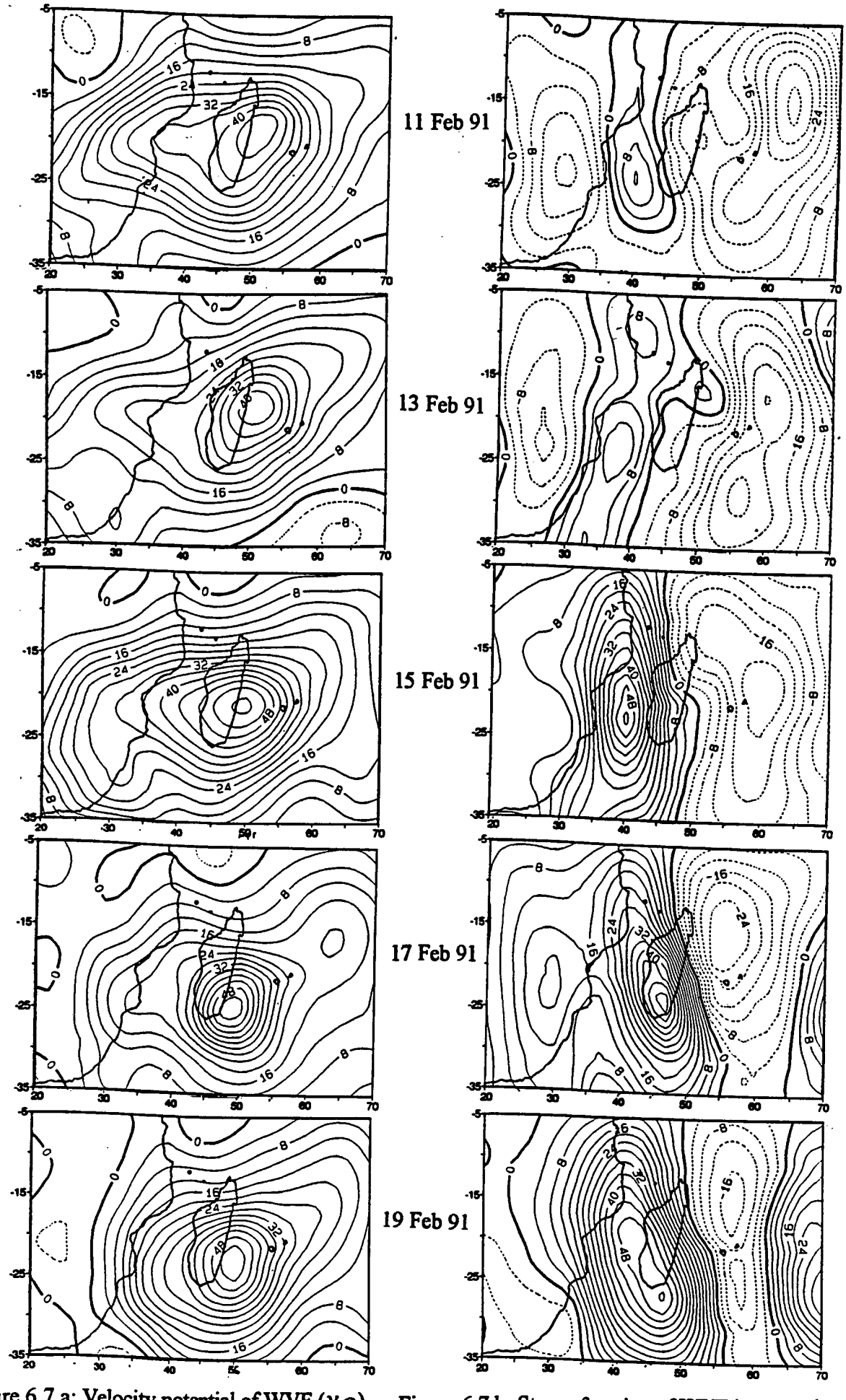

Figure 6.7.a: Velocity potential of WVF (XQ) integrated from the surface to 500 hPa. Contour interval 4 x 10^9 kg s^{-1}

Figure 6.7.b: Streamfunction of WVF integrated from the surface to 500 hPa. Contour interval 4 x 10^9 kg s^{-1}

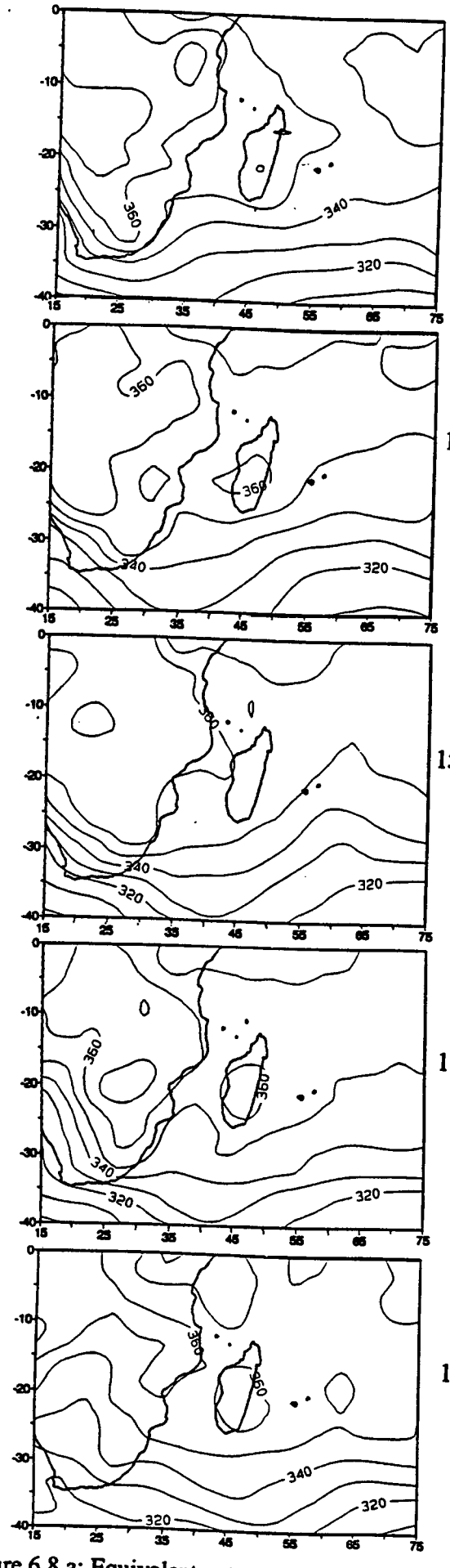

Figure 6.8.a: Equivalent pot. temp. at 1000 hPa. Contour interval 10°K

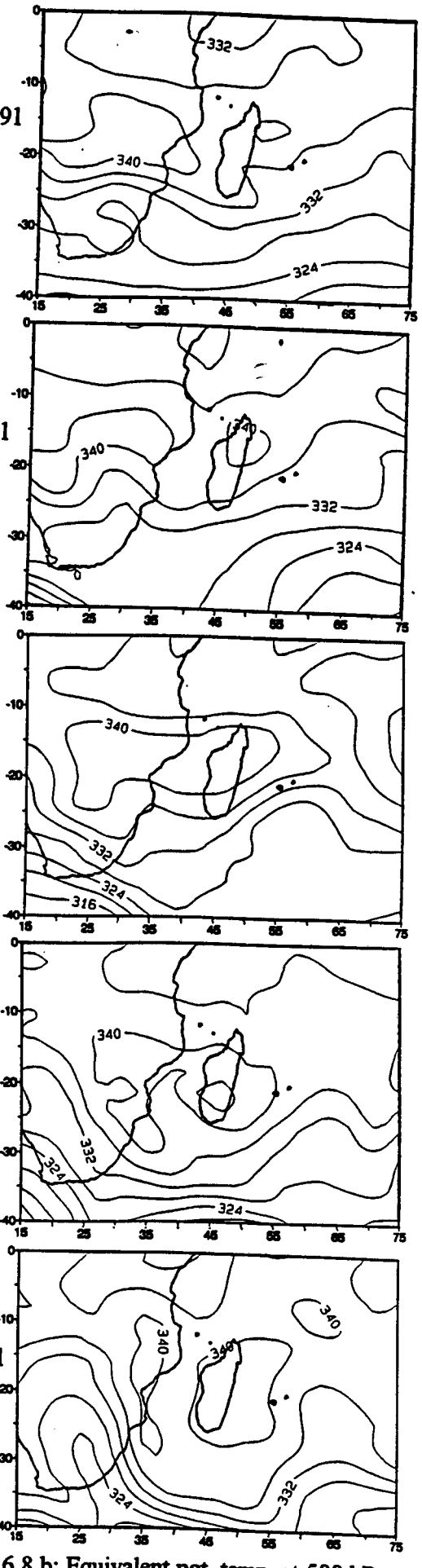

Figure 6.8.b: Equivalent pot. temp. at 500 hPa. Contour interval 4°K

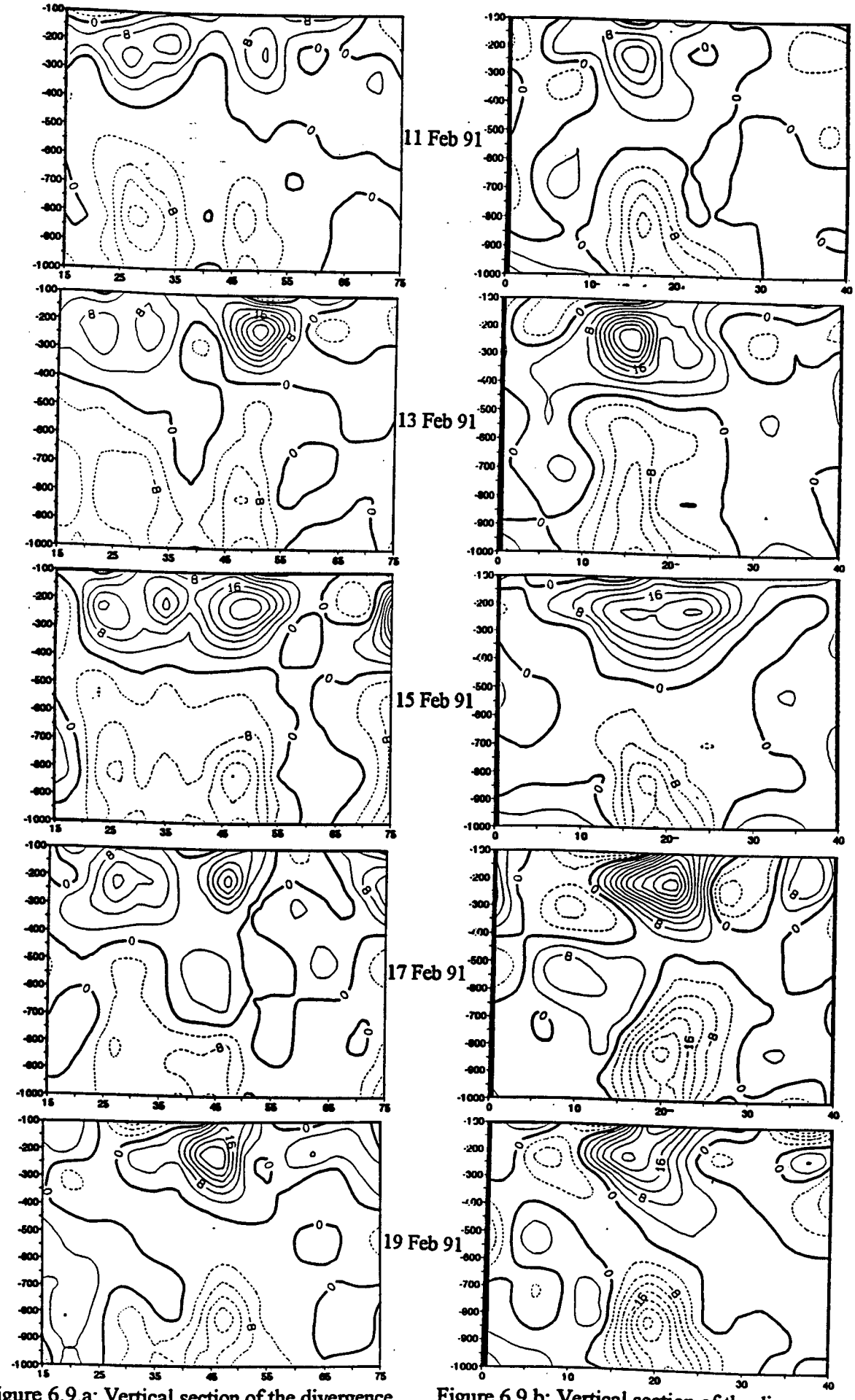

Figure 6.9.a: Vertical section of the divergence field along 16°S.
Contour interval 4 x 10^{-6} s^{-1}

Figure 6.9.b: Vertical section of the divergence field along 46°E.
Contour interval 4 x 10^{-6} s^{-1}

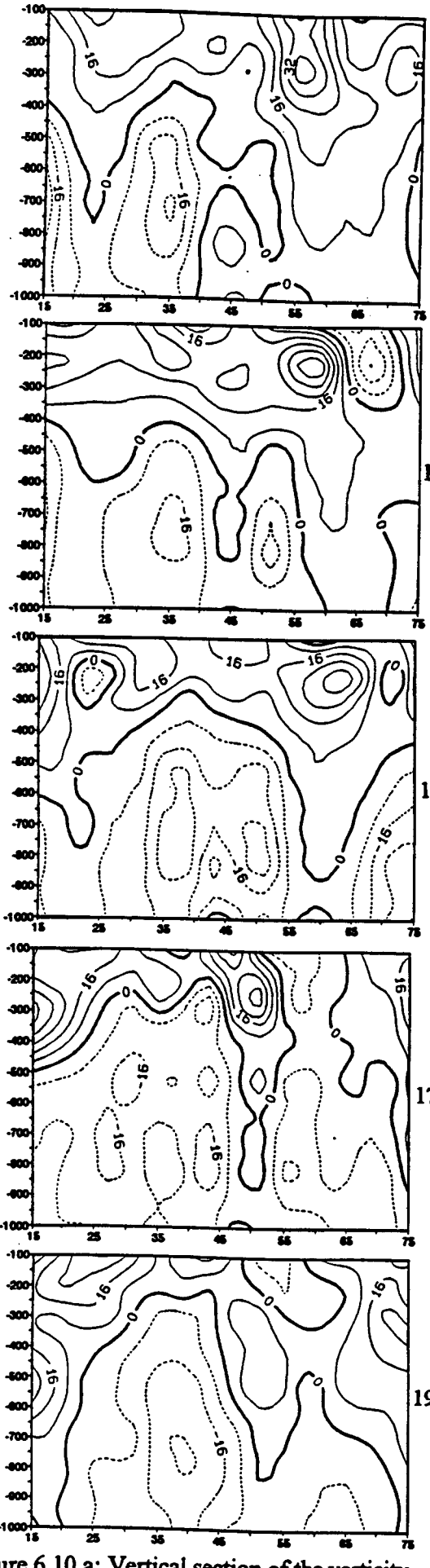

Figure 6.10.a: Vertical section of the vorticity field along 16°S.
Contour interval 8 x 10^{-6} s^{-1}

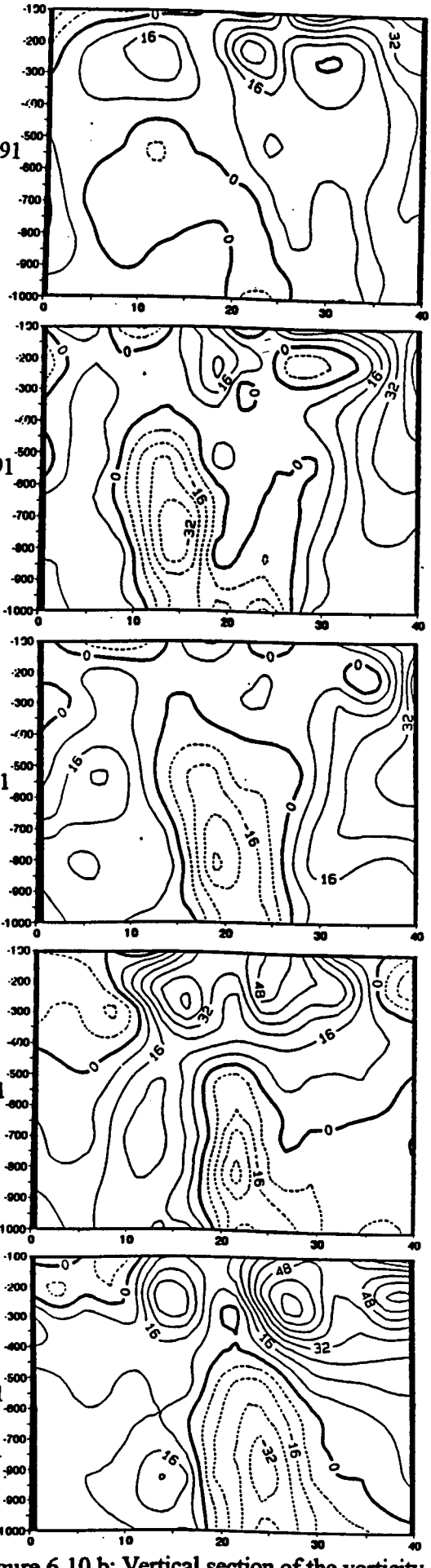

Figure 6.10.b: Vertical section of the vorticity field along 46°E.
Contour interval 8 x 10^{-6} s^{-1}

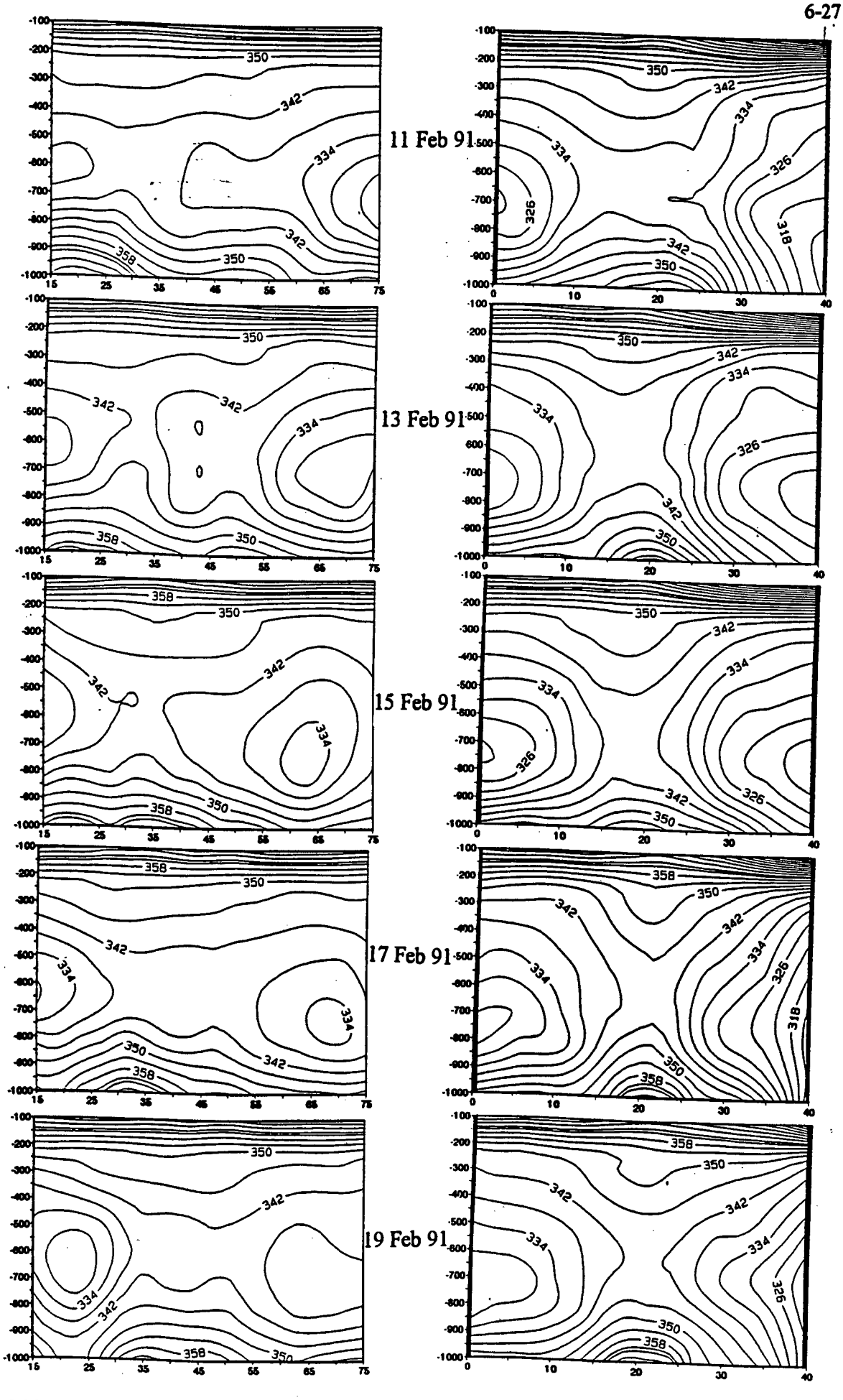

Figure 6.11.a: Vertical section of EPT along 16°S. Contour interval 4°K

Figure 6.11.b: Vertical section of EPT along 46°E. Contour interval 4°K

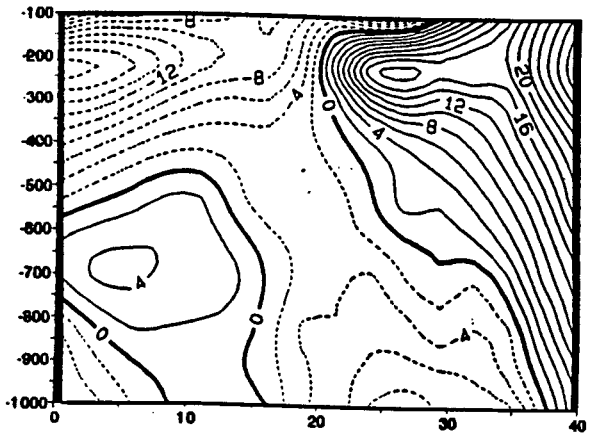

11 Feb 91

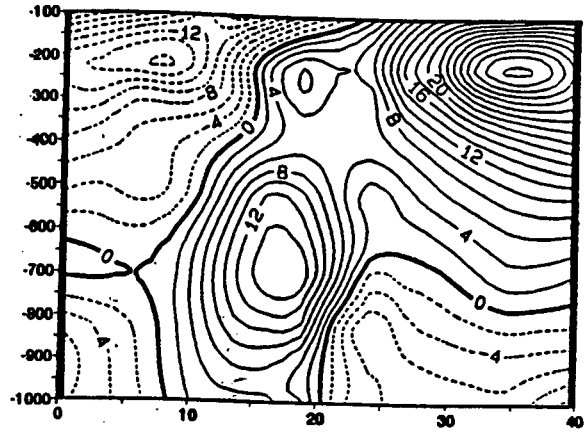

17 Feb 91

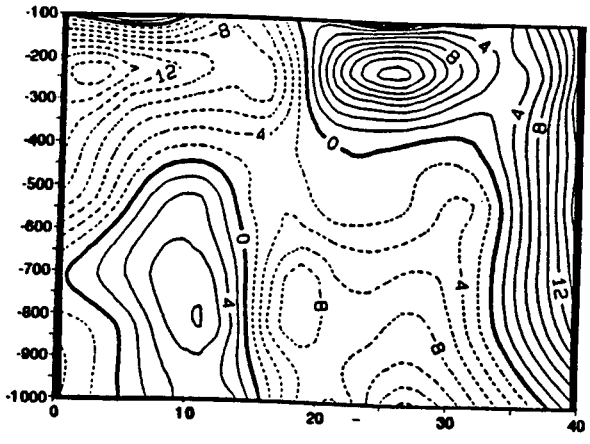

13 Feb 91

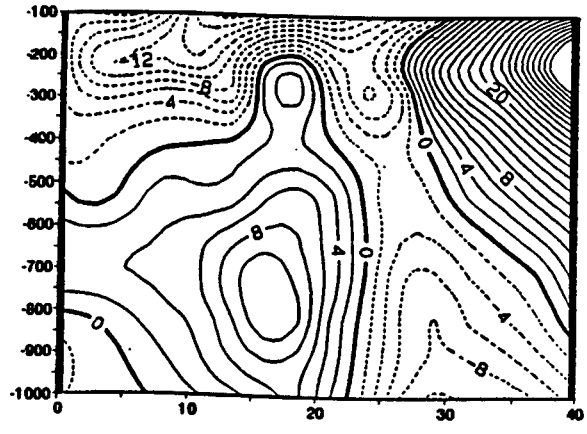

19 Feb 91

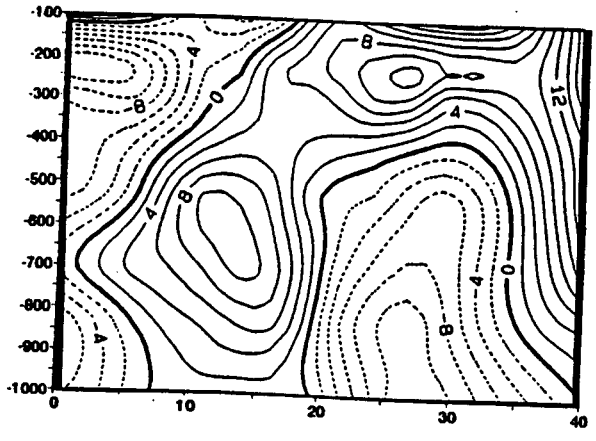

15 Feb 91

Figure 6.12: Vertical section of the u-component of the horizontal wind along 46°E. Contour interval 2 m s^{-1}

6.2 The 1992 extreme rainfall event :

In January 1992, the NW region of Madagascar experienced another severe flood event due to the passage of TC Bryna resulting in many casualties. The system formed from a cloud cluster in the Indian Ocean northeast of the island between the latitude 10-15°S where the SST was 28-29°C. The surface pressure chart showed a cold front to the south of Madagascar moving eastward since 30 December. At lower levels, a northerly monsoon flow of 10-15 m s^{-1} was noted along the east coast of Africa before swinging to westerly to the north of Madagascar to converge into the TC. At the same time, the wind shear between 1000-500 hPa weakened in the area of formation, and the post-frontal anticyclone in the subtropics intensified. The development of the TC will be investigated using the ECMWF data in the same way as it has been done for TC Cynthia.

6.2.1 Dynamic and kinematic results :

6.2.1.1 Geopotential height :

The 1000 hPa geopotential height pattern on 28 December 1991 shows a low pressure area of 70 gpm in the I-O at 10°S, 65°E; over southern Africa exists a trough and a ridge axis is oriented along the coast of Mozambique (Fig 6.13). In the upper troposphere at 200 hPa level, a trough axis over Madagascar separates two anticyclones, one over Africa at 10°S, 30°E and another in the I-O at 20°S, 75°E; over Cape Town (South Africa) exists a cut-off low. On the 30th of December in the 1000 hPa level, the low system (80 gpm) moves westward toward Madagascar and an anticyclone of 200 gpm develops to the south of the Mozambique Channel. In the 200 hPa level, the upper-level trough moves southeastward. On 1 January 1992, in the 1000 hPa level the subtropical anticyclone intensifies to 210 gpm and moves eastward followed by the frontal

trough axis oriented meridionally along 30°E, the low system (TC Bryna) is located at 15°S, 52°E off the NE coast of Madagascar and intensifies to 70 gpm. In the upper level, a cut-off low forms over the southern Mozambique Channel, the anticyclone in the I-O moves over eastern Madagascar. On the 3rd of January, in the 1000 hPa level the low system weakens to 80 gpm over NW Madagascar at 17°S, 47°E; the frontal trough moves farther east to the SE of Reunion, followed by a post frontal high of 200 gpm located to the SW of the Channel. In the 200 hPa level, a high pressure area (12420 gpm) extends from Africa to the Mascarenes. To its east exists a trough oriented NW-SE at 65°E, and to the SW of the Channel lays a second trough over the SE coast of Africa. On the 5th of January, in the surface level the subtropical anticyclone moves east and weakens (180 gpm) followed by a frontal trough over South Africa, the low system continues to weaken (90 gpm) and moves southward to be located over SW Madagascar at 24°S, 43°E. In the upper level, the high pressure area strengthens to 12440 gpm and the upper-subtropical trough moves to the south of the Channel (Fig 6.13). Throughout the sequence the surface pressure minima is only 70 gpm. The system moves southwestward from 12°S, 64°E to 24°S, 42°E.

6.2.1.2 Horizontal wind :

The horizontal wind vector patterns at the 1000 hPa level reveal that on the 28th of December, the monsoon flow and the easterlies are converging over Madagascar. In the 200 hPa level exists a trough axis to the SW of the Mozambique Channel with strong subtropical westerlies. To the north of 15°S the upper-level easterlies are blowing toward the equator (Fig 6.14). On the 30th, the monsoon flow weakens and a cyclonic circulation forms to the east of the island at 10°S, 60°E. Both trade and monsoon winds converge into the vortex, and to the south of the Mozambique Channel an anticyclonic circulation forms. At 200 hPa,

the upper-level trough is shifted to the SE of the island and behind it, there is an anticyclonic circulation centered at 32°S, 44°E. The upper-level easterlies become less organized over the tropics. On the 1st of January at the surface level, the low system intensifies, moves westward and is located off the east coast of the island; while monsoon winds strengthen off the northern tip of the island. The subtropical anticyclone shifts east with stronger easterly flow. In the 200 hPa level, the system tilts south with height, the upper-level trough moves farther east and a cyclonic circulation develops over Mozambique. The upper-level easterlies weaken. On the 3rd, the surface pattern shows that the TC moves over the NW region of the island and weakens, the surface easterlies weaken and northwesterly monsoon flow converges into the system. In the 200 hPa level, the anticyclonic flow associated with the system is weak, whilst over the Mascarenes exists an anticyclonic circulation. On the 5th, the system is over the SW region of the island and to its south, there is an anticyclonic circulation. In the upper level, a trough axis develops to the south of the Channel and to the north of 10°S the upper-level easterlies become stronger in the tropics. A significant feature of the sequence is the persistence of subtropical upper westerlies in "front" of the TC.

6.2.1.3 Temperature gradient :

On 28 December, the vertical gradient of upper-level temperature between 500-100 hPa reveals the existence of instability over the I-O to the east of Madagascar and over Africa with a maximum of 76°C centered at 10°S, 30°E over Mozambique. From 28 December 1991 to 5 January 1992, the upper instability over the region increases and the maximum area shifts SE from the Congo basin to the northern Mozambique Channel; while in the I-O the area of high instability shifts NE toward the equator (Fig 6.15.a). As was seen in the case of TC Cynthia,

the latent heating in the mid-level and the upper radiative cooling contributes to positive feedback in the convective process.

6.2.1.4 Vertical wind :

On the 28th of December 1991, there is upward motion over Africa along the latitude 10°S with maximum -6 x 10^{-1} Pa s^{-1} over northern Mozambique and a weak uplift area to the NE of Madagascar. On the 30th, the area of upward motion expands over southern Africa and a second one develops over the island with its maximum (-4 x 10^{-1} Pa s^{-1}) on the NE coast. On 1 January 1992, the upward motion over Africa weakens and ascent over the island moves to its southern part (20°S, 47°E). In the I-O, the negative area enclosed by the 0-isoline extends from Madagascar eastward. Two days later on the 3rd, the areas of upward motion are located over tropical Africa, over Madagascar and at 8°S, 65°E in the I-O. On the 5th, the upward motion over the island intensifies with a maximum of -8 x 10^{-1} Pa s^{-1} over its SE coast (Fig 6.15.b). The vertical wind pattern at 500 hPa level suggests that the area of active convection over northern Mozambique moves eastward toward Madagascar as the TC moves westward. These factors contribute to the occurrence of heavy rainfall over the area although the TC weakened over land.

6.2.1.5 Divergence :

On the 28th of December (Fig 6.16), the 1000 hPa divergence pattern exhibits an area of convergence with a maximum of -8 x 10^{-6} s^{-1} along the latitude band 5-15°S extending southward over Madagascar to cover the entire island. The lower-level convergence area is overlaid by upper-level divergence with a maximum of 28 x 10^{-6} s^{-1} at the 200 hPa level. On the 30th of December, the convergence area over Africa weakens, while the one over the island intensifies to

-12×10^{-6} s^{-1} at 20°S, 47°E. In the upper level the zonal band of divergence splits into two parts, one over Africa and another one extending from Madagascar eastward with a maximum of 28×10^{-6} s^{-1} at 5°S, 60°E. On 1 January, the convergence area at 1000 hPa over the island is oriented NE-SW and continues to intensify with a maximum value of -16×10^{-6} s^{-1} off its NE coast. In the 200 hPa level an area of divergence (24×10^{-6} s^{-1}) exists above the lower-level convergence area. On the 3rd, the surface convergence is oriented N-S over the island and weakens to -12×10^{-6} s^{-1}. In the upper level, the zonal band of divergence is established along the latitude 15°S, extending southeastward over Madagascar where it has a maximum value of 16×10^{-6} s^{-1}. On the 5th, the upper divergence-lower convergence dipole starts to tilt. The convergence area at the surface over the island intensifies to a value of -16×10^{-6} s^{-1} as does the upper-level divergence (28×10^{-6} s^{-1}) at 200 hPa level.

6.2.1.6 Vorticity :

On the 28th of December 1991, there is in the 1000 hPa level a cyclonic vorticity area extending from the eastern Mozambique Channel northeastward to the I-O with a maximum of -40×10^{-6} s^{-1} (Fig 6.17). In the upper level (200 hPa) a belt of anticyclonic values is oriented NW-SE over the tropics from Africa to the I-O; to its south exists a band of cyclonic vorticity with a maximum of -60×10^{-6} s^{-1} over Botswana. The southern tip of Africa is covered by a positive area, and to the NE of Madagascar lays a weak area of cyclonic vorticity. On the 30th, the surface cyclonic vorticity over the island weakens (-16×10^{-6} s^{-1}) and in the I-O at 10°S, 65°E a negative area develops (-24×10^{-6} s^{-1}). In the upper level, the subtropical anticyclonic area moves to the south of Madagascar pushing the negative area north forming an inverted V-shape over the Channel. The region to the east of Mauritius and the interior southern Africa are cover by positive

vorticity areas. On 1 January 1992, the cyclonic vorticity in the I-O intensifies to a value of -32 x 10^{-6} s^{-1} and moves toward Madagascar to cover its northern region. In the 200 hPa level, the island is under an anticyclonic vorticity area. A negative area develops with a maximum of -48 x 10^{-6} s^{-1} over Mozambique and the eastern Channel. On the 3rd, the lower cyclonic vorticity extends over the island with a maximum value of -24 x 10^{-6} s^{-1} over its SW region. In the upper level a band of positive values extends NW-SE from tropical Africa to the I-O with a maximum of 48 x 10^{-6} s^{-1} to the south of the Mascarenes at 25°S, 50°E. On the 5th, the lower cyclonic vorticity shifts SW over the Channel connecting a negative area in the subtropics to the SE of South Africa and another along the 10°S latitude in the I-O. In the 200 hPa level, the area of positive vorticity intensifies to 60 x 10^{-6} s^{-1} at 27°S, 55°E and over the southern Channel a cyclonic vorticity area of maximum value of -60 x 10^{-6} s^{-1} develops.

6.2.2 Moisture and thermodynamic results :

6.2.2.1 Precipitable water :

The field of precipitable water (PW) integrated from the surface to 300 hPa reveals that there is an excess of moisture over 50 mm in northern Madagascar throughout the sequence while over tropical Africa, PW does not exceed 30 mm (Fig 6.18.a). On 28 December 1991, the 40 mm-isoline covers the tropical region of I-O with a maximum of 60 mm at 10°S, 72°E. On the 30th, this 40 mm-isoline extends southward and the area of maximum moisture content shifts to the east of Mauritius at 20°S, 75°E. On 1 January 1992, the area of maximum PW content moves to the NE coast of Madagascar. On the 3rd, it is located over the NW region of the island, and then shifts SE over the eastern region on the 5th of January. The PW pattern suggests that prior to the development of TC Bryna, the

branch of the ITCZ in the I-O was convectively active and moist in contrast with the one over the Congo basin.

6.2.2.2 Water vapour flux :

The WVF pattern is similar to the surface level wind circulation and emphasises the TC vortex (Fig 6.18b). On 28 December, there is a low-level circulation over western Madagascar due to the convergence of monsoon flow and easterlies in the area, another low system exists in the I-O at 12°S, 70°E which will develop later into TC Bryna. On the 30th, TC Bryna intensifies, moves westward and is now at 11°S, 60°S. To the south of the Mozambique Channel an anticyclonic flux develops while the low system over the island weakens. On the 1st of January 1992, the TC intensifies and is located off the NE coast of the island, while the subtropical anticyclonic circulation moves east. On the 3rd, the TC is over NW Madagascar and weakens due to the relief of the region. The easterly flow weakens which suggests that a majority of moisture converging into the system comes from the monsoon flow. On the 5th, the monsoon moisture flux continues.

6.2.2.3 Velocity potential of water vapour flux :

The velocity potential of the WVF integrated from the surface to 500 hPa reveals that the area of positive maximum value (convergent WVF) shifts from northern Mozambique and the I-O to SE Madagascar from 28 December to 5 January (Fig 6.19.a).

On the 28 of December, the SE Africa region is dominated by an area of convergent WVF with a maximum of 28 x 10^9 kg s^{-1} at 15°S, 38°E over Mozambique. To the SE of Mauritius however exists a weak area of divergent WVF (-4 x 10^9 kg s^{-1}). On the 30th, the area of maximum convergent WVF shifts

southeastward to be located off the east coast of Madagascar while the area of divergent WVF in the subtropics moves to the south of the island. On 1 January 1992, the area of convergent WVF intensifies to a value of 36 x 10^9 kg s^{-1} to the north of Reunion. Its center shifts westward off the east coast of Madagascar on the 3rd of January. On the 5th, the area of maximum convergent WVF shifts to the SE coast of the island and intensifies to 44 x 10^9 kg s^{-1} centered at 23°S, 50°E.

6.2.2.4 Streamfunction of water vapour flux :

The streamfunction of the WVF integrated from the surface to the 500 hPa level (Fig 6.19.b) exhibits on 28 December two positive areas (cyclonic circulation), one over SE Madagascar with a maximum of 16 x 10^9 kg s^{-1}, and another to the east of longitude 60°E with a maximum of 16 x 10^9 kg s^{-1} at 17°S, 68°E. These two areas are separated by a negative band (anticyclonic circulation) oriented N-S along 55°E with a maximum of -16 x 10^9 kg s^{-1} at 10°S, 52°E. On the 30th, the positive area in the I-O extends up to Madagascar and intensifies to a value of 52 x 10^9 kg s^{-1}. The anticyclonic circulation area shifts westward with a maximum value of -28 x 10^9 kg s^{-1} over the SE coast of Africa. On 1 January, the moisture flux circulation weakens. The positive area (36 x 10^9 kg s^{-1}) continues its westward movement and is centered at 17°S, 55°E. On 3 January it is located over Madagascar (20°S, 47°E) with a maximum value of 40 x 10^9 kg s^{-1} and extends over the northern Mozambique, while a negative area lays over southeastern Africa. On the 5th, the positive area weakens over the SW of the island and in the I-O a negative area of -32 x 10^9 kg s^{-1} develops over the Mascarenes.

6.2.2.5 Equivalent potential temperature :

The EPT field highlights an area of convective potential along the ITCZ with instability over the interior of Africa (Fig 6.20).

On 28 December, at the 1000 hPa level there are warm sector areas bounded by the 350°K-isolines over tropical Africa and in the I-O at 10°S, 65°E. In the 500 hPa level, the warm sector (>340°K) is confined over 10°S, 30°E. On the 30th, the surface warm sector in the I-O extends from 55°E eastward and in the 500 hPa level there is a belt of warm area (>330°K) along 12°S. On 1 January, the 350°K-isoline in the 1000 hPa level covers tropical Africa and extends a zonal band along 15°S toward the I-O. In the upper level (500 hPa) exists two warm areas, one over the Congo basin and another over the I-O from the northern tip of Madagascar. On the 3rd, at the surface there are two areas of maximum EPT, over the Congo basin and over NW Madagascar, this structure is reflected in the 500 hPa level suggesting a region of convective potential. In the 5th, the maximum warm area over the island shifts to its SE coast (Fig 6.20).

6.2.3 Vertical section analysis of the 1000-100 hPa layer :

6.2.3.1 The vertical section of the divergence field :

The E-W vertical section of divergence along the 16°S (Fig 6.21.a) shows that on the 28th of December, there is a convergent area over NW Madagascar (47°E) from the surface tilted NW with height with a maximum of -8×10^{-6} s^{-1} at 700 hPa. This lower tropospheric convergence is overlaid by upper-level divergence (8×10^{-6} s^{-1}) at 300 hPa. On the 30th, the lower convergence maximum moves down to 800 hPa while in the upper level, the area of maximum divergence remains at 300 hPa. Over the interior of southern Africa (20°S), there is weak low level convergence extending up to 400 hPa just below upper divergence with a maximum value of 20×10^{-6} s^{-1} at 250 hPa. On 1 January 1992, maximum convergence over the island is located at the surface while above it upper divergence moves to the 300 hPa level and tilts NW. In the mid-troposphere

over SE Africa and the Mozambique Channel, exists a divergence area overlaid by an upper-level convergence field. On the 3rd, maximum convergence over the island deepens and is still overlaid by the upper-level divergence field. Over Africa a convergence field develops in the lower troposphere up to 400 hPa. The mid-troposphere over the Mozambique Channel is dominated by divergence. On the 5th, the lower-level convergence over the island intensifies (-12×10^{-6} s^{-1}) as well as the upper-level divergence (24×10^{-6} s^{-1}) and the dipole system shifts westward with the upper-level divergence slightly ahead.

The N-S vertical section of the divergence field along 46°E (Fig 6.21.b) reveals on 28 December, the existence of a convergence area over the latitude band 14-28°S which extends up to 700 hPa over NW Madagascar (17°S). Above this lower-level convergence area is a field of divergence with a maximum of 12×10^{-6} s^{-1} at 250 hPa. On the 30th, the system intensifies and shifts northward with the lower-level convergence extending up to 400 hPa and the upper-level divergence with a maximum of 20×10^{-6} s^{-1} over 17°S. On the 1st of January, throughout the troposphere exists alternate layers of convergence and divergence tilted north with height. The lower-level convergent area is confined near 22°S with upper-level divergence at 200 hPa. On the 3rd, the dipole structure over the island intensifies with maximum convergence (-24×10^{-6} s^{-1}) at the surface in NW Madagascar (16°S) and a maximum divergence of 28×10^{-6} s^{-1} over 14°S at 250 hPa. On the 5th, the upper-level divergence continues to intensify.

The vertical section of the divergence indicates that in the lower level, the area of convergence is mainly confined over the NW of Madagascar, being enhanced by the topography of the island. Before the flood event, the convergence-divergence dipole over the region weakens through interaction of the TC with the eastern mountainous region. The monsoon flow converging into the area enhances uplift and intensifies the convergence-divergence dipole.

6.2.3.2 The vertical section of the vorticity field :

The E-W vertical section of the vorticity field along 16°S (Fig 6.22.a) indicates on the 28th of December, in the mid-troposphere between Africa and Madagascar the existence of negative (cyclonic) vorticity with a maximum of -16 x 10^{-6} s^{-1} at 650 hPa over the Mozambique Channel (45°E). Above it, there is a layer of anticyclonic vorticity with a maximum (40 x 10^{-6} s^{-1}) over 35°E. On the 30th, the negative area over the Channel (35-46°E) extends throughout the troposphere with a maximum of -56 x 10^{-6} s^{-1} at 250 hPa. The upper-level positive area shifts westward over Mozambique (30°S). To the east of Madagascar in the I-O a cyclonic vorticity area develops at 700 hPa over 65°E, and above it lays an area of positive vorticity. On the 1st of January, the whole system moves westward, the lower negative area in the I-O moves over the island extending from the surface to 650 hPa. In the upper level the area of anticyclonic vorticity in the I-O intensifies with a maximum of 32 x 10^{-6} s^{-1} over 65°E, while the negative vorticity over the Channel in the upper level weakens to -24 x 10^{-6} s^{-1}. On the 3rd, the lower cyclonic vorticity over the island extends upward and it is now juxtaposed with the positive vorticity area aloft. On the 5th, the system weakens with the area of anticyclonic vorticity covering the upper troposphere.

The N-S vertical section of vorticity along longitude 46°E (Fig 6.22.b) shows on 28 December 1991, the existence of a lower level negative vorticity area with a maximum of -40 x 10^{-6} s^{-1} over Madagascar (12-25°S). To the south of it, there is a positive area (32 x 10^{-6} s^{-1}). In the upper level exists an area of positive vorticity (40 x 10^{-6} s^{-1}) at 300 hPa over 10°S. On the 30th, the vorticity structure weakens, in the lower level the cyclonic area is confined to 15°S and in the upper level, a positive vorticity area (80 x 10^{-6} s^{-1}) develops over the subtropics. On the 1st of January, positive vorticity dominates the troposphere except that in the lower level there are two columns of negative area bounded by 0-isolines over 14

and 26°S up to 700 hPa. On the 3rd, the lower-level negative area develops and extends throughout the troposphere between the latitude band 10-25°S with a maximum of -48 x 10^{-6} s^{-1} at 800 hPa. In the upper level the anticyclonic vorticity weakens (32 x 10^{-6} s^{-1} at 200 hPa) and extends from 750 hPa upward near 25°S. On the 5th, the lower-level cyclonic vorticity area weakens and shifts south over the latitude band 16-27°S.

6.2.3.3 The vertical section of the EPT field :

The E-W vertical section of EPT along 16°S (Fig 6.23.a) exhibits land heating effects over Madagascar and the plateau of SE Africa. On the 28th of December 1991, there is a warm layer over the interior of Africa in the lower troposphere, and a dry stable sector extends from the Mozambique Channel to 70°E in the mid-troposphere with minimum 326°K at 750 hPa over Madagascar (45°E). On the 30th, the cold area of EPT in the mid-troposphere moves westward over the Channel. From the 1st of January onward, the lower and mid-tropospheric layer becomes warmer from Madagascar to Africa suggesting deep convection potential over the region. The dry stable area in the mid-troposphere shifts toward the I-O. It is clear that the main low EPT layer eroding the TC is in the mid-troposphere layer 700-500 hPa.

The N-S vertical section of EPT along the longitude 46°E (Fig 6.23.b) reveals high convective potential over Madagascar throughout the sequence. On 28 December, there is a warm sector at the surface up to 700 hPa over the island at 22°S. On the 30th, the lower layer of the troposphere over the island (10-25°S) becomes warmer up to 3 January. On the 5th, this lower-level warm area over the island shifts southward. This indicates that deep convection follows the TC poleward.

6.2.3.4 The vertical section of the zonal wind field :

The N-S vertical section of the zonal wind along longitude 46°E indicates on the 28th of December that there is a negative (easterly wind) layer at the equator throughout the troposphere (Fig 6.24). To the south of 5°S the troposphere is covered with a positive (westerly wind) field (32 m s^{-1} at 250 hPa) in the subtropics. In the latitude band 19-29°S up to 700 hPa there exists a negative trade wind zone. On the 30th, to the north of 10°S, there are monsoon westerlies at the surface and easterlies aloft. Between 15-35°S exists a negative area throughout the troposphere and to the south of it a column of westerly winds. On the 1st of January, to the north of 15°S exists a dipole of lower positive-upper negative zonal tropical winds and to its south there is a negative area in the lower level and positive area in the upper level extending southward to the mid-latitudes. On the 3rd, at the surface between the latitude band 15-30°S exists a negative area extending upward over 20°S throughout the troposphere. To the south of it lays a positive area with maximum 30 m s^{-1} at 200 hPa. To the north of 15°S the dipole system weakens. On the 5th, the pattern is disorganized similar to the one on 28 December.

The meridional section of the zonal wind reveals that surface easterly winds weaken at the expense of the tropical westerlies. Two days prior to the event the shear line tilts with height and a double dipole is present. Organization of the double dipole is a useful forecast indicator of the flood event (Fig 6.24).

6.2.4 Summary :

TC Bryna was the longest lived depression of the 1991-92 season, its initial vortex was first located to the south of Agalega in the I-O on 26 December 1991. It dissipated to the SE of Fort-Dauphin, Madagascar in the subtropics on the 10th of January. Its intensity was moderate but it brought considerable precipitation to

NW Madagascar (up to 347 mm rainfall in 24 hours at Mahajanga) where floods caused a lot of destruction. Although the TC weakened over land on 2 January 1992, the monsoon flow enhanced uplift and associated convective activity over the eastern Channel.

The analysis of meteorological parameters associated with the TC reveals that the system moves westward from the I-O. Its surface pressure deepens and the subtropical anticyclone strengthens prior to the event. An upper cut-off low forms on the SW of the Mozambique Channel two days prior to the event. Subtropical upper westerlies are a key feature of the flood event, since the same phenomena was observed in the case of TC Cynthia. As the TC moves toward Madagascar, the low-level convergence area from northern Mozambique shifts over the island and the upper-level divergence associated with the system increases prior to the event. The PW field indicates that the I-O branch of the ITCZ is more active prior to the development of the TC. The WVF pattern suggests that four days prior to the flood event, moisture from the monsoon flux increases over NW Madagascar. Throughout the process areas of maximum positive velocity potential of the WVF increase and converge from northern Mozambique and the central I-O to SE Madagascar.

The vertical section of the troposphere allowed the following observation. The lower-level convergence is confined over the island due to its topography and although the TC weakens after its landfall, the increase of the monsoon flow converging into the area enhances uplift. The EPT field shows that the area of convective potential extends from SE Africa to the island prior to the event. The zonal wind field exhibits the weakening of the easterlies, while the westerlies strengthen and tilt equatorward with height two days prior to the event.

The main differences between the two TC events is the direction of propagation, lifespan and surface wind speeds.

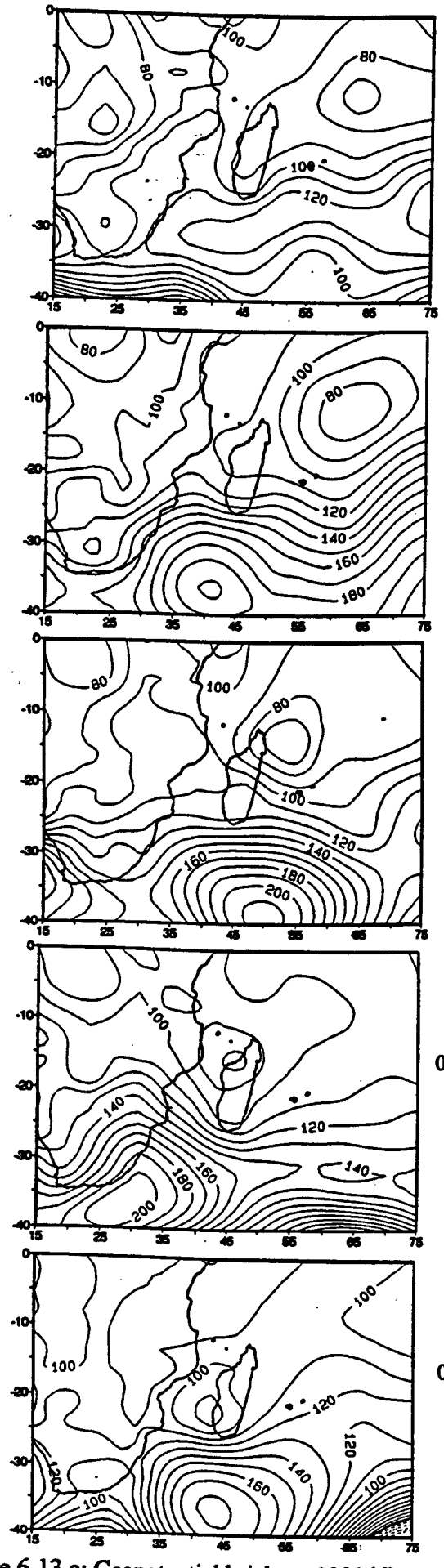

Figure 6.13.a: Geopotential height at 1000 hPa. Contour interval 10 gpm.

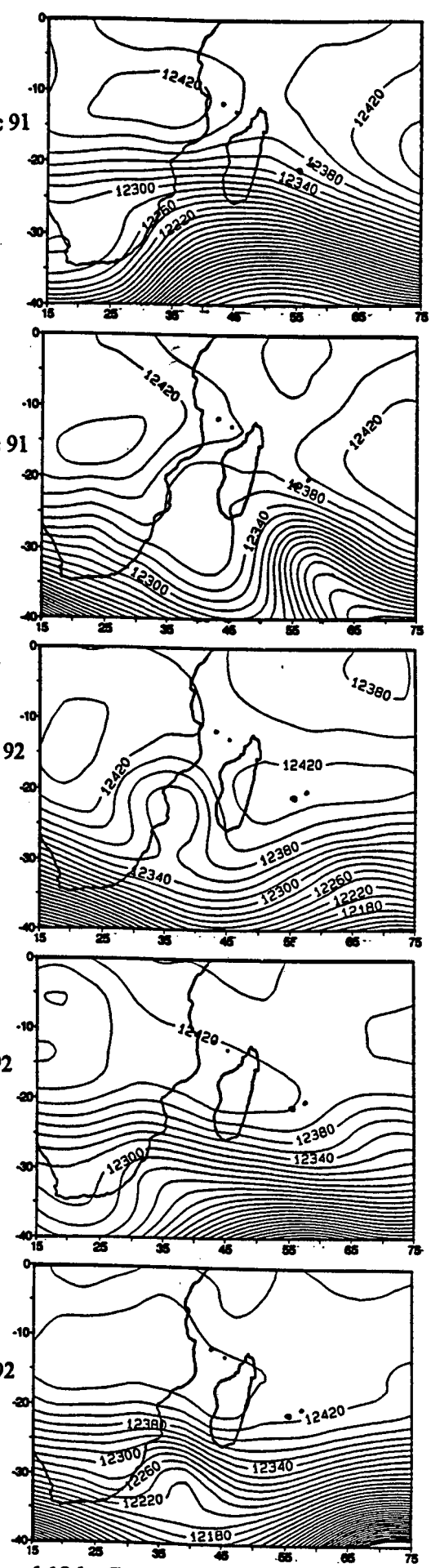

Figure 6.13.b: Geopotential height at 200 hPa. Contour interval 20 gpm

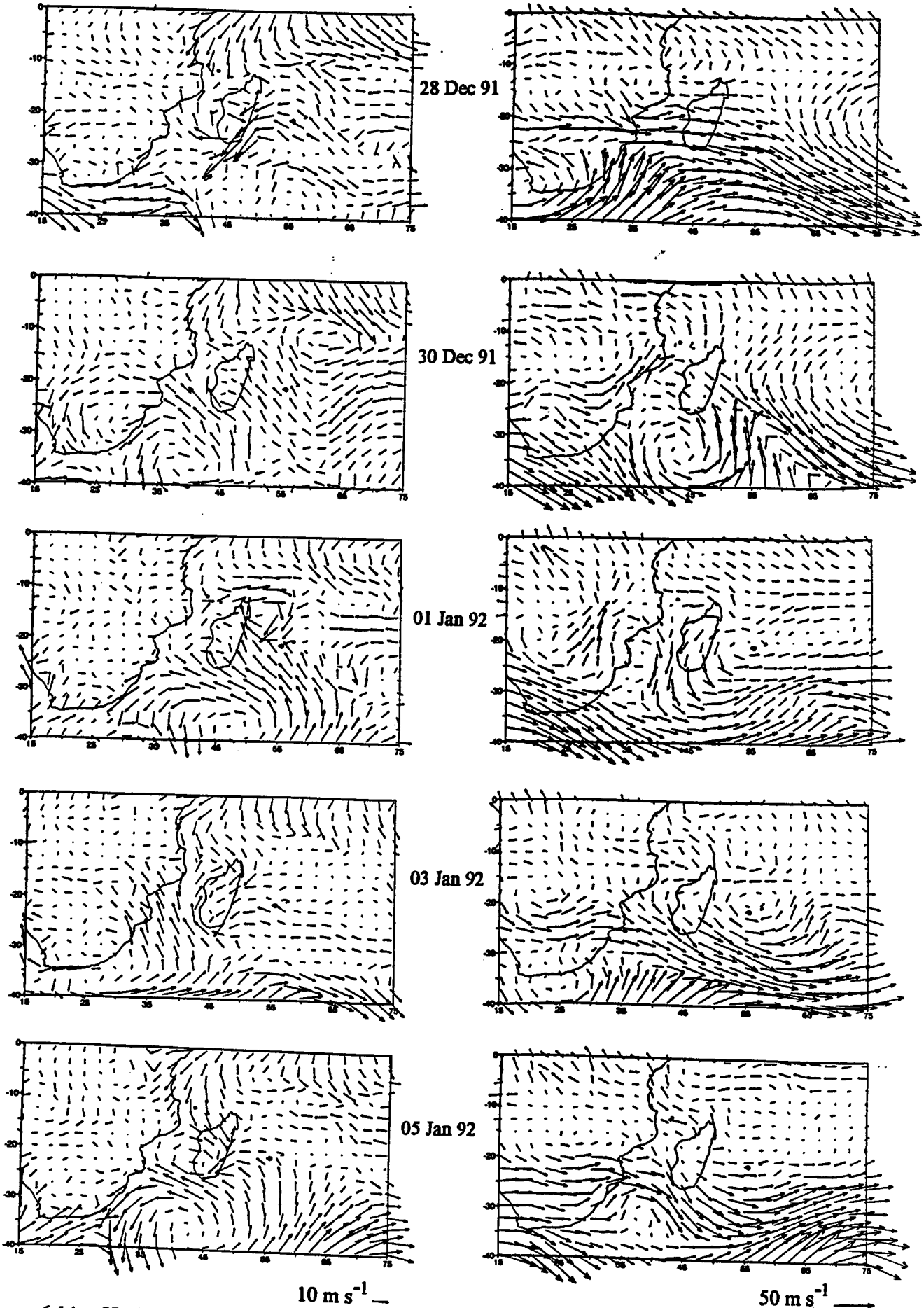

Figure 6.14.a: Horizontal wind at 1000 hPa.

Figure 6.14.b: Horizontal wind at 200 hPa.

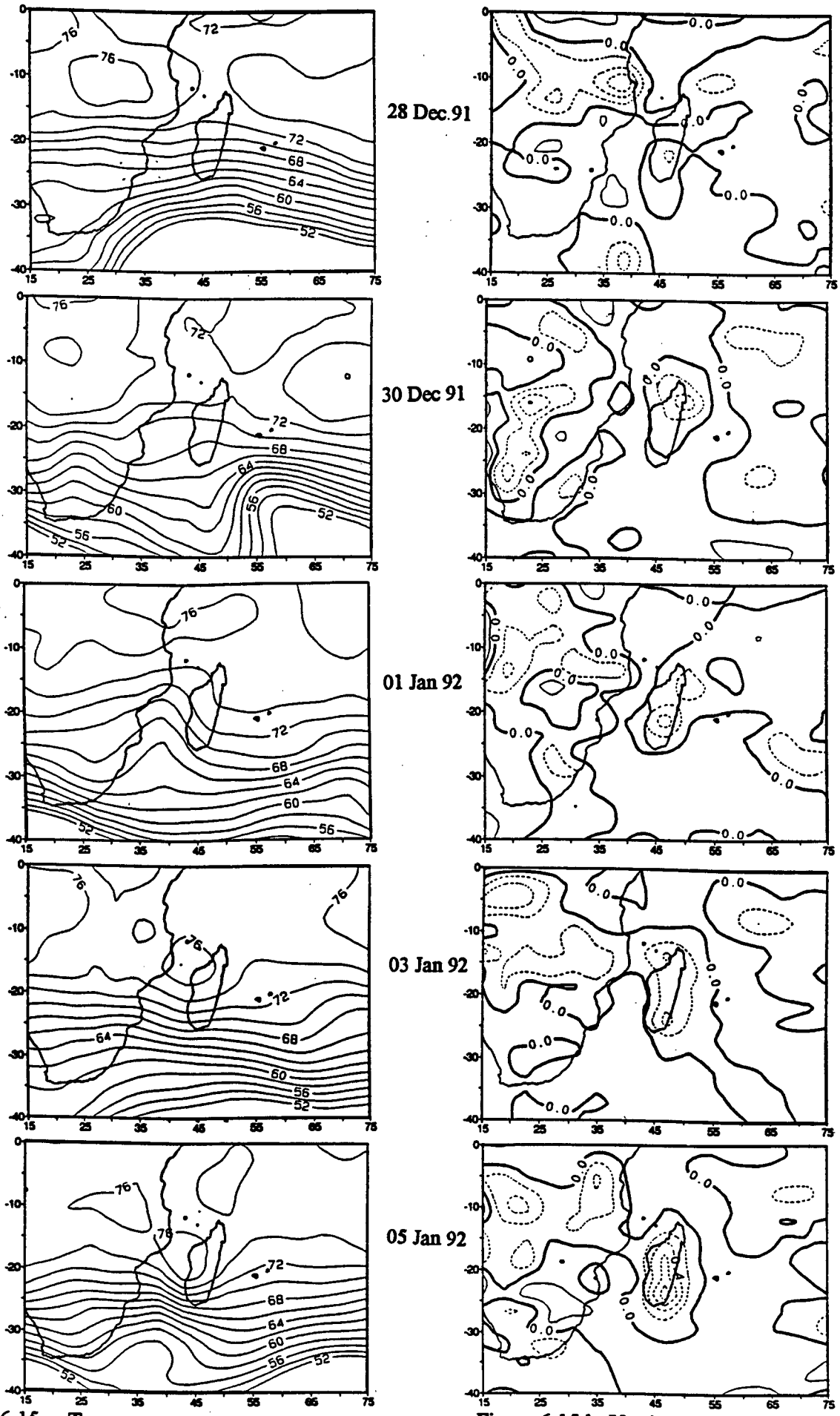

Figure 6.15.a: Temperature gradient between 500-100 hPa. Contour interval 2°C

Figure 6.15.b: Vertical wind at 500 hPa. Contour interval 0.2 Pa s^{-1}

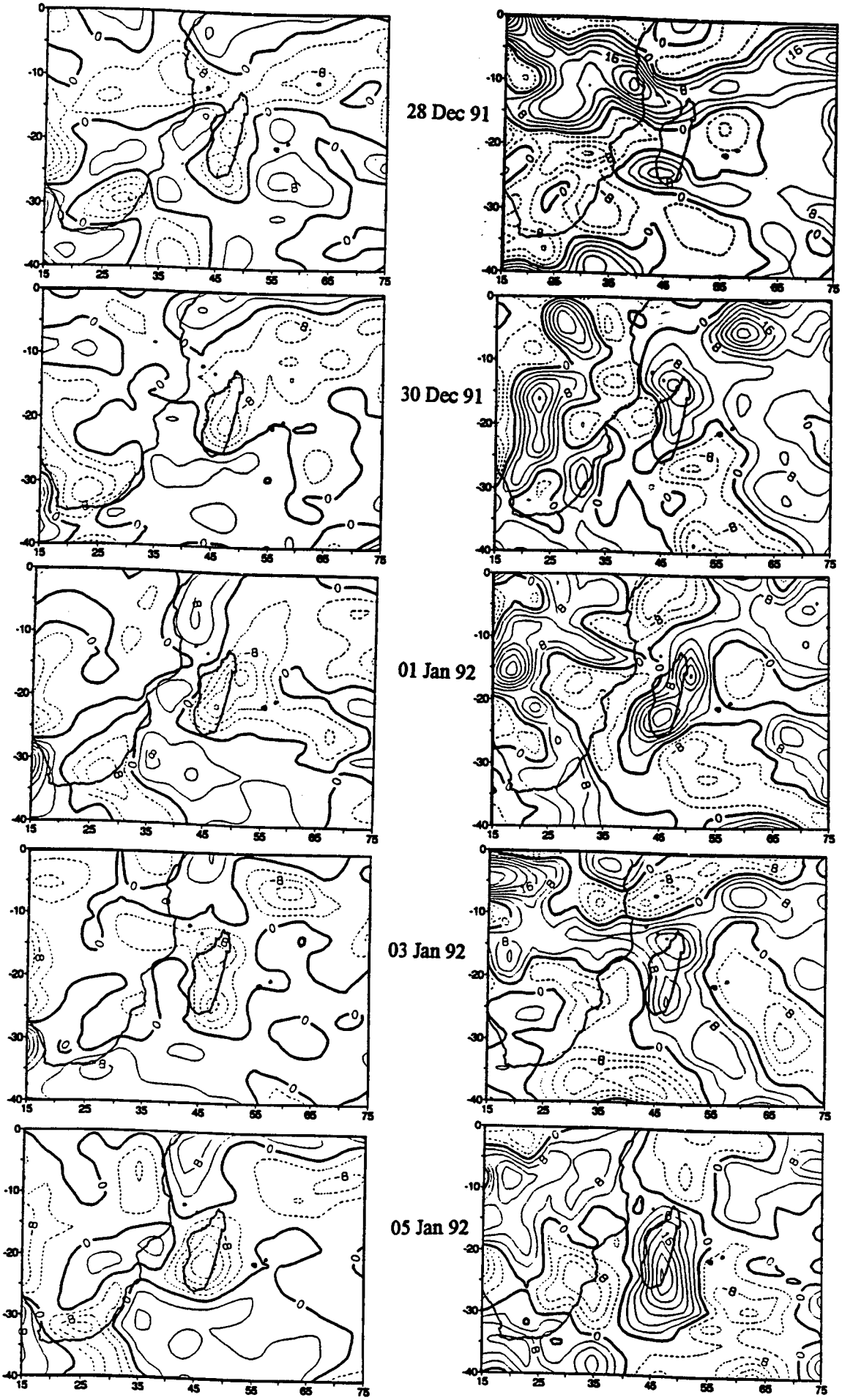

Figure 6.16.a: Divergence at 1000 hPa.
Contour interval 4 x 10^{-6} s^{-1}

Figure 6.16.b: Divergence at 200 hPa.
Contour interval 4 x 10^{-6} s^{-1}

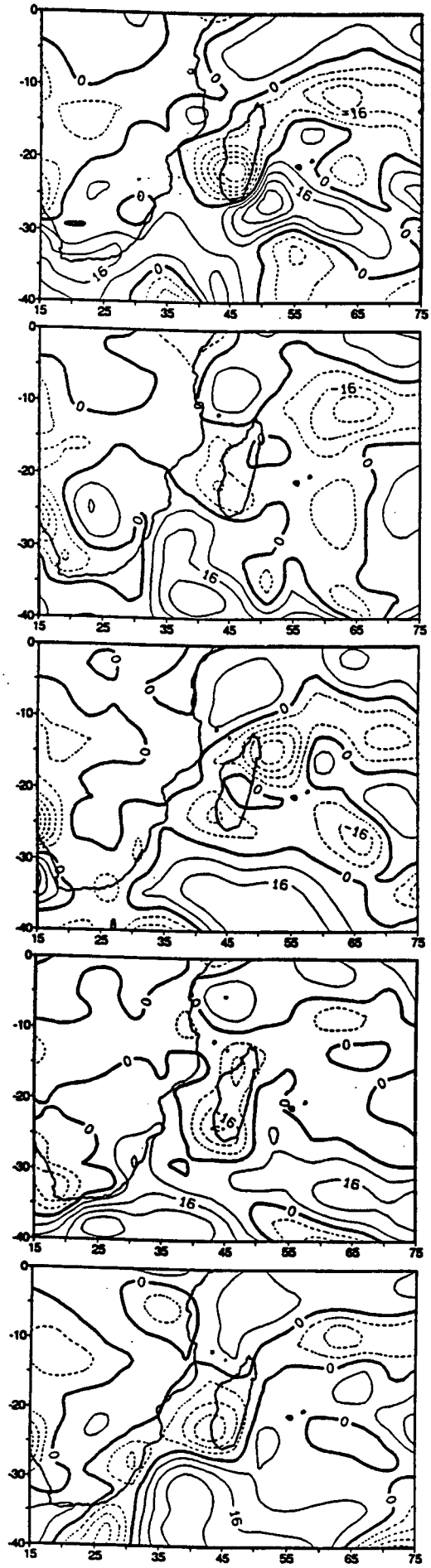

Figure 6.17.a: Vorticity at 1000 hPa.
Contour interval 8 x 10^{-6} s^{-1}

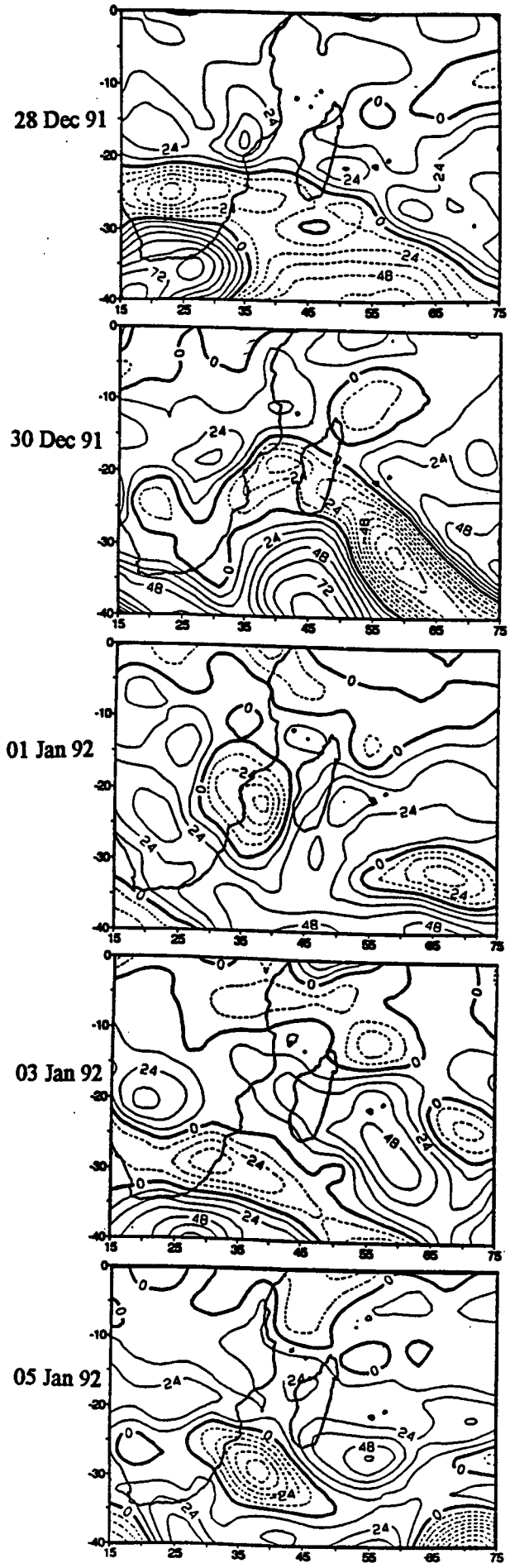

Figure 6.17.b: Vorticity at 200 hPa.
Contour interval 12 x 10^{-6} s^{-1}

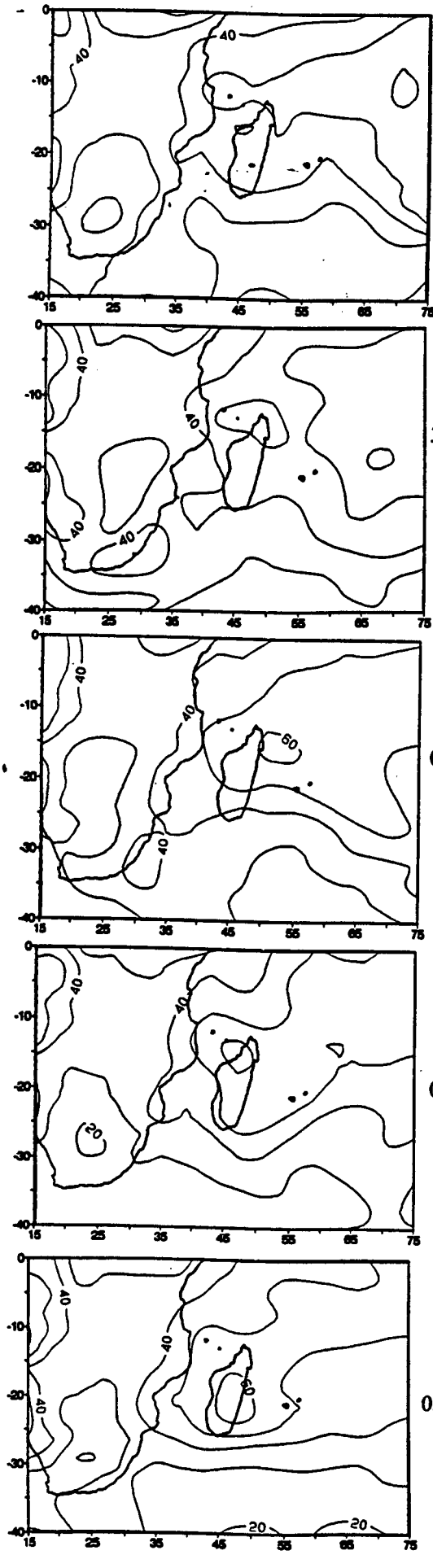

Figure 6.18.a: Precipitable water integrated from the surface up to 300 hPa. Contour interval 10 mm.

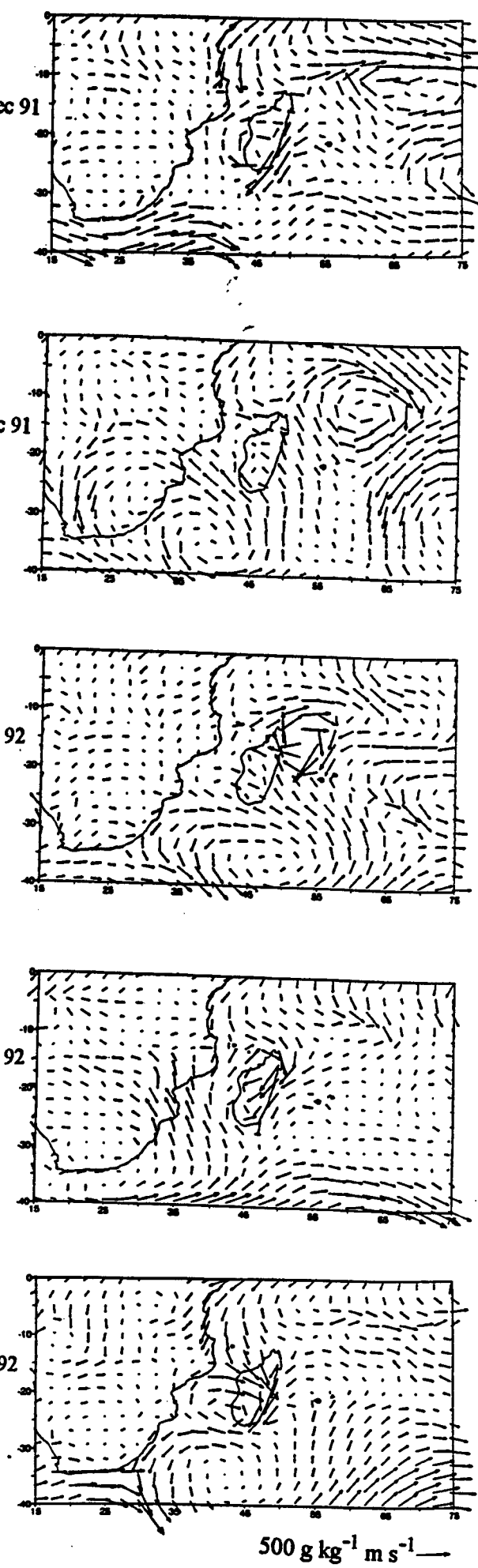

Figure 6.18.b: Water vapour flux integrated from the surface up to 500 hPa.

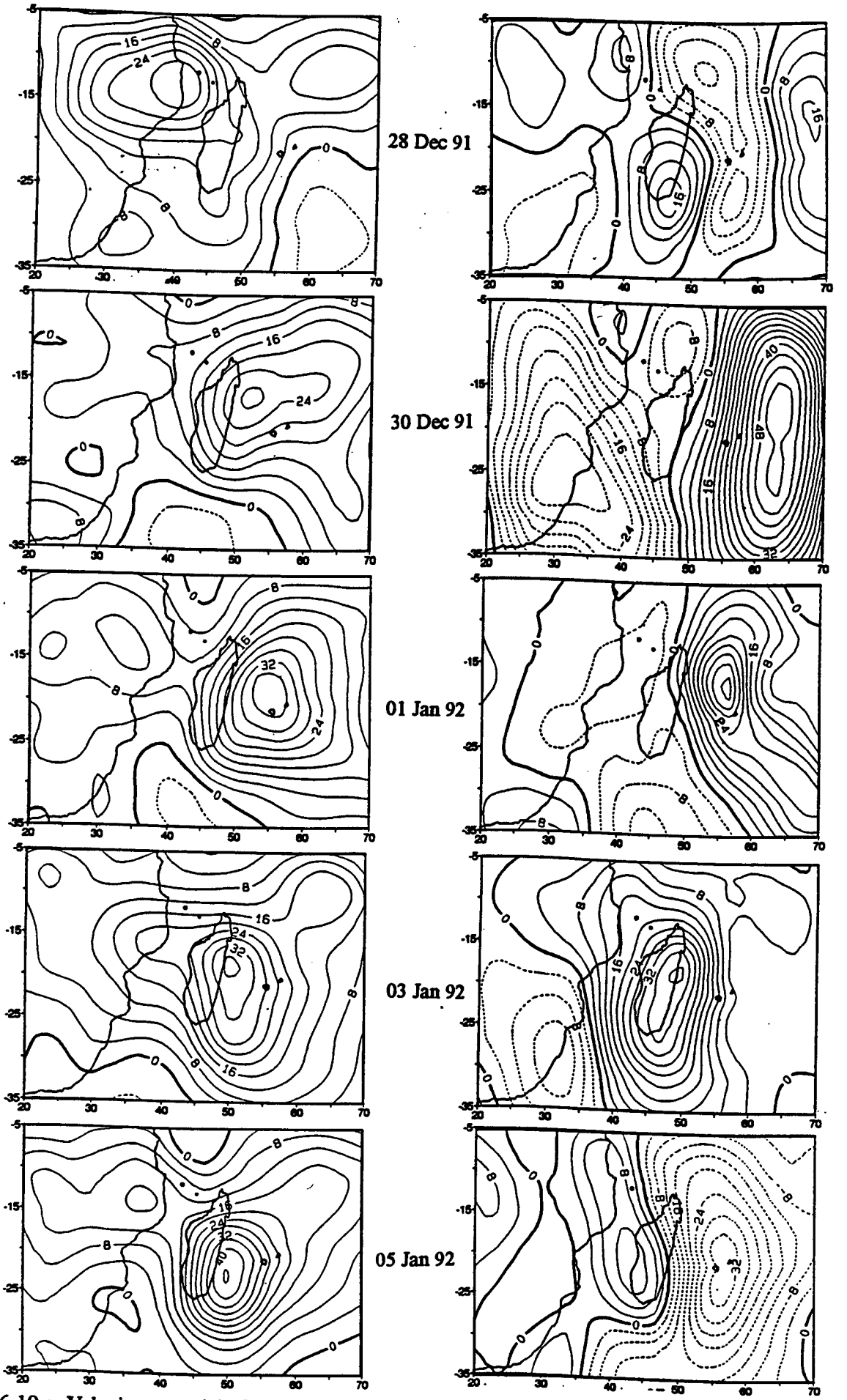

Figure 6.19.a: Velocity potential of WVF (χQ) integrated from the surface to 500 hPa. Contour interval 4 x 10^9 kg s^{-1}

Figure 6.19.b: Streamfunction of WVF integrated from the surface to 500 hPa. Contour interval 4 x 10^9 kg s^{-1}

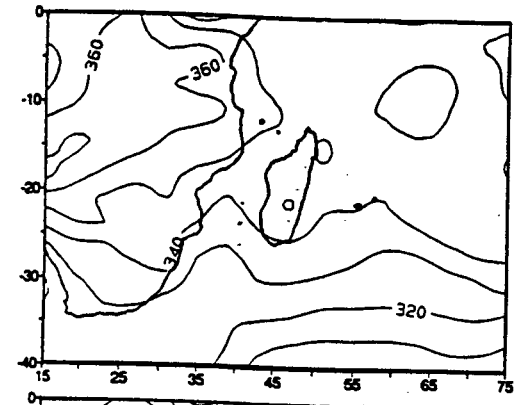

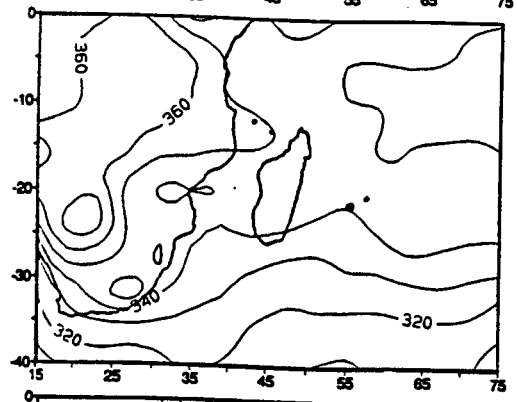

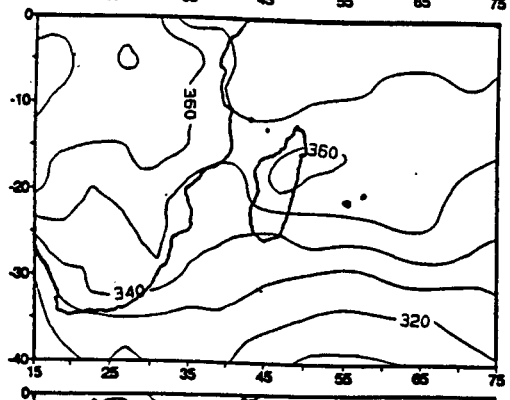

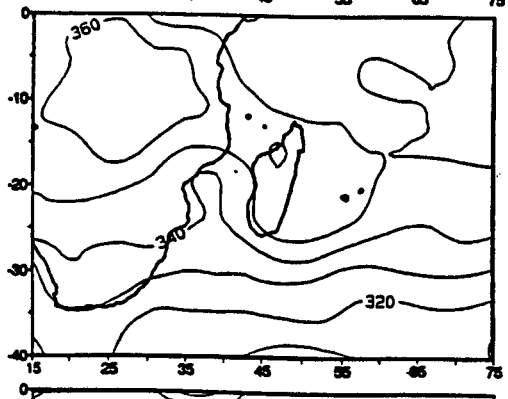

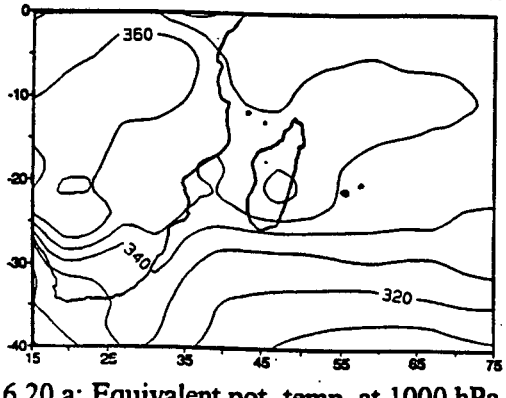

Figure 6.20.a: Equivalent pot. temp. at 1000 hPa. Contour interval 10°K

28 Dec 91

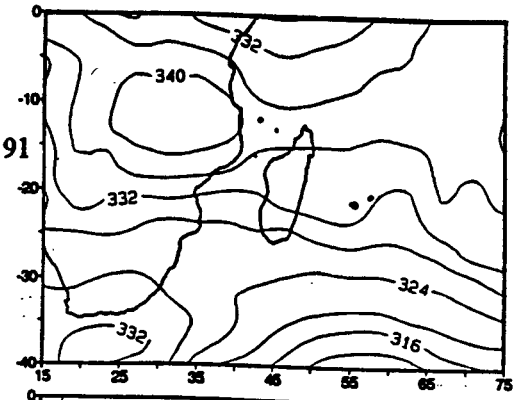

30 Dec 91

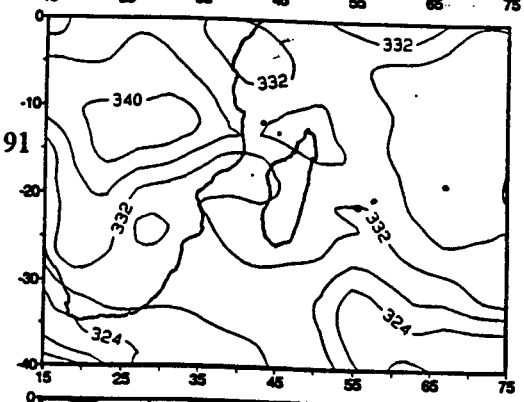

01 Jan 92

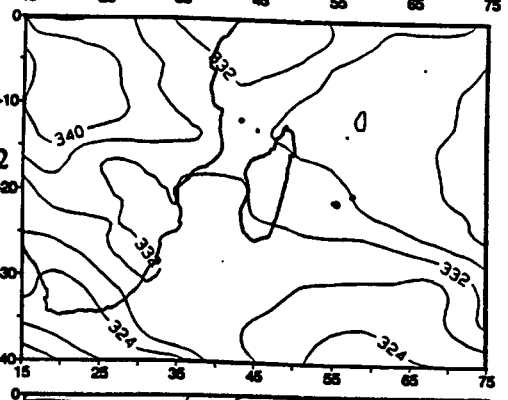

03 Jan 92

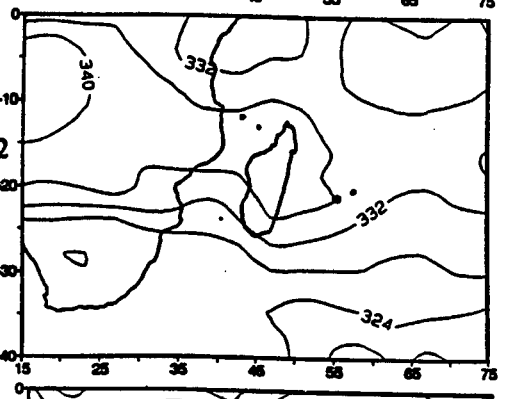

05 Jan 92

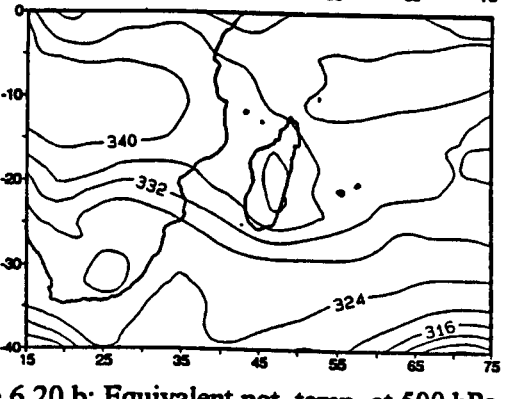

Figure 6.20.b: Equivalent pot. temp. at 500 hPa. Contour interval 4°K

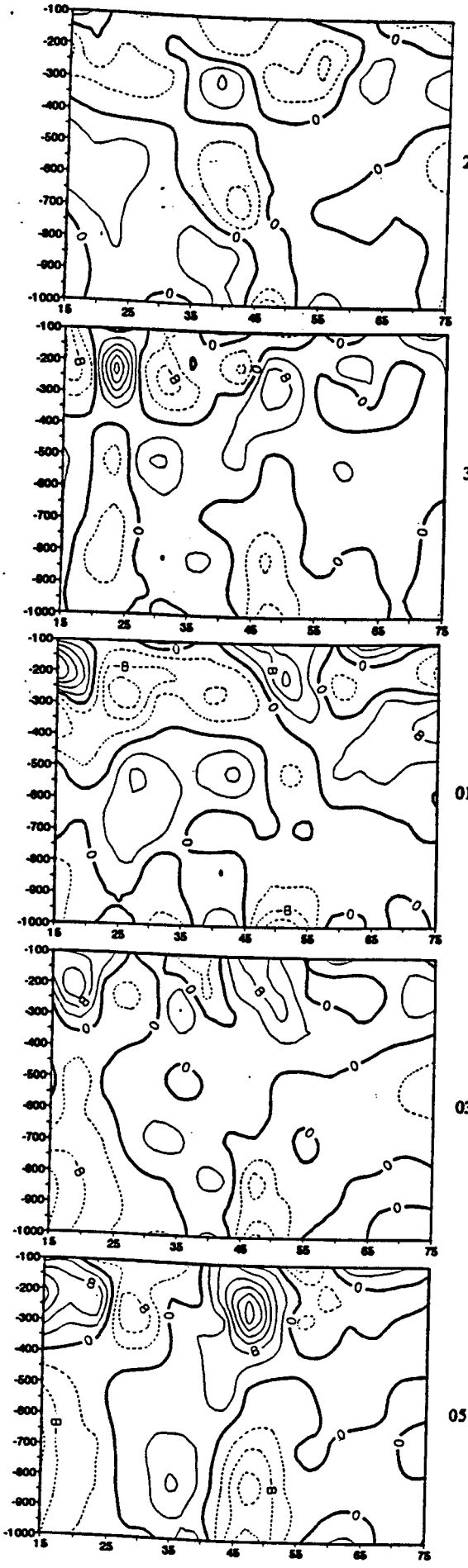

Figure 6.21.a: Vertical section of the divergence field along 16°S.
Contour interval 4 x 10^{-6} s^{-1}

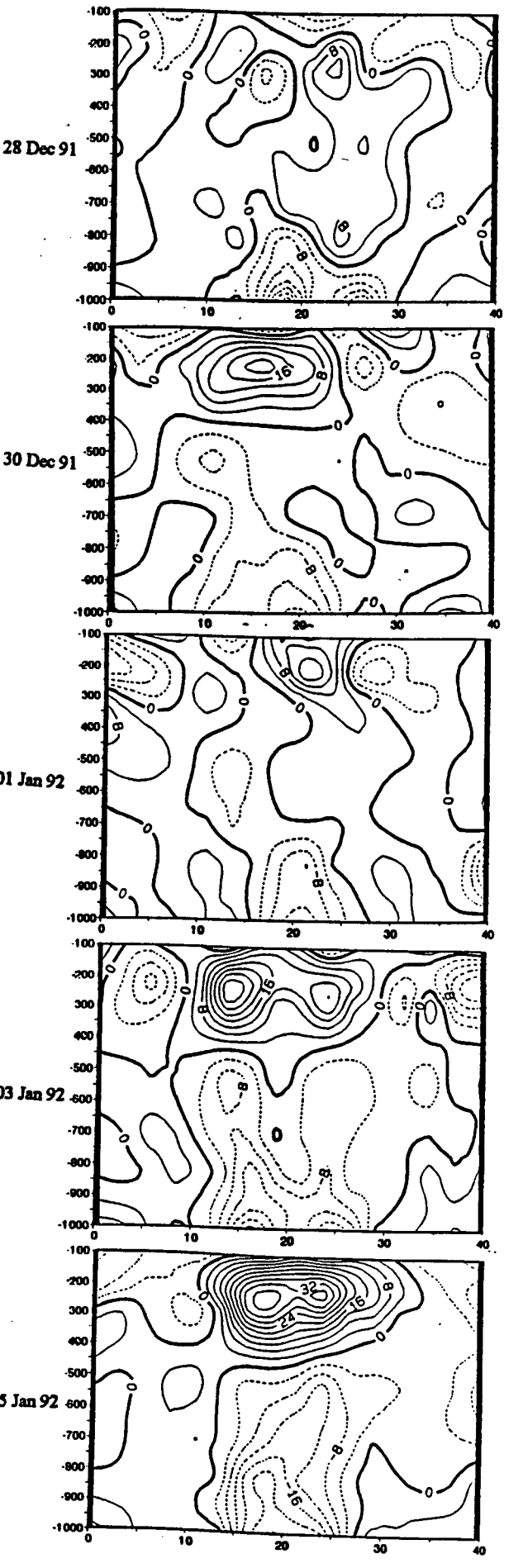

Figure 6.21.b: Vertical section of the divergence field along 46°E.
Contour interval 4 x 10^{-6} s^{-1}

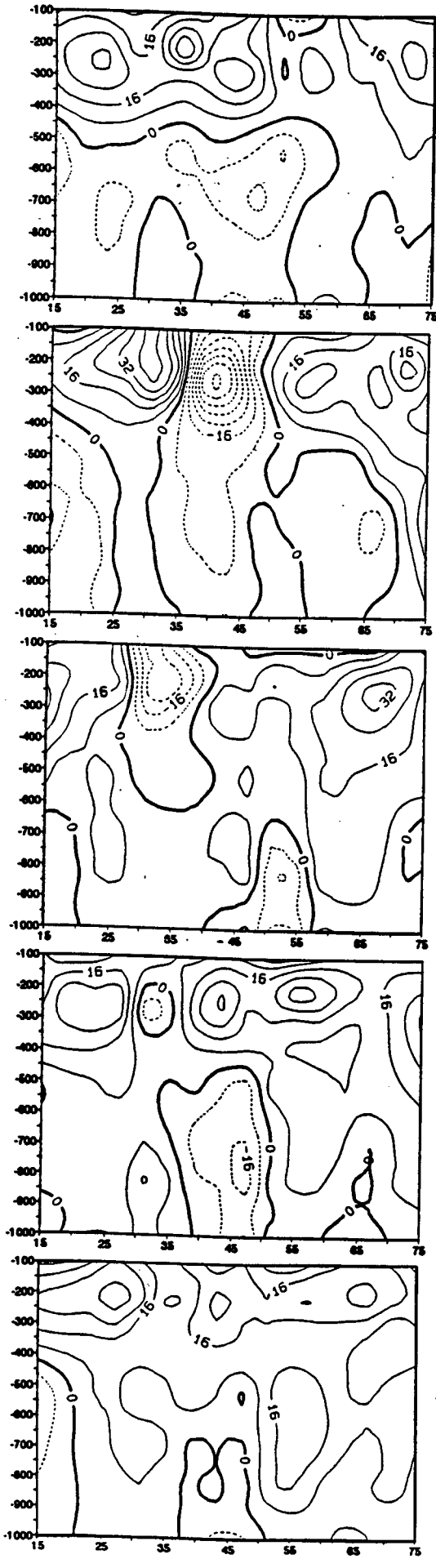

Figure 6.22.a: Vertical section of the vorticity field along 16°S.
Contour interval 8 x 10^{-6} s^{-1}

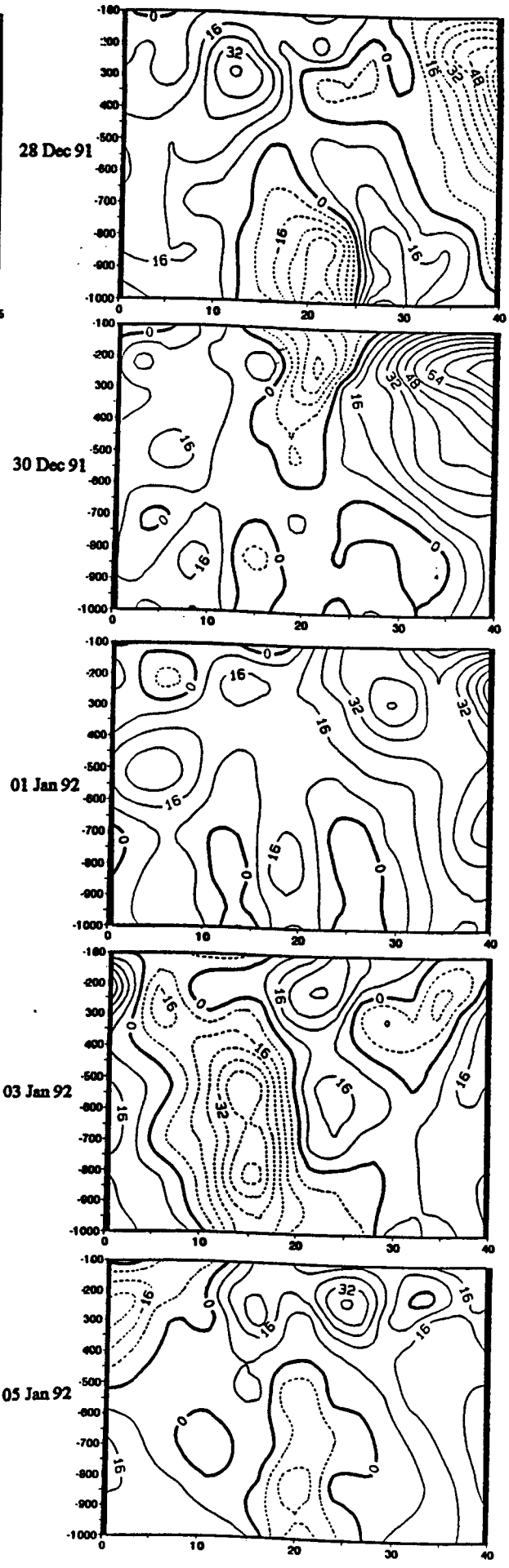

Figure 6.22.b: Vertical section of the vorticity field along 46°E.
Contour interval 8 x 10^{-6} s^{-1}

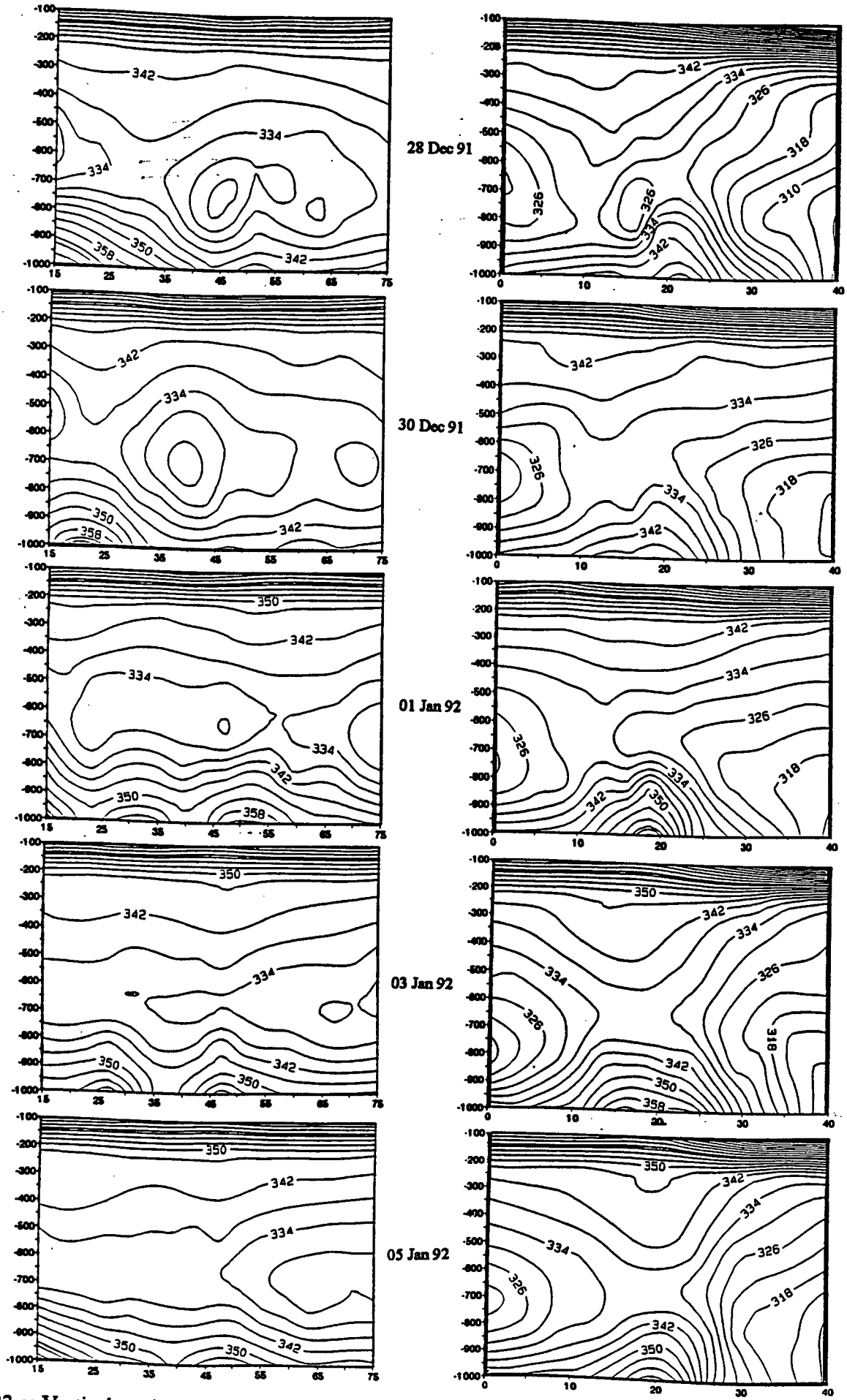

Figure 6.23.a: Vertical section of EPT along 16°S. Contour interval 4°K

Figure 6.23.b: Vertical section of EPT along 46°E. Contour interval 4°K

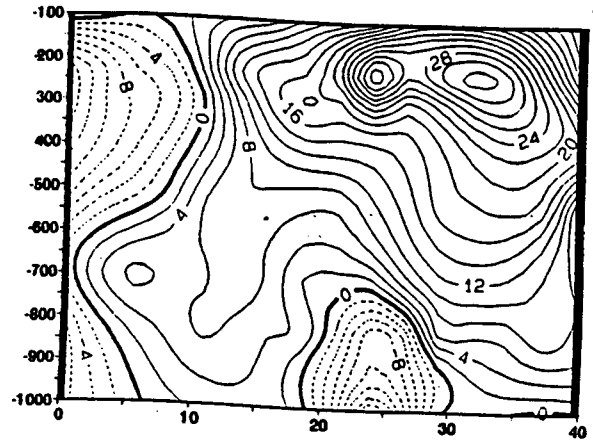

28 Dec 91

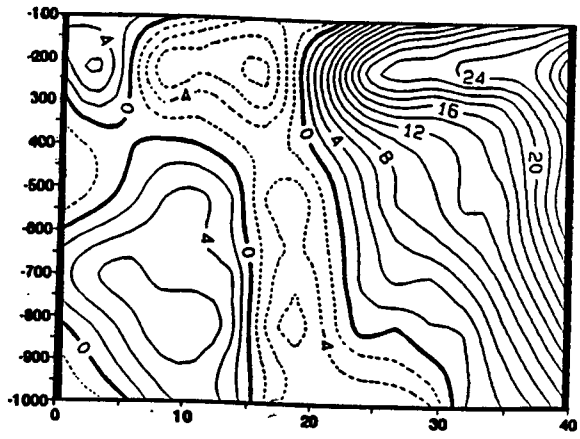

03 Jan 92

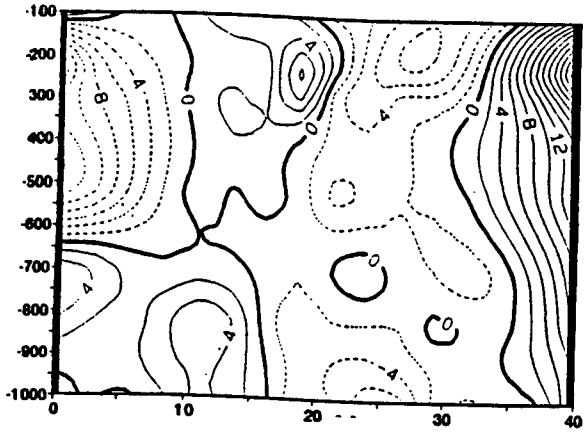

30 Dec 91

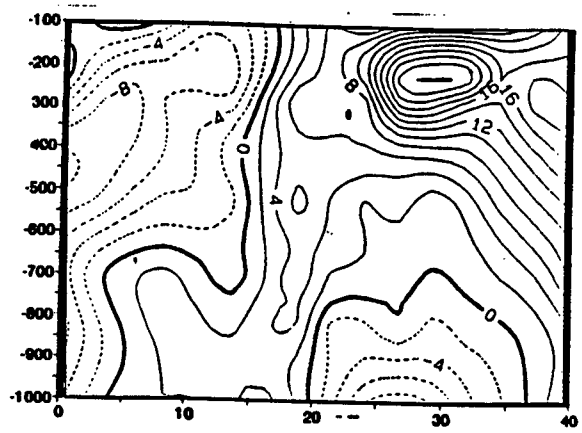

05 Jan 92

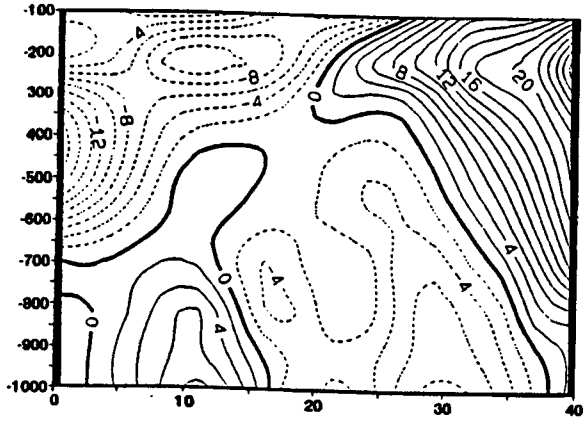

01 Jan 92

Figure 6.24: Vertical section of the u-component of the horizontal wind along 46°E. Contour interval 2 m s^{-1}

Bryna was the longest lived depression of the 1991-92 season. It brought up to 347 mm rainfall over the north and northwest regions of Madagascar where floods caused a lot of destruction. Strong wind and bad weather are concentrated in the TC's south quadrant, at Antalaha in the TC's northern quadrant, gusts of 15 m s^{-1} and rainfall of 110.6 mm were recorded, while at Mahajanga in the TC's southern quadrant, gusts of 23 m s^{-1} and rainfall of 346.6 mm was recorded in 24 hr. Although the TC weakened over land on 2nd January 1992, the monsoon flow enhanced uplift and associated convective activity over the Channel (fig B-4).

Damage was confined to roads, bridges and houses due to flooding over the north of the island. Only few deaths were recorded, this is due to its weak intensity and ample warning provided by the Madagascar Meteorological Department. The TC had a stable trajectory prior to landfall.

The westward tilt with height of the TC agreed with Douglas (1992) and coincide with upper easterlies and QBO in E-phase.

TC IN THE MOZAMBIQUE CHANNEL

The cyclonic seasons 1967/68 to 1991/92:

Climatology:

Cyclogenesis:

The tropical cyclones affecting the Mozambique Channel may be classified into two categories: TC from the Indian Ocean and TC originating in the Channel.

Frequency:

Observation have been improved since the use of satellite imagery in the region in 1968. During the season 1967/1968 up to 1991/1992, 37 tropical

depressions/cyclones (intensity > 2.5T in the Dvorak scale) have been observed moving from the Indian Ocean into the Channel, and 36 have been formed within the Channel. The least active seasons were 1981/82, 1986/87 and 1987/88 with no formation, while the most active seasons were 1970/71, 1974/75 and 1985/86 with 3 formations each.

Characteristics:

Concerning the Channel area, among these 36 TD/TC, 27 formed during January and February and 19 have westward trajectory.

a- Cyclonic activity:

Cyclonic activity is defined as the total of days where the storm's intensity were at least 2.5T.

The longest lived depression has 11 days of activity such as TC Joelle in 1970/71, and TD Debra in 1990/91 (in the Indian Ocean 22 days for the longest lived TC Alibera in 1989/90); and the shortest one has 2 days of activity such as TD Adele in 1974/75.

b- Intensity:

The intensity of the TC originated in the Channel is relatively weak. From that period 1967/68 to 1991/92, only 9 of the 36 TD formed reached TC intensity that is T number greater than 4.5 in the Dvorak scale.

These characteristics agreed with LeBorne (1987) who stated that the TC formed in the Channel are distinguished by small radius, relatively weak intensity, short lifespan, and rapid formation.

CHAPTER 7

DISCUSSION

Rainfall rates during wet events in NW Madagascar in the summer often exceed 70 mm per day, suggestive of deep tropical convection associated with monsoon type conditions. In this regard, the hypothesis addressed was that a tropical vortex is developed in the area as a result of localized enhancement of a transient tropical storm system. These events recur somewhat randomly, but in some years with a cyclic periodicity primarily associated with surges of the NW monsoon. The dynamics of the tropical weather have been characterised by studies of rainfall periodicity, through compositing of wet events, using various diagnostic analyses in a time frame from -4 days to +2 days, and through case studies.

7.1 Rainfall variability:

Summer season rainfall over NW Madagascar in the period 1960-1992 exhibits spectral peaks around 2.3 and 3.6 years, which are attributed to global oscillations. During the low phase of the SO, the ascending branch of the Walker circulation lies over and east of the island (Tyson 1986, Lindesay 1988). The ITCZ reaches it southernmost limit in the longitudes of Madagascar as a result of the cross-equatorial penetration of the NW monsoon and the lee-side trade wind trough developed over the eastern Mozambique Channel by the mountains of Madagascar (Jury and Pathack, 1991). The low phase of the SO and east phase of the QBO leads to enhanced lower-level convergence over Madagascar. However in many years the global oscillations play secondary roles, particularly at shorter

time scales. Ecormier (1992) and Donque (1979) indicate that extreme rainfall in the NW region of Madagascar is related to the passage of TC over the area.

Monsoon variability at the intra-seasonal scale is an important modulator of TC genesis potential. Over India and Australia the duration of wet spells in respective summer seasons is 15-20 days (Ananthakrishnan and Soman, 1988, Hendon and Liebmann 1990) and related to active periods of equatorial zonal flow. The mean onset of monsoon rainfall in the NW Madagascar region is near Christmas and the wet spell duration of 2-3 pentads is consistent to that found elsewhere. Westward moving convective systems are another frequent phenomenon in the SWIO and display a lifespan of 10-20 days. These easterly waves are considerably slower moving than their northern hemisphere counterparts and induce spectral peaks in low level meridional wind components near 20 days in the latitude band from 15-25°S. The spectrum of Madagascar daily rainfall is generally flat, and singular peaks are rare. This reveals the complex interplay between the convective forcing features (monsoon surges, easterly waves, African tropical troughs and mid-latitude westerly waves). Cycles of 10-20 and 40 days which are apparent in most cases can be attributed to transient waves and monsoon surges modulated by the Madden-Julian oscillation respectively.

The intraseasonal distribution of the rainfall during each season reveals the existence of several dry spells. The analysis of meteorological fields indicates a weakening of both monsoon and easterly wind regimes prior to the dry spell. At upper levels the westerly subtropical jet intensifies and the upper tropical easterly winds die off, particularly during summers with west phase QBO (Jury, 1992). An east-west dipole may often be present such that dry spells over Madagascar coincide with wet spells over southern Africa. The PW and the vertical section of the EPT patterns suggest the shifting of the active branch of the ITCZ toward eastern Africa prior to the occurrence of the dry spell.

7.2 Composite Study

The analysis of a 16-event composite was carried out in Chapter 5. These events lay in a period of below normal seasonal rainfall (1987-1992). The analysis of the meteorological anomalies indicates that two days prior to the event there is:

1] an intensification of the surface convective area over Mozambique and an eastward shift over Madagascar, coincident with strengthening of upper level divergence over the island.

2] an intensification and shifting of the surface cyclonic vorticity from Mozambique to the island and a strengthening of upper anticyclonic vorticity, assisted by the sub-tropical jet.

3] a strengthening of monsoon flow and weakening of the easterlies in the surface layer, and development of northwestward outflow.

4] an eastward shift in the velocity potential of the WVF field indicating moisture flux convergence over the island.

The above is in agreement with Lyons (1991) who found a northeastward propagation of a sub-tropical trough combined with a monsoon trough moving southward across east Africa. The composite analysis reveals the importance of an upper sub-tropical trough in cyclogenesis (McBride and Keenan 1982), and emphasizes the eastward movement of the flood-producing system from Mozambique to Madagascar in PW anomaly fields. The EPT field indicates the existence of a warm moist mid-troposphere and the intensification of convective potential over the Channel extending eastward from day-4 to day 0 near 700 hPa. The WVF indicates an increase of monsoon moisture flux converging into the lower-level cyclonic circulation throughout the process while the moisture flux associated with the lower easterlies weakens two days prior to the event. The streamfunction of WVF reveals a positive area (cyclonic anomaly) persists over

eastern Africa and extends toward Madagascar during the monsoon surge wet phase. The composite vortex analysis thus demonstrates a number of common meteorological patterns which may be of use in operational forecasting. One problem is that both dry spells and composite wet events show negative upper geopotential anomalies to the south. However in the dry spells sub-tropical westerlies are 5° further north.

7.3 TC Cynthia and TC Bryna cases :

Individual cases of destructive TC events were studied in Chapter 6. The first flood event was due to TC Cynthia which had a southeastward trajectory according to Meteosat imagery (Fig 7.1). During its period of development a cloud band spread from the Congo basin south to a low depression area over Mozambique. To the south of the Mozambique Channel a cold front moved eastward, as confirmed by lower geopotential heights. The northwesterly monsoon flow from the north of the Channel increased progressively from 13 February to reinforce the cloud vortex over the area. The Meteosat imagery on 15 February shows two cloud clusters, one on the northwest coast of Madagascar and the other over Mozambique. On the 16th, the two clusters fused to form one cloud system with outflow of cirrus to the north coinciding with upper easterlies, and deep convection to the southwest. The TC reached the west coast of Madagascar near Morondava and the local topography altered the system's trajectory to SE. The presence of a transient trough on the 19th to the southwest of the Channel assisted in steering the system southward. The system dissipated following the intrusion of dry subtropical westerlies in the lower troposphere.

Although TC Cynthia had only three day's lifespan, the Madagascar National Weather Service reported that the damage in the region of NW Madagascar was considerable. Surface observing meteorological stations in the

region indicate that maximum wind and heavy rainfall were recorded on the northern quadrant of the system near maturity on 17 February 1991. A pressure minimum of 979 hPa, peak gusts of 50 m s^{-1} and rainfall of 420 mm in 24 hours were recorded at Maintirano. It is of interest to note that Dvorak criteria do not fit reality in the Mozambique Channel. Surface observations suggest that the system reached TC intensity (T > 4.5) but no eye was detected in the satellite imagery analysis. TC in the Channel are more violent than those moving westward from the Indian Ocean.

The second flood event studied in Chapter 6 is TC Bryna which had a westward trajectory according to Meteosat imagery (Fig 7.2). TC Bryna formed from a cloud cluster in the Indian Ocean between the latitudes 10-15°S where the SST was 28-29°C. A cold front to the south of Madagascar moved eastward. Monsoon winds flowed along the east coast of Africa, then swung to westerly over the Comoros Islands to converge into the TC. The system moved slowly westward toward Madagascar coincident with a strengthening of the I-O sub-tropical anticyclone on 30 December 1991. The zonal vertical section of the vorticity field indicates a deepening of the cyclonic vorticity layer, in agreement with Davidson et al. (1990) as a precursor of TC genesis. The TC intensified to the northeast of Madagascar on the 1st of January 1992. An upper level cut-off low over the Channel pulled the system westward. Although the TC weakened over land on 2 January 1992, the monsoon flow enhanced uplift and associated convective activity over the Channel. This explains the torrential rain over northwest Madagascar. Highest wind and rainfall were concentrated in the TC's south quadrant. At Antalaha in the TC's northern quadrant, gusts of 15 m s^{-1} and rainfall of 110.6 mm were recorded, while at Mahajanga in the TC's southern quadrant, gusts of 23 m s^{-1} and rainfall of 347 mm was recorded in 24 hr. Although damage

was considerable, only a few deaths were recorded. This was due to the TC's weaker intensity and ample warning provided by the Madagascar Meteorological Department. TC Bryna had a stable trajectory prior to landfall.

The direction of propagation, lifespan and peak winds of these two TCs were entirely different. The dynamic and thermodynamic analyses of the meteorological parameters related to each TC indicate the existence of an upper-level cut-off low to the south prior to the flood event, which stirred the upper-level divergence and anticyclonic vorticity of the system. The persistent moisture flux convergence over Madagascar was enhanced by the island's topography which deflected the low level easterlies, leaving a leeside vortex over the warm Mozambique Channel. The strengthening of the moist monsoon northwesterlies deepened the semi-permanent low over the eastern Mozambique Channel, probably attracting convective activity from tropical Africa. When the easterlies weakened with the arrival of a frontal trough in the subtropics, uplift accelerated.

The intensity of the monsoon northwesterlies and topographically steered trade winds are key features of flood producing systems over the NW Madagascar in general, and TC development in the Mozambique Channel in particular. In the cases analysed here, strong wind and heavy rain are located to the northern / southern sector of the system for an eastward / westward moving TC.

Further studies of the destructive 1994 TC season could be undertaken using a similar approach. The mechanisms which trigger and sustain TCs in the region could be more accurately understood using additional derivative meteorological products and numerical model investigations.

11 Feb 91

17 Feb 91

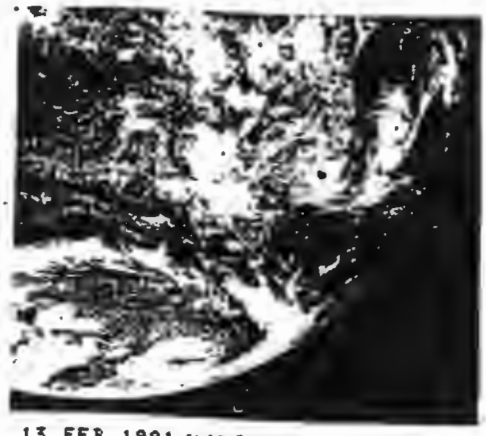

13 Feb 91

19 Feb 91

15 Feb 91

Figure 7-1: Satellite imagery of TC Cynthia.

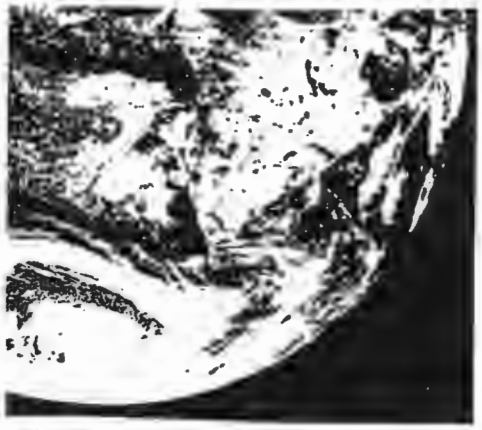

28 Dec 91

03 Jan 92

30 Dec 91

05 Jan 92

01 Jan 92

Figure 7-2: Satellite imagery of TC Bryna.

ACKNOWLEDGMENTS

Sincere thanks to my supervisor Dr. Mark Jury, of Oceanography Department, University of Cape Town (UCT), for his tireless support and advice at all stages of my research. Under his guidance the objectives of this work were achieved. Thanks are due to Kevin Levey and Bhawoodien Parker, graduate students in the Climate and Weather Research Lab UCT, for assistance in writing the programs needed to process the data, to Amos Makarau of the Zimbabwe Meteorological Service for his assistance and valuable discussions. Special thanks are also extended to Professor Geoff Brundrit, Head of the Oceanography Department for helping with administrative procedures, to S. Courtney for his computer assistance, to J. Williams for his assistance with the satellite images and to my wife Voahanginantenaina Julie for her tireless patience, understanding and encouragement throughout this research. The " Direction de la Météorologie et de l ' Hydrologie de Madagascar ", particularly the Director, is thanked for enabling me to pursue this study, while on leave from the national meteorological office of Madagascar.

I wish to thank the Foundation for Research Development Special Programme on Climatic Variability (SACCAIM), Dynamics of Marine Weather Systems Project for funding this research.

REFERENCES

Anathakrishnan, R., and M. K. Soman, 1988: The onset of south-west monsoon over Kerala: 1901-1980. *J. Climatol.*, **8**, 283-296.

Anthes, R. A., 1982: Tropical cyclones: their evolution, structure and effect, Meteor. Monogr., N°41, *Amer. Meteor. Soc.*, 208pp.

Asnani, G. C., 1993: Tropical Meteorology. Volume I. *Noble Printers Pvt. Ltd.*, Pune (India). 603pp.

Barnett, T. P., 1991: The interaction of multiple time scales in the tropical climate system. *J. Climatol.*, 4, 269-285.

Berlage, H. P., 1957: Fluctuations in the general atmospheric circulation of more than one year, their nature and prognostic value. K. Ned. Meteor. Inst. Meded. Verh., 69.

Betts, A. K., 1974: Further comments on "A comparison of the equivalent potential temperature and static energy", *J. Atmos. Sci.*, **32**, 1934-1945.

Bjerknes, J., 1969: Atmospheric teleconnections from the equatorial Pacific, *Mon. Wea. Rev.*, **97**, 163-172.

Bolton, D., 1980: The computation of equivalent potential temperature, *Mon Wea. Rev.*, **108**, 1046-1053.

Bosart, L. F., and J. A. Bartlo, 1991: Tropical storm formation in a baroclinic environment. *Mon. Wea. Rev.*, **119**, 1979-2013.

Cadet, D. L., 1985: The Southern Oscillation over the Indian Ocean. *J. Climatol.*, **5**, 189-212.

Chao, Y., and G. H. Phinlander, 1993: On the structure of the southern Oscillation. *J. Atmos. Sci.*, **6**, 450-469.

Chen, T.-C., and R. Y. Tzeng, 1990: Global-scale intra-seasonal and annual variation of divergent-water vapour flux. *Meteorol. Atmos. Phys.*, **151**, 133-151.

Chen, T.-C., M-C. Yen, K.-D Wu, and N. G. Thomas, 1992: Long-range prediction of the low-frequency mode in the low-level Indian monsoon circulation with a simple statistical method. *Tellus*, **44 A**, 324-330.

Davidson, N. E., and G. J. Holland, 1987: A diagnostic analysis of two intense monsoon depressions over Australia. *Mon. Wea. Rev.*, **115**, 380-392.

Davidson, N. E., and H. H. Hendon, 1989: Downstream development in the South Hemisphere monsoon during FGGE / WMONEX. *Mon. Wea. Rev.*, **117**, 1458-1470.

Davidson, N. E., Holland G. J., McBride J. L., and Keenan T. D., 1990: On the Formation of AMEX Tropical Cyclones Irma and Jason. *Mon. Wea. Rev.*, **118**, 1981-2000.

Davidson N. E., and A. Kumar, 1990: Numerical simulation of the development of AMEX tropical cyclone Irma. *Mon. Wea. Rev.*, **118**, 2001-2019.

Donque, G., 1975: *Contribution Geographique à l'étude du Climat de Madagascar*, N. Impr. Art. Graph, Antananarivo, Madagascar. 417 pp.

Douglas, 1992a: Structure and dynamics of two monsoon depressions. Part I: Observed structure. *Mon. Wea. Rev.*, **120**, 1524-1547.

Douglas, 1992b: Structure and dynamics of two monsoon depressions. Part II: Vorticity and heat budgets. *Mon. Wea. Rev.*, **120**, 1548-1564.

Duvergé P., 1949: *Principes de météorologie dynamique et types de temps à Madagascar*. Sce Met. M/car, N° **13**, Impr Paoli et Fakra Tananarive Madagascar. 134 pp.

Ecormier, J., 1992: *Cyclone tripical du sud-ouest de l' Océan Indien: Le cas de l' Ile de la Réunion*. Météo France, Reunion. 479 pp.

Ferranti, L., T. N. Palmer, F. Molteni, and E. Klinker, 1990: Tropical-extratropical interaction associated with the 30-60 day oscillation and its impact on medium and extended range prediction. *J. Atmos. Sci.*, **46**, 2177-2199.

Garanganga, B. J., 1989: The onset of 1982/83 summer monsoon over Southern Africa: A diagnostic study. *M. Sc.* thesis, Office of Graduate Studies of Texas A & M University.

Gray, W. M., 1979: Hurricanes: Their formation, structure and likely role in the tropical circulation. *Meteorology over the tropical Oceans*. D. B. Shaw, Ed., Roy. Meteor. Soc., 278pp.

Hendon, H. H., N. E. Davidson, and B. W. Gunn, 1989: Australian summer monsoon onset during AMEX 1987. *Mon. Wea. Rev.*, **117**, 370-390.

Hendon, H. H., and B. Liebmann, 1990: A composite study of the onset of Australian summer monsoon. *J. Atmos. Sci.*, 47, 2227-2240.

Hess, P. G., D. S. Battisti, and P.-J. Rasch, 1993: Maintenance of the Intertropical Convergence Zones and the Large-Scale Tropical Circulation on a Water-covered Earth. *J. Atmos. Sci.*, **50**, 691-713.

Holland, G. J., 1986: Interannual variability of the Australian summer monsoon at Darwin: 1952-82. *Mon. Wea. Rev.*, **114**, 594-604.

Jury, M. R., B. Pathack, G. Campbell, B. Wang, and W. Landman, 1991: Transient convective waves in the tropical SW Indian Ocean. *Meteorol. Atmos. Phys.*, **47**, 27-36.

Jury, M. R., and Pathack, B.,1991: A Study of Climate and Weather Variability over the Tropical Southwest Indian Ocean. *Meteorol. Atmos. Phys.*, **47**, 37-48.

Jury, M. R., 1992: A climatic dipole governing the interannual variability of convection over the SW Indian Ocean and SE Africa region. *Geophys. Res. Trends*, **1**, India, 165-172.

Jury, M. R., B. Pathack, B. Wang, M Powell and N. Raholijao, 1993a: A destructive tropical cyclone season in the SW Indian Ocean: January-February 1984. *S. Afr. Geogr. J.*, **72**, 53-59.

Jury, M. R., K. Levey, C. McQueen, B. Parker, A. Lee-Thorpe, A. Makarau, and B. Pathack, 1993b: Correlation Atlas of climatic determinants for sub-tropical Southern Africa and the SW Indian Ocean. *Technical rep.*, Oceanogr. Dept., UCT, Cape Town.

Jury, M. R., 1993: A preliminary study of climatological associations and characteristics of tropical cyclones in the SW Indian Ocean. *Meteorol. Atmos. Phys.*, **51**, 101-115.

Jury, M. R., B. Parker, and D. Waliser, 1994: Evolution and variability of the ITCZ in the SW Indian Ocean: 1988-1990. *Theor. Appl. Climatol.*, **48**, 187-194.

Kiladis, G. N., and H. Van Loon, 1988: The southern oscillation. Part VII: Meteorological anomalies over the Indian Ocean and the Pacific sectors associated with the extremes of the oscillation. *Mon. Wea. Rev.*, **116**, 120-135.

Latif, M., A. Sterl, E. Maier-Reimer, and M. M. Junge, 1993: Structure and predictability of the El Niño / Southern Oscillation phenomenon in a coupled Ocean-Atmosphere general circulation model. *J. Climate*, **6**, 700-708.

Laing, A. G., and J. M. Fritsch, 1993: Mesoscale convective complexes over the Indian monsoon region. *J. Climate*, **6**, 911-919.

Le Borne, J., 1987: *Climatologie du sud-ouest de l'Océan Indien, Tome 1: Le cas de l'Ile Maurice.* Collection travaux et documents N° 204, ORSTOM, France. 358 pp.

Lindesay, J. A., M. S. J. Harrison, and M. P. Haffner, 1986: The southern Oscillation and South African rainfall. *S. Afr. J. Sci.*, **82**, 196-198.

Lindesay, J. A., 1988: The southern oscillation and atmospheric circulation changes over Southern Africa. *Ph.D Thesis*, Univ. of Witwatersrand, Johanesbourg, 285pp.

Lindzen, R. S., and S. Nigam, 1987: On the role of sea surface temperature gradients in forcing low level winds and convergence in the tropics. *J. Atmos. Sci.*, **44**, 2440-2458.

Lyons, S. W., 1991: Origins of convective variability over equatorial Southern Africa during austral summer. *J. Climate*, **4**, 23-39.

Magaña V., and M. Yanai, 1991: Tropical-midlatitude interaction on the time scale of 30 to 60 days during the northern summer of 1979. *J. Climate*, **4**, 180-201.

McBride, J. L., and R. Zehr, 1981: Observational analysis of tropical cyclone formation. Part II: Comparison of non-developing versus developing systems, *J. Atmos. Sci.*, **38**, 1132-1151.

McBride, J. L., and T. D. Keenan, 1982: Climatology of tropical cyclone genesis in the Australian region. *J. Climatol.*, **2**, 12-33.

Montgomery, M., and B. Farrell, 1993: Tropical Cyclone Formation. *J. Atmos. Sci.*, **50**, 285-310.

Molinari, J., and D. Vallaro, 1990: External influences on hurricane intensity. Part II: Vertical structure and response of the hurricane vortex. *J. Atmos. Sci.*, **46**, 1902-1918.

Murakami, T., L.-X. Chen, and A. Xie, 1986: Relationship among seasonal cycles, low-frequency oscillations, and transient disturbances as revealed from outgoing longwave radiation data. *Mon. Wea. Rev.*, **114**, 1456-1465.

Ogallo, L. J., Okoola R. E., and D. N. Wanjohi, 1993: Characteristics of quasi-biennial oscillation over Kenya and their predictability potential for the seasonal rainfall. *Techn. report. Meteorol. Dept.*, University of Nairobi, Kenya.

Padya, B. M., 1989: *Weather and climate in Mauritius*, M. Gandhi Instutite, Mauritius. 283 pp.

Rasmusson, E. M., and Carpenter, T. H., 1982: Variations in tropical sea surface temperature and surface wind fields associated with the Southern Oscillation / El Niño, *Mon. Wea. Rev.*, **110**, 354-384.

Riehl, H.,1979: *Climate and weather in the Tropics*. London: Academic Press, 611 pp.

Ropelewski, C. F., M. S. Halpert, and X. Wang, 1992: Observed tropospheric biennial variability and its relationship to the Southern Oscillation. *J. Climate*, **5**, 594-614.

Schneider, E. K., and R. S. Lindzen, 1977: Axially symmetric steady state models of the basic state for instability and climate studies. Part I: Linear calculations. *J. Atmos. Sci.*, **34**, 253-279.

Shi, J. J., S. W. Chang, and S. Raman, 1990: A numerical study of the outflow layer of tropical cyclones. *Mon. Wea. Rev.*, **118**, 2042-2055.

Shukla, J., and D. A. Paolino, 1983: The Southern Oscillation and Long-Range Forecasting of the Summer Monsoon Rainfall over India, *Mon. Wea. Rev.*, **111**, 1830-1837.

Slingo, J. M., Mohanty U. C., Tiedke M., and R. P. Pearce, 1988: Prediction of 1979 summer monsoon onset with modified parametrization schemes. *Mon. Wea. Rev.*, **116**, 328-346.

Soman, M. K. and K. K. Kumar, 1993: Space-time evolution of meteorological features associated with the onset of Indian summer monsoon. *Mon. Wea. Rev.*, **121**, 1177-1194.

Streten, N. A., 1980: Some synoptic indices of the southern hemisphere mean sea level circulation 1972-77. *Mon. Wea. Rev.*, **108**, 18-36.

Taljaard, J. J., 1967: Development, distribution, and movement of cyclones and anticyclones in the Southern Hemisphere during the IGY. *J. Appl. Meteor.*, **6**, 973-987.

Tiedtke, M., W. A. Heckley, and J. Slingo, 1988: Tropical forecasts at ECMWF: The influence of physical parametrization on the mean structure of forecasts and analyses. *Quart. J. Roy. Meteor. Soc.*, 114, 639-664.

Troup, A. J., 1961: Variations in upper tropospheric flow associated with the onset of Australian summer monsoon. *Indian J. Meteor. Geophys.*, **12**, 217-230.

Tyson, P. D., 1981: Atmospheric circulation variations and the occurence of extended wet and dry spells over South Africa. *J. Climatol.*, **1**, 115-130.

Tyson, P. D., 1986: *Climatic change and variability in Southern Africa.* Oxford Univ. Press, Capetown, 220 pp.

Walker, N. D., 1989: Sea surface temperature-rainfall relationships and associated ocean-atmosphere coupling mechanisms in the southern African region. *Ph.D thesis*, Oceanogr. Dept. Univ. Cape Town, 173pp.

Williams, J. B., 1990: Some temporal and regional variations of climate in Madagascar, *Tech. Rep. Overseas Devep. Nat. Res. Inst.*, Chatham Maritime, Kent, pp 144.

Xu, J.-S., 1992: On the relationship between the stratospheric quasi-biennial oscillation and the tropospheric southern oscillation. *J. Atmos. Sci.*, 49, 725-734.

Yanai, M., 1968: Evolution of a tropical disturbance in the Caribbean sea region. *J. Meteor. Soc. Japan*, **46**, 86-108.

Zehnder, J., A., 1991: The interaction of planetary-scale tropical easterly waves with topography: A mechanism for the initiation of tropical cyclones. *J. Atmos. Sci.*, **48**, 1217-1230.

APPENDIX A

CALCULATION OF MIXING RATIO:

A] CONDENSATION LEVEL TEMPERATURE T_L :

$$T_L = [1 / \{1 / (T_K - 55) - (\ln (RH/100) / 2840\}] + 55 \qquad \text{Eq. A-1}$$

where : T_K = temperature (°K)

RH = relative humidity (%)

B] VAPOUR PRESSURE :

$$e = \exp(3.5 \times \ln T_K - (2840 / (T_L - 55)) - 4.805 \qquad \text{Eq. A-2}$$

C] MIXING RATIO :

The mixing ratio (x) is the ratio of the mass of water vapour to the mass of dry air. It is dependent on vapour pressure and total atmospheric pressure and can be derived using temperature and relative humidity (Bolton, 1980).

Using e from eq.A-2

$$x = (0.622 \times e) / (P - e) \qquad \text{Eq. A-3}$$

where : P = set-level pressure (hPa)

e = vapour pressure

From this precipitable water, water vapour flux and its derivative products can be computed.

APPENDIX B

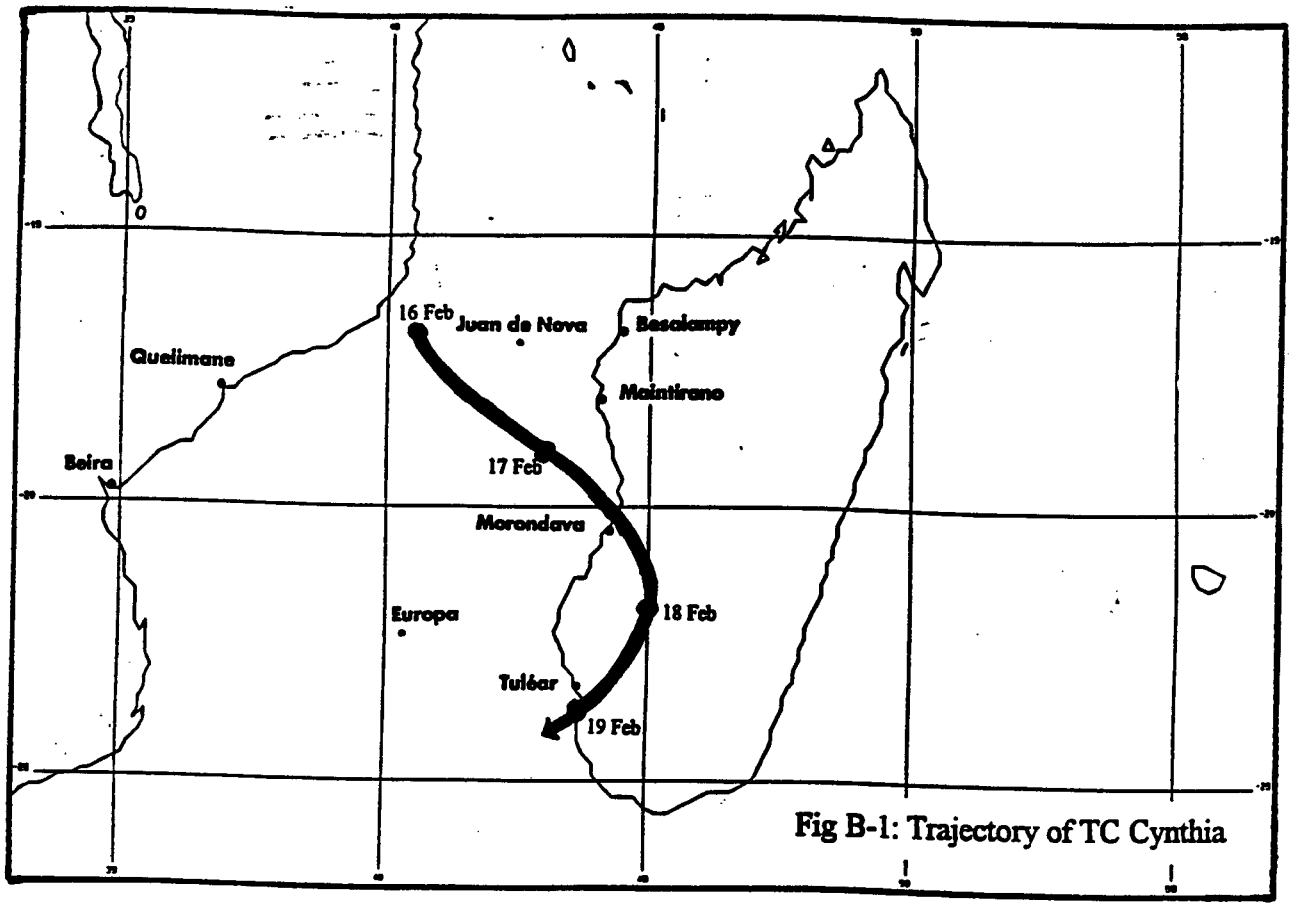

Fig B-1: Trajectory of TC Cynthia

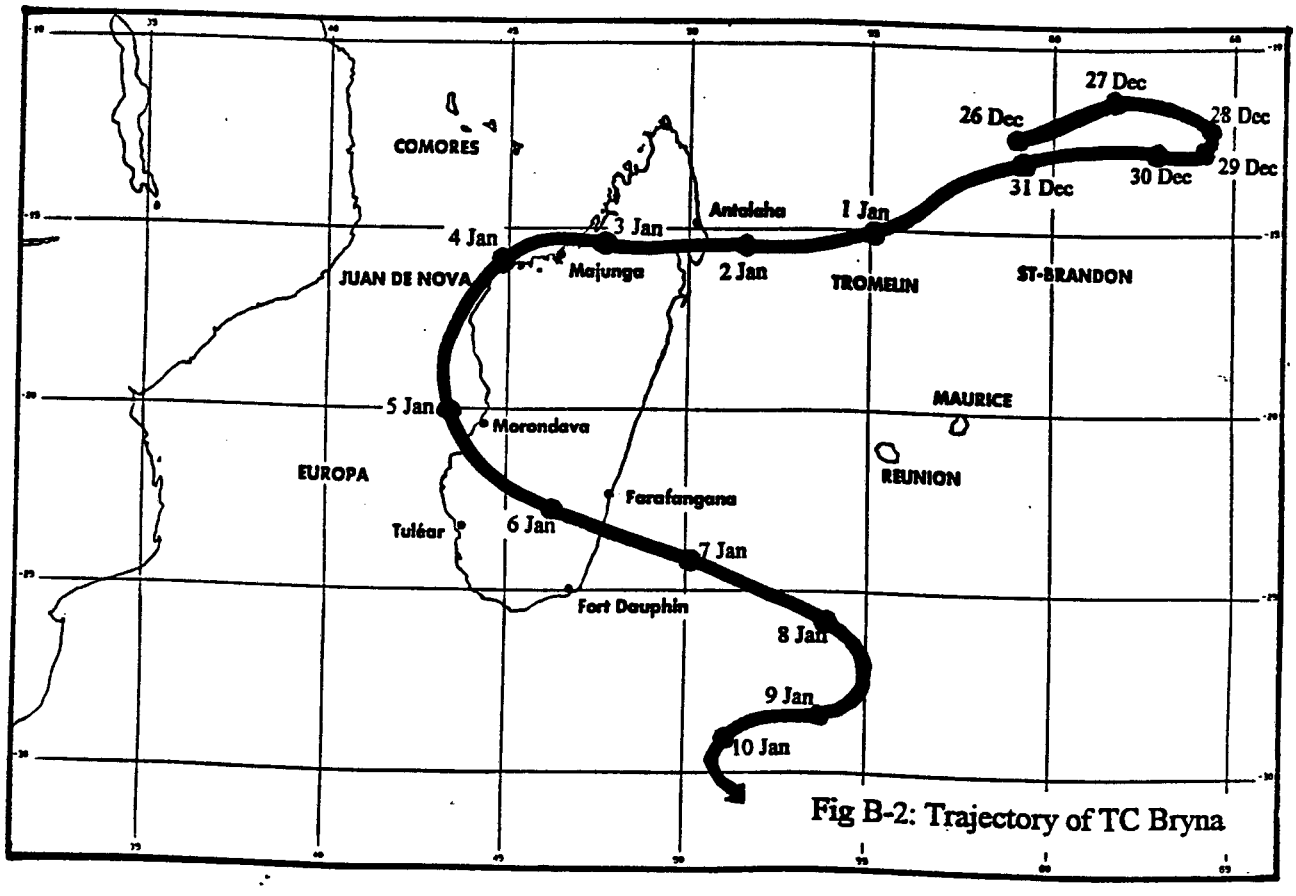

Fig B-2: Trajectory of TC Bryna